Barts and The London
School of Medicine and Dentistry

Elucidating the Expression Pattern and Role of the Oncogenic GLI Transcription Factors in Basal Cell Carcinoma

Doctorate of Philosophy

Lucia Bianchi

Supervisors: Dr. G.W. Neill and Professor M.P. Philpott

Centre for Cutaneous Research
Blizard Institute of Cell and Molecular Science (BICMS)
Barts and The London School of Medicine and Dentistry
4 Newark street, London E1 2AT

Abstract

Basal Cell Carcinoma (BCC) is the most common type of skin cancer; its development is associated with mutational inactivation of the PTCH1 tumour suppressor gene leading to deregulation of the Hedgehog pathway through increased expression of the downstream GLI (GLI1 and GLI2) transcription factors. The high expression of GLI1 and GLI2 has also been shown to be maintained through a positive feedback mechanism in human keratinocytes, but this has partly relied upon mRNA expression and has not been fully explored at the protein level. Moreover, expression analysis in human BCCs has largely relied upon in situ hybridization or RT-PCR and no studies have investigated co-expression of the GLI1 and GLI2 proteins.

Whereas an active mutant of GLI2 (GLI2ΔN) has been shown to increase endogenous GLI1 protein expression in normal human keratinocytes, preliminary evidence suggests that ectopic GLI1 suppresses endogenous GLI2 protein expression, which refutes the presence of a positive GLI feedback loop. In human BCC samples, there was a relatively high degree of heterogeneity in the expression pattern of GLI1 and GLI2 with the various antibodies employed and this was also affected by how the tissue was processed i.e. frozen versus formalin-fixed. Surprisingly, many BCCs displayed strong epidermal GLI1 expression that was decreased in the basal layer and tumour islands. In most tumours GLI1 and GLI2 showed areas of co-expression, but this was not uniform and in many areas one protein was more abundant than the other. Moreover, there was no clear difference in the expression level of GLI1 or GLI2 between BCC subtypes (aggressive versus non-aggressive). Finally, one antibody (GLI1 H-300) detected strong GLI1 expression in mesenchymal cells surrounding tumour islands (in frozen samples) but this did not correlate with epithelial Sonic Hedgehog ligand expression, suggesting a lack of paracrine Hedgehog signalling in BCC biology. In summary, this project has shown that GLI regulation and expression are more complex than previous studies have suggested and that research in this field is hampered by a lack of consistency and reliability of commercial GLI antibodies.

Declaration

The work contained in this thesis is the independent work of the author (except where stated) with guidance and advice from the supervisors Dr. Graham Neill and Professor Mike Philpott. The copyright of this thesis rests with the author and no quotation from it or information derived from it may be published without the prior written consent of the author.

Acknowledgements

I would like to thank my supervisors Dr Graham Neill and Professor Mike Philpott for their advice and guidance throughout these four years. I would also like to thank Eleni Pantazi and Jane Elliott for their friendship and support, and everyone at the Centre for Cutaneous Research for their help. I am grateful to all my friends (you know who you are) who never stopped believing in me. Finally, I would like to thank my Mum and Dad for helping shape me into the person I am today. Without your example and support, I would never have achieved this.

To my Mum,
and to the memory of my Dad.
I hope I made you proud.

"Quando si dice la verità non bisogna dolersi di averla detta.
La verità è sempre illuminante.
Ci aiuta ad essere coraggiosi."

Aldo Moro

"Abbiamo lavorato vanamente, ma non invano."

Guy Debord

Contents

List of Figures

List of Tables

Abbreviations

Abs Absorbance

BMP Bone Morphogenetic Protein

BCC Basal Cell Carcinoma

BSA Bovine Serum Albumin

cDNA Complementary DNA

CYC Cyclopamine

DAB 3, 3'-Diaminobenzidine tetrahydrochloride

DAPI 4'6'-Diamidine-2'-phenylidole dihydrochloride

DED Depidermalised dermis

DHH Desert Hedgehog

DMEM Dulbecco's Modified Eagle's Medium

DMSO Dimethyl sulphoxide

DNA Deoxyribonucleic acid

ECL Electrochemiliuminescence

ECM Extra Cellular Matrix

EDTA Ethylenediamineacetic acid

EGF Epithelial Growth Factor

EGFR Epithelial Growth Factor Receptor

FBS Fetal Bovine Serum

FCS Fetal Calf Serum

FGF Fibroblast Growth Factor

g Gram

GAPDH Glyceraldehyde-3-phosphate dehydrogenase

GFP Green Fluorescent Protein

HGF Hepatocyte Growth Factor

H&E Hematoxylin and Eosin

HH Hedgehog

HPE Holoprosencephaly

hr Hours

IGF insulin-like growth factor

IHH Indian Hedgehog

IRS Inner root sheath

KAAD-cyclopamine
3-keto, N-aminoethyl-aminocaproyl-dihydrocinnamoyl-cyclopamine

kDa Kilodalton

KGM Keratinocyte Growth Medium

L Litre

M Molar

MEFs Mouse Embryonic Fibroblasts

min Minutes

mg Milligram

ml Millilitre

mM Millimolar

MMP Matrix Metallo Proteinase

mRNA Messenger RNA

μg Microgram

μl Microlitre

μM Micromolar

μm Micrometre

ng Nanogram

nl Nanolitre

nM Nanomolar

NBCCS Nevoid Basal Cell Carcinoma Syndrome

NHS Normal Human Skin

nm Nanometre

ORS Outer root sheath

PTCH Patched

PBS Phosphate buffered saline

qPCR Real-time Polymerase Chain Reaction (quantitative PCR)

RAS RAt Sarcoma protein

RFU Relative Fluorescence Unit

RNA Ribonucleic acid

rpm Revolutions per minute

RT Room Temperature

RT Reverse Transcription

RT-PCR Reverse Transcriptase Polymerase Chain Reaction

SANT-1
4-Benzyl-piperazin-1-yl-3,5-dimethyl-1-phenyl-1H-pyrazol-4-ylmethylene-amine

SDS Sodium Dodecyl Sulphate

SDS-PAGE SDS-Polyacrylamide Gel Electrophoresis

SFM Serum Free Media

SHH Sonic hedgehog

siRNA Short interfering RNA

SMO Smoothened

SuFu Suppressor of Fused

TBS Tris buffered saline

TEMED NNN', N'-tetramethylethylenediarnine

TGFβ Transforming Growth Factor-beta

v/v Volume / Volume

VEGF Vascular Endothelial Growth Factor

w/v Weight / Volume

WNT Wingless + Int1

Chapter 1

1 Introduction

1.1 The skin

1.1.1 Structure of the skin

Skin is the largest organ of the body and performs a vital role in acting as barrier against the outside world, as it prevents the ingress of harmful chemicals and pathogenic organisms. The skin is composed by three layers: the epidermis, dermis, and the subcutaneous layer (fat layer) (Fig. 1.1 a).

The epidermis is a stratified structure mainly composed by keratinocytes; scattered throughout the epidermis there are also melanocytes, responsible for skin pigmentation, Langerhans' cells, which are part of the immune system and Merkel cells which have sensory roles (Freinkel and Woodley, 2001). The epidermis is a continually renewing epithelia in a basal to superficial direction: the end point is terminally differentiated and metabolically inactive keratinocytes known as corneocytes which are periodically shed from the skin surface. The dermis is a thick layer of fibrous and elastic tissue (made mostly of collagen, elastin, and fibrillin) that gives the skin its flexibility and strength, but is also involved in the regulation of the body temperature. The subcutaneous layer helps insulate the body from heat and cold and serves as an energy storage area where fat cells are held together by fibrous tissue.

Hair follicles (see section 1.2) are skin appendages that consist of downward growths of epidermal tissue into the dermis in which hair is produced. In the deep dermis there are also sebaceous glands that connect to the surface of the skin through sweat ducts: the hair follicle and associated sebaceous gland are named the ‘pilosebaceous unit’.

1.1.2 Layers of the epidermis

The epidermis is divided into layers (basal, spinous, granular and cornified)(Fig. 1.1 b) which can be distinguished histologically and correspond to distinct stages in the differentiation of the keratinocyte (Freinkel and Woodley, 2001).

The basal layer is a single layer of cells located at the dermal-epidermal junction. Keratinocytes proliferation takes place exclusively in the basal layer and the cells generated undergo a differentiation process as they are displaced outwards until they reach the outer surface of the epidermis where they are shed. Maintenance of epidermal homeostasis depends upon a fine balance between cell proliferation in the basal layer and cell death in the stratum corneum. Keratinocyte regeneration is maintained by stem cells resident in the basal cell layer: these cells divide asymmetrically to generate a transient-amplifying cell which gives rise to a basal keratinocyte and a stem cell to maintain the stem cell pool. In addition to the basal layer, skin epidermal stem cells are also found in the hair follicle bulge and at the base of the sebaceous glands (Watt *et al.*, 2006). Next to the basal layer is the spinous layer which consists of multiple rows of keratinocytes in which the synthesis of characteristic keratins, proteins and lipids takes place. Lamellar granules are also synthetised; these lipid-rich structures are later discharged into the intercellular space and contribute to the water-proof qualities of the epidermis. On top of the spinous layer sits the granular layer; granular keratinocytes are characterized by keratohyalin granules composed of proteins profilaggrin, locrin and keratins intermediate filaments. The stratum lucidum is an additional epidermis layer only found in thick skin (the palms of the hands and the soles of the feet) that helps reduce friction forces between the stratum corneum and stratum granulosum. During the transition from the granular to the cornified layer keratinocytes become metabolically inactive losing their organelles and nuclei, while lipids are released into the extracellular space. Corneocytes are composed by 80% keratins which linked with lipids provide a waterproof barrier. When corneocytes reach the surface of the epidermis they become less tightly associated with each other as desmosomes undergo proteolytic degradation and are eventually shed into the environment. The process of differentiation in the epidermis is also known as keratinisation: all keratinocytes contain cytoplasmic keratin filaments, the nature of which is dependent upon their location within the epidermis. The keratins serve a structural role and are classified as either acidic (type I, keratins K10 to K20) and basic (type II, keratins K1 to K9). Keratins assemble into filaments as obligate heteropolimers, meaning a member of each family (acidic and basic) must be coexpressed and form a filament structure (Freinkel and Woodley, 2001). Basal keratinocytes contain bundles of K5 and K14,

while K1 and K10 are newly synthesized in the spinous keratinocytes. In hyperproliferative epidermis, such as during wound healing, K1 and K10 are downregulated while K6 is induced. Keratin K2e is a marker of late epithelial differentiation.

Keratinocytes in the epidermis are connected to each others through protein adhesion structures named desmosomes; keratinocytes in the basal layer are anchored to the basement membrane via hemidesmosomes. Attachment of the epidermis to the underlying dermis is mediated by adhesive interactions between the basal keratinocytes and the basement membrane, which contains a layer of proteins including laminins, collagens and fibronectin. These extracellular matrix proteins serve as ligands for integrin receptors expressed on basal keratinocytes, which anchor the cells to the basement membrane.

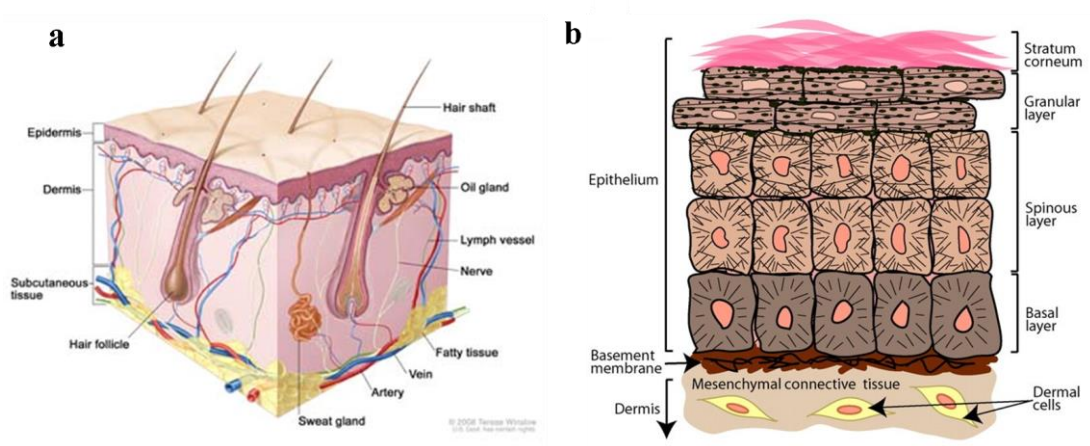

Figure 1.1: Anatomy of the skin and structure of the epidermis

Diagram of the skin, showing the epidermis, dermis, and subcutaneous layer (a) and section of epidermis highlighting the different cell layers present in the epidermis (b).
(Modified from http://www.cancer.gov/cancertopics/pdq/treatment/skin/Patient and Alonso and Fuchs, 2003).

1.2 The Hair Follicle

Hair follicles are mammalian skin appendages that produce hairs, whose functions include thermoregulation, sensory information collection and social communication (Stenn and Paus, 2001; Botchkarev and Paus, 2003) (Fig. 1.2a). The hair follicle develops during embryogenesis and consists of three concentric cylinders: the central one is the hair fiber, the middle one constitutes the inner root sheath (IRS) and the outermost one the outer root sheath (ORS) (Stenn and Paus, 2001). At the base of the hair follicle is located a region containing specialized dermal cells, named the dermal papilla. Hair follicles contain two major types of cell: dermal papilla cells, derived from the mesenchyme, and epithelial cells of the root sheaths and hair fiber, derived from the epithelium (Hardy, 1992). The sebaceous gland buds from the upper outer root sheath; sebocytes secrete lipid-rich sebum into the hair canal that empties out to the skin surface.

All mature follicles undergo successive cycles consisting of phases of active growth (anagen), followed by regression (catagen) and inactivity (telogen) (Fig. 1.2 b). During each anagen phase a new hair fiber is produced, while in the catagen phase the follicle partially degenerates and the hair moves it towards the skin surface for subsequent shedding. Telogen is a phase of relative quiescence before the follicle receives new signals that would determine its re-entry into anagen.

At a molecular level, the Sonic Hedgehog (SHH) (see section 1.4), WNT/β-catenin (WNT) (see section 1.9) and Bone Mophogenic Protein (BMP) signalling pathways are involved in both hair follicle morphogenesis and adult hair cycle. BMP factors together with WNT and SHH activating signals stimulates hair-follicle induction during embryogenesis (Botchkarev and Paus, 2003). Hedgehog signalling (HH) is required for hair morphogenesis during embryonic development: in Sonic Hedgehog (SHH) knockout mice no mature hair follicles are present as formation of the dermal papilla fails to occur (St-Jacques et al., 1998; Chiang et al., 1999). Overexpression of a stabilized form of β-catenin (which mimics activated WNT signalling) induces de-novo formation of hair follicles in the skin of transgenic mice (Gat et al., 1998). Also, transient activation of β-catenin signaling in adult mouse epidermis is sufficient to induce new hair follicles and growth of existing follicles (Lo Celso et

al., 2004). Reciprocally, loss of β-catenin expression in mice does not allow hair follicle development (Huelsken *et al.*, 2001). As SHH expression is absent in β-catenin knockout mice, SHH signaling has been proposed to act downstream of WNT signalling in hair follicle development (Huelsken *et al.*, 2001). Hedgehog signaling also plays a key role in adult hair follicle growth (Sato et al., 1999; Wang et al., 2000b) in association with the WNT signalling pathway. Whereas SHH signaling is responsible for the downgrowth of the follicular epithelium to form a follicle, WNT/β-catenin signaling has a key role in initiating formation of the hair bud (in adult mice skin the hair follicle is unable to enter anagen following β-catenin ablation (Huelsken *et al.*, 2001).

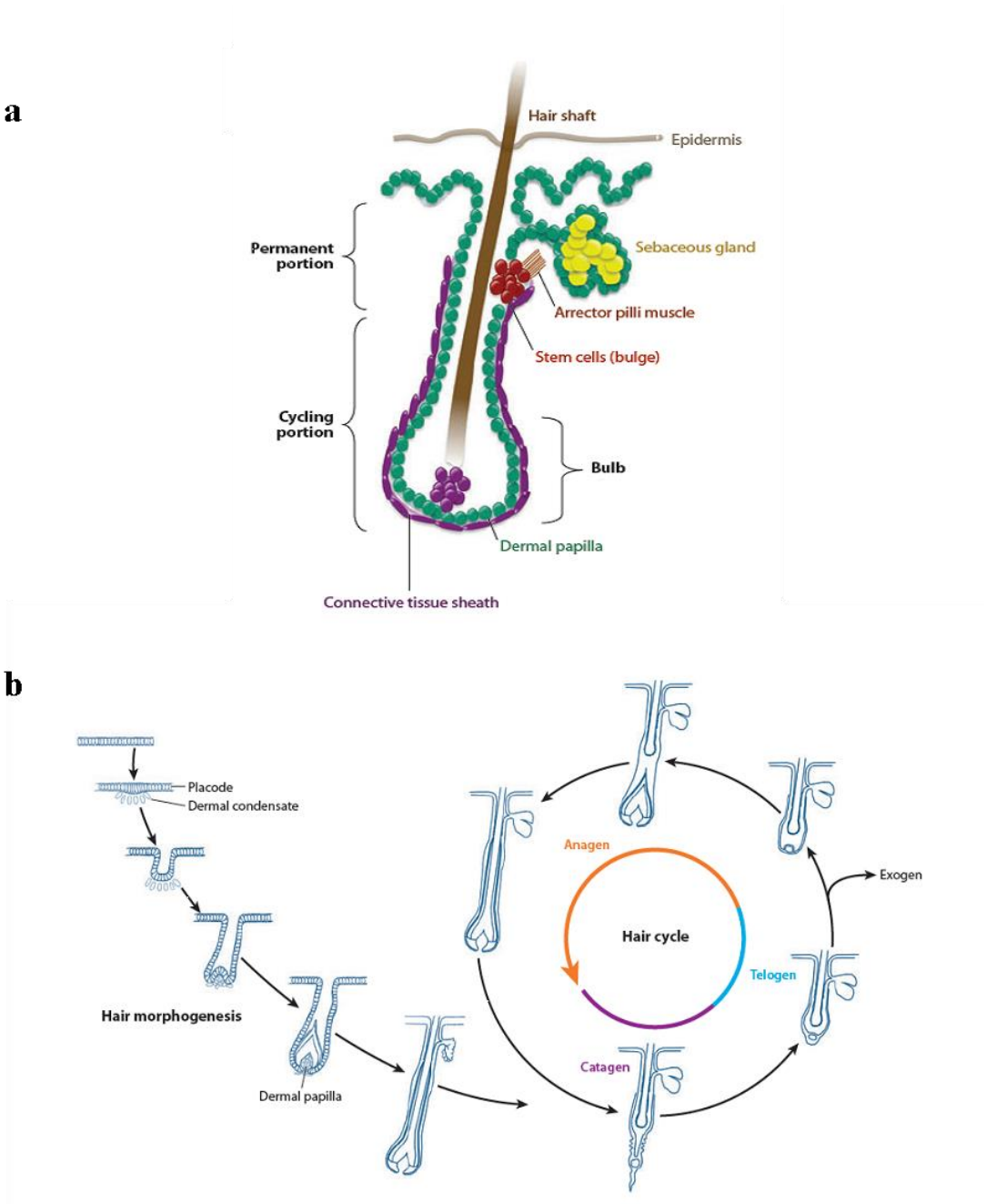

Figure 1.2: Hair follicle structure and hair cycle

Schematic representation of a hair follicle (a) and of hair follicle morphogenesis and hair cycle (b). (Adapted from Shimomura and Christiano, 2010).

1.3 Basal Cell Carcinoma

1.3.1 Incidence and aetiology

Basal Cell Carcinoma (BCC) is the most common malignant cancer that affects the Caucasian population and its incidence rate is on the increase (Crowson, 2006). Although rarely metastatic, it is capable of extensive local growth and its surgical extirpation can have adverse cosmetic effect since they are most common on the head and neck region (Miller, 1995). Known risk factors for BCC development include ultraviolet light, exposure to arsenic or ionizing radiation, and a compromised immune system (Crowson, 2006). The molecular mechanisms underlying BCC development, which involve deregulation of the Hedgehog pathway, were deduced from studies of a rare hereditary disorder, Gorlin's syndrome, which is characterized by hundreds of these tumours (Gorlin, 1995; Hahn et al., 1996b).

1.3.2 Classification

Basal Cell Carcinomas can be broadly classified into three subtypes on the basis of their histological appearance: Nodular, Micronodular, Superficial, and Morpheic / Infiltrative, the latter being the less frequent but most aggressive type (Crowson, 2006) (Fig. 1.3).

Nodular BCC, the most common subtype, begins as a papule or nodule on or within the skin, which grows slowly and has a pearly translucence. These BCCs are characterized by discrete nests of basaloid cells; tumour cells tend to align more densely in a palisading pattern at the periphery of the nests. Nodular BCCs can become very large and destroy deeper structures. Micronodular BCCs are histologically similar to Nodular BCCs, manifesting as tumour nests of basaloid cells, although they tend to be smaller and widely dispersed. Superficial BCC lesions appear as flat wrinkled superficial ulcerations, often larger than 1 cm in diameter. Histologically they appear as aggregates of basaloid cells located within and just underneath the epidermis. Morphoeic and Infiltrative BCCs appear as plaques with irregular contours and small irregular islands of tumour cells embedded in a heavily collagenized fibrous stroma (Halpern and Hanson, 2004). Histologically they present as elongated strands of basaloid cells extending into the surrounding tissue

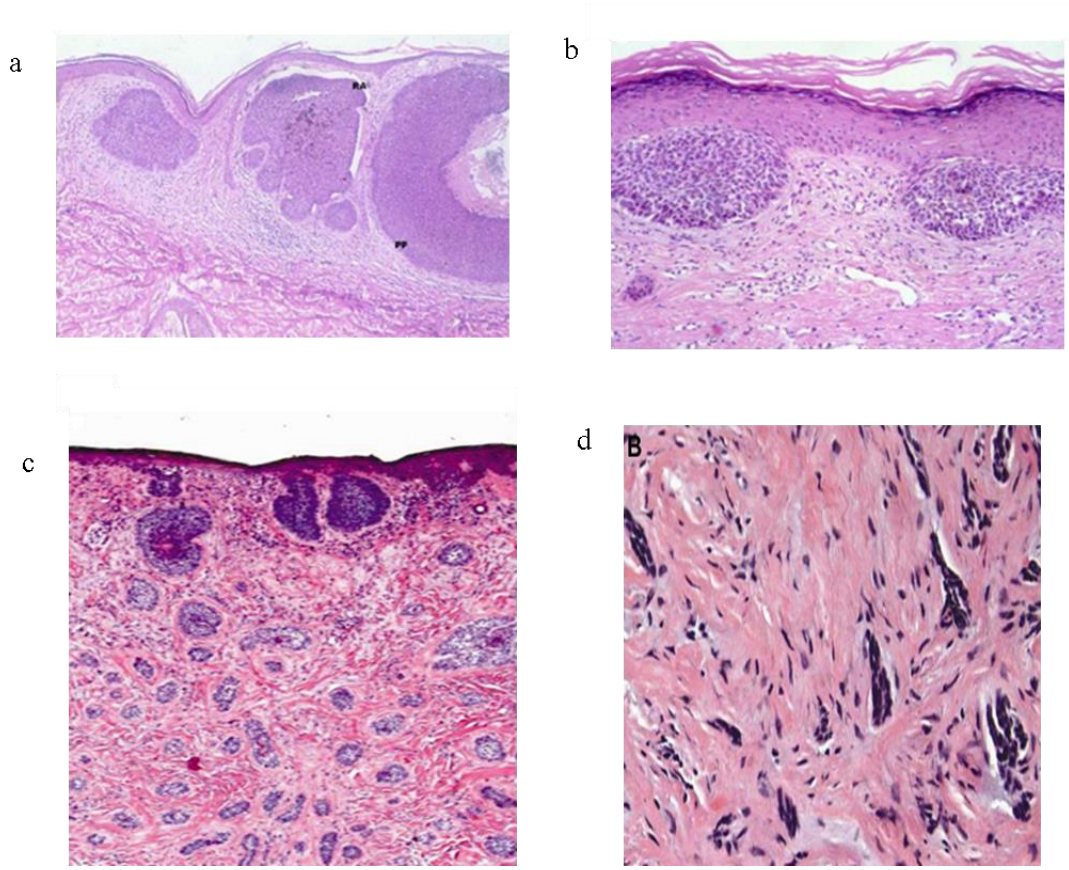

Figure 1.3: Histological analysis of Basal Cell Carcinomas belonging to different subtypes

Haematoxylin and eosin staining of nodular (a), superficial (b), micronodular (c) and morpheic (d) Basal Cell Carcinomas. (Adapted from Crowson, 2006).

1.3.3 Origin of Basal Cell Carcinoma

The molecular mechanisms underlying Basal Cell Carcinoma development, which involve deregulation of the Hedgehog pathway (see section 1.7), were deduced from studies of a rare hereditary disorder, Gorlin's syndrome, which is characterized by hundreds of these tumours (Gorlin, 1995; Hahn et al., 1996b). Since mutations affecting the Hedgehog pathway result in the development of BCC and SHH activity in the skin is mostly confined to hair follicles, it has been hypothesized that cells of the hair follicle may be an important target for BCC carcinogenesis; alternatively, BCC may also originate from the basal layer of interfollicular epidermis that, as a result of oncogenic mutation, are able to re-enter into the into the cell cycle. Different theories regarding the cell of origin of BCCs are present in the literature. BCCs have been proposed to derive from basal keratinocytes of the interfollicular epidermis which are positive for the expression of keratin 5 and keratin 14 and negative for differentiation markers (Miller, 1995; Crowson, 2006) this is consistent with the role of SHH pathway in skin, which is implicated in the maintenance of the epidermal stem cell population present in the epidermal basal layer and in the hair follicle bulge (Blanpain and Fuchs, 2006). Due to the role of SHH signaling in the hair follicle morphogenesis and cycle, these tumours may also be derived from undifferentiated cells of the outer root sheath of the hair follicle (Blanpain and Fuchs, 2006)Blanpain and Fuchs, 2006; Crowson, 2006; Hutchin et al., 2005).

Upon wounding, follicular stem cells migrate and contribute to the healed wound epithelium; using different genetic mouse models of BCC, it has been shown that oncogene-expressing follicular stem cells promote the formation of BCCs after wounding (Kasper et al., 2011; Wong and Reiter, 2011). The neuroepithelial stem cell marker nestin, which is expressed in the hair follicle papilla, is also present in the stroma of BCCs, suggesting a similarity between the BCC stroma and the mesenchyme surrounding of the hair follicle (Sellheyer and Krahl, 2011). Recently, some papers have tried to identify the cell of origin of BCC by taking advantage of mouse models expressing HH pathway components in specific skin regions. In Youssef et al. (Youssef et al., 2010), an activated form of SMO (SMOM2, see section 1.4) is conditionally expressed in either hair follicle bulge stem cells, hair follicle transit amplifying cells or basal epidermal cells (from which all other

epidermal layer are generated). No BCC originating from bulge stem cells and their progenies were observed, while constitutive SMOM2 activation in basal keratinocytes leaded to tumour formation; BCC are therefore proposed to arise from interfollicular epidermis. Another recent publication uses a constitutively active form of GLI2 (GLI2ΔN, see section 1.8) and argues that tumor phenotype depends on the cell targeted and the level of oncogenic HH signaling, as well as the hair cycle proliferation phase (Grachtchouk et al., 2011). GLI2ΔN is proposed to be a more potent activator of HH signalling than SMOM2; GLI2ΔN induction in hair follicle stem cells gives rise to nodular BCCs, while its expression in interfollicular epidermis results in superficial BCCs. Nodular BCCs skin tumors arise from a subset of hair follicle stem cells that expresses the Lrg5 marker; moreover, GLI2ΔN induction during the anagen phase of the hair cycle enhances its tumorigenic properties. In Ptch1 heterozygous mice X-ray induced BCC develop from hair follicle bulge stem cells (Wang et al., 2011). Selective deletion of p53 enhances tumor formation from the hair follicle bulge and also leads to BCC development from the intefollicular epidermis; the latter event is due to increased SMO expression in interfollicular epidermis as a result of p53 loss. This could also partly explain the discrepancies with the result of Youssef et al., where BCCs are observed in interfollicular epidermis as a result of targeted expression of SMO, which is not expressed at a significative level in interfollicular skin of Ptch1 + / - mice. PTCH1 may have non HH-related functions (Barnes et al., 2001) which are required for BCC formation from the hair follicle but not from the intefollicular epidermis in the presence of mutated SMO. Although expression of downstream HH pathway components result in murine BCC development, Ptch1 + / - mouse model are proposed to be a more relevant model of human BCC tumorigenesis as nearly 90% human BCC have mutations in at least one copy of the PTCH1 gene.

1.3.4 Treatment

Treatment options for BCC include surgical excision, Moh's micrographic surgery, curettage and electrodesiccation, cryosurgery, treatment with chemicals that interfere with DNA synthesis (5-Fluorouracil) or that modulate the immune response (Imiquimod) (Ceilley and Del Rosso, 2006). Recently, synthetic SMO inhibitors have been tested for the treatment of human BCC but have shown limited efficacy so far (Von Hoff *et al.*, 2009; Yauch *et al.*, 2009).

1.4 The Hedgehog signalling pathway

The Hedgehog (HH) signaling pathway is one of the most fundamental signal transduction pathways in embryonic development and it is conserved from flies to humans (Hooper and Scott, 1989; Goodrich et al., 1996; Hahn et al., 1996a). Hedgehog was initially identified as a segment polarity gene that controls Drosophila embryonic pattern during a large-scale screen for mutations that impair the development in the fruit fly (Nussleinvolhard and Wieschaus, 1980)

The pathway takes its name from its polypeptide ligand, called Hedgehog (HH) in Drosophila. Three vertebrate homologs of the Drosophila hedgehog gene have been identified: Sonic Hedgehog (SHH), Desert Hedgehog (DHH), and Indian Hedgehog (IHH) (Echelard et al., 1993). SHH is the most broadly expressed member of this family and most likely responsible for all the major effects on development of the brain, spinal cord, axial skeleton, and limbs (Chiang et al., 1996). IHH has been implicated in regulation of cartilage differentiation in the growth of long bones (Lanske et al., 1996; St-Jacques et al., 1999). DHH exerts its effect mainly in the developing germline and in Schwann cells of the peripheral nervous system (Bitgood et al., 1996; Mirsky et al., 1999). Sonic Hedgehog ligand (SHH) is the most widely expressed Hedgehog ligand (Chiang et al., 1996); it encodes a 45 kDa protein that undergoes autocatalytic cleavage and modification to give a 20 kDa active N-terminal fragment covalently bound to cholesterol (Porter *et al.*, 1996).

The Patched gene (PTCH) was originally identified in Drosophila: in humans it consists of 23 exons and encodes a glycoprotein with 12 membrane-spanning domains (Hooper and Scott, 1989; Nakano et al., 1989) and two large extracellular loops that are required for Hedgehog ligand binding (Marigo *et al.*, 1996) (Stone *et al.*, 1996). There are two Patched genes in humans: Patched 1 (PTCH1) is the major receptor molecule for all three forms of Hedgehog ligand, and mutations in this gene are associated with a wide variety of birth defects and development of specific tumours. (Hahn et al., 1996a; Goodrich et al., 1997). Patched 2 (PTCH2) is a close homolog of Patched, which function is still unclear (Smyth et al., 1999). From here onward Patched1 (PTCH1) will be referred as PTCH unless otherwise specified.

Smoothened (SMO) is a 115 kDa protein containing seven membrane spanning domains which shows structural similarity to serpentine G-protein coupled receptors (Alcedo et al., 1996; vandenHeuvel and Ingham, 1996).

The Hedgehog signal is received and transduced via a receptor complex consisting of PTCH1 and SMO. The exact nature of the interaction between PTCH1 and SMO is still unclear, but it involves change in the cellular localization and stability of PTCH1 and SMO upon Hedgehog ligand binding (Denef et al., 2000). Under physiological condition PTCH1 localisation to the cellular cilia inhibits Hedgehog signaling by excluding SMO (Rohatgi et al., 2007); upon ligand binding SMO translocates to the cilia, where it activates the transduction cascade leading to the activation of the GLI transcription factors (Fig. 1.4). The net effect of pathway stimulation is the activation of members of the GLI family of zinc finger transcription factors (Kasper *et al.*, 2006) (see section 1.8). In the absence of ligand, GLI proteins are linked to the cytoskeleton by interaction with a multiprotein complex that includes Fused (Fu) and Suppressor of fused (SuFu) (Murone et al., 2000). Upon ligand binding GLI proteins are translocated into the nucleus (Kogerman et al., 1999; Sheng et al., 2006) where they activate transcription of target genes, including genes involved in cell proliferation (e.g. cyclin D), apoptosis (Bcl2, c-Flip), invasion (Snail), and maintenance of the stem cell pool (Sox-9) (Duman-Scheel *et al.*, 2002; Mill *et al.*, 2003; Aberger and Frischauf, 2006; Kasper *et al.*, 2006). GLI target genes include PTCH1 itself (Nilsson *et al.*, 2000). A negative feedback loop of PTCH1 on GLI1 has recently been described (Rahnama *et al.*, 2006). This effect is observed even in the presence of the Hedgehog pathway inhibitor cyclopamine. Moreover, PTCH1 C-terminal region (proposed to play a role in HH/SMO signalling) is dispensable for this inhibition, indicating this effect is independent of canonical Hedgehog signaling. Recent evidence indicates that Hedgehog pathway remains active in a subset of cells in the adult (stem cells) (Ruiz i Altaba et al., 2002) and contribute to tissue homeostasis in some organs, including the skin. Aberrant reactivation of Hedgehog pathway in adult tissue has been linked with development of different types of cancer (di Magliano and Hebrok, 2003).

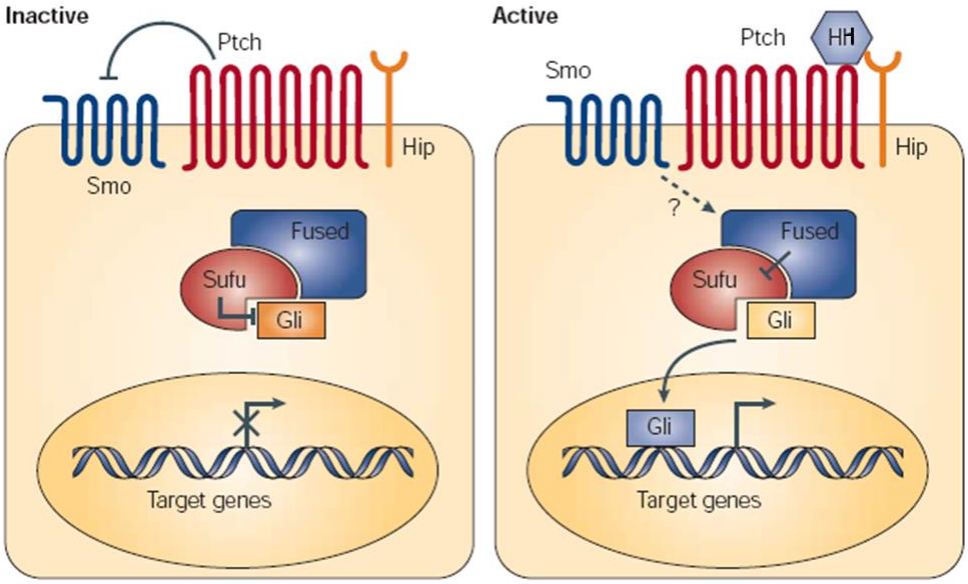

Figure 1.4: The Hegdehog signalling pathway

Diagram of the Hedgehog signalling pathway main components in the absence (left) or in the presence (right) of the Hedgehog (HH) ligand. (Adapted from di Magliano and Hebrok, 2003).

1.5 Hedgehog signalling in cancer

Hedgehog signalling deregulation due to mutation in the pathway components has been shown to cause formation of Basal Cell Carcinoma (BCC), a nonmelanoma skin cancer, and of medulloblastomas, a primitive neuroectodermal tumour of the brain (di Magliano and Hebrok, 2003); mutations in Hedgehog pathway components have been found both in familial and sporadic cases of BCC.

Interestingly, Hedgehog signalling seems to be required also for the growth and maintenance of other types of cancer, including pancreas, prostate, lung and digestive tract (Berman *et al.*, 2003; Watkins *et al.*, 2003; Karhadkar *et al.*, 2004; Nolan-Stevaux *et al.*, 2009) which are caused by mutations in different pathways (Thayer *et al.*, 2003; Watkins *et al.*, 2003; Karhadkar *et al.*, 2004; Sarangi *et al.*, 2009; Zhao *et al.*, 2009). This discovery could have important therapeutic implication as Hedgehog signalling inhibitors could be an alternative approach for tumours that are difficult to treat by conventional means.

1.5.1 Antagonists of Hedgehog signalling

Screens of different molecules have led to the identification of several diverse antagonists of Hedgehog signalling, some of which may have potential therapeutic application. The first Hedgehog signalling antagonist discovered was cyclopamine, a steroidal alkaloid found in lily (Veratrum californicum). When pregnant sheep ate lilies, this resulted in severe holoprosencephaly in developing embryos, also referred as ‘cyclopia’; the relevant chemical from the lily was then named 'cyclopamine'. Holoprosencephaly (HPE) is a developmental disorder characterized by an absence of midline facial structures and development of fused nasal chambers at a location overlying a cyclopic eye. As holoprosencephaly is also a characteristic feature of SHH-/- knockout mice (Chiang et al., 1996) and human HPE is associated with loss of function mutation at the human SHH locus (Belloni et al., 1996), it was suggested that cyclopamine works by repressing the Hedgehog pathway (Cooper et al., 1998) acting on the SMO protein (Taipale et al., 2000). Cyclopamine inhibits the growth of human medulloblastoma and glioma cell lines (Dahmane et al., 2001) and also of mouse embryonic fibroblasts (MEFs) lacking a functional copy of PTCH1 (Taipale et al., 2000): therefore, cyclopamine has been proposed as treatment for tumour

displaying aberrant activation of the Hedgehog pathway. KAAD-cyclopamine (3-keto, N-aminoethyl-aminocaproyl-dihydrocinnamoyl-cyclopamine) is a potent synthetic cyclopamine derivative (Taipale et al., 2000) while SANT-1 (4-Benzyl-piperazin-1-yl)-(3,5-dimethyl-1-phenyl-1H-pyrazol-4-ylmethylene)-amine is a synthetic SMO antagonist. The use of cyclopamine and its derivative as cancer therapeutics is hindered by their teratogenic effects. A recently developed synthetic inhibitors of SMO, GDC-0449, has given promising preliminary results in the treatment of medulloblastoma and metastatic BCC (Von Hoff et al., 2009; Yauch et al., 2009). However, other anti-SMO inhibitors appear to be effective in reducing BCC tumour growth in mouse models but have shown limited success in the treatment of human BCCs (Williams *et al.*, 2003; Tang *et al.*, 2011).

1.5.2 Paracrine Hedgehog signalling in cancer

The interaction between tumour cells and stromal cells has been shown to be linked to the tumorigenic process and to play a fundamental role in tumour invasion. Recently, Hedgehog signalling has been proposed to regulate tumour growth by acting in a paracrine manner (Fig. 1.5). In mouse xenotrasplantation models of pancreatic and colorectal cancer the effect of Hedgehog ligands is not predominantly exerted in tumour cells; instead, the proteins are secreted to activate the Hedgehog pathway in non-malignant stromal cells (Yauch et al., 2008). This closely resemble the typical role of Hedgehog signalling in development, which is mediated by paracrine effects on mesenchymal cells (Ingham and McMahon, 2001). HH ligand produced by cancer cells activates the pathway in tumour stroma, which in turn affects tumour development, possibly by secretion of chemokines and growth-promoting factors. Specific inhibition of Hedgehog signaling with Hedgehog pathway antagonist or by genetic deletion of SMO in the stroma of mice results in growth inhibition of HH ligand-expressing xenografts (Yauch et al., 2008). Additional evidence for paracrine Hedgehog signalling in cancer came from mouse models of pancreatic cancer (Nolan-Stevaux *et al.*, 2009; Tian *et al.*, 2009). Inhibition of Hedgehog signalling in the stroma has been shown to alter the secretion of factors, such as insulin-like growth factor receptor and WNT signalling pathway components, that are linked to cancer pathogenesis (Yauch *et al.*, 2008; Scales and de Sauvage, 2009). Moreover, in a mice model of pancreatic cancer tumour-

associated fibroblasts expressed GLI1 and also stained positive for vascular endothelial growth factor (VEGF) (Bailey et al., 2009). A better understanding of paracrine Hedgehog signaling mechanism in cancer can therefore be useful to develop targeted tumour therapies.

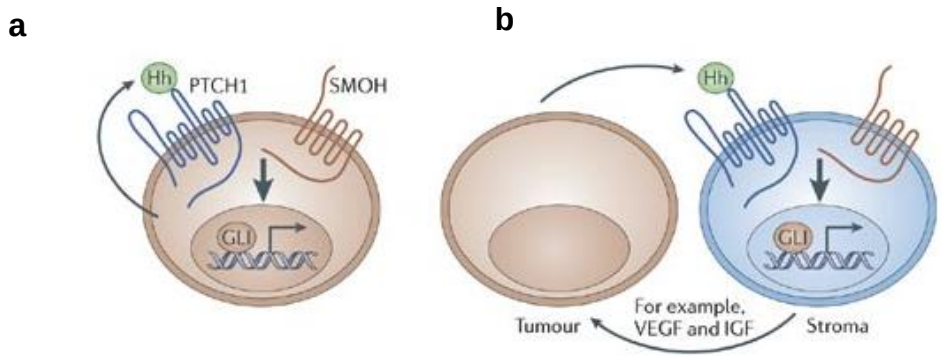

Figure 1.5: Proposed autocrine and paracrine mode of Hedgehog signalling in cancer

Requirement for autocrine Hedgehog signalling has been reported in epithelial tumours (a); recent publications also highlight a paracrine mode of Hedgehog action in cancer (b), in which the stromal compartment contributes to tumour formation via mechanisms that remained to be characterized (Adapted from Rubin, 2006).

1.6 Role of tissue stroma in cancer

Epithelial cells are surrounded by the stroma, which is composed by the extracellular matrix (ECM) as well as cellular components such as fibroblasts and cells belonging to the immune and vascular systems.

Cancer cells can modify their adjacent stroma through the expression of growth factors that promote angiogenesis and alter ECM protein expression, leading to increased inflammatory cell recruitment and also activating surrounding fibroblasts (Tlsty and Coussens, 2006). Activated fibrobroblasts play a prominent role in cancer progression via secretion of ECM components, growth factors, chemokine and proteases. The growth factors secreted by fibroblasts belongs to different families, including the fibroblast growth factor (FGF) family, the insulin-like growth factor (IGF) family, the epithelial growth factor (EGF) family, hepatocyte growth factor (HGF), the vascular endothelial growth factor family (VEGF) and the transforming growth factor (TGF-β) family (Bhowmick et al., 2004). During malignant tumour progression cells acquire the ability to invade the surrounding tissues; specifically, keratinocytes are able to cross the basement membrane barrier by promoting extracellular matrix degradation and activating cell motility mechanisms (Liotta and Kohn, 2001). Degradation of basement membranes components is achieved by secretion of matrix metalloproteinase (MMP), while cytoskeletal changes favour migratory movement.

The microenvironment of a tumour is constituted of a heterogenous population of stromal cells, extracellular matrix components and secreted factors, which make it distinct from that of normal tissue and therefore a potential site for therapeutic intervention.

1.7 Hedgehog signalling in Basal Cell Carcinoma

Insight into the molecular mechanism underlying Basal Cell Carcinoma (BCC) development came from the study of Gorlin-Goltz's syndrome, also known as Nevoid Basal Cell Carcinoma Syndrome (NBCCS) (Gorlin, 1995). Gorlin's syndrome is an autosomal dominant condition that results in a variety of developmental and skeletal defects and is associated with an increased risk for some types of cancers, most notably BCCs, but also fibrosarcomas and rhabdomyosarcomas. Gorlin-Goltz's syndrome maps to chromosome 9q22.3; the majority of sporadic BCCs display loss of heterozigosity on chromosome 9q22 suggesting that inactivation of a tumour suppressor in this location is an important step in BCC formation (Gailani et al., 1996a). Tumour suppressor genes normally exert a negative control on cell growth, and inactivation of both homologues is required for a tumorigenic effect (Weinberg, 1995). In accordance with Knudson's two hits hypothesis of tumorigenesis, heritable mutations in the human homologue of the Drosophila Patched gene were identified in patients with NBCCS syndrome and somatic loss of heterozygosity in the tumour suppressor Patched gene resulted in BCC development (Hahn et al., 1996b; Johnson et al., 1996). The Patched gene was originally identified as a gene regulating segmentation and polarity during Drosophila development (Hooper and Scott, 1989; Nakano et al., 1989). The transmembrane receptor PTCH1 is part of the Hedgehog pathway and it is conserved in eukaryotic organisms (Goodrich et al., 1996; Hahn et al., 1996a), where this pathway plays a role in development and tissue homeostasis. Mutations in the Patched gene (Gailani et al., 1996b; Gailani and Bale, 1997; Aszterbaum et al., 1998) and other components of the Hedgehog pathway were subsequently identified also in sporadic BCCs. The mutational spectrum of Patched in sporadic BCCs suggests that environmental factors other than ultraviolet B (UVB), the predominant carcinogenic component of sunlight, may play a role in tumorigenesis. UVB typically causes formation of photodimers that result in G·C to A·T transitions opposite dipyrimidine sites (Quinn, 1997). Mutations in p53 occur in ~50% of BCCs (Ziegler et al., 1993); less frequently occurring mutations in the Ras family of proto-oncogenes (Vanderschroeff et al., 1990) are often of the type caused by UVB. However, only

about 50% of the Patched mutations in sporadic BCCs have the typical UVB signature (Gailani and Bale, 1997).

Activation of SMO, similar to PTCH1 inactivation, result in transcription of Hedgehog target genes; activating mutations in the SMO gene (SMOM1, SMOM2) have been detected in of sporadic BCCs (Xie et al., 1998) SMOM2 mutation (Trp535Leu), which maps in the seventh transmembrane domain of SMO, has been detected in almost all BCCs lacking PTCH1 mutations. In contrast to wild-type SMO, the mutant form has been shown to result in BCC-like tumours in transgenic mice expressing this mutant gene under the control of an epidermal promoter (Yang et al., 2008). Other rare mutations in the Hedgehog pathway that causes BCC are Sonic Hedgehog ligand (SHH) activating mutations and possibly gain-of-function mutation in GLI proteins (Khavari, 2006).

1.7.1 Other signaling pathways implicated in Basal Cell Carcinoma pathogenesis

Hedgehog and WNT signalling have been shown to interact both in normal development (Mullor et al., 2001) and in vitro oncogenic cell transformation (Li et al., 2007). Cross talk between the Hedgehog and WNT pathways has also been suggested to be implicated in Basal Cell Carcinoma pathogenesis. In a mouse model of skin cancer activation of WNT signalling pathway has been shown to be required for the development of follicular hamartomas, a type of benign tumour associated with deregulated Hedgehog signalling (Yang et al., 2008). Constitutive activation of Hedgehog signaling by targeted expression of an oncogenic form of SMO (SMOM2) in the skin induces WNT signalling, and this induction is required for tumour development, as expression of the secreted WNT pathway inhibitor Dkk1 in the skin prevents tumour formation. In mice where activation of the secreted WNT inhibitor Dkk1 could be achieved in the skin compartment tumour formation was abolished. These results suggest WNT signaling inhibition as a potential therapeutic target in BCC, although further studies are required to address the importance of this interaction in human neoplasia.

TGFβ pathway components (see section 1.10) have been shown to be present in the epithelial and stromal components of BCCs (Schmid et al., 1996; Furue et al., 1997;

Verhaegh et al., 1997; Gambichler et al., 2007) and to promote invasion by acting on the stroma (Marsh et al., 2008), although their precise role in the development of this epithelial tumour remains to be fully elucidated. TGFβ has been shown to induce GLI1 and GLI2 expression in keratinocytes and fibroblasts even in the presence of cyclopamine, suggesting this activation is not be dependent on canonical Hedgehog signalling through PTCH1 and SMO (Dennler *et al.*, 2007).

1.8 GLI proteins and their role in Basal Cell Carcinoma

The GLI family of transcription protein control transcriptional programs in response to Hedgehog pathway activation. Following ligand binding GLI proteins translocate into the nucleus (Fig 1.6); three vertebrate Gli genes - Gli1, Gli2 and Gli3 have been identified (Kinzler et al., 1988; Ruppert et al., 1988). They regulate defined transcriptional programs in a context-dependent and cell-type specific manner.

GLI1, GLI2, and GLI3 encode transcription factors that share five highly conserved tandem cysteine-histidine C2-H2 zinc fingers motif (F/YXCX2-4CX3FX5LX2HX3-4HX5) and a consensus histidine-cysteine linker sequence between zinc fingers (Ruppert et al., 1988). The GLI1 and GLI3 proteins recognize a conserved GACCACCCA sequence in the promoters of target genes (Kinzler and Vogelstein, 1990; Ruppert et al., 1990; Vortkamp et al., 1995), and GLI2 recognizes a nearly identical GAACCACCCA motif (Tanimura et al., 1998). Full length GLI proteins have been speculated to have activator as well as repressor functions, the latter as a result of carboxyl-terminal cleavage by the proteasome (Ruiz i Altaba et al., 2002). In the absence of Hedgehog signalling proteolytic processing leads to the formation of a GLI3 repressor form (GLI3-R) which represses GLI factor transcriptional activity (Wang et al., 2000a).

GLI1 was originally identified as a gene that was amplified in human glioma (Kinzler et al., 1987) and subsequently shown to be a transcription factor that binds DNA in a sequence-specific manner (Kinzler and Vogelstein, 1990). GLI1 has been classified as an oncogene on the basis of its ability to transform cells in cooperation with adenovirus E1A (Ruppert et al., 1991). To date, different GLI1 isoforms have been described: GLI1ΔN, which encodes an N-terminal truncated protein generated by skipping exons 2 and 3 (Shimokawa *et al.*, 2008) and tGLI1, an in-frame deletion spanning the entire exon 3 and part of exon 4 (Lo *et al.*, 2009). GLI1ΔN is a less potent transcriptional activator compared to full-length GLI1; the expression ratio of the two GLI1 isoforms is greatly variable in tumour cell lines. tGLI1 has been discovered during the analysis of human glioblastoma multiforme samples and has been shown to confer enhanced migratory properties to cells. Moreover, other two GLI1 isoforms have been described by transfecting full length GLI1 into glioma cells

(Altaba, 1999; Stecca and Ruiz i Altaba, 2009), one deleted at the amino-terminal (positions 1 – 231) and the other missing a large portion at the carboxyl-terminal (position 515 to the end of the protein) (see also section 4.3.5 and Figure 4.53).

GLI2ΔN is a constitutively active form of GLI2 lacking the amino-terminal repressor domain (which was identified in 2005); this truncated form of GLI2 was thought to represent the whole protein but has been revealed to be a much more potent transcriptional activator than the full length GLI2 in vitro (Roessler et al., 2005). In the absence of HH ligand, full length GLI2 is a weak transcriptional activator; in response to Hedgehog signalling, proteolytic removal of the amino terminal repressor domain, or its inactivation, appears to be required for full GLI2 activator function (Roessler et al., 2005). Four different GLI2 isoforms have been described: alpha (α), beta (β), gamma (γ) and delta (δ), whose transcripts are generated by combinations of two independent alternative splicing sites (Tanimura et al., 1998). Alternative splicings result in a 51-base deletion of the coding frame in the beta (β) and delta (δ) isoforms, and a 1,231-base deletion in the gamma (γ) and delta (δ) isoforms.

GLI3 has been reported to be phosphorylated by protein kinase A (PKA), casein kinase 1 (CK1), and glycogen synthase kinase 3β (GSK3β) and targeted for ubiquitination by β-TrCP ubiquitin ligase, in order to be converted into a truncated transcriptional N-terminal repressor (Wang *et al.*, 2000a; Pan *et al.*, 2006b). GLI2 contains PKA and GSK3β phosphorylation sites, but appears to be inefficiently processed *in vivo* in mouse (Pan *et al.*, 2006b). However, using a biochemical approach in different cell lines, several protein fragments smaller than full-length GLI2 have been detected, similarly to what has also been observed for GLI1 (Altaba, 1999; Aza-Blanc *et al.*, 2000). GLI2 has also been shown to be phosphorylated by PKA, CK1 and GSK3β in C-terminal activation domain (Pan *et al.*, 2006a; Riobo *et al.*, 2006b) and targeted for ubiquitination and proteasome mediated full protein degradation by β-TrCP ubiquitin ligase (Bhatia *et al.*, 2006; Pan *et al.*, 2006b). GLI1 has also been shown to be degraded via the proteasome in vivo in mice (Huntzicker *et al.*, 2006). GLI proteins processing and degradation are inhibited by activated SHH signalling.

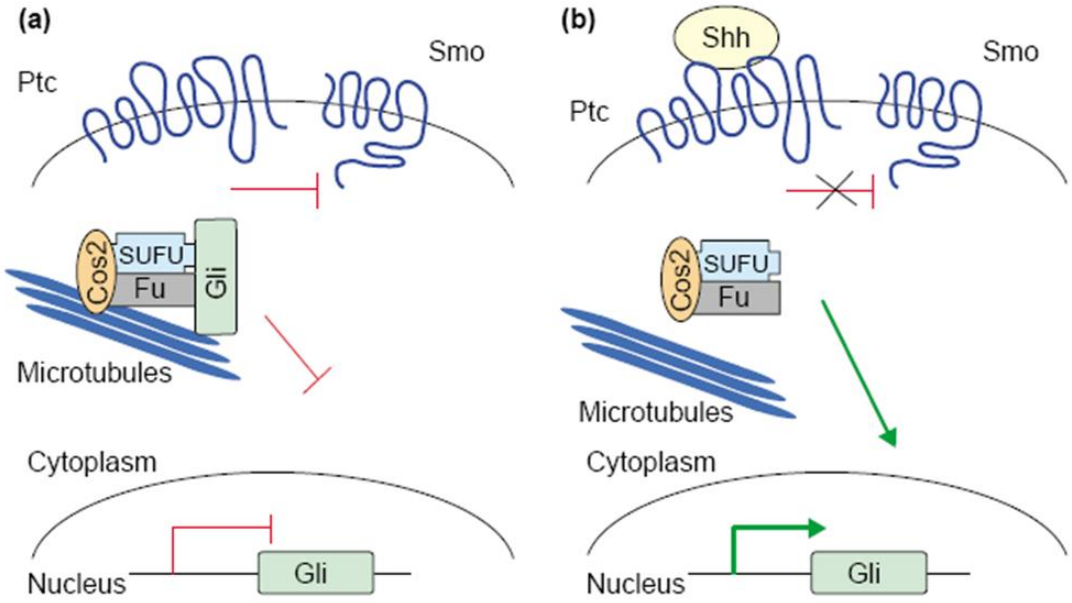

Figure 1.6: Components of the Hedgehog pathway in vertebrates.

GLI factors are retained in the cytoplasm in association with the cytoskeleton (a), while in the presence of Sonic Hedgehog ligand (SHH) they traslocated to the nucleus when they activate the transcription of target genes (b). (Adapted from Wetmore, 2003).

1.8.1 Mouse models of Basal Cell Carcinoma

GLI1 and GLI2 knockout mice display different phenotypes. In knockout mice, GLI2 mutants which lacked most of the zinc-finger domains exhibited developmental defects in several organ systems including the skin (Mo et al., 1997; Ding et al., 1998; Hardcastle et al., 1998; Motoyama et al., 1998). Conversely, mice homozygous for a mutation that removes most of the GLI1 zinc-finger domains develop normally (Matise et al., 1998; Park et al., 2000). However, overlapping function between GLI1 and GLI2 in development also exist, as GLI2−/− developmental phenotype in mice can be substantially rescued by the expression of GLI1 from the GLI2 locus (Bai and Joyner, 2001). Both GLI1 and GLI2 result in epithelial tumours with characteristics of BCC when overexpressed in the basal epidermal layer of mice or frog skin (Dahmane et al., 1997; Grachtchouk et al., 2000; Nilsson et al., 2000; Sheng et al., 2002). Targeted expression of human GLI2ΔN in the basal layer of mouse skin results in basal cell carcinoma-like downgrowths indicating the ability to activate cell proliferation in a HH-independent manner similar to mouse GLI2ΔN but not full-length GLI2 (Grachtchouk et al., 2003; Mill et al., 2003; Hutchin et al., 2005). PTCH1 knockout mice (Ptch1 $^{-/-}$) are not viable; mice who are heterozygous for PTCH1 (Ptch1 $^{+/-}$) develop tumours similar to human trichoblastomas. Exposure to ultraviolet or ionizing radiation increases in the number of these tumours and cause their histology to be more similar to human BCCs (Aszterbaum *et al.*, 1999; Mancuso *et al.*, 2004). It is however still debated how closely these mice tumours can mimic their human counterparts.

1.8.2 In vitro models of Basal Cell Carcinoma and their use in elucidating GLI1 – GLI2 interactions

Keratinocytes derived from BCC are been proven difficult to culture in vitro (Asada *et al.*, 1992; Grando *et al.*, 1996) and the reasons for this may include dependence of the tumours on the surrounding stroma.

Expression of GLI factors in human keratinocyte cell lines helped dissected the potential molecular mechanisms by which GLI factors contribute to BCC tumorigenesis. GLI1 or GLI2ΔN expression in human keratinocytes increases proliferation of cells in confluent cultures, possibly opposing cell cycle arrest of keratinocytes (Regl et al., 2004a). Using a gene expression profiling approach GLI2 has been shown to induce genes involved in cell cycle progression and represses genes associated with epidermal differentiation (Regl et al., 2004a). GLI2 also contributes to tumorigenesis via the induction of Bcl-2 (Regl et al., 2004b), a key molecule involved in the prevention of the intrinsic apoptotic pathway, and by upregulating cFlip which antagonizes death ligand mediated apoptosis (Kump et al., 2008).

GLI1 expression in human keratinocytes has been shown to induce GLI2 mRNA; reciprocally, GLI2 specifically binds to the GLI1 promoter to induce its expression. Based on mRNA induction kinetics, activation of GLI2 by GLI1 is likely to be indirect (Regl et al., 2002) The in vivo relevance of the proposed GLI1-GLI2 feedback for BCC development remains yet to be addressed. Ectopic GLI2 has also been shown to induce endogenous GLI1 protein expression in keratinocytes by Western Blotting; GLI2 protein induction by GLI1 was not analysed as no commercially available antibodies against GLI2 were available at the time (Ikram et al., 2004).

In previous studies carried out in the Neill Group by Mr Sandeep Nadendla and Dr Graham Neill, an unexpected observation was made: GLI2 protein is downregulated upon ectopic expression of GLI1 in both primary prostate cells (PrEc) and immortalised keratinocytes (N/Tert-1). In Western Blotting analysis, ectopic GLI1 suppresses a high molecular weight band corresponding to endogenous GLI2 in primary prostate epithelial cells (PrECs) (Fig. 1.7 a , lanes 1 and 2). Ectopic GLI2ΔN

was expressed for comparison and two distinct bands were detected (Fig. 1.7 a, lane 3): although the strength of the upper band may suggest it represents the ectopic protein, it is likely to be an endogenous isoform as its molecular weight is similar to the band detected in the pBabe lysate (Fig 1.7 a, lane 1); the lower band represents the ectopic mutant. A weak band representing endogenous GLI1 is detected in the PrEC-GLI2ΔN lysates (Fig. 1.7 b, lane 3) which correlates with previously published work in human primary keratinocytes (Ikram et al., 2004). Subsequently, GLI2 protein expression was analysed in N/Tert-1 keratinocytes overexpressing GLI1 using the same vector system (pBabePuro) (work performed by Dr Graham Neill). As for PrECs, ectopic GLI1 suppressed the expression of a high molecular weight band corresponding to endogenous GLI2 (Fig. 1.8, cf. lanes 1 and 2). However, a slightly lower molecular weight band was also observed (Fig. 1.8, lane 2). To help identify this band, N/Tert-1 GLI2ΔN lysates were included for comparison (Fig. 1.8, lane 3). Three bands were detected: the highest band represents endogenous GLI2; the middle band co-migrates with the lower band in N/Tert-1 GLI1 lysates; the lowest band represents ectopic GLI2ΔN as it is unique to lane 3. By comparison with the upper and lowest band, the middle band in lane 3, which is also detected in N/Tert-1 GLI1 (lane 2), could represent a GLI2 degradation or cleaved product or, alternatively, a novel GLI2 isoform (i.e. because ectopic GLI2ΔN induces endogenous GLI1 which may in turn induce this isoform) but this is unlikely because the expression of ectopic GLI2ΔN is weak and because no induction of endogenous GLI1 was actually observed by Western blot (Fig. 1.8 b, lane 3). At this point these observations were not investigated further but it is important to note that the PrECs and N/Tert-1 cells in these experiments were cultured in specialist serum free media (SFM). As part of my PhD project, I tried to further extend these observations as described in Chapter 3.

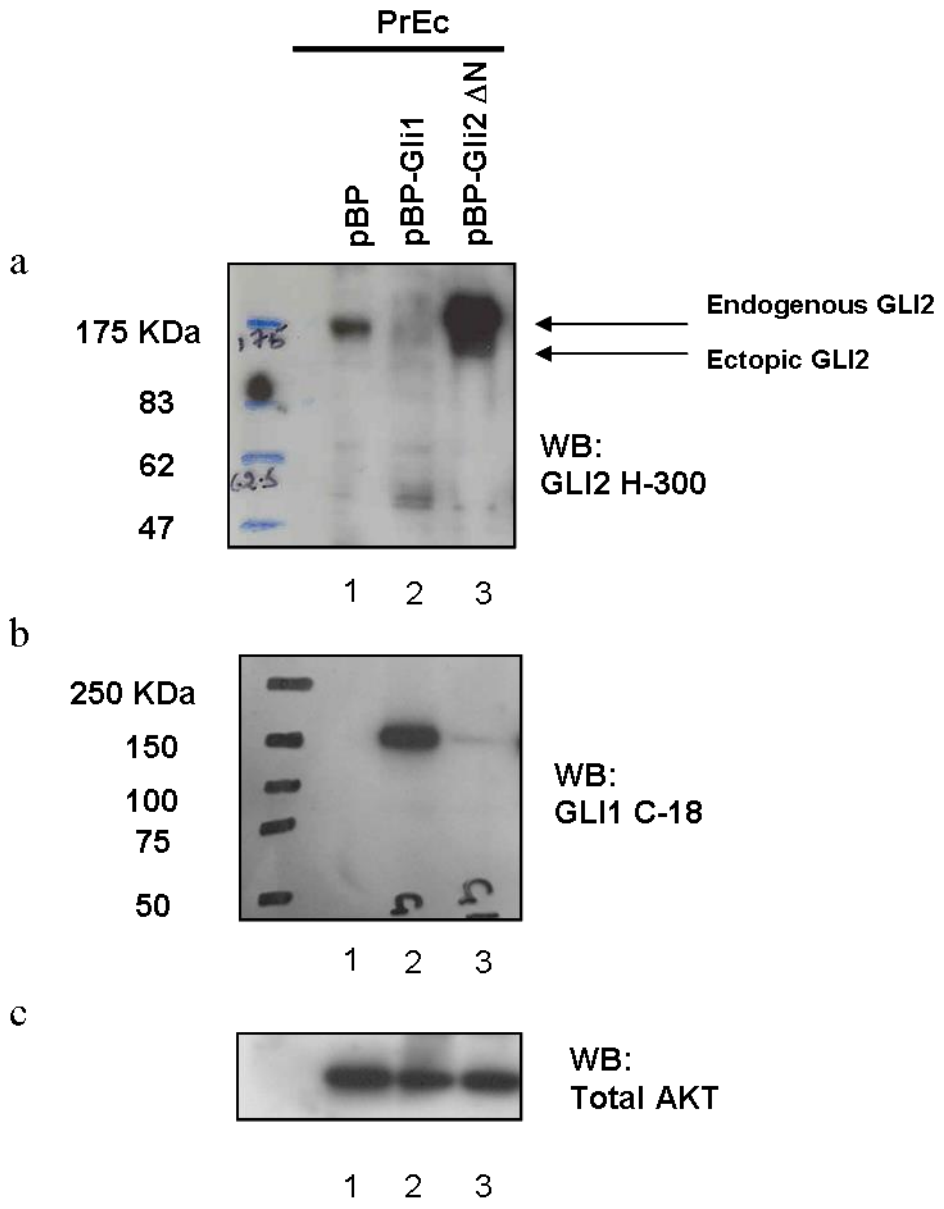

Figure 1.7: Western Blotting for GLI2 protein levels in primary epithelial prostate cells (PrEC) overexpressing either GLI1 or GLI2ΔN

Effect of GLI1 overexpression in primary epithelial prostate cells (PrEC) cells. Ectopic expression of GLI1 (Fig 1.7 b, lane 2) results in endogenous GLI2 protein downregulation (Fig 1.7 a, lane 2). Cells were grown in SFM (serum-free media). pBP, pBabePuro empty vector control. Total AKT was used as a loading control (Fig 1.7 c).

Experiment was performed by Mr. Sandeep Nadendla, Centre for Cutaneous Research, BICMS, QMUL.

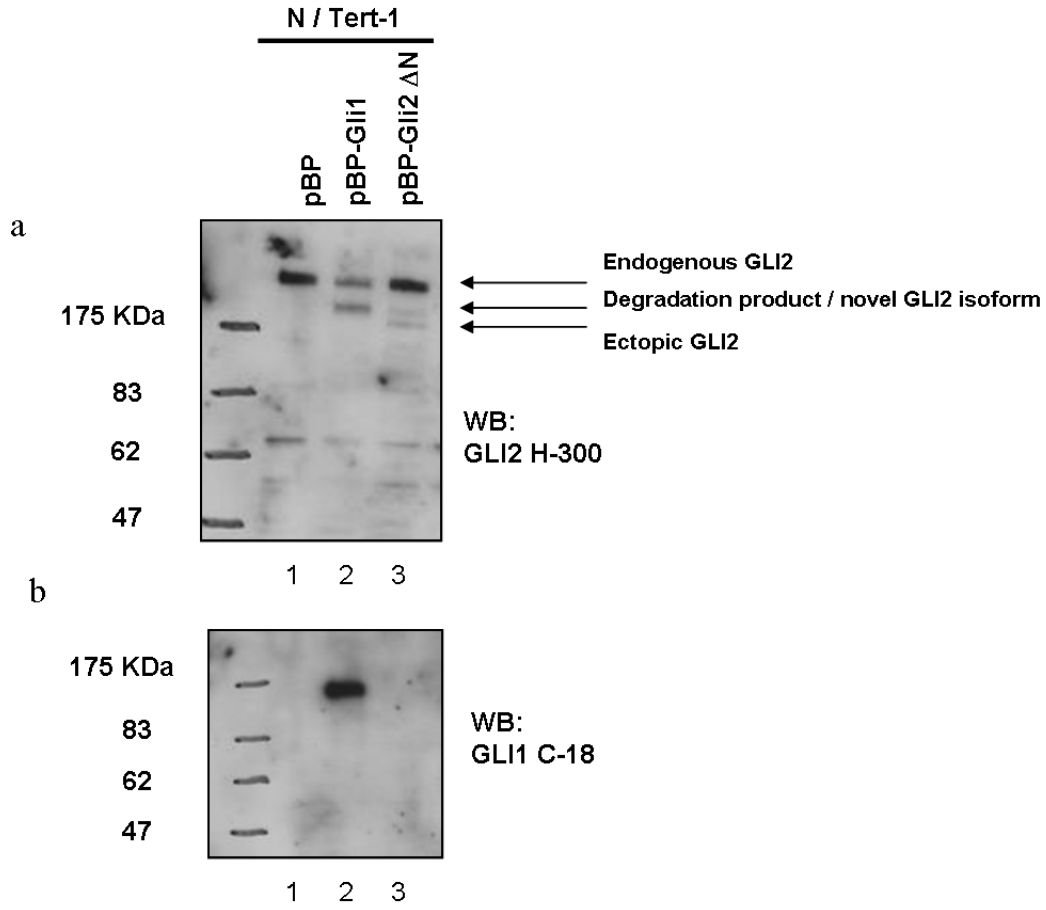

Figure 1.8: Western Blotting for GLI2 protein levels in N/Tert-1 keratinocytes overexpressing either GLI1 or GLI2ΔN

Effect of GLI1 overexpression in N/Tert-1 keratinocytes. Ectopic expression of GLI1 (Fig 1.8 b, lane 2) results in GLI2 protein downregulation and appearance of a slightly lower molecular weight band (Fig 1.8 a, lane 2). Cells were grown in SFM (serum-free media). pBP, pBabePuro empty vector control.

Experiment was performed by Dr. Graham Neill, Centre for Cutaneous Research, BICMS, QMUL.

1.8.3 GLI factors expression in human Basal Cell Carcinoma

The literature on GLI1 and GLI2 levels in BCC is not extensive and relies heavily on the measurement of mRNA levels, either by RT-PCR or in-situ hybridisation; only three publications analyse GLI expression in BCCs at a protein level. High level of GLI1 has been shown to be present in Basal Cell Carcinomas by reverse transcriptase polymerase chain reaction (RT-PCR) (Bonifas et al., 2001), and GLI1 has been proposed as a molecular marker to distinguish BCCs from other skin tumours (Hatta et al., 2005). Another study reported GLI1 transcript was absent in normal skin, while 13 out of 14 BCCs analysed expressed GLI1; the presence of GLI1 in BCCs's epithelial component was confirmed by in situ hybridization (Green et al., 1998). Dahmane et al. analysed 47 human BCC samples by in situ hybridization: all but one of the 47 BCCs examined showed expression of GLI1, although the level of expression varied. GLI1 gene expression was not detected in normal regions of skin distant from the tumour site, although GLI1 mRNA was present in normal basal keratinocytes immediately surrounding the tumour site. Single cells surrounding the main BCC tumour masses were rarely positive for GLI1; they were proposed to be either early invading tumour cells or other cell types that express GLI1 in response to a secreted tumour-derived factor (Dahmane et al., 1997). Two papers describe immunostaining of GLI1 in human BCC samples, Ghali et al. (Ghali et al., 1999), and Dahmane et al. (Dahmane et al., 1997). Ghali et al. reported GLI1 expression in BCCs by DAB immunohistochemistry on wax-sections using two different antibodies, one which recognises the carboxyl-terminal end of GLI1 and another which binds to the amino-terminus: staining was predominantly cytoplasmic. GLI1 immunostaining was also detected in some regions of normal human skin, specifically in the outer root sheath keratinocytes of some hair follicles, in a subpopulation of mesenchymal cells in the vicinity of the bulge region of adult hair follicles and in the dermal sheath cells of developing hair follicles. Dahmane et al. used an in-house made antibody against the zinc finger domain of GLI1 and reported cytoplasmic expression of GLI1 by immunofluorescence in 6 out of 6 BCCs analysed. GLI2 expression at mRNA level in BCCs has been analysed in two publications. In Tojo et al. (Tojo et al., 2003), quantitative reverse transcriptase–polymerase chain reaction performed on a series of 16 samples revealed GLI2 mRNA upregulation in BCCs compared to normal skin and other skin tumours. GLI2

protein exists in four isoforms, GLI2 α, β, γ, and δ, resulting from combinations of two independent alternative splicing processes of the GLI2 gene (Tanimura et al., 1998). The GLI2β isoform was shown to be the most expressed isoform in the 16 BCCs analysed (Tojo et al., 2003). Using by in situ hybridization Ikram et al. (Ikram et al., 2004) reported GLI2 mRNA expression in 8 BCC samples, intefollicular skin and outer root sheath of hair follicles. Only one report describe GLI2 expression in the outer root sheath cells of hair follicles and BCCs by immunohistochemistry (Regl et al., 2004b) using an antibody against the amino-terminal of GLI2, though the number of BCC samples analysed is not specified. A comprehensive analysis of GLI1 and GLI2 at protein level to determine if they are co-expressed in BCC based on putative feedback loop described in Regl et al (Regl et al., 2002) has not been reported so far. The existence of a previously described positive GLI1-GLI2 feedback loop in vitro would raise the question of why GLI1 has not been detected in normal human skin; this also suggests GLI1 – GLI2 interplay may be different in normal skin compared to BCCs, and it would be therefore important to understand these differences as they could be linked to the tumorigenic process.

1.8.4 Non canonical induction of GLI factors

GLI2 has been shown recently to be induced by transforming growth factor beta (TGFβ) (Dennler et al., 2007; Dennler et al., 2009), therefore non-canonical activation of GLI2 may also play a role in BCC tumorigenesis. TGFβ has been shown to induce GLI1 and GLI2 expression in keratinocytes even in the presence of cyclopamine, suggesting this activation may not be dependent on canonical Hedgehog signalling through PTCH1 and SMO (Dennler *et al.*, 2007). During embryogenesis GLI2 is expressed in response to fibroblast growth factor (FGF) signalling (Brewster et al., 2000), and deletion of Notch in mice skin leads to development of BCCs associated with GLI2 upregulation (Nicolas et al., 2003). This suggests that in some instances GLI2 can function independently of canonical Hedgehog signalling. Moreover, GLI protein activity has also been shown to be modulated by interaction with other cellular pathways frequently activated in human malignancies such as RAS and EGFR (Riobo *et al.*, 2006a; Lauth and Toftgard, 2007; Schnidar *et al.*, 2009).

1.9 The WNT signalling pathway

The WNT signaling pathway is a highly conserved signal transduction cascade that has a central role in embryonic development, tissue regeneration, and, when deregulated, in tumorigenesis (Giles et al., 2003; Clevers, 2006). Many of the genes in the WNT pathway, which were first discovered as genes affecting segmentation in Drosophila embryos, were later shown to act as oncogenes and tumour suppressors when deregulated in human cancer (Rijsewijk et al., 1987; Nusse et al., 1991).

The WNT ligands are a family of 19 secreted glycoproteins (Miller, 2002) that, by interacting with different receptors present on the plasma membrane, regulate cell fate specification, proliferation, migration and adhesion (Wodarz and Nusse, 1998; Nusse, 2005). WNT signaling has been classified into two pathways: the canonical and non canonical pathways, or β-catenin-dependent and β-catenin-independent pathways (Chien et al., 2009) (Fig 1.9). Once secreted, WNT proteins act in a cell-non autonomous fashion and bind to two distinct families of cell-surface receptors, the Frizzled (Fz) proteins and the low-density lipoprotein receptor-related proteins 5 and 6 (LRP5/6). WNT ligand binding to Fzd and low-density lipoprotein receptor related protein 5/6 (LRP5/6) co-receptors leads to the activation of Dvl, although the mechanisms underlying this activation are still unclear. Canonical WNT signalling is characterized by signalling through β-catenin. β-catenin has two major functions: first, in simple epithelia, it is an integral part of adherens junctions, connecting E-cadherin to the actin skeleton via α-catenin (Peifer et al., 1992); second, dimers of β-catenin are one of the members of the TCF/LEF (T cell factor/lymphoid enhancer factor) family that function as a transcription factor when localized in the nucleus. In the absence of WNT ligand, the cytoplasmic pool of β-catenin is depleted by the action of a destruction complex which targets β-catenin for ubiquitin-dependent proteosomal degradation. The tumour suppressor protein Axin acts as the scaffold of this complex as it interacts with all other components: β-catenin, the tumour suppressor protein APC, and the two kinases CK1α and GSK3β. In the absence of the WNT ligand CK1 and GSK3β sequentially phosphorylate β-catenin in a series of Ser/Thr residues near its N- terminus; phosphorylated β-catenin is then recognized by the F box/WD repeat protein β-TrCP, a component of a dedicated E3 ubiquitin ligase complex. As a consequence, β-catenin is ubiquitinated and targeted for rapid

destruction by the proteasome (Aberle et al., 1997; Gao et al., 2002). Upon inhibition of GSK3 activity by WNT signaling dephosphorylated β-catenin translocates into the nucleus and activates expression of specific target genes by interacting with transcription factors of the T-cell factor (TCF) and lymphoid-enhancing factor (LEF) families (Behrens et al., 1996; vandeWetering et al., 1997).

Numerous Tcf/Lef target genes have been identified, and many WNT target genes appear to be cell type specific. Some of them, such as cMyc and Cyclin D1, contribute to the oncogenic potential of disregulated WNT signaling (He et al., 1998; Tetsu and McCormick, 1999). Overexpression of different WNT ligands in epithelial cells led to the identification of a subset of WNT ligands capable of regulating morphological transformation of cells in the absence of β-catenin stabilization: this in turn led to the discovery of non-canonical WNT signalling (Shimizu et al., 1997; Veeman et al., 2003).

Potential mechanisms of non-canonical WNT signal transduction are diverse, including signaling through calcium flux, JNK, and both small and heterotrimeric G proteins (Veeman et al., 2003). Examples of non-canonical WNT signalling are the planar cell polarity (PCP) pathway and the Ca2+ dependent WNT signalling pathway. Many functions of non-canonical WNT signalling have been described: for example, signalling by the PCP pathway in Drosophila and Xenopus embryos results in polarization of cells and directs cell motility (Seifert and Mlodzik, 2007). WNT signalling has been shown to be regulated by secreted proteins, including the Dickkopf (DKK) family and Frizzled-related proteins (sFRPs) (Kawano and Kypta, 2003). The two major classes of WNT antagonists function in different ways: the sFRP class binds to WNT ligands, while the Dkk class binds to WNT coreceptors LRP5/6. The predicted theoretical outcome is that sFRPs inhibit canonical and non-canonical pathways whereas Dkks inhibit only the canonical pathway.

Uncontrolled WNT–β-catenin signalling associated with elevated β-catenin levels, either by mutations in components of the destruction complex or by stabilizing mutation in β-catenin itself, has been linked to the development of different kind of cancers (Morin et al., 1997; Rubinfeld et al., 1997; Polakis, 2007). The non canonical ligand WNT5a has been proposed to suppress tumour formation by promoting GSK-3 independent β-catenin degradation in colon cancer cells (Topol et al., 2003).

WNT5a, however, does not seem to act as a tumour suppressor as WNT5a expression levels have been found to positively correlate with the severity of certain melanomas; modulation of WNT5a signaling can affect the motility and invasiveness of melanoma cells (Weeraratna et al., 2002). WNT5a expression also affect invasion of breast and gastric cancer cell lines (Kurayoshi et al., 2006; Pukrop et al., 2006). Another non canonical WNT, WNT11, has been shown to promotes migration of IEC6 intestinal epithelial cells (Ouko et al., 2004). Interestingly, the WNT proteins known to affect cell adhesion and movements in embryos can also affect cell migration in some cancers.

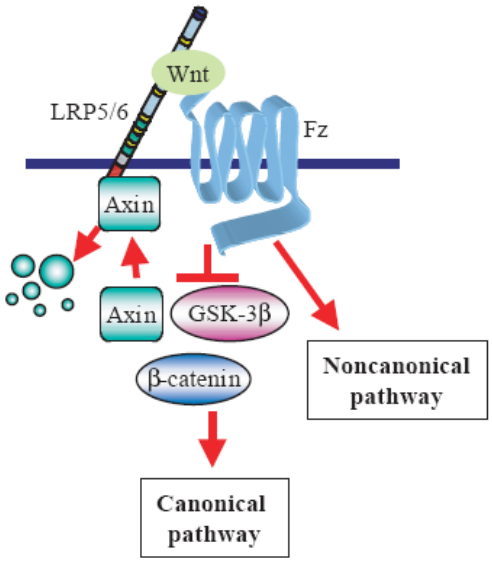

Figure 1.9: The WNT signalling pathway

Schematic representation of activated WNT pathway; binding of WNT proteins to membrane bound receptors initiate the signal transduction cascade, although the partial overlap between the canonical and non-canonical pathways has in some instances made it difficult to distinguish between the two (Adapted from Kawano and Kypta, 2003).

1.10 The TGFβ signalling pathway

The transforming growth factor beta (TGFβ) superfamily is a composed by related cell regulatory proteins involved in vertebrate embryogenesis and in tissue homeostasis in adult organism; the main sub-groups of TGFβ-like genes include the TGFβs I-V, the activins and inhibins and Bone Morphogenetic Proteins (BMPs) (Massague, 1998). TGFβ is a cytokine that controls proliferation, differentiation, migration, and apoptosis of different cell types (Massague et al., 2000). TGFβ was first described as a growth factor capable of inducing a transformed morphology in mouse cell lines (Moses et al., 1981), although it had been subsequently demonstrated that it can have both tumour suppressor and oncogenic activities. TGFβ is synthesized as part of a precursor form that is cleaved before secretion from the cell (Derynck et al., 1985).

The TGFβ propeptide, or latency associated peptide (LAP), remains noncovalently bound to TGFβ after secretion, retaining TGFβ in a latent form. In addition, latent TGFβ can contain a protein of variable size called the Latent TGFβ Binding Protein (LTBP); LTBP is implicated in TGFβ secretion, storage in the extracellular matrix, and activation (Miyazono et al., 1993). Both the LAP and the LTBP must be removed before the mature protein can function; activation can occur by the action of proteases, integrins, the glycoprotein thrombospondin-1, reactive oxygen species (ROS) and changes in pH (Yu and Stamenkovic, 2000; Annes et al., 2003). TGFβ superfamily members require two different serine/threonine kinase receptors to signal, a type I (TβR-I) and a type II (TβR-II) (Wrana et al., 1992). The TGFβ ligand binds to a type II receptor dimer, which recruits a type I receptor dimer forming a hetero-tetrameric complex; type II receptor phosphorylate and activate type I receptor and this allows transduction of the signal to the nucleus (Wrana et al., 1994). The most studied signaling pathway downstream of TGFβ receptors is the Smad pathway (Liu et al., 1996), although other signaling pathways can also be activated in response to TGFβ, such as the mitogen-activated protein kinase (MAPK) pathway (Lee et al., 2007; Yamashita et al., 2008). The Smad family includes the receptor-regulated Smads (R-Smads) Smad1, 2, 3, 5, 8, the co-Smad Smad4, and the inhibitory Smads Smad6 and 7 (Massague et al., 2005). Upon ligand binding the R-

Smads are phosphorylated by the type I receptors, form homomeric and heteromeric complexes with Smad4 and subsequently accumulate in the nucleus where they regulate the transcription of target genes. TGFβ signalling is involved in different cellular processes and TGFβ responsive regions have been identified in the cyclin-dependent kinase inhibitors p15Ink4b (Hannon and Beach, 1994) and p21Cip1 (Datto et al., 1995), and in genes encoding extracellular matrix proteins such as collagen (Ritzenthaler et al., 1993) and elastin (Marigo et al., 1994). A TGFβ responsive element has also been recently identified in the promoter of GLI2 (Dennler et al., 2009), a transcription factor part of the Hedgehog pathway.

In normal skin TGFβ it is located in the keratinocytes in the epidermis and is present throughout the basal lamina in the extracellular matrix (Okane and Ferguson, 1997). TGFβ has been shown to promote wound healing by recruiting inflammatory cells and fibroblasts to the wound site and by inducing fibroblasts to produce increased amounts of collagen and fibronectin (Montesano and Orci, 1988).

TGFβ plays a dual role in tumorigenesis, acting as a tumour suppressor at early stages and as a tumour promoter at later stages (Wakefield and Roberts, 2002). Cancer progression is often accompanied by a decreased responsiveness of the cancer cells to TGFβ mediated growth inhibition but display enhanced migration and invasive behavior in response to TGFβ stimulation (Cui et al., 1996; Oft et al., 1998).

Notably, TGFβ pathway components have been shown to be present in the epithelial and stromal components of BCCs (Schmid et al., 1996; Furue et al., 1997; Verhaegh et al., 1997; Gambichler et al., 2007) and to promote invasion by acting on the stroma (Marsh et al., 2008), although their precise role in the development of this epithelial tumour remains to be fully elucidated.

1.11 Aims of the project

Molecular mechanisms involved in the aetiology of human Basal Cell Carcinoma are not yet fully understood, partly due to the difficulty in growing these tumours as explants.

GLI transcription factors overexpression, though to be primarily mediated by the Sonic Hedgehog (SHH) signalling pathway activation, are associated with BCC development; to date, GLI1 and GLI2 expression has mainly been analysed at mRNA levels in in-vitro models and in a limited number of human BCC samples.

Whether GLI1 or GLI2 is the primary effector with regard to BCC formation is currently debated, and their interplay has not yet been fully elucidated. BCC are rarely metastatic, although the morphoiec subtype has been shown to be more invasive than the others.

The aims of this study are:

(i) characterise GLI1 and GLI2 expression pattern at protein level in a panel of human BCC samples in order to better understand their clinical relevance for the aetiology of this kind of cancer; determine if there is a correlation with tumor aggressiveness

(ii) clarify the interplay between GLI1 and GLI2, and their relation with other components of the HH pathway

(iii) study the effects of the overexpression of an activated form of GLI2 on cell migration and invasion taking advantage of in-vitro organotypics models

Chapter 2

2 Materials and Methods

2.1 Cell Culture

2.1.1 Cell Lines

N/TERT-1 immortalised keratinocytes

N/Tert-1 cells are human keratinocytes immortalized by ectopical expression of the telomerase catalytic subunit hTERT (Dickson et al., 2000). N/Tert-1 cells were a kind gift from professor J. Rheinwald and were grown in RM+ Medium (see Appendix I for details).

N/TERT-1 GFP and N/TERT-1 GLI2ΔN immortalised keratinocytes cell line

The N/Tert-1 GLI2ΔN immortalised keratinocytes cell line had been previously created and characterized in the lab (E. Pantazi et al, unpublished data). The construct CMV-EGFP-GLI2ΔN was cloned into the pSIN plasmid, and the GFP-GLI2ΔN fusion protein is stably expressed under the control of the CMV promoter. GLI2ΔN is a constitutively active form of GLI2 lacking the N-terminal repressor domain. N/Tert-1 GFP keratinocytes were transduced with the pSIN CMV-EGFP empty vector alone and used as the control cell line

N/TERT-1 pBabe, N/TERT-1 pBGLI1 and N/TERT-1 pBGLI2ΔN immortalised keratinocytes cell line

N/Tert-1 pBGLI1 and N/Tert-1 pBGLI2ΔN clonal cell lines, which stably express either GLI1 or GLI2ΔN, along with its respective empty vector control N/Tert-1 pBabe, were created and characterised in the lab by Dr Wesley Harrison.

NEB-1 immortalised keratinocytes

NEB-1 cells are human keratinocytes which have been immortalized by transduction with HPV16 (Morley et al., 1995). NEB-1 cells were grown in KGM Medium (see Appendix I).

NEB-1 pBabe, NEB-1 pBGLI1 and NEB-1 pBGLI2ΔN immortalised keratinocytes cell line

NEB-1 pBGLI1 and NEB-1 pBGLI2ΔN clonal cell lines, which stably express either GLI1 or GLI2ΔN, along with its respective empty vector control NEB-1 pBabe, were created and characterised in the lab by Dr Wesley Harrison.

NEB-1 PTCH1 knockdown cells keratinocyte cell line

NEB-1 PTCH1 knockdown keratinocyte clonal cell line (shPTCH1 189A) and its respective scramble control (shCON) were created and characterised in the lab by Mr Muhammad Rahman. NEB-1 cells were retrovirally transduced with either a shRNA construct that target exon 24 of human PTCH1 (shPTCH1 189A) or a non-targeting scramble control vector (shCON); the clone with the lowest PTCH1 levels was then selected, expanded and characterised (Rahman et al., unpublished results).

N/TERT-1 EGFP and N/TERT-1 EGFP-GLI1 immortalised keratinocytes cell line

Clonal N/Tert-1 keratinocytes stably expressing EGFP or an EGFP-GLI1 fusion protein were created in the lab by Dr Graham Neill (Neill *et al.*, 2008 and Neill et al., unpublished results).

Hacat immortalised keratinocytes

Hacat are in vitro spontaneously transformed keratinocytes (Boukamp *et al.*, 1988). Hacat cells were grown in KGM Medium (see Appendix I).

Du145 prostate cancer epithelial cell line

Du145 is a prostate carcinoma cell line derived from a brain metastasis (ATCC); Du145 cells were grown in RPMI 1640 media (see Appendix I).

Human epidermal primary keratinocytes

Human primary keratinocytes enzymatically isolated from redundant human skin obtained from facelift surgery were a kind gift from Mr. Sreekanth Vootukurireddy. Human primary keratinocytes were grown in RM+ Medium in the presence of 3T3 mouse fibroblast feeder cells (Rheinwald and Green, 1975). 3T3 cells were previously lethally irradiated to prevent cell proliferation. 2 x 10^6 3T3 fibroblasts

were seeded into a 75 cm^2 cell culture flask (T75) and incubated overnight; the next day 2 x 10^6 primary keratinocytes were seeded on top of the feeders cells.

Human primary dermal fibroblasts

Human dermal primary fibroblasts isolated from human redundant facelift skin removed during surgery were a kind gift from Jane Elliott. Human primary fibroblasts were grown in supplemented DMEM High Glucose (4.5 g / l) Medium (see Appendix I).

Mouse 3T3 fibroblasts

3T3 fibroblasts is a spontaneously immortalized cell line established from primary mouse embryonic fibroblast (Todaro and Green, 1963); they secrete growth factors that help the growth of primary keratinocytes and therefore routinely used for the cultivation of this type of cells. Irradiated 3T3 cells were a kind gift from Sreekanth Vootukurireddy and were grown in supplemented DMEM High Glucose (4.5 g / l) Medium (see Appendix I).

2.1.2 Culture conditions and passaging of cells

Adherent keratinocytes or fibroblasts were routinely grown on tissue culture treated flasks or dishes; all cells were incubated at 37ºC in a humidified atmosphere of 90% air / 10% CO_2. Cells were passaged upon reaching approximately 70% confluence, counted and reseeded at the desired density. Cell media was replaced on alternate days or upon passaging. All tissue culture was carried out under aseptic conditions.

2.1.2.1 Routine cell passaging

Cell culture medium was aspirated from flasks and the cell monolayer was then washed with sterile phosphate buffered saline (PBS) to remove any trace of media. The PBS was then aspirated and trypsin – EDTA was added to disrupt cell adhesion; flasks were incubated for 5 min at 37°C 90% air / 10% CO_2 and the progress of cell detachment from the flask surface monitored under a light microscope. Detached cells were removed from the flasks and transferred to a sterile falcon tube where the trypsinisation process was inhibited by the addition of an equal volume of media containing 10% (v/v) FCS. The process was repeated until all cells could be brought

into suspension. The cells were centrifuged at 1000 rpm for 5 min at RT (room temperature), the supernatant aspirated and the cell pellet resuspended in culture media for counting.

The passaging of cells co-cultured with 3T3 feeders requires aspiration of culture media, washing with PBS and treatment with Versene (Invitrogen, U.K.) for 5 minutes. Versene treatment results in detachment of feeders cells but not keratinocytes from the culture dish; 3T3 feeders could therefore be selectively removed and primary keratinocytes subsequently trypsinised.

2.1.2.2 Cell counting

The number of cells per unit volume of cell suspension is determined using a haematocytometer. The haematocytometer is a glass chamber engraved with perpendicular lines to form squares: since the area bounded by the lines and the depth of the chamber is known, it is possible to calculate the concentration of cells. 10 μl of cell suspension was pipetted into the haematocytometer and cells were counted using a light microscope; the number of cells per milliliter of media is calculated by multiplying the mean of the number of cells in each of the four squares by 10^4. It is then possible to calculate the number of cells present in the whole of the cell suspension and seed the required number of cells into new flasks.

2.1.3 Cryopreservation

Cells not needed for experiments or propagation were trypsinised, centrifuged at 1000 rpm for 5 min at RT and resuspended in freezing solution (see Appendix I) at a concentration of $2x10^6$ cells per milliliter. Aliquots of 1 ml of cell suspension were then transferred into individual cryovials (Corning Life Sciences, U.S.A.), put into a freezing container (Nalgene, U.K.) and stored at -80°C. The freezing container allows a steady cooling rate of about 1°C / hour to prevent damage to the cells. After 1-2 days the vials were transferred into a liquid nitrogen tank for long term storage. When required, cells were thawed by defrosting vials in a 37°C waterbath, mixing of cell suspension with equal amount of cell media, centrifugation to remove freezing solution and resuspension of the cells pellet into the required amount of culture media.

2.2 De-epidermalized dermis (DED) based organotypic raft culture system

In contrast to conventional submerged cultures, growth of keratinocytes on dermal substrates allows epithelial differentiation and recreates a situation closely related to the physiological setting; this system has been previously used to study different processes, including cell migration and invasion. The epidermis was removed from cadaveric skin using two different methods: in half of the skin removal was achieved by soaking in PBS plus antibiotics / antimycotics, while in the other half the epidermis was enzymatically removed using Dispase, a bacterial protease. Glycerol-preserved skin (Euro Skin Bank, The Netherlands) was washed in PBS and incubated in PBS containing antibiotic mix (Antibiotic-Antimycotic Solution, PAA Laboratories GmbH, Austria) at 37°C 90% air / 10% CO_2 for three weeks. Every 2 days the antibiotic-antimycotic solution was replaced and the bottle gently shaken to facilitate epidermis detachment from the dermis. The remaining skin was treated with Dispase (Dispase, Roche, U.K.) at a 2 U/ml concentration overnight. The skin was then cut into 1.5 cm x 1.5 cm square pieces using a scalpel and the remaining epidermis scraped off with forceps.

The squares of skin were placed on their reticular side in a 6-well plate, covered with a 1 cm diameter stainless steel ring and 1 x 10^6 human dermal fibroblasts seeded within the metal ring. 2-3 ml of fibroblast growth media was also pipetted into each well to prevent desiccation of the DED and the plate incubated overnight at 37°C 90% air / 10% CO2. 1 x 10^6 human dermal fibroblasts were also seeded in a 24 well plate to allow verification of cell confluence, since the area delimited by the metal ring and that of a well of a 24 well plate are comparable.

After 48 hours the rings were removed, the DED turned on their papillary surfaces and the rings subsequently put back into place. 1 x 10^6 human keratinocytes were seeded within each metal ring, 2-3 ml of media were added to each well to prevent desiccation and the plate incubate at 37°C 90% air / 10% CO_2. 1 x 10^6 human keratinocytes were also seeded in a 24 well plate to allow verification of cell confluence.

After 48 hours a number of stainless steel grids equal to the number of the DEDs were placed in a new six-well plate. The DEDs were cut in half using a scalpel and carefully placed on top of the grids; 3-4 ml of keratinocyte media was added to each well so that the liquid meniscus would reach the bottom of the DED. This allows growth of keratinocytes on top of DEDs at the air-liquid interface, therefore mimicking the physiological setting in vivo.

Keratinocyte media was replaced every 2-3 days and the DEDs harvested by either snap-freezing in liquid nitrogen or fixing in a 4% (v/v) paraformaldehyde (PAF) solution. Snap-frozen tissue was subsequently embedded in OCT and stored at –80°C while fixed tissue was incubated overnight at +4°C. The following day the PAF solution was removed by washing with PBS and the DEDs placed in 70% (v/v) ethanol ready for processing. The fixed tissue was dehydrated and impregnated with paraffin using a tissue processor (Tissue Tek VIP 3000, Sakura, Japan). The next day processed tissue was embedded into wax blocks using moulds.

Frozen tissue samples were sliced using a cryostat (OTF5000, Bright Instrument, U.K.) and 7 μm thick slices were mounted onto Superfrost Plus microscope slides (ThermoScientific, Germany). Sections were stored at –80°C until required.

Paraffin embedded tissue samples were sliced using a microtome (RM 2235, Leica Microsystems, U.S.A.) and 7 μm thick slices were mounted onto Polysine microscope slides (ThermoScientific, Germany). Sections were stored at RT.

2.2.1.1 DED optimisation

Two different methods of epidermis removal were tested: in half of the skin removal was achieved by soaking in PBS plus antibiotics / antimycotics, while in the other half the epidermis was enzymatically removed using Dispase, a bacterial protease.

The effect of growth supplement media was also tested, as some of the DEDs were fed with RM+ media, namely DMEM: Ham's F12 3:1 ratio with addition of RM+ supplement (see Appendix I), while the others were feed with the same media but lacking the RM+ supplement.

A total of four DEDs were generated using primary keratinocytes, by combining epidermis removal with PBS or Dispase and feeding with or without RM+ supplement.

In all experiments 1 × 106 cells were used and both fibroblasts and keratinocytes were left to seed on the DEDs for 48 hours prior to the DEDs being raised to the grids. Dispase treatment did not seem to facilitate keratinocytes adhesion to the DED surface as primary keratinocytes were unable to adhere on Dispase-treated dermis (Fig. 2.1 a, b). When DEDs where fed with media lacking the RM+ supplement no keratinocytes attachment was observed, regardless of the method used for epidermis removal (PBS soaking or Dispase treatment) (Fig. 2.1 a, c).

Primary keratinocytes grown on PBS-treated DED in the presence of RM+ supplement seem to adhere and differentiate properly, as judged by the appearance of the stratum corneum (Fig. 2.1 d): therefore these conditions were selected to perform the subsequent experiments.

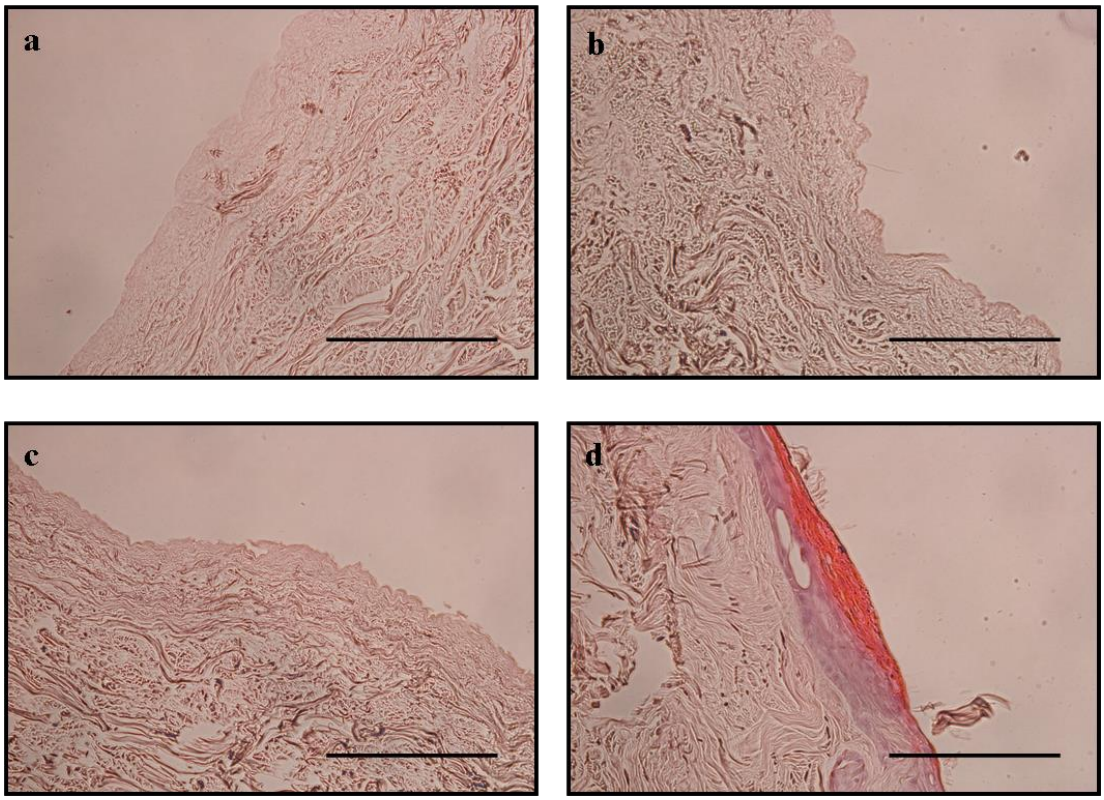

Figure 2.1: Human primary keratinocytes organotypic raft cultures obtained using different methods of epidermis removal and differently supplemented growth media

Haematoxylin and eosin stained transverse section of organotypic cultures of primary keratinocytes on De-Epidermalized Dermis (DED). Human primary keratinocytes were plated on top of DED and grown at the air-liquid interface for 13 days. (a) Primary keratinocytes organotypic raft, epidermis removed by Dispase treatment and grown in the absence of RM+ media supplement (b) Primary keratinocytes organotypic raft, epidermis removed by Dispase treatment and grown in the presence of RM+ media supplement (c) Primary keratinocytes organotypic raft, epidermis removed by PBS soaking and grown in the absence of RM+ media supplement (d) Primary keratinocytes organotypic raft, epidermis removed by PBS soaking and grown in the presence of RM+ media supplement. Scale bar represents 200 µm.

2.3 Collagen-matrigel based organotypic raft culture system

Type I collagen is the most abundant collagen found in the human body and it is commonly employed in the manufacture of artificial skin substitutes (Auger *et al.*, 1998). Matrigel is a basement membrane preparation containing extracellular matrix components such as laminin, collagen IV, heparan sulfate proteoglycans and different growth factors including transforming growth factor beta (TGFβ), epidermal growth factor (EGF), insulin-like growth factor (IGF), fibroblast growth factor (FGF) and tissue plasminogen activator (TPA). Extracellular matrix based substrata provide a physiological environment that supports cellular functions, and collagen-matrigel gels are widely used in the study of cell migration and invasion.

Collagen-matrigel gels were prepared by mixing 3.5 volumes of type I collagen (Rat tail collagen type I, BD Biosciences, U.S.A.), 3.5 volumes of Matrigel (Matrigel Basement membrane matrix, BD Biosciences, U.S.A.), 1 volume of 10x DMEM, 1 volume of fetal calf serum (Biosera, U.K.) and one volume of growth media containing 5×10^5 human dermal fibroblasts. Aliquots of this suspension were placed in a 24-well plate (1 ml per well) and incubated at 37°C 90% air / 10% CO_2 for 1 hour to allow the components to solidify. The gels were then detached from the sides of the wells by using a sterile pipette tip, covered with 1 ml growth media and incubated overnight at 37°C 90% air / 10% CO_2.

The next day the media was carefully aspirated from the wells, a plastic cloning ring was placed on each gel ring and a suspension of 5×10^5 human keratinocytes was seeded within the plastic ring. 5×10^5 keratinocytes were also seeded in a 48 well plate to allow verification of cell confluence and the plates incubated overnight at 37°C 90% air / 10% CO_2. The following day cell confluence of the keratinocytes plated in the 48 well was assessed and, if the confluence reached 100%, rings were removed from the gels. For each gel a sterile stainless steel grid was placed in a new 6 well plate and gels were carefully lifted with a spatula and placed on the top of the grids; 3-4 ml of keratinocyte media was added to each well so that the liquid meniscus would reach the bottom of the grid. This setting allows growth of keratinocytes at the liquid-air interface, similar to the physiological situation.

Growth media was replaced every 2-3 days and gels were harvested after 14 days and preserved by freezing in dry ice. Gels were subsequently embedded in OCT media, sectioned using a cryostat (OTF5000, Bright Instrument, U.K.) and 7 μm thick sections were mounted onto Superfrost Plus microscope slides (ThermoScientific, Germany). Sections were stored at –80°C until required.

2.4 Hematoxylin and eosin staining of paraffin sections

Hematoxylin and eosin (H&E) is a histological stain used to reveal the morphology and structure of a tissue. Hematoxylin has a deep blue-purple color and stains nuclei, while eosin is pink and stains proteins. Sections of tissue mounted on slides were placed into a rack and sequentially immersed in jars containing different chemicals as follows: tissue were deparaffinized by dipping into xylene I (5 minutes) and xylene II (3 minutes), then rehydrated by immersion in a scale of decreasing ethanol (EtOH) concentrations (EtOH I 100% (v/v) 3 minutes, EtOH II 100% (v/v) 3 minutes, EtOH 90% (v/v) 3 minutes, EtOH 70% (v/v) 3 minutes). After a brief rinse in distilled water sections were immersed in hematoxylin for 3-5 minutes, washed in running tap water to remove excess stain and differentiated by dipping into acidic alcohol 2-6 times. The rack was placed in running tap water until the nuclei turned blue (approximately 5 minutes), then dipped into eosin for 2 minutes. The excess stain was removed by immersing in running tap water and the section were dehydrated using a scale of increasing ethanol concentrations (EtOH I 70% (v/v) 3 minutes, EtOH II 90% (v/v) 3 minutes, EtOH 100% (v/v) 3 minutes, EtOH 100% (v/v) 3 minutes). Slides were then immersed in clean xylene (xylene I 2 minutes, xylene II 2 minutes) and coverslipped with glass slides (VWR International, U.K.) using DePeX Mounting Medium (BDH Laboratory Supplies, U.K.). Slides were observed using a light microscope.

2.5 Hematoxylin and eosin staining of frozen sections

Sections of frozen tissue mounted on slides were retrieved from the -80°C freezer, incubated at RT for 5 minutes to allow defrosting and then placed into a rack. Slides were immersed in a 95% (v/v) ethanol solution for 2 minutes and then washed briefly in distilled water. Slides were then immersed in a 1x solution of Scott’s tap water

(see Appendix I) for 2 minutes and then stained with hematoxylin. From this step onward the protocol used was identical to the one used to hematoxylin and eosin stain paraffin sections.

2.6 RNA interference

2.6.1 Principles of RNA interference

Gene expression in eukaryotes can be modulated by double-stranded RNA (dsRNA) molecules that result in the degradation of a specific messenger RNA (mRNA) (Cerutti and Casas-Mollano, 2006). This mechanism, known as RNA interference, is evolutionarily conserved and provides a mean of modulating gene expression at a transcriptional level. The RNA interference process has been widely exploited in molecular biology to silence expression of a particular gene of interest. Short interfering RNAs (siRNAs) are synthetic duplexes of RNA about 21 bases in length with 3' overhanging ends which are introduced into cells by electroporation or lipid mediated transfection.

Once inside the cell one strand of the siRNA will be incorporated into the RNA induced silencing complex (RISC) where it will guide the cleavage of single-stranded mRNAs that show complementarity with the siRNA sequence leading to its degradation (Fig. 2.2).

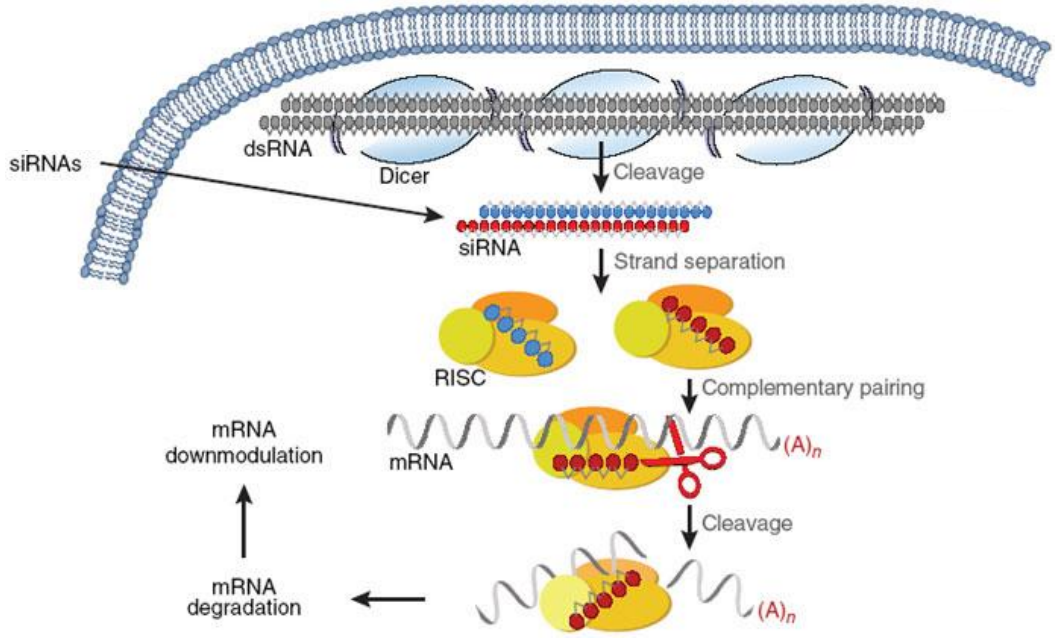

Figure 2.2: Cellular mechanism of RNA interference

(Adapted from Bumcrot *et al.*, 2006).

2.6.2 siRNA reverse transfection

Short interfering RNAs are introduced into the cells by opening transient pores in the cell membrane: this process is known as transfection and was achieved by taking advantage of the lipid-based reagent Hiperfect (Qiagen, U.K.). Sequences of siRNAs used can be found in Appendix II. siGLO Cyclophilin B siRNA (Dharmacon, U.S.A.) was used as a transfection control: siGlo is a fluorescently labelled siRNA against Cyclophilin B which localises to the endoplasmic reticulum and is used to assess transfection efficiency. A second non-fluorescent control was also used, Silencer Negative Control #1 siRNA (Ambion, U.K.). This scramble control (siAmb) is designed to have no significant sequence similarity to known human transcripts and was shown to have no impact on cell viability.

Hiperfect was added to serum-free media (SFM) in polypropylene flow cytometry tubes and incubated for 5 minutes. The siRNA of interest (or siGLO) was pipetted into the well of a cell culture plate to obtain a 30nM final concentration, then the Hiperfect-SFM solution was added on top, mixed and incubated for 20 minutes. In the meantime, cells were trypsinised and counted; cells were then re-suspended in the appropriate volume of media before being added to the plates and incubated at 37°C,

10% CO_2 overnight. siGLO fluorescence was observed under a fluorescence microscope after 24 hours to visually assess transfection efficiency. Media was changed after 48 hours and cells either harvested or fixed for analysis after 96 hours.

2.7 Protein harvesting and quantification

Whole cell protein lysates were obtained by adding 220 μl of pre-heated buffer A (50 mM Tris-HCl pH 8.0, 2% (w/v) SDS, 1 mM Na_3OV_4) for each 60 mm dish onto cells after media removal and PBS washing. Cells were scraped off the dishes, collected in eppendorf tubes and boiled at 95°C for 5 minutes, then incubated on ice. The lysate solutions were then mixed 3 times using a syringe with needle to help reduce viscosity and therefore enhance the release of proteins into solution. Protein concentration was determined using the DC Protein Assay (Bio-Rad Laboratories, U.S.A.): this assay is based on the Lowry assay method and relies on the shift in the absorbance of a chemical compound depending on the amount of proteins present in the solution. A stock colourimetric solution (Buffer AS) was made up according to the manufacturer's instructions consisting of 2 μl of Buffer S to 98 μl of Buffer A per sample. 20 μl of cell lysate was then added to 100 μl of Buffer AS in a clean eppendorf tube, and 800 μl of Reagent B were subsequently added. The reactions were incubated for 15 minutes at RT and then transferred into optical cuvettes for absorbance reading (Abs) at 655 nm using a spectrophotometer. The spectrophotometer was calibrated using a blank solution in which 20 μl of lysis buffer were added to the previously described buffers instead of 20 μl of cell lysate. Protein concentration is calculated using the equation ((Abs + 0.0009) / 0.213) = concentration (μg/μl) based on a standard curve generated using bovine serum albumin (Fig 2.3). A standard curve is made by measuring the absorbance of protein samples of known concentration, giving a range of absorbance values related to the varying concentrations of proteins. To determine the protein concentration of a sample from it absorbance, the standard curve is used to find the concentration of proteins that would have the same absorbance as the sample. 50 μl of loading buffer was subsequently added and the lysated, followed by boiling at 95°C for 1 minute. Since the original sample in which the absorbance has been measured is diluted as a result of the addition of the loading buffer, a correction factor (0.8 = 200 μl / 250 μl)

is added to the equation to give (((Abs + 0.0009) / 0.213)*0.8) = concentration (µg/µl). The protein samples were then either used for Western Blotting analysis immediately or stored at -20°C until required.

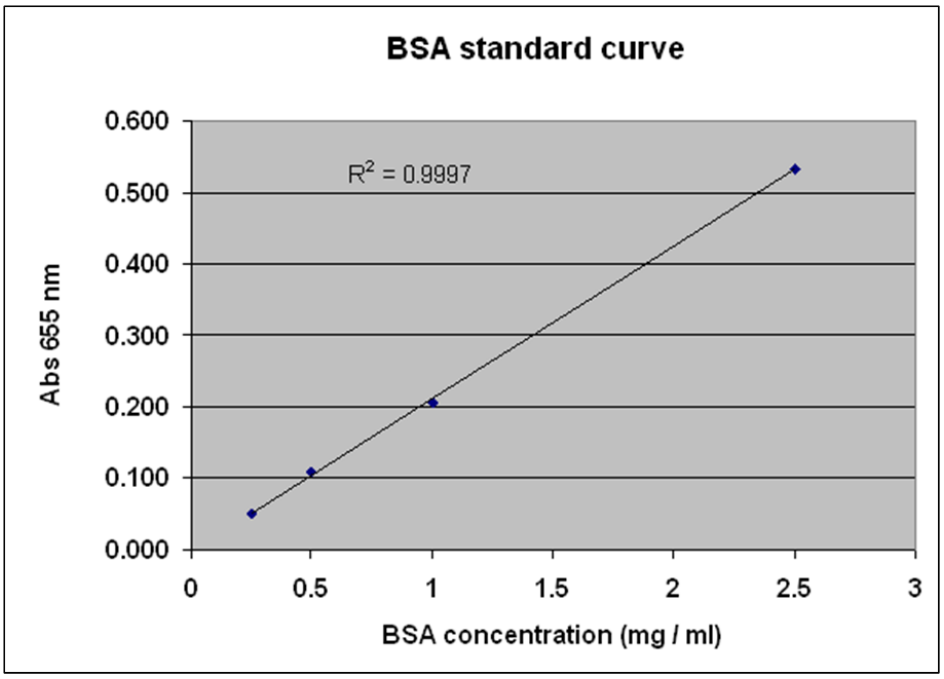

Figure 2.3: BSA standard curve for protein assay.

2.8 Western Blotting

2.8.1 SDS-polyacrylamide gel electrophoresis (SDS-PAGE)

SDS-PAGE is a technique used to separate proteins taking advantage of their different electrophoretic mobility. SDS binds to proteins and confers them a negative charge proportional to the length of the polypeptide: when the proteins are loaded onto a polyacrylamide gel in the presence of an electric field they migrate toward the positive electrode (anode) and are separated on the basis of their molecular masses. Gels were assembled using a specific apparatus (Mini-PROTEAN 3 Cell, BioRad, U.S.A.) and consist of two parts, stacking and resolving (see Appendix I): the stacking gel function is to concentrate (or 'stack,) the protein samples loaded into wells into tight bands, while the resolving gels separate the proteins depending on their molecular weight. Proteins of known molecular weight (Prestained Protein Marker, New England Biolabs, U.K.) were used as reference. Samples were loaded

in the wells of 5% stacking - 10% resolving gels, the tank was filled with running buffer (see Appendix I) and proteins separated at by applying a 120V difference in potential until the dye front reached the base of the gel.

2.8.2 Electrotransfer

This technique allows the transfer of proteins from an electrophoretic gel to a solid support, usually a nitrocellulose membrane. Transfer was achieved by using a specific apparatus after the gel had been placed onto a nitrocellulose membrane (Amersham Hybond ECL, GE Healthcare, U.K.) and sealed in place with blotting paper and sponges. The tank was then filled with transfer buffer (see Appendix I) and a 100V difference in potential was applied for one hour.

2.8.3 Immunoblotting

Immunoblotting is a technique that allows the detection of a particular protein by using a specific antibody. Non-specific binding sites on the nitrocellulose membrane containing the proteins were saturated by placing the membrane in a small plastic bag, covering with a solution of 10% (w/v) milk TBS-T and leaving on a gently shaking rotor for 1 hour. The first antibody to be applied (primary, see Table 2.1) is specific for protein of interest and, after being diluted in 5% (w/v) milk TBS-T, was incubated with the membrane on a gently shaking rotor at +4°C overnight. The next day, the membrane was put in a small plastic box and washed 3 times for 5 minutes with TBS-T to remove the unbound primary antibody. The secondary antibody (see Table 2.1), which binds to the primary, was then diluted 1:2000 in 5% (w/v) milk TBS-T and incubated with the membrane in a small plastic box for 45 min-1 hour. The unbound secondary antibody was then removed by 3 washing with TBS-T, 5 minutes each. The secondary antibody is linked to an enzyme that allows visual identification of proteins (see section 2.8.4).

2.8.4 Enhanced chemiluminescence detection and development

Chemiluminescent detection methods rely on a secondary antibody linked to a reporter enzyme (horseradish peroxidase) which can convert an appropriate substrate into a luminescent product. The light emitted is then detected by using a photographic film: bands corresponding to the detected protein of interest will appear

as dark regions on the developed film. ECL plus reagent A and B (ECL Plus Western Blotting Detection Reagents, GE Healthcare, U.K.) were mixed in a ratio of 40:1 and put onto the membrane for 3-5 minutes to allow the reaction to develop. The signal was then detected by exposing the membrane to a photographic film (Hyperfilm, GE Healthcare, U.K.) for 1-5 minutes followed by development using an automatic film processor.

Table 2.1:List of antibodies used for Western Blotting

Protein	Primary antibody and concentration	Secondary antibody (HRP conjugated) and concentration
GLI-1	GLI-1 (C-18): sc-6152 (Santa Cruz, U.S.A.) 1:1000	Rabbit anti-Goat (P0449, DakoCytomation, Denmark) 1:2000
GLI-1	GLI-1 (Part 965884, ExactaChIP Kit) (R D Systems Inc, U.S.A.) 1:1000	Rabbit anti-Goat (P0449, DakoCytomation, Denmark) 1:2000
GLI-2	GLI-2 (H-300): sc-28674 (Santa Cruz, U.S.A.) 1:1000	Swine Anti-Rabbit (P0399, DakoCytomation, Denmark) 1:2000
GLI-2	GLI-2 (ab26056) (Abcam, U.K.) 1:1000	Swine Anti-Rabbit (P0399, DakoCytomation, Denmark) 1:2000
ERK	p44/42 MAPK (Erk1/2) (#9102) (Cell Signaling, U.S.A.) 1:1000	Swine Anti-Rabbit (P0399, DakoCytomation, Denmark) 1:2000

2.9 Immunohistochemistry

2.9.1 Basal Cell Carcinoma tissue samples

Normal human hair bearing skin and Basal Cell Carcinoma tumour samples were obtained from the tissue banks of the Royal London Hospital, London, U.K., with the approval of local ethical committees. Samples had been previously snap frozen in liquid nitrogen, transferred into cryovials and stored at –80°C.

2.9.2 Samples preparation

Tissues were included in OCT embedding medium (Cryo-M-bed, Bright Instrument, U.K.), placed onto a cork disc and put onto dry ice to allow the OCT to solidify. Samples were sectioned using a cryostat (OTF5000, Bright Instrument, U.K.) and 7 μm thick sections were mounted onto Superfrost Plus microscope slides (ThermoScientific, Germany). Sections were stored at –80°C until required.

2.9.3 Immunofluorescent histochemistry on BCC frozen sections

Immunohistochemistry is a technique used to reveal the presence of a specific protein in a tissue of interest by using a primary antibody that binds to the protein and a secondary antibody labeled with either a fluorescent dye or an enzyme that allows for detection. Immunofluorescent histochemistry was used to determine the protein expression pattern of GLI factors in normal human hair bearing skin and in Basal Cell Carcinomas (BCC) samples (see Table 2.2 for list of antibodies used).

Tissue sections were allowed to defrost for 10 minutes at RT and then fixed in ice-cold acetone for 15 minutes at –20°C. Samples were then washed in PBS for 15 minutes before being transferred into 1% (w/v) milk-PBS blocking solution for another 15 minutes. Slides were washed in 0.05% (v/v) Tween 20-PBS for 5 minutes prior to being covered with a drop of 0.05% (v/v) Tween 20, 5% (v/v) serum PBS in which the primary antibody had been diluted. Slides were put into a humidified chamber and incubated with the primary antibody overnight at +4°C .The next day the slides were washed three times for 5 minutes in 0.05% (v/v) Tween 20-PBS and then covered with a drop of 0.05% (v/v) Tween 20, 5% (v/v) serum PBS containing the diluted secondary antibody. Sections were incubated for 30 minutes in the dark at

RT, and then washed 3 times for 5 minutes. Slides were then incubated in PBS containing 4',6-diamidion-2-phenylindole dihydrochloride (DAPI) (1:10000, Invitrogen, U.K.) for 10 minutes to allow visualization of the cells' nuclei. Slides were then washed 2 times in PBS (2 minutes each). Sections were subsequently coverslipped with glass slides (VWR International, U.K.) using Vectashield mounting medium (Vector Laboratories, U.S.A.). Slides were observed using a confocal microscope.

Table 2.2: List of antibodies used for fluorescent immunohistochemical analysis of Hedgehog pathway components in Human Skin and Basal Cell Carcinomas

Protein	Primary antibody and dilution	Secondary antibody (fluorescent dye conjugated) and dilution
GLI-1	GLI-1 (H-300): sc-20687 (Santa Cruz, U.S.A.) 1:100	Alexa Fluor® 488 goat anti-rabbit (Invitrogen, U.K.) 1:500
GLI-1	GLI-1 (MAB3324) (R&D Systems, U.S.A.) 1:100	Alexa Fluor® 488 donkey anti-rat (Invitrogen, U.K.) 1:500
GLI-1	GLI-1 (C-18): sc-6152 (Santa Cruz, U.S.A.) 1:100	Alexa Fluor® 488 donkey anti-goat (Invitrogen, U.K.) 1:500
GLI-2	GLI-2 (H-300): sc-28674 (Santa Cruz, U.S.A.) 1:100	Alexa Fluor® 488 goat anti-rabbit (Invitrogen, U.K.) 1:500
GLI-2	GLI-2 (ab26056) (AbCam, U.K.) 1:100	Alexa Fluor® 594 goat anti-rabbit (Invitrogen, U.K.) 1:500
SHH	SHH (ab19897) (AbCam, U.K.) 1:100	Alexa Fluor® 594 goat anti-rabbit (Invitrogen, U.K.) 1:500
Vimentin	Vimentin 550513 - clone RV202 (BD Biosciences, U.S.A.) 1:1000	Alexa Fluor® 488 donkey anti-mouse (Invitrogen, U.K.) 1:500

2.9.4 Immunofluorescent histochemistry on De-epidermalised dermis (DED) wax-embedded sections

Tissue were deparaffinized and rehydrated by transferring slides into xylene I (5 minutes) and xylene II (5 minutes), ethanol (EtOH 100% (v/v) 5 minutes, EtOH 90% (v/v) 5 minutes, EtOH 70% (v/v) 5 minutes, EtOH 50% (v/v) 5 minutes), then distilled water (5 minutes) and PBS (5 minutes). Antigen retrieval was performed by incubating the slides in a 0.01 M Sodium Citrate solution and microwaving at 800 Watt for three cycles of 5 minutes each; slides were then left to cool down to room temperature. Blocking of aspecific binding sites was achieved by incubation in a 5% (v/v) serum PBS solution for 1 hour. Slides were then covered with a drop of 5% (v/v) serum PBS solution in which the primary antibody had been diluted. Slides were put into a humidified chamber and incubated with the primary antibody overnight at +4°C. The next day the slides were washed three times for 5 minutes in 0.05% (v/v) Tween 20-PBS and then covered with a drop of 5% (v/v) serum PBS solution containing the diluted secondary antibody. Sections were incubated for 1 hour in the dark at RT, and then washed 3 times for 5 minutes. Slides were then incubated in PBS containing 4',6-diamidion-2-phenylindole dihydrochloride (DAPI) (1:10000, Invitrogen, U.K.) for 10 minutes to allow visualization of the cells' nuclei. Slides were then washed 2 times in PBS (2 minutes each). Sections were subsequently coverslipped with glass slides (VWR International, U.K.) using Vectashield mounting medium (Vector Laboratories, U.S.A.). Slides were observed using a confocal microscope.

Table 2.3: List of antibodies used for fluorescent immunohistochemical analysis of differentiation markers on De-epidermalised dermis (DED) sections

Protein	Primary antibody and dilution	Secondary antibody (fluorescent dye conjugated) and dilution
Human Keratin 1	Human Keratin 1 (AF 87) (Covance, U.S.A.) 1:400	Alexa Fluor® 488 goat anti-rabbit (Invitrogen, U.K.) 1:800
Human Involucrin	Human Involucrin (clone SY7) Cancer Research UK antibody production facility 1:500	Alexa Fluor® 488 donkey anti-mouse (Invitrogen, U.K.) 1:800
Human Involucrin	Human Involucrin (clone SY5) Cancer Research UK antibody production facility 1:500	Alexa Fluor® 488 donkey anti-mouse (Invitrogen, U.K.) 1:800
Human Loricrin	Human Loricrin (AF 62) (Covance, U.S.A.) 1:500	Alexa Fluor® 488 goat anti-rabbit (Invitrogen, U.K.) 1:800
Human E-cadherin	Human E-cadherin (clone HECD-1) Cancer Research UK antibody production facility 1:100	Alexa Fluor® 488 goat anti-mouse (Invitrogen, U.K.) 1:800

2.10 Image acquisition, image processing and data analysis of Basal Cell Carcinomas immunofluorescent staining

Fluorescence quantification is a sequential process involving image acquisition, image preprocessing, and data analysis steps. Confocal imaging was performed using a Zeiss LSM 510 META microscope (Carl Zeiss, Germany) and associated software (Zeiss LSM Image Browser v. 4.2.0.121). Fluorochrome excitation of secondary antibodies was achieved by 488-nm or 543-nm filtered emission from a laser source. All images have been acquired using a pre-determined Multi Track Configuration (either DAPI – 488nm or DAPI – 488nm – 543nm); using this option, sequential scanning are performed. Optimal power values for each laser were already set by Dr Ann Wheeler (BICMS Imaging Facility manager) for each configuration and have not been altered. A frame size (number of pixels) of 1024 was selected for every image, with a dynamic range of 12 Bit per pixel (4096 gray levels). For each channel pinhole size was set to 1 Airy unit. Line averaging (to improve the image by increasing the signal to noise ratio) was set as 4. Images were acquired using as follows: an objective was selected (either Plan-Neurofluar 10x / 0.3 Ph1or Plan-Neurofluar 20x / 0.5 Ph2) and continuous fast scanning was used to put the image into focus. By using the 'Palette' and 'Range Indicator' options the image was converted into grayscales in which areas which exceed the maximum limit of detection (saturation) were shown as red whereas areas which are below detection were shown as blue. Red saturation over the maximum was minimized by decreasing the Detector Gain, while undetected blue areas were reduced by increasing the Amplifier Offset. Amplifier Gain was kept as 1. These steps were repeated for each individual channel, ensuring images were within the linear range of the photomultiplier tube detectors. For quantification purposes, each flourescence measurement was normalised against the value of the black background of the same slide. Image noise was further reduced using Image J software (v.1.41, NIH, U.S.A.) during the image preprocessing step. The 'Threshold' tool in Image J allows the user to set lower and upper threshold values on the fluorescence intensity distribution histogram, segmenting the image into features of interest. Pixels with brightness values included in a specified range can be highlighted and their average fluorescence intensity calculated. Taking advantage of this feature the fluorescence

intensity of the signal in the epithelial and in the mesenchymal components of each tumour was measured. Conventional statistical analysis on the intensity of the fluorescence signals of different samples was performed to obtain graphical representations of the results (Student's T-Test, two-sample assuming unequal variance).

2.11 Immunoperoxidase - DAB immunohistochemistry

Normal human skin and Basal Cell Carcinoma tumour samples were obtained from the tissue banks of the Royal London Hospital, London, U.K., with the approval of local ethical committees. Samples had been previously fixed, dehydrated and paraffin wax embedded. Wax embedded tissue samples were sliced using a microtome (Leica RM2235, Leica, Germany) and 7 μm thick slices were placed onto Poly-L-Lysine Coated Microscope Slides (ThermoScientific, Germany).

Sections were stained using the streptavidin/biotin-based staining technique. The streptavidin/biotin is an indirect immunohistochemical staining method based on the high affinity that streptavidin has for biotin. Streptavidin has four binding sites for biotin and this allow macromolecular complexes (ABCs) to be formed between streptavidin and biotinylated molecules, including enzymes and antibodies. In this technique the primary antibody is applied to the tissue, followed sequentially by the biotinylated secondary antibody and by a preformed streptavidin-biotin -peroxidase complex (ABC technique) (Hsu *et al.*, 1981). The horseradish peroxidase (HRP) linked to streptavidin catalyzes hydrogen peroxide oxidation of the 3,3'-Diaminobenzidine tetrahydrochloride (DAB) substrate to yield a brown staining product wherever primary and secondary antibodies are attached to the tissue (DAB staining), providing a high and specific signal at the antigen binding site location.

Tissue were deparaffinized and rehydrated by transferring slides into xylene I (2 minutes) and xylene II (2 minutes), ethanol (EtOH 100% (v/v) 2 minutes, EtOH 70% (v/v) 2 minutes) and then running water (5 minutes).

Since wax-embedded tissues are fixed with formaldehyde prior to embedding, an antigen retrieval step is required to remove the methylene bridges formed due to the formaldehyde treatment as they could mask the antigen.

Antigen retrieval step was performed using different conditions depending on the primary antibody used (conditions are listed in Table 2.4). Briefly, slides were placed in a rack and immersed in the appropriate antigen unmasking solution, then either microwaved in a plastic container or put into a coplin jar into the waterbath. Endogenous peroxidase activity was then inhibited by immersing the slides in a solution of 3% (v/v) hydrogen peroxide for 15 minutes, followed by washing in running water for 5 minutes. Slides were then placed in a staining chamber and covered with a drop of wash buffer (Dako, Denmark).

All subsequent steps were performed using the Vectastain® Universal Elite® ABC kit (Vector Laboratories, California) according to the manufacturer's instructions; incubations were carried out at room temperature in a humidified chamber. The wash buffer was removed and the sections covered with a drop of horse serum for 20 minutes to block non-specific binding sites. Serum was then removed and primary antibody (see Table 2.4) was diluted in Antibody Diluent solution (Dako, Denmark) and applied to the tissue for 40 minutes. Slides were washed twice with wash buffer (2 minutes each) and the tissues covered with either biotinylated anti rabbit and mouse solution (from Vectastain® Universal Elite® ABC kit) or biotynilated anti-rat secondary antibody (Anti-Rat Immunoglobulins/HRP, Dako, Denmark, 1:300 dilution) for 30 minutes. After washing the Vectastain ABC reagent was applied for 30 minutes. Slides were washed twice with wash buffer (2 minutes each) and DAB solution was prepared in the meantime by adding one drop of DAB chromogen to 1 ml of DAB substrate buffer (Vector Laboratories, California). Tissues were incubated with DAB solution for 5 minutes followed by washing in running water for 5 minutes. Sections were counterstained in Gill's haematoxylin and subsequently dehydrated and mounted using DePex mounting media (Sigma, Poole, U.K.) under 22 x 64 mm coverslips (VWR, U.K.) using an automated coverslipping machine (ThermoScientific, Germany). Negative controls were performed in which the diluted primary antibody was omitted from the staining procedure.

2.11.1 Antigen retrieval optimization procedure

In order to find the optimal antigen retrieval condition for each antibody, an optimization procedure that tests twelve different conditions was employed. This procedure gives a quick indication of the most suitable method, which can then be

fine tuned if required. The twelve conditions differ in pH of the antigen retrieval solution, heating method (microwave or waterbath) and time of incubation; conditions are listed in Table 2.4.

Table 2.4: List of antigen retrieval conditions

Antigen retrieval solution and pH	Microwave	Microwave	Waterbath	Waterbath
Vector Antigen unmasking solution pH 6.0 (VectorLab, USA)	10 min (condition 1)	35 min (condition 2)	10 min (condition 3)	35 min (condition 4)
Tris EDTA Citrate unmasking solution pH 8.1	10 min (condition 5)	35 min (condition 6)	10 min (condition 7)	35 min (condition 8)
Tris EDTA Citrate unmasking solution pH 9.0	10 min (condition 9)	35 min (condition 10)	10 min (condition 11)	35 min (condition 12)

Table 2.5: List of antibody used for DAB immunohistochemical analysis of GLI factors in Human Skin and Basal Cell Carcinomas

Protein	Primary antibody and dilution	Secondary antibody (biotin conjugated) and dilution
GLI-1	GLI-1 (H-300): sc-20687 (Santa Cruz, U.S.A.) 1:100	biotinylated anti rabbit and mouse solution from Vectastain® Universal Elite® ABC kit (Vector Laboratories, California) 1 drop according to manufacturer's instructions
GLI-1	GLI-1 (MAB3324) (R D Systems Inc, U.S.A.) 1:100	Anti-Rat Immunoglobulins/HRP (Dako, Denmark) 1:300
GLI-2	GLI-2 (H-300) sc-28674 (Santa Cruz, U.S.A.) 1:100	biotinylated anti rabbit and mouse solution from Vectastain® Universal Elite® ABC kit (Vector Laboratories, California) 1 drop according to manufacturer's instructions
GLI-2	GLI-2 (ab26056) (AbCam, U.K.) 1:100	biotinylated anti rabbit and mouse solution from Vectastain® Universal Elite® ABC kit (Vector Laboratories, California) 1 drop according to manufacturer's instructions

2.12 Immunofluorescent cytochemistry and quantification

Cells were seeded onto sterile 19 mm cover slips within 6- well tissue culture plates ($2x10^4$ cells each) and cultured to subconfluence. Culture media was removed and cells washed twice in PBS and fixed in 4% (w/v) paraformaldehyde overnight. The next day paraformaldehyde was removed and cells washed in PBS (three times, 5 minutes each). Keratinocytes were permeabilised in 0.1% (v/v) Triton X-100 -PBS and aspecific binding sites were subsequently blocked with 3% (w/v) BSA-PBS (Sigma-Aldrich, U.K.). The blocking solution was removed and primary antibody (see Table 2.5) diluted in 3% (w/v) BSA-PBS was added to the wells for 1 hour 30 minutes. Cells were washed in PBS (three times, 5 minutes each) to remove the unbound primary antibody and subsequently incubated with the appropriate secondary antibody (Alexa Fluor, Invitrogen, U.K.) for 1 hour 30 minutes in the dark. After washing with PBS (three times, 5 minutes each), cells were incubated in a 4',6-diamidion-2-phenylindole dihydrochloride (DAPI) solution (1:5000 in PBS, Invitrogen, U.K.) for 5 minutes. Unbound DAPI was removed by washing with PBS (5 minutes) and coverslips inverted and mounted onto slides with fluorescent mounting media (Vector Laboratories, U.S.A.). Slides were observed using a Zeiss LSM 510 META microscope (Carl Zeiss, Germany). Image quantification was performed with Image J software (v.1.41, NIH, U.S.A.). Briefly, using the 'freehand selection tool' the contour of a cell is selected and its area and fluorescence intensity values are measured; by multiplying the area by the fluorescence intensity an integrated fluorescence density value is obtained. The integrated fluorescence density of ten randomly selected cells is measured for each picture. Relative fluorescence density values are obtained by dividing integrated fluorescence density values of a sample by the integrated fluorescence density values of an appropriate control (e.g. untreated cells). Results are expressed as a relative fluorescence increase or decrease compared to control taken as 1.

Table 2.6: List of antibodies used for immunofluorescent cytochemistry

Protein	Primary antibody and dilution	Secondary antibody (fluorescent dye conjugated) and dilution
GLI-1	GLI-1 (H-300) sc-20687 (Santa Cruz, U.S.A.) 1:500	Alexa Fluor® 488 goat anti-rabbit (Invitrogen, U.K.) 1:800
GLI-1	GLI-1 (MAB3324) (R D Systems Inc, U.S.A.) 1:500	Alexa Fluor® 488 donkey anti-rat (Invitrogen, U.K.) 1:800
GLI-1	GLI-1 (Part 965884, ExactaChIP Kit) (R D Systems Inc, U.S.A.) 1:500	Alexa Fluor® 488 donkey anti-goat (Invitrogen, U.K.) 1:800
GLI-2	GLI-2 (H-300) sc-28674 (Santa Cruz, U.S.A.) 1:500	Alexa Fluor® 488 goat anti-rabbit (Invitrogen, U.K.) 1:800
GLI-2	GLI-2 (ab26056) (AbCam, U.K.) 1:500	Alexa Fluor® 488 goat anti-rabbit (Invitrogen, U.K.) 1:800

2.13 Total RNA extraction from cultured cells

All work surface and pipettes were cleaned with RNase Zap (Ambion, U.K.) to remove RNAses. Total RNA extraction was achieved using RNeasy Mini Kit (Qiagen, U.K.) following the manufacturer's instructions. Briefly, 10 μl of β-mercaptoethanol were added to each 1 ml of kit component Buffer RLT and this solution used to scrape cells off the culture dishes after the media had been removed. Buffer RLT disrupts the cell membrane allowing release of RNA into the solution; it also contains a denaturing agent that inactivates RNase enzymes, thus preserving RNA integrity.

All centrifugation steps were performed at 13,000 rpm for 15 sec at room temperature and all flow-throughs were discarded unless stated otherwise. Cell lysates were homogenized using a QIAshredder Mini Spin column (Qiagen, U.K.) by centrifugation at 13,000 rpm for 2 min. One volume of 70% (v/v) ethanol was added

to the flow through solution, the sample was transferred into an RNeasy Mini Spin column and centrifuged. Genomic DNA was digested by adding 10 μl DNase I stock solution to 70 μl Buffer RDD (RNase Free DNase Set, Qiagen, U.K.) and placing the 80 μl solution on top of the column for 15 min at room temperature. 700 μl of RW1 buffer was then added to the column and the samples centrifuged, followed by two washing with 700 μl and 500 μl of RPE buffer (last centrifugation step was performed at 13,000 rpm for 2 min). Finally, the column was transferred to a fresh RNase-free microfuge tube and the RNA was eluted by addition of 40 μl RNase free water to the column followed by centrifugation at 10,000 rpm for 1 min. The last step was repeated using the resulting eluate to yield higher RNA concentrations. The RNA was quantified (see section 2.15) and stored at -80C until required.

2.14 Total RNA extraction from tissue

2.14.1 Whole frozen tissue

Frozen normal human skin or BCC samples were placed in a sterile eppendorf tube, covered with lysis buffer (approx 300 μl, depending on sample size) from the RNeasy Fibrous Tissue Mini Kit (Qiagen, U.K.) and homogenized using a Tissue Rupture (Qiagen, U.K.) according to manufacture's instructions. Extraction of total RNA was subsequently achieved using the RNeasy Fibrous Tissue Mini Kit (Qiagen, U.K.). The RNA extraction procedure is similar to that employed for RNA extraction from cultured cells (see sections 2.13) except for additional digestion with 10 μl of proteinase K solution at 55°C for 10 min followed by centrifugation before the ethanol precipitation step.

2.14.2 Sectioned frozen tissue

Frozen normal human skin samples were sectioned using a cryostat (OTF5000, Bright Instrument, U.K.) and sections of 7 μm thickness were placed into a sterile eppendorf tube containing 100 μl lysis buffer. Extraction of total RNA was subsequently achieved using the RNeasy Micro Kit (Qiagen, U.K.). The RNA extraction procedure is similar to that employed for RNA extraction from cultured

cells (see sections 2.13) except for one extra washing with buffer RW1 and scaling down of volumes according to sample size.

2.14.3 Sectioned wax-embedded tissue

Wax-embedded normal human skin tissue samples were sectioned using a microtome (RM 2235, Leica Microsystems, U.S.A.) and 7 μm thick sections were placed into a sterile eppendorf tube containing 100 μl lysis buffer. Extraction of total RNA was subsequently achieved using the RNeasy FFPE Kit (Qiagen, U.K.). The RNA extraction procedure is similar to that employed for RNA extraction from cultured cells (see sections 2.13) except for previous removal of paraffin by sequential addition of 1 ml xylene and 1 ml 100% ethanol to the samples, followed by centrifugation. Also, an additional digestion with 10 μl of proteinase K solution at 55°C for 10 min followed by centrifugation was performed before the ethanol precipitation step.

2.15 RNA quantification

Isolated RNA was quantified using a NanoDrop ND-1000 Spectrophotometer (Labtech, U.K.). The sample RNA concentration and purity was estimated from a 1 μl aliquot loaded on the spectrophotometer. The 260/280 nm ratio of absorbance was used to assess RNA purity; for RNA a ratio significatively lower than 2.0 indicates the presence of protein or phenol contaminants. A 260/230 nm ratio was also measured as values appreciably lower than 2 denote contamination from carryover of reagents used in the extraction process.

2.16 Reverse transcriptase complementary DNA synthesis

Reverse transcriptase is used to copy the RNA into its complementary DNA sequence (cDNA). The synthesis of cDNA from total RNA template was achieved using SuperScript III First-Strand Synthesis SuperMix (Invitrogen, U.K.). In RNA-free microcentrifuge tubes the components listed in Table 2.6 were added and the mixture incubated for 10 min at 65^{o}C to denature secondary structures and allow primers (random hexamers) binding.

Table 2.7: Primers annealing reaction components

Component	Amount
Up to 5 μg total RNA	X μl (variable)
50 ng / μl Random hexamers	1 μl
10 mM deoxyribonucleotides (dNTPs)	1 μl
DEPC-treated water	to 10 μl (final volume)

After chilling on ice for 1 minute 10 μl of the cDNA synthesis mix (see Table 2.7) was added to each tube, the solution mixed gently and incubated for 10 minutes at RT and then for 50 minutes at 50°C. The reverse transcriptase was omitted in the negative control (-RT).

Table 2.8: cDNA synthesis mix components

Component	Amount
10 X RT Buffer	2 μl
25 mM MgCl2	4 μl
0.1 DTT	2 μl
RNase OUT (40 U/ μl)	1 μl
SuperScript III RT (200 U/ μl)	1 μl

The reaction was terminated by heating at 85°C for 5 minutes. After chilling on ice 1 μl of RNase H was added to each tube to remove any RNA/DNA duplex and the reaction incubated at 37°C for 20 minutes. cDNA was stored at -20C until needed.

2.17 Real-time polymerase chain reaction (qPCR)

Real-time polymerase chain reaction or quantitative PCR (qPCR), is a technique based on the polymerase chain reaction (PCR), which is used to amplify and simultaneously quantify a targeted DNA or c-DNA molecule in a given sample. Selective amplification is obtained by using primers specific for the gene of interest: primers are short oligonucleotides that serve as a starting point for the DNA

synthesis catalysed by the polymerase. Quantification is achieved using fluorescent molecules that correlate qPCR product concentration to fluorescence intensity. Fluorescence is monitored during each cycle of amplification allowing the detection of the reaction in real time. The three major steps in a qPCR reaction, which are repeated for a definite number of cycles, are: denaturation, annealing and extension. The reaction mixture is heated causing the double strand of DNA to melt open (denaturation); primers anneal to the complementary regions in the DNA (annealing) giving rise to short region of double strand DNA that are extended by the polymerase (extension). Primers are designed to amplify a product of a specified size range, for qPCR they should be between 70-150 bp in length. Taq polymerase is used in qPCR reactions as it is a very processive enzyme and it also can withstand the high temperatures needed for DNA strand separation. During each cycle the Taq polymerase synthesises new DNA, creating more template DNA for the next cycle. The reaction proceeds in an exponential manner, doubling the amount of target during each cycle until one of the reagents becomes limiting and the reaction reaches a plateau. In qPCR a specific (TaqMan probes) or non-specific (SYBR Green) detection chemistry allows the quantification of the amplified product. The amount of cDNA detected at a certain point of the run is directly related to the initial amount of target in the sample. SYBR Green, the most used non-specific dye, it is an intercalating molecule that fluoresces once bound to double strand DNA; the amount of fluorescence emitted is related to the amount of target amplified. Since SYBR Green will bind to any double strand DNA, primer dimers or unspecific products can interfere with the quantification. To check for the specificity of the product amplified, it is common practice to run a melting curve at the end of the qPCR run; since every product will have a different dissociation temperature depending on their size and base contents, it is possible to check the number of products amplified. A valid primer pair should produce a single peak on the melting curve. At the beginning of the qPCR reaction there is a linear ground phase (usually the first 10 cycles) where fluorescence emission has not yet risen above background which is used to calculate baseline fluorescence. During the exponential amplification phase the software generates a curve plotting the fluorescence values of each sample in relation to the cycle number. A fluorescence threshold value is selected (manually or automatically) where all the samples are undergoing exponential amplification. The

Ct value is defined as the cycle number at which a specific sample reaches the threshold value. The Ct value is dependent on the amount of the target initially present in the sample: the more abundant the template sample, the quicker this point is reached, giving lower Ct values. There are two different methods to measure the levels of expressed genes by qPCR based on Ct values, absolute and relative quantification. Absolute quantification relates the fluorescent signal to initial target amount using a standard curve, while relative quantification measures the relative change in mRNA expression level (comparative Ct method). In these experiments absolute quantification was used: a standard curve was generated for every primer pairs with serially diluted standards of known concentrations (100 ng, 50 ng, 10 ng, 1ng, 0.1 ng) using cDNA from cells that express the genes of interest. The level of expression of the gene of interest was subsequently normalised to a housekeeping gene (a gene that is expressed at a constant level), namely Glyceraldehyde 3-phosphate dehydrogenase (GAPDH). Normalised values are then expressed as fold change expression relative to an appropriate control e.g. normal tissue, empty vector etc. taken as 1. Each qPCR reaction contained the components listed in Table 2.8 in a final volume of 20 μl.

Table 2.9: qPCR reaction components

Component	Amount
SYBR Green MasterMix	10 μl
Forward + Reverse Primers 5 μM stock solution	1.2 μl
Template cDNA 2 ng / μl	5 μl
DNase free water	3.8 μl

Every reaction was performed in duplicate and a negative control by omission of cDNA (no template control) was added to each experiment. Plates were run on an Applied Biosystem 7500 qPCR machine (Applied Biosystem, U.K.).

The qPCR program was set for an initial holding step of 10 minutes at 95°c followed by the cycling stage. The denaturation stage was set at 95°c for 15 seconds, followed by the annealing and extension stage which lasted for 1 minute at 60°c; the qPCR machine recorded SYBR green fluorescence values during the extension step. The cycling stage (denaturation / annealing / extension) was repeated 40 times before the final dissociation stage which generated a melting curve.

2.18 Primer design and selection

Genomic DNA sequences for human GLI1 were obtained using Entrez, an online DNA sequence search engine (www.ncbi.nlm.nih.gov/entrez/query.fcgi) using the GenBank accession number GLI1 NM_005269.

Primers were then designed using Primer3, an online PCR primer design program (www.genome.wi/mit.edu/cgi-bin/primer/primer3www.cgi), and compared against human sequences using an online sequence comparison program, BLAST (www.ncbi.nlm.nih.gov/BLAST) to ensure specific binding. Primers were designed to be around 20 nucleotides in length, with a 40%-60% GC content and minimal inter- and intra-complementary sequences to prevent hairpin and primers dimer formation. Sequences of both newly designed primers and primers derived from previous publications are reported in Table 2.10.

Table 2.10: Primer sequences for qPCR analysis

Gene and primers name	Forward primer (5'-3')	Reverse primer (5'-3')
GLI1 (GLI1 RD – newly designed)	CTGGACCTGCAGACGGTTAT	GGTGCCAATGGAGAGATGAC
GLI1 (GLI1 H300 – newly designed)	CCCAGGAACCTTCCTACCAG	CTTGTGATTGGGCAAGTTGG
GLI1 (Yauch R et al., 2008)	GTTCACATGCGCAGACACACT	TTCGAGGCGTGAGTATGACTTC
GLI1 used in Ch 3	GAAGACCTCTCCAGCTTGGA	GGCTGACAGTATAGGCAGAG
GLI2 (Regl G et al., 2002)	GGGTCAACCAGGTGTCCAGCACTGT	GATGGAGGGCAGGGTCAAGGAGTTT
GLI2 used in Ch 3	TGCCACTGGGAAGACTGCACC	AAGGGCTTCTGCTCCGCGGT
PTCH1 (Yauch R et al., 2008)	CGGCAGCCGCGATAAG	TTAATGATGCCATCTGCATCCA
PTCH1 (1) used in Ch 3	TGAGTGGAGTTCTGTGCGACA	CTCCCAAGCAAATGTACGAGC
PTCH1 (2) used in Ch 3	ACTCGCCAGAAGATTGGAGA	TCCAATTTCCACTGCCTGTT
GAPDH (Van Trappen P et al. 2001)	GAAGGTGAAGGTCGGAGT	GAAGATGGTGATGGGATTTC

2.19 Agarose gel electrophoresis

Agarose gel electrophoresis was used to check the integrity of the extracted RNA. Agarose powder was poured in TAE buffer (tris-acetate ethylediaminetetra-acetic acid, see Appendix I) to obtain a 1% (w/v) agarose - TAE solution. The solution was heated up in the microwave to dissolve the agarose and then poured in a tank; a small comb was placed into the solution to create wells to load the samples. When the agarose was set, samples were loaded onto the gel placed into a tank filled with TAE running buffer. To allow visualization of RNA 1 μg/ml SYBR Green II RNA Gel Stain (Invitrogen, U.K.) was added to the gel before solidification. RNA bands were visualized using an U.V. translilluminator (Alpha Innotech Corporation, USA).

2.20 Transwell migration assay

The movement of cells from one area to another in response to a chemical signal is a central function in wound repair, development and the tumour metastasis. The transwell migration assay is a widely used test to study the migratory response of cells to chemotattic stimuli. The transwell is placed into a 12 well plate to form a system comprised of a lower and an upper chamber containing the cell suspension. During the assay cells are placed on the upper chamber on top of a coated cell permeable membrane; following an incubation period the cells that have migrated through the membrane are stained and counted. Cell migration assay was performed in Transwell chambers (tissue culture treated, 10 mm diameter, 8 μm pores, Nunc, USA). Cells were serum starved in RM+ media containing 0.5% (v/v) FBS overnight and transwells were coated with either 100 μg / ml collagen or 10 μg / ml fibronectin. The following day 30000 cells per well were resuspended, added to the top of each chamber and allowed to migrate. After 4 hours cells that had not migrated were removed by using a cotton swab whereas migrated cells were fixed with 4% paraformaldehyde, stained with 1% (w/v) crystal violet and counted.

2.21 Adhesion assay

Adhesion assays are widely used to assess the adhesive properties of cells. Cells were serum starved in RM+ media containing 0.5% (v/v) FBS overnight and 96 well plates were coated with either 100 μg / ml collagen or 10 μg / ml fibronectin. The following day cells were resuspended, placed in a 50 ml falcon tube and left in agitation on a rotating wheel for 1 hour. 10000 cells were placed in each 96 well and left to adhere for different amounts of time (45, 30, 15 or 1 minutes) before fixation with 4% (v/v) paraformaldehyde. Each timepoint was repeated in triplicate. Cells were stained with 1% crystal violet for 10 minutes, washed with PBS and 20% (w/v) SDS was then added to solubilise the crystal violet. The plated was put on a laboratory shaker for 10 minutes at 130 rpm and absorbance values at 550 nm were subsequently read using a spectrophotometer (Synergy HT, BioTek, USA).

Chapter 3

3 Analysis of the putative feedback loop between GLI1 and GLI2 in human epithelial cells

3.1 Introduction

Basal Cell Carcinoma development is associated with loss of the PTCH1 tumour suppressor gene resulting in increased expression of the GLI (GLI1 and GLI2) transcription factors which are thought to be vital for tumour formation. Overexpression of either GLI1 or GLI2 in the basal layer of mice or frog skin results in BCC-like tumours (Dahmane et al., 1997; Grachtchouk et al., 2000; Nilsson et al., 2000; Sheng et al., 2002). Both GLI1 and GLI2 possess tumorigenic properties, though their sequence of activation is still debated; moreover it is not clear whether one has a predominant role in the genesis of the tumours or if they have a synergistic effect. This would be ideally investigated using in vitro models of BCC, though at the moment a very limited number exist (see section 1.8.2). From mammalian developmental studies, the activation of GLI1 is thought to depend upon GLI2 (Bai and Joyner, 2001). Indeed, using a cell-based inducible system, Regl et al. (2002) (Regl et al., 2002) showed that a constitutively active mutant of GLI2 (GLI2ΔN) induces endogenous GLI1 mRNA expression in HaCat cells and this was later confirmed at the protein level in primary human keratinocytes (Bonifas *et al.*, 2001; Ikram *et al.*, 2004). Regl et al (2002) also showed that ectopic GLI1 induces endogenous GLI2 mRNA expression and thus proposed the presence of a positive GLI1-GLI2 feedback loop that may perpetuate the oncogenic effects of both transcription factors in BCC. Based upon the kinetics of transcripts expression, GLI1 is thought to be a direct transcriptional target of GLI2ΔN; moreover, GLI2ΔN binds to the human GLI1 promoter (Bonifas *et al.*, 2001; Ikram *et al.*, 2004). On the other hand, based upon the kinetics of transcript expression and by comparison with the induction of PTCH1 mRNA, GLI2 appears to be an indirect target of GLI1 (Regl et al., 2002).

In contrast to these studies based on mRNA levels, previous work in the lab had found evidence that endogenous GLI2 protein is suppressed in prostate cells by ectopic GLI1 (see section 1.8.2). We proposed to analyse the GLI1-GLI2 feedback

loop at protein level in N/Tert-1 keratinocytes. Clarifying this interplay in skin cells and understanding its relevance for BCC development may be useful for choosing the appropriate target for therapeutic intervention.

3.2 Results

3.2.1 GLI2 protein appears to be downregulated upon ectopic expression of GLI1 in immortalised keratinocytes (N/Tert-1)

Continuing work previously carried out in the Neill group (described in section 1.8.2), I analysed GLI2 protein levels in GLI1-expressing N/Tert-1 keratinocytes. At the time I started this project, the Neill group employed N/Tert-1 keratinocytes cultured in KGM which contains 10% FCS. This was done because maintaining expression of ectopic proteins (GLI1 and GLI2ΔN) during serial passage was not possible in cells cultured in SFM. Using the same antibody employed in the past (GLI2 H-300, Santa Cruz) but different aliquots, expression of GLI2 in clonal N/Tert-1 cells stably expressing EGFP or an EGFP-GLI1 fusion protein was analysed. The pattern of GLI2 expression was different to that observed in N/Tert-1 cells cultured in SFM with the most notable difference being the presence of a very strong band migrating between the 47 and 62 kDa marker proteins (cf. Fig. 1.8, lane 1 and Fig. 3.1, lane 1). The identity of this band has not been established but it has also been observed in LNCaP and DU145 prostate cancer cells cultured in RPMI 1640 medium containing 10% FCS (Mr Sandeep Nadendla, data not shown). However, it likely represents GLI2 as, along with several other distinct bands, its expression appears to be suppressed in the N/Tert-1 EGFP-GLI1 lysate (Fig. 3.1 a, lane 2).

This Western Blotting experiment was repeated using the same lysates but probing the membrane with a different aliquot of the GLI2 H-300 antibody. The expression of several bands was suppressed in EGFP-GLI1 cells suggesting that ectopic GLI1 may suppress GLI2 protein expression in human keratinocytes (Fig. 3.2).

GLI2 protein expression was also analysed in N/Tert-1 keratinocytes overexpressing GLI1 using the pBabePuro vector system and cultured in KGM media (10% FCS). N/Tert-1 pBabe, N/Tert-1 pBGLI1 and N/Tert-1 pBGLI2ΔN cell lines were previously generated in the lab by Dr Wesley Harrison by transduction followed by drug selection; these keratinocytes stably express either GLI1 or GLI2ΔN. In pBGLI1 keratinocytes, a reduction in the level of endogenous GLI2 is observed (Fig 3.3 a, lane 2) by Western Blotting. GLI2 is downregulated upon GLI1 expression,

although not as strongly as in the EGFP – EGLI1 system (Fig 3.1). A slight reduction in the intensity of the lower molecular band at around 60 KDa is also observed; because of the strength of the band, this is more evident with a lower time exposure (Fig 3.3 a, lower panel). A third aliquot of the GLI2 H-300 antibody, different from the ones used previously, was employed. GLI1 was detected taking advantage of a newly commercialized antibody, GLI1 965 RD (GLI1 Part 965884, ExactaChIP Kit, R&D Systems), whose epitope sequence or localization could not be disclosed by R&D Systems technical service. Two bands are detected and, since they are only present in the pBGLI1 lane (Fig 3.3 b, lane 2), they likely represent ectopic expressed GLI1 and either a degradation product or an induced isoform. Different GLI1 variants have been described in the literature (Shimokawa et al., 2008; Lo et al., 2009; Altaba, 1999; Stecca and Ruiz i Altaba, 2009).

NEB1 pBabe, NEB1 pBGLI1 and NEB1 pBGLI2ΔN cell lines, also created by Dr Wesley Harrison, were also tested. No ectopic GLI1 (Fig 3.9 b, lane 2) nor GLI2 expression (Fig 3.9 a) could be detected; concerning the latter, no unique band is present in the pBGLI2ΔN lane compared to pBabe and pBGLI1, suggesting ectopic GLI2 is not detected. Two bands are observed in all lanes (pBabe, pBGLI1 and pBGLI2ΔN), whose intensity is overall similar, with a slight decrease in the pBGLI2ΔN lane. They likely represent endogenous GLI2, although it is unusual for GLI2 to be weaker in pBGLI2ΔN cells as it is usually the same strength or even stronger in the pBGLI2ΔN lane compared to pBabe (cf. Fig 1.7 a, Fig 1.8 a and Fig 3.3 a). The intensity of the lower molecular band at around 60 KDa is comparable in all lanes. Analysis of levels of endogenous GLI2 protein expression pattern in NEB1 keratinocytes will need to be addressed in further studies, as it may differ from those of other cell lines previously analysed; moreover, the identity of the lower molecular band should be confirmed, as argued in the Discussion section.

The extent of GLI2 downregulation in N/Tert-1 keratinocytes (grown in serum-containing media KGM) was not as strong using the pBabe expression system compared to the EGFP system (based on pSIN vectors, see Materials and Methods), as observed comparing Fig. 3.1 and Fig. 3.3. To help understand this discrepancy, qPCR experiments were performed.

In N/Tert-1 pBGLI1 keratinocytes there is a roughly 6 fold increase (logarithmic scale) in the mRNA levels of GLI1 compared to pBabe control, as expected (Fig. 3.4); GLI2 mRNA levels are increased less than 2-fold. Conversely, N/Tert-1 pBGLI2ΔN keratinocytes show a 5 fold increase for both GLI2 and GLI1 mRNA levels. These observations are consistent with previous publications, as GLI1 is thought to be a direct transcriptional target of GLI2ΔN, while activation of GLI2 by GLI1 is likely to be indirect (Bonifas et al., 2001; Ikram et al., 2004; Regl et al., 2002). Levels of GLI target gene PTCH1 were also measured, using two different pairs of primers: a similar increase in PTCH1 mRNA (between 2.5 – 3 fold) is observed in both pBGLI1 and pBGLI2ΔN cells, regardless of the pair of primers used (Fig 3.4).

Levels of PTCH1 mRNA were also analysed in NEB1 keratinocytes: PTCH1 is induced only about 1 fold in pBGLI1 keratinocytes compared to control, whereas virtually no PTCH1 induction is detected in pBGLI2ΔN keratinocytes (Fig 3.10). These data, combined with the fact no ectopic GLI1 or GLI2 is detected by Western Blotting in NEB1 keratinocytes (Fig 3.9), suggest the proteins are either not strongly expressed or not very active; therefore, experiments with NEB1 cells were no longer pursued.

To further analyse GLI1-induced downregulation of GLI2 at protein level, immunofluorescence cytochemistry experiments were performed on N/Tert-1 pBabe, N/Tert-1 pBGLI1 and N/Tert-1 pBGLI2ΔN keratinocytes. Staining with GLI1 965 RD is stronger in pBGLI1 cells, as it would be expected, as both endogenous and ectopic GLI1 are detected; of note, GLI1 staining is heterogeneous in both intensity and localisation, e.g. some cells stain stronger than others, and GLI1 can be nuclear and cytoplasmic or predominantly nuclear (Fig 3.5 c). Although not statistically significative, quantification of GLI1 965 RD staining reveals an increase in GLI1 staining in pBGLI1 keratinocytes compared to N/Tert-1 and N/Tert-1 pBabe cells, and also a slight increase of GLI1 in pBGLI2ΔN cells (Fig 3.6).Similarly to what has been observed for GLI1, GLI2 H-300 staining is more intense in pBGLI2ΔN keratinocytes; again, staining heterogeneity is striking feature, as different staining intensities are present even in the same colony of cells (Fig. 3.7 d). Staining quantification highlights the increase in GLI2 in pBGLI2ΔN cells and shows a

negligible increase in pBGLI1 cells compared to N/Tert-1 and pBabe cells, which is not statistically significative (Fig 3.8).

To address the physiological relevance of these preliminary findings, and to determine the extent of GLI1 – GLI2 co-expression in vivo (which has never been previously investigated) immunohistochemical analysis for GLI1 and GLI2 in human BCCs samples has been performed (see Chapter 4).

Please note: GLI1 965 RD (GLI1 Part 965884, ExactaChIP Kit, R&D Systems) was only made commercially available after this thesis was originally submitted; experiments performed with this antibody were added subsequently to that date as part of the thesis corrections. This is the reason why GLI1 965 RD has not been used in immunofluorescence experiments on Basal Cell Carcinoma sections (which could be part of future work concerning this project) and is not further discussed in the following sections.

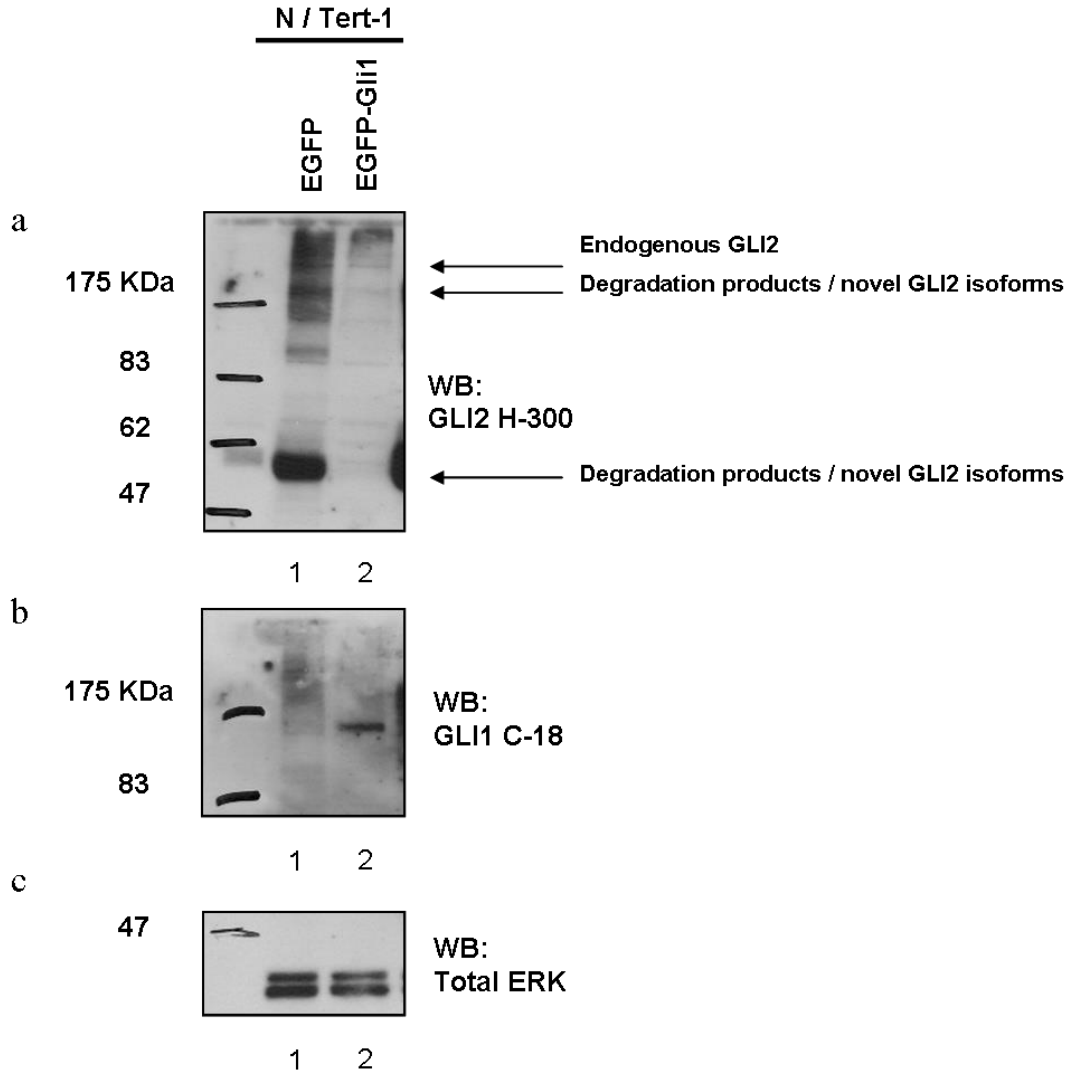

Figure 3.1: Western Blotting for GLI2 protein levels in N/Tert-1 keratinocytes overexpressing GLI1 (GLI2 H-300 antibody - batch 1)

Effect of GLI1 overexpression in N/Tert-1 keratinocytes. In EGFP empty vector control cells endogenous GLI2 as well as lower molecular bands are present, the strongest at about 50 KDa (Fig 3.1 a, lane 1). Ectopic expression of GLI1 (Fig 3.1 b, lane 2) seems to induce full length GLI2 protein downregulation and disappearance of the lower molecular weight product (Fig 3.1 a, lane 2). Total ERK was used as a loading control (Fig 3.1 c). Cells were grown in KGM (10% serum media).

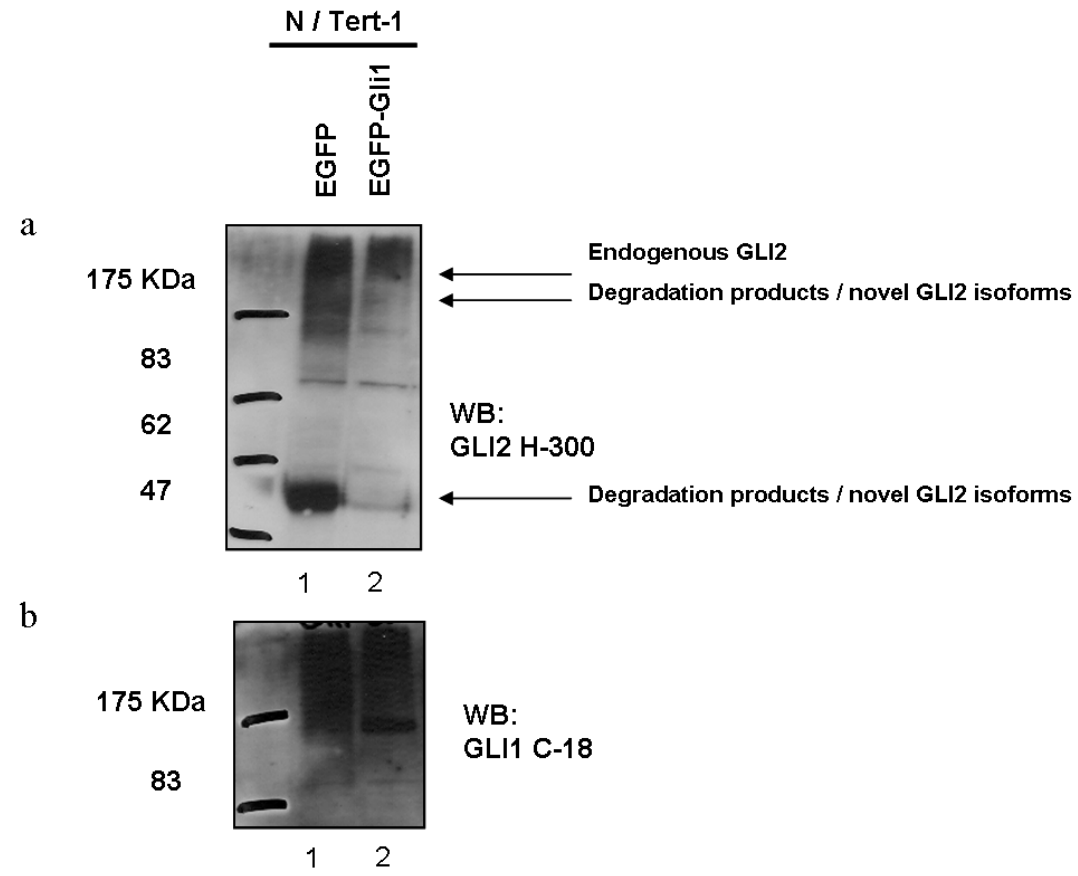

Figure 3.2: Western Blotting for GLI2 protein levels in N/Tert-1 keratinocytes overexpressing GLI1 (GLI2 H-300 antibody - batch 2)

Effect of GLI1 overexpression in N/Tert-1 keratinocytes. Lysates from Figure 3.1 were run on a new gel and the membrane probed with a different batch of GLI2 H-300 antibody compared to the one used in Figure 3.1 (Fig 3.2 a, batch 2, Figure 3.1 a, batch 1). In EGFP empty vector control cells endogenous GLI2 as well as lower molecular bands are present, the strongest at about 50 KDa (Fig 3.2 a, lane 1). Ectopic expression of GLI1 (Fig 3.2 b, lane 2) seems to induce full length GLI2 protein downregulation (Fig 3.2 a, lane 2) and disappearance of the lower molecular weight product (Fig 3.2 a, lane 2). Cells were grown in KGM (10% serum media).

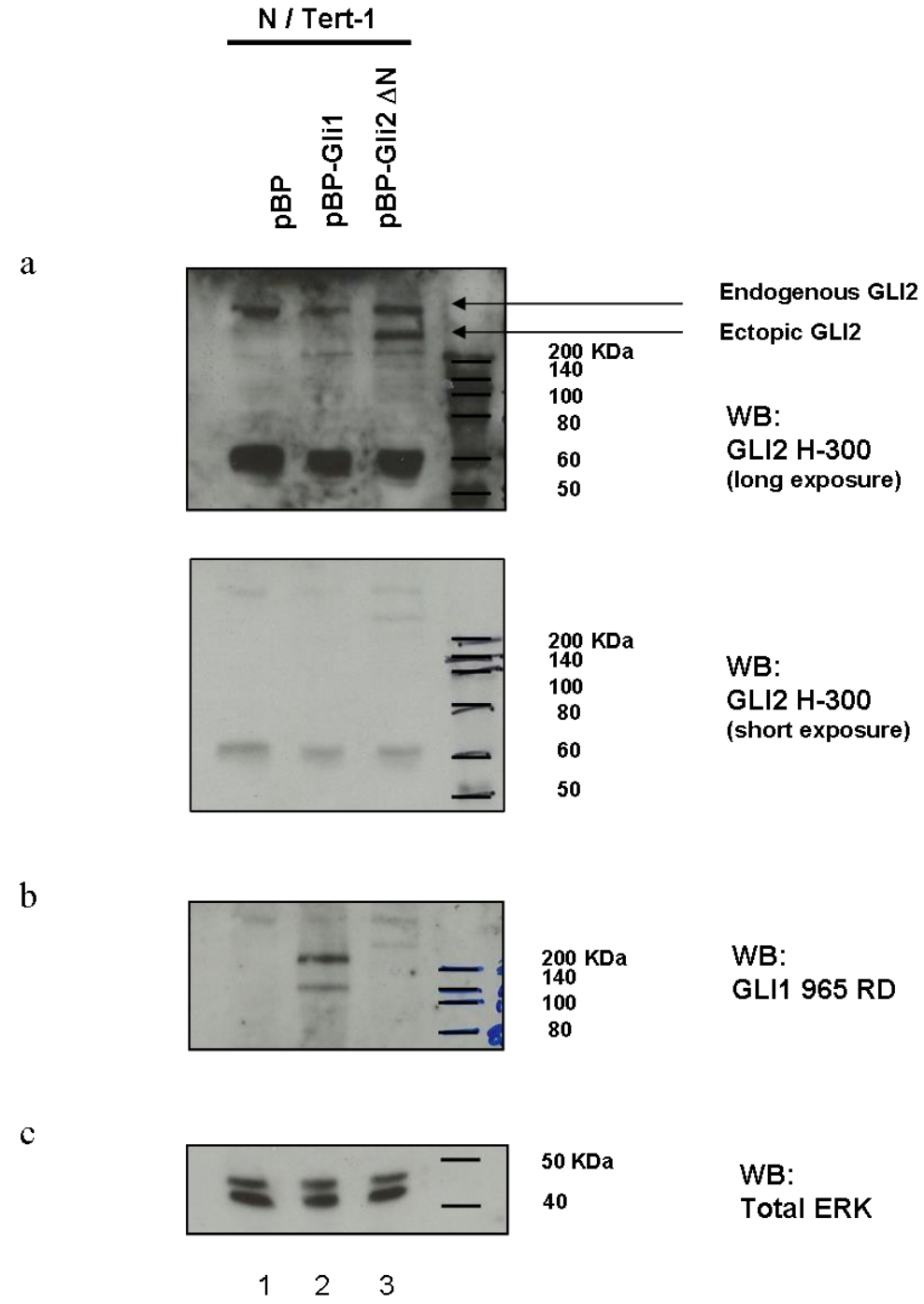

Figure 3.3: Western Blotting for GLI2 protein levels in N/Tert-1 keratinocytes overexpressing either GLI1 or GLI2ΔN

Effect of GLI1 overexpression in N/Tert-1 keratinocytes. Ectopic expression of GLI1 (Fig 3.3 b, lane 2) slightly reduces GLI2 protein levels (Fig 3.3 a, lane 2). Total ERK was used as loading control (Fig 3.3 c).Cells were grown in KGM (10% serum media). pBP, pBabePuro empty vector control.

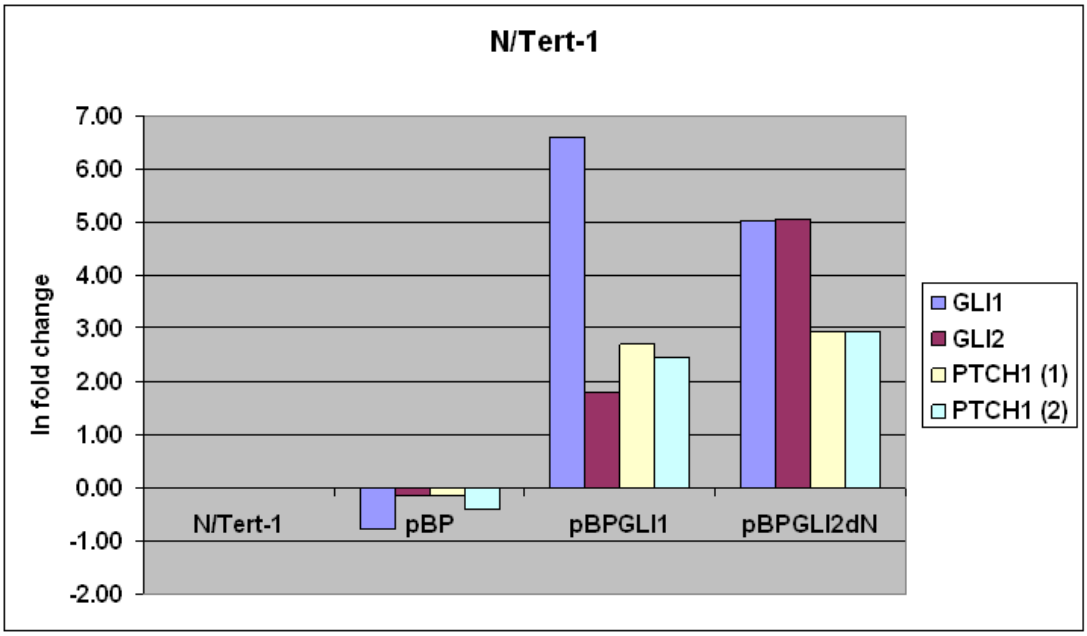

Figure 3.4: qPCR analysis of N/Tert-1 keratinocytes overexpressing either GLI1 or GLI2ΔN

qPCR measurements of mRNA levels of GLI1, GLI2 and PTCH (two different sets of primers) in N/Tert-1 keratinocytes stably expressing GLI1 or GLI2ΔN. All values refer to mRNA levels normalised to GAPDH and are expressed as logarithmic fold changes relative to untransduced N/Tert-1 cells taken as 1.

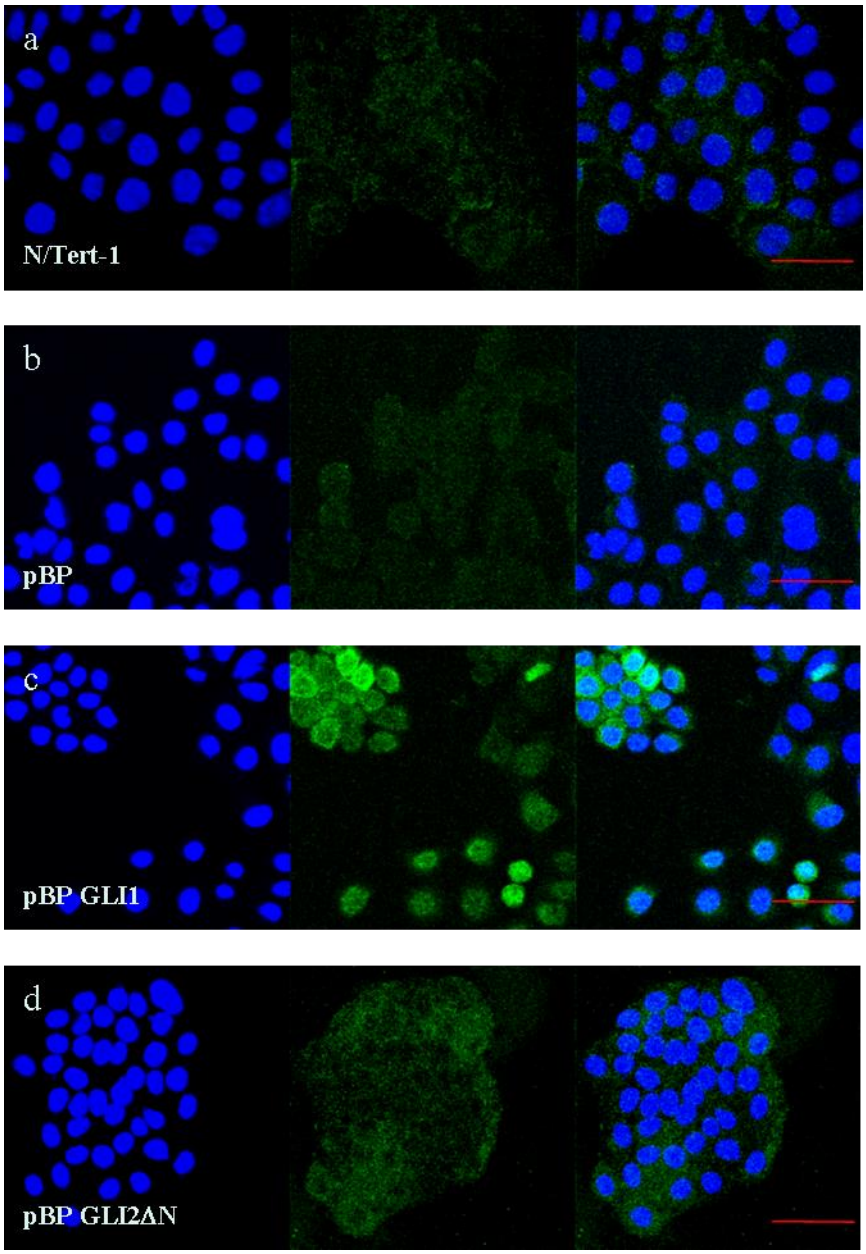

Figure 3.5: Immunofluorescent analysis of N/Tert-1 keratinocytes overexpressing either GLI1 or GLI2ΔN using GLI1 965 RD antibody

N/Tert-1 (a), N/Tert-1 pBP(b), N/Tert-1 pBP GLI1 (c) and N/Tert-1 pBP GLI2ΔN (d) keratinocytes were fixed and stained with GLI1 965 RD antibody. Scale bar represents 20 µm.

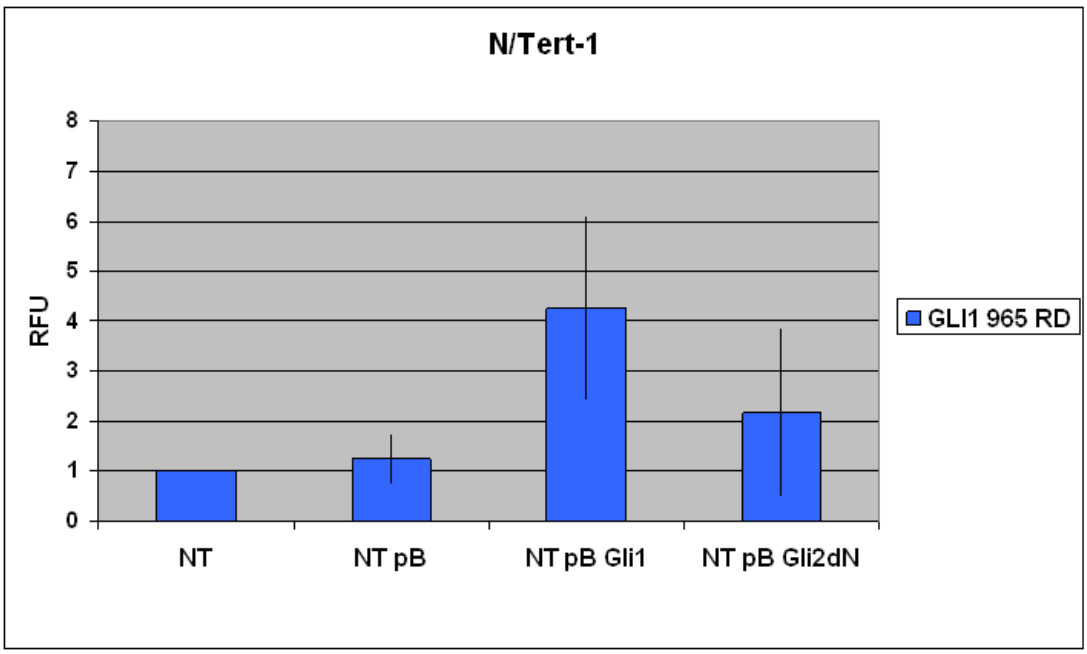

Figure 3.6: Quantification of immunofluorescent analysis of N/Tert-1 keratinocytes overexpressing either GLI1 or GLI2ΔN using GLI1 965 RD antibody

Quantification of GLI1 965 RD antibody fluorescence intensity in N/Tert-1, N/Tert-1 pBP, N/Tert-1 pBP GLI1 and N/Tert-1 pBP GLI2ΔN keratinocytes. Images displayed in Fig. 3.5 were quantified using the image processing software Image J. Data are expressed as mean ± standard deviation. RFU, Relative Fluorescence Units.

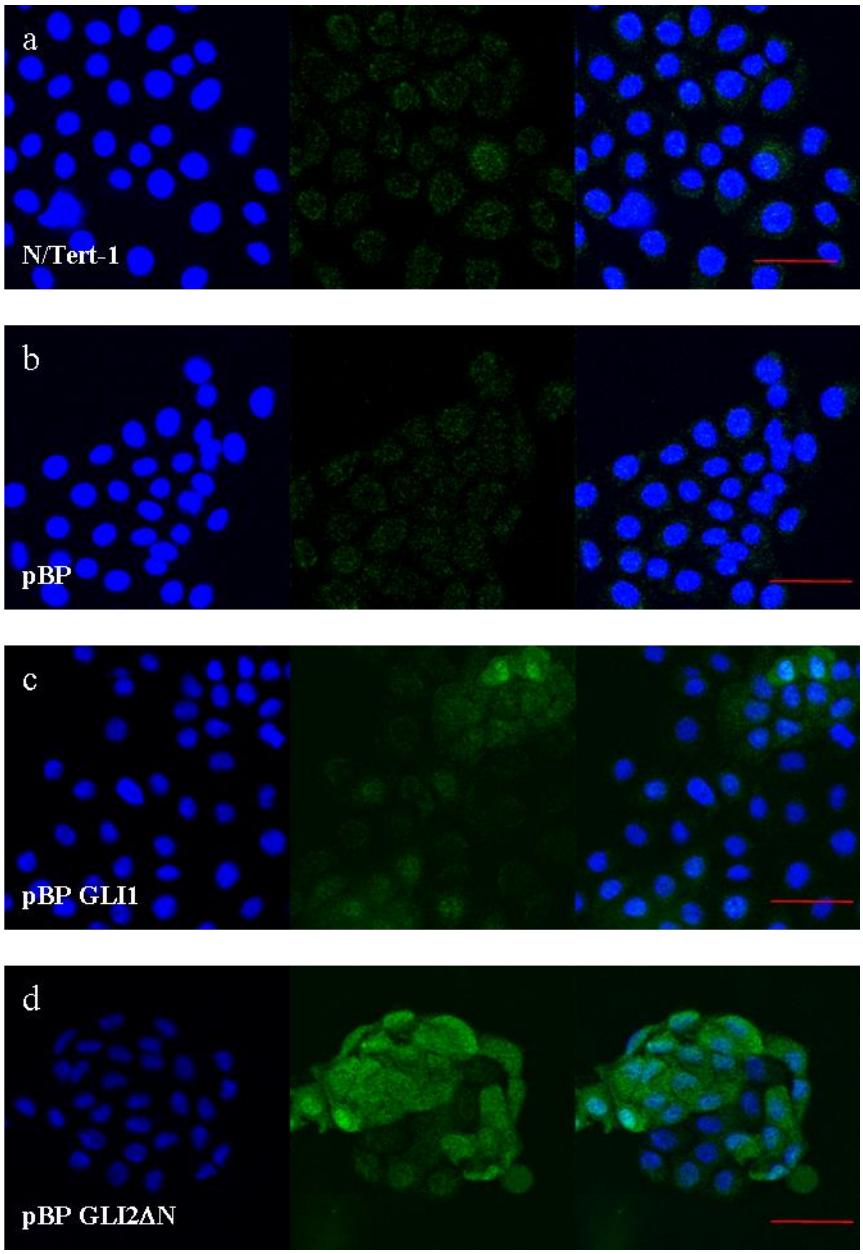

Figure 3.7: Immunofluorescent analysis of N/Tert-1 keratinocytes overexpressing either GLI1 or GLI2ΔN using GLI2 H-300 antibody

N/Tert-1 (a), N/Tert-1 pBP(b), N/Tert-1 pBP GLI1 (c) and N/Tert-1 pBP GLI2ΔN (d) keratinocytes were fixed and stained with GLI2 H-300 antibody. Scale bar represents 20 µm.

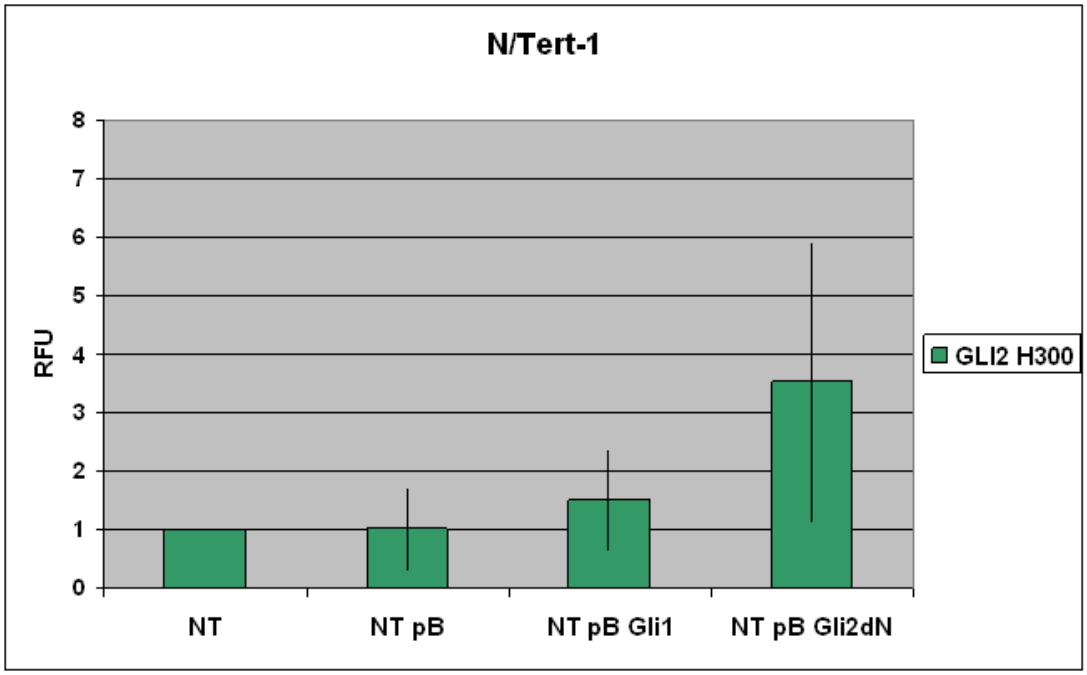

Figure 3.8: Quantification of immunofluorescent analysis of N/Tert-1 keratinocytes overexpressing either GLI1 or GLI2ΔN using GLI2 H-300 antibody

Quantification of GLI2 H-300 antibody fluorescence intensity in N/Tert-1, N/Tert-1 pBP, N/Tert-1 pBP GLI1 and N/Tert-1 pBP GLI2ΔN keratinocytes. Images displayed in Fig. 3.7 were quantified using the image processing software Image J. Data are expressed as mean ± standard deviation. RFU, Relative Fluorescence Units.

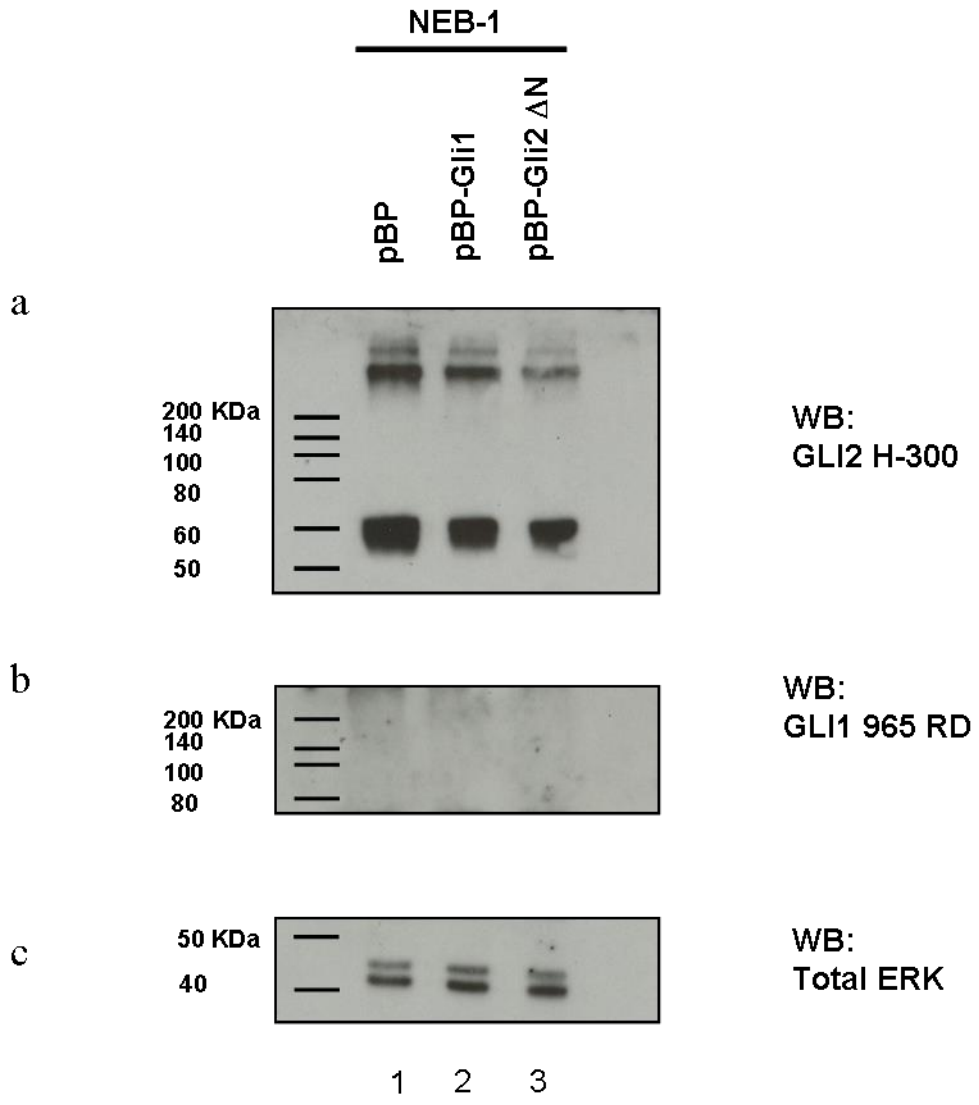

Figure 3.9: Western Blotting for GLI2 protein levels in NEB1 keratinocytes overexpressing either GLI1 or GLI2ΔN

Effect of GLI1 overexpression in NEB1 keratinocytes. No ectopic GLI1 (Fig 3.4 a, lane 2) nor GLI2 expression (Fig 3.4 b) could be detected. Total ERK was used as a loading control (Fig 3.4 c). Cells were grown in KGM (10% serum media). pBP, pBabePuro empty vector control.

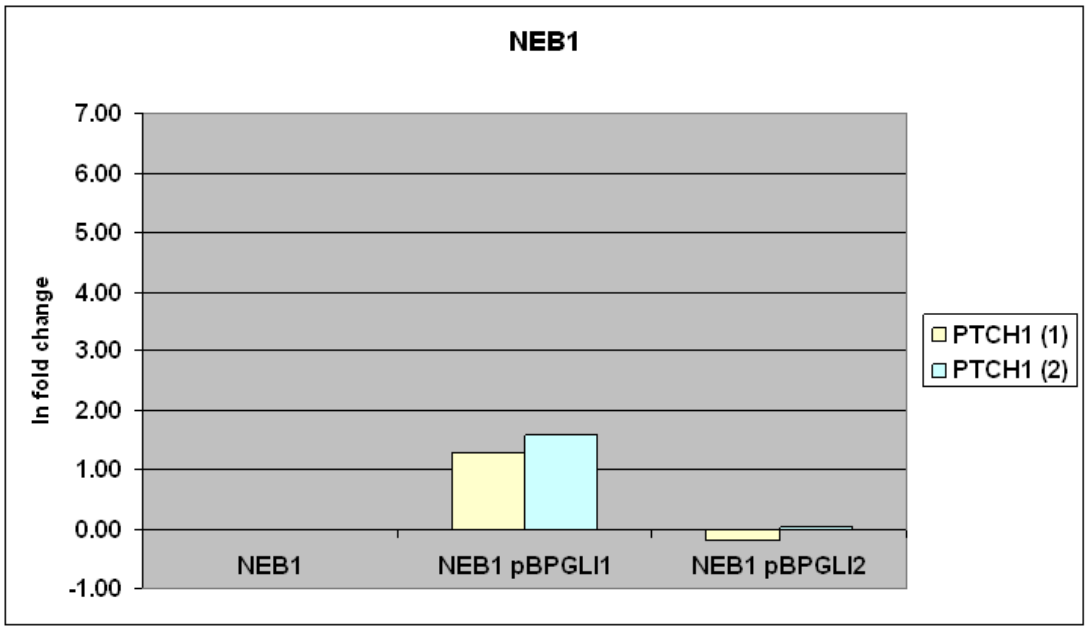

Figure 3.10: qPCR analysis of NEB1 keratinocytes overexpressing either GLI1 or GLI2ΔN

qPCR measurements of mRNA levels of PTCH (two different sets of primers) in N/Tert-1 keratinocytes stably expressing GLI1 or GLI2ΔN. All values refer to mRNA levels normalised to GAPDH and are expressed as logarithmic fold changes relative to untransduced NEB1 cells taken as 1.

3.3 Discussion

GLI2 Western Blot analysis of epithelial cells upon GLI1 overexpression revealed an unexpected downregulation of GLI2 as well as differences in GLI2 expression pattern between different cell types (see Fig. 1.7, 1.8, 3.1 and 3.3). To interpret these results, it is useful to consider a number of complexities which are intrinsic to Hedgehog /GLI signalling.

Full length GLI proteins have been speculated to have activator as well as repressor functions, the latter as a result of carboxyl-terminal cleavage by the proteasome (Ruiz i Altaba et al., 2002). Two GLI1 splice variants (Shimokawa *et al.*, 2008; Lo *et al.*, 2009) and four different isoforms of GLI2 have so far been described (Tanimura et al., 1998); moreover, GLI2 transcript has been shown to be subject to alternative splicing in different cell lines (Speek *et al.*, 2006). The complete full length GLI2 sequence had only been discovered in 2005 (Roessler et al., 2005); before this date a truncated form of GLI2, subsequently named GLI2ΔN, was thought to represent the whole protein.

In some contexts GLI proteins have been shown to be activated independently of HH signalling in response to fibroblast growth factor (FGF) signalling (Brewster et al., 2000), loss of the tumour suppressor Notch (Nicolas et al., 2003) or exposure to TGFβ ligand (Dennler et al., 2007; Dennler et al., 2009). GLI protein activity has also been shown to be modulated by interaction with other cellular pathways frequently activated in human malignancies such as RAS and EGFR (Lauth and Toftgard, 2007; Schnidar *et al.*, 2009).

Normal, immortalised and malignant epithelial cell lines have different genetic arrangements, and specific signalling pathways may be active in each cell: this could explain the different GLI2 expression pattern observed in primary prostate epithelial cells (PrEc) compared to the immortalised keratinocytes cell line N/Tert-1 (both grown in serum-free media). In N/Tert-1 keratinocytes the amount of full-length GLI2 is reduced upon GLI1 overexpression, together with the appearance of a slightly lower molecular band that could be either a degradation product or a yet unidentified GLI2 isoform (Fig 1.8). In PrEc cells this lower band is not noticeable while full-length GLI2 is almost absent when GLI1 is overexpressed (Fig 1.7). A

lower band at about 50 kDa is observed but because of its weakness it is difficult to interpret.

GLI2 pattern of expression seem also to be influenced by the culture media used, as it presents some differences in N/Tert-1 grown in serum free media (Fig 1.8) compared to KGM (10% serum, Fig 3.1 and 3.2). While in SFM a single full-length GLI2 band is present in control cells, multiple bands are observed in serum-containing media; of particular interest is a strong band of about 50 kDa molecular weight that is present in control cells but is downregulated upon GLI1 overexpression. This low molecular band has also been detected in prostate cancer cell lines (Mr. Sandeep Nadendla and Dr. Graham Neill, unpublished data) grown in serum-containing media (RPMI 1640), raising the hypothesis that expression of this putative degradation product or novel isoform could be the result of cellular pathway(s) that are only activated in the presence of serum.

GLI2 possesses an amino-terminal repressor domain, a central zinc-finger DNA-binding domain and a carboxyl-terminal activator domain; it can act as activator or a repressor of transcription. In the absence of HH signalling, GLI2 is converted from a transcriptional activator to a transcriptional repressor: protein kinase A (PKA) phosphorylation leads to a proteasome-mediated processing which yields a carboxyl-terminus truncated repressor (Ruiz i Altaba et al., 2002; Sasaki et al., 1999; Pan et al., 2009). As a result of HH binding processing of GLI2 is inhibited, leading to the accumulation of its full-length form and the activation of specific target genes (Stecca and Ruiz i Altaba, 2010). Full length GLI2 is a weak transcriptional activator; in response to HH signalling, proteolytic removal of the amino terminal repressor domain appears to be required to convert GLI2 into a strong activator (Sasaki et al., 1999; Sheng et al., 2002; Roessler et al., 2005). A study in mice revealed full length GLI2 is highly unstable in the absence of HH signalling; GLI2 degradation is dependent on consecutive phosphorylations by PKA, CK1 and GSK3, which result in interaction with the β-TrCP ubiquitin ligase and proteasome-mediated degradation (Pan et al., 2006b). The hyperphosphorylation of GLI2 creates binding sites for the β-TrCP ubiquitin ligase; the mutation of serine 662 to alanine in the binding motif of GLI2 significantly impairs its ability to interact with β-TrCP (Bhatia et al., 2006). Mice GLI2 has been reported to be inefficiently proteolytically

processed to form a transcriptional repressor in vivo (Pan et al., 2006b). Both processing and degradation of GLI2 are inhibited by activated HH signalling. In biochemical studies based on exogenous GLI2 overexpression several protein fragments smaller than full-length GLI2 have been detected, which provide further evidence of GLI2 proteolytic processing (Altaba, 1999; Aza-Blanc et al., 2000). GLI2 proteolytic processing adds a layer of complexity to the regulation of HH signalling and its relevance for BCC development has not been fully elucidated yet.

Four different GLI2 isoforms have been reported, alpha (α), beta (β), gamma (γ) and delta (δ), whose transcripts are generated by combinations of two independent alternative splicing sites (Tanimura et al., 1998). Alternative splicings result in a 51-base deletion of the coding frame in the beta (β) and delta (δ) isoforms, and a 1,231-base deletion in the gamma (γ) and delta (δ) isoforms. The longest clone, alpha (α), was thought to consists of 4,961 bp and to encode a 1,258 amino acids protein.

A previously unidentified 328 amino acids long N-terminal domain of the human GLI2 protein has later been described (Roessler et al., 2005), and now the full-length protein is thought to be composed of 1586 amino acids. Four different protein variants are encoded by the four transcripts, with the region between amino acids positions 394 and 410 missing in the beta (β) and delta (δ) isoforms and the region between amminoacids positions 1158 and 1586 is missing in the gamma (γ) and delta (δ) isoforms (according to UniProtKB/Swiss-Prot database, GLI2_HUMAN, accession number P10070, see also Appendix III). Predicted molecular weights for alpha (α), beta (β), gamma (γ) and delta (δ) protein isoforms are, respectively, 133-, 131-, 88-, and 86-kDa (Tanimura et al., 1998). Differences in size between alpha (α) (133 kDa) and beta (β) (131 kDa) and between gamma (γ) (88 kDa) and delta (δ) (86 kDa) are too small to be detected by Western Blot (only a few kDa difference); however, alpha (α) plus beta (β) isoforms can be distinguish from gamma (γ) plus delta (δ) as the difference in molecular weight is around 50 kDa (133 and 131 kDa alpha (α) plus beta (β) versus 88 and 86 kDa gamma (γ) plus delta (δ)).

Using an in-house antibody against a region present in all the isoforms and located at the N-terminus of human GLI2, these alpha / beta (α/β) and gamma / delta (γ/δ) isoforms have been detected by Western Blot (Tanimura et al., 1998) in Hut 102

cells (Fig 3.7). This antibody was raised against amino acids 1 to 506 of human GLI2; bearing in mind that the full-length GLI2 was only discovered afterward, that would mean the region recognised would correspond to amino acids 328 to 834 (328 + 506 = 834): nonetheless, all the isoforms would be recognised. This observation could offer a possible explanation of the discrepancy between the predicted molecular weights of alpha (α) plus beta (β), around 133 kDa, and the migration observed upon Western Blot analysis, around 155 kDa (Fig 3.11) (Tanimura et al., 1998). GLI2 N-terminal domain, discovered in 2005, is composed of 328 amino acids (Roessler et al., 2005); considering the average molecular weight of one amino acid to be around 135 daltons (da), 328 amino acids would amount to approximately 44 kDa. These additional 44 kDa would make GLI2 molecular weight about 170 kDa; a similar case could be made for gamma (γ) plus delta (δ) isoforms, which would go from 88 to 120 kDa. This observation highlights how molecular weights should be interpreted with caution.

GLI2 protein isoforms were described by Tanimura et al. using Hut102, a T-cell lymphoma cell line grown in media containing 10% serum. Of note, a lower molecular band is detected by Western blot, which is hyphothesised to be a degraded fragment of GLI2 but whose identity is not further investigated in the paper. It is tempting to speculate this band could be related to the one observed in N/Tert-1 keratinocytes grown in serum-containing media (Fig 3.1 and 3.2).

The antibody used for Western Blotting, GLI2 H-300 (Santa Cruz), is a rabbit polyclonal raised against amino acids 841-1140 mapping near the C-terminus of human GLI2; all known GLI2 isoforms mRNA encode this region and therefore this antibody could recognise all protein variants. Other commercially available antibodies against human GLI2, though raised against different sequences, also recognise all isoforms. If a similar pattern of band would be observed by Western Blot analysis using a different GLI2 antibody this would confirm the specificity of the bands observed.

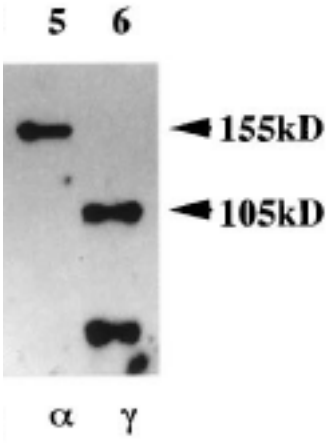

Figure 3.11: Identification of protein isoforms of human Gli2 in Hut102 cells by Western blot analysis (Adapted from Tanimura et al., 1998).

Discriminating between alpha (α) (133 kDa) and beta (β) (131 kDa) and between gamma (γ) (88 kDa) and delta (δ) (86 kDa) by Western Blotting is not a feasible approach as the difference in molecular weight is tiny; even if a specific antibody against those 17 amino acids could be generated, differences in migration would not be appreciable on a Western Blot. However, an antibody whose epitope would fall in the region between positions 1158 and 1586, which are missing in the gamma (γ) and delta (δ) isoforms, would only recognise the alpha (α) and beta (β) isoforms and could be used by immunoprecipitation to specifically separate these isoforms.

The identity of the novel GLI2 bands observed in N/Tert-1keratinocytes (Fig 1.8, 3.1) remains to be addressed, as discussed below. Nonetheless, would they be proven to be novel GLI2 isoforms, targeted antibodies could be generated that would recognise only one or a specific subset of isoforms based on the differences in their sequence. It is likely that those antibodies will need to be custom-made, as commercially available antibodies are generally raised against conserved sequences.

Upon GLI1 overexpression, disappearance of the main GLI2 band is accompanied by appearance of lower molecular weight bands that could be either degradation productions or differentially induced novel isoforms. To distinguish between these two possibilities proteasome inhibitors like MG-132 could be used; if the low molecular weight bands would not disappear after MG-132 treatment they are likely

to be novel GLI2 isoforms. Another possible approach would be using immunoprecipitation (IP) followed by mass spectroscopy (MS) to see if the bands are yet unidentified variant of the GLI2 protein. Specificity of the bands observed could be further investigated by performing short interfering RNA (siRNA) experiments. For siRNA experiments, different harpins against different regions of GLI2 mRNA could be needed: if a harpin targets a region which is not present in the putative short new isoform, the correspondent mRNA would not be targeted for degradation. Consistent with the hypothesis of the existence of yet unidentified GLI2 isoforms, novel alternatively spliced forms of GLI2 generated by skipping exon 3, or exons 4 and 5 were recently reported (Speek *et al.*, 2006). These variants were shown to be differentially expressed in normal human tissues and in a panel of cell lines; the presence of these transcripts could be investigated in PrEc and N/Tert-1 cells by RT-PCR. Serial analysis of gene expression (SAGE) analysis could also be perform in order to identify novel GLI2 isoforms; this technique relies on bioinformatics to predict novel splicing variants that can be subsequently validated by RT-PCR using specifically designed primers.

Previous work in the lab revealed GLI1 expression from a pBabe plasmid is able to downregulate GLI2 protein levels in both primary prostate cells (work performed by Mr Sandeep Nadendla, Fig. 1.7) and N/Tert-1 immortalised keratinocytes (work performed by Dr. Graham Neill, Fig. 1.8). Of note, in both experiments cells were grown in serum-free media (SFM). When I started this project, N/Tert-1 keratinocytes were routinely cultured in serum-containing media (KGM, 10% FCS). This choice was made as maintaining expression of ectopic proteins (GLI1 and GLI2ΔN) during serial passage was not possible in cells cultured in SFM (Neill et al., unpublished results). In the experiments I performed, GLI2 downregulation upon GLI1 overexpression in N/Tert-1 keratinocytes grown in serum-containing media (KGM) appears to be strong when cells are transduced with the EGFP – EGLI1 system (which is based on pSIN vectors, Fig. 3.1); this phenomena, although less evident, is still observed when cells are transduced using the pBabe system (Fig. 3.3). Moreover, GLI2 expression pattern as well as the extent of GLI2 downregulation in N/Tert-1 keratinocytes differs from cells grown in serum-free media. A strong band of around 50 kDa (thought to be a GLI2 novel isoform or degradation product) is specifically observed in 10% serum and downregulated upon GLI1 expression in

EGFP-GLI1 cells but not affected in pBGLI1 keratinocytes (cf. Fig. 3.1 and Fig. 3.3). A different putative GLI2 novel isoform / degradation product, whose molecular weight is intermediate between endogenous and ectopic GLI2, is specifically observed in pBGLI1 keratinocytes only when grown in serum-free media (cf. Fig. 1.8 and Fig. 3.3). Since, as mentioned before, two different expression system were used (pBabe or pSIN – based vectors) those differences cannot be solely attributed to the presence or absence of serum, although it definitely has an influence: it has been shown serum plays a role in regulating GLI protein levels (as suggested by the fact that ectopic GLI expression is lost upon passaging in SFM); moreover, serum-modulated cellular pathways such as RAS and EGFR are known to influence GLI protein activity (Riobo et al., 2006a; Lauth and Toftgard, 2007; Schnidar et al., 2009). The expression system used also plays a role in the intracellular levels of ectopic GLI1, and therefore on its ability to downregulate GLI2. The EGFP – EGLI1 system is based on the pSIN vector (Neill et al., 2008) and ectopic gene expression is driven by the cytomegalovirus (CMV) promoter, whereas in the pBabe system the viral Long Terminal Repeats (LTR) act as the promoter; LTR are prone to be methylated, which results in loss of gene expression. GLI1 expression levels using pBabe may be lower compared to EGFP – EGLI1: if we assume the negative feedback loop only operates at high GLI1 levels (e.g. over a certain threshold), it could explain why GLI2 downregulation is not as effective. In addiction to the intracellular amount of GLI1, the level of its transcriptional activity could influence its ability to downregulate GLI2; as mentioned before, there are evidences GLI protein activity is dependent on the culture media used. In the latest experiments (Fig. 3.4 and Fig 3.10), GLI1 mRNA levels were measured by qPCR: although in N/Tert-1 pBGLI1 keratinocytes there is an increase of about 6 folds (logarithmic scale) compared to pBabe control (Fig. 3.4), higher levels of GLI1 may be required for effective GLI2 downregulation (moreover, measured mRNA levels may be different from protein levels due to post-transcriptional regulation mechanisms). qPCR for the GLI target gene PTCH1 was also performed in order to evaluate how active GLI1 was in these cells: an increase in PTCH1 mRNA of about 3 fold (logarithmic scale) was observed in N/Tert-1 pBGLI1 keratinocytes compared to pBabe control (Fig 3.4). This increment, although informative about the fact GLI1 is indeed active in these cells, may not be sufficient to strongly inhibit GLI2

expression and therefore explain why only a partial reduction in GLI2 protein levels is observed in N/Tert-1 pBGLI1 keratinocytes (Fig. 3.3).

Virtually no PTCH1 induction was observed in NEB1 pBGLI1 and NEB1 pBGLI2ΔN cells, suggesting GLI proteins are not very active (Fig 3.10); therefore, NEB1 keratinocytes were not analysed further.

Immunofluorescence cytochemistry experiments performed on N/Tert-1 pBabe, N/Tert-1 pBGLI1 and N/Tert-1 pBGLI2ΔN keratinocytes confirmed GLI1 or GLI2 overexpression (respectively) as well as highlighting heterogeneity in GLI protein levels and localisation (Fig 3.5 – 3.8). No clear GLI2 staining intensity decrease was observed in pBGLI1 cells compared to N/Tert-1 and pBabe cells (Fig 3.7 b, 3.8). Although this result slightly differs from what has been observed by Western Blotting, it is most likely due to the heterogeneity in GLI2 staining intensities (Fig 3.7 c). While immunofluorescence is an informative technique regarding GLI protein staining heterogeneity and localisation, it is focused by its nature on detecting phenomena at cellular level; in Western Blotting, on the other hand, a substantial number of cells is analysed and may therefore be more informative on what happens in the whole cell population.

In conclusion, despite the differences in the magnitude of GLI2 downregulation upon GLI1 expression (due to the different expression systems and growth conditions are used), this phenomena was observed in both prostate cells (Fig. 1.7, Mr Sandeep Nadendla work) and N/Tert-1 keratinocytes (Fig 1.8 and this Chapter). This unexpected result questions the existence of a positive feedback loop between GLI1 and GLI2 in human Basal Cell Carcinoma, which had been proposed based on mRNA levels. Consistent with this hypothesis, another project in the group (M. Rahman et al., unpublished results) has shown that PTCH1 suppression in NEB1 human keratinocytes leads to an increase of GLI1 but not GLI2 mRNA. In order to address the biological relevance of these preliminary data, the GLI1-GLI2 interplay was analysed ex-vivo by immunostaining of normal human skin and Basal Cell Carcinoma samples; to our knowledge, this is the first study to address GLI proteins expression in a large number of BCC tumors (see Chapter 4).

Chapter 4

4 Immunohistochemical staining for GLI proteins in Normal Human Hair Bearing Skin and in Basal Cell Carcinomas

4.1 Introduction

The Hedgehog pathway (HH) and GLI transcription factors have been shown to be involved in hair follicle development (St-Jacques et al., 1998; Chiang et al., 1999), hair regeneration (Sato et al., 1999; Wang et al., 2000b) and Basal Cell Carcinoma (BCC) etiology (Daya-Grosjean and Couve-Privat, 2005).

Overexpression of either GLI1 or GLI2 in mouse or frog skin lead to the development of BCC-like tumors. (Dahmane et al., 1997; Grachtchouk et al., 2000; Nilsson et al., 2000; Sheng et al., 2002; Hutchin et al., 2005). At a molecular level, GLI factors are though to contribute to BCC tumorigenesis by opposing cell cycle arrest of keratinocytes (Regl et al., 2004a); moreover, GLI2 has been shown to induce anti-apoptotic genes and to repress genes associated with epidermal differentiation (Regl et al., 2004a; Regl et al., 2004b; (Kump et al., 2008). Whether GLI1 or GLI2 has a predominant role in the genesis of the tumours is still debated; moreover, there are only a few publications which have analysed GLI protein expression in human BCCs. GLI1 has been shown to be expressed in human BCCs by RT-PCR and in situ hybridization (Dahmane et al., 1997; Green et al., 1998). In a subsequent study, GLI1 protein was confirmed to be present in BCCs and was also observed in normal human skin, specifically in the outer root sheath of hair follicles and in a subset of surrounding mesenchymal cells. Of note, GLI1 was found to be expressed at higher levels in the ORS compared to tumour islands (Ghali et al., 1999). GLI2 was shown to be expressed in normal skin (interfollicular epidermis and outer root sheath of hair follicles) and also in BCCs by in situ hybridisation (Bonifas *et al.*, 2001; Ikram *et al.*, 2004). GLI2 mRNA was also detected in skin and BCCs using q-PCR (Regl et al., 2002) and GLI2 protein observed by immunohistochemistry in outer root sheath cells of hair follicles and one BCC (Regl et al., 2004b).

Most of these studies analysed GLI factors mRNA levels; GLI protein expression by immunohistochemistry has been performed on a limited number of samples. Studies were also hindered by the lack of commercially available antibodies against GLI proteins. Recently, different antibodies against GLI transcription factors have been made commercially available: some of these were tested and optimised for detection of GLI proteins by immunohistochemistry in normal human hairy skin and in BCCs. The aim of this chapter is to characterise GLI1 and GLI2 expression pattern at the protein level in a panel of human BCC samples in order to better understand their relevance to tumor development and to determine if there is any correlation with tumor aggressiveness. Details on antigens used to generate the different antibodies are highlighted in Appendix III.

4.2 Results

4.2.1 Lists of Human Hair Bearing Skin (NHS) and Basal Cell Carcinomas samples stained with antibodies against Hedgehog pathway components

A panel of Hair Bearing Skin (NHS) and Basal Cell Carcinomas samples were stained with antibodies against Hedgehog pathway components, as summarised in Tables 4.1 and 4.2 and described in the following sections.

Table 4.1: List of Hedgehog pathway antibodies optimised using Human Hair Bearing Skin Samples (NHS)

	NHS 1 Source: Abdominoplasty	NHS 2 Source: Facelift
Gli1 SC H-300	X	X
Gli1 SC C-18	X	
Gli1 R&D rat monoclonal	X	
Gli2 SC H-300	X	
Gli2 Abcam	X	
Gli1 R&D rat monoclonal + Gli2 Abcam	X	
Gli1 R&D rat monoclonal + SHH Abcam	X	

Table 4.2: List of all Basal Cell Carcinomas samples stained with different antibodies against Hedgehog pathway components

BCC Code	Histologic Subtype	Gli1 SC H-300	Gli1 R&D rat monoclonal	Gli2 SC H-300	Gli1 R&D rat monoclonal + Gli2 Abcam	Gli1 R&D rat monoclonal + SHH Abcam
AC 636	superficial	X			X	
AK 674	nodular	X	X		X	
AV 501	nodular	X		X	X	X
BB 638	nodular	X				
BD 641	nodular	X			X	X
DF 572	superficial	X				
DP 712	nodular	X				
DS 327	nodular	X	X		X	
EC M59	superficial				X	
EK F55	superficial				X	X
EL 652	nodular	X			X	
FP200	nodular	X			X	
GJ 106	nodular	X			X	X
HP 115	superficial	X				
JG 138	morphoeic	X				
JK 959	nodular	X				
JS 668	nodular / morphoeic	X				
JW 611	nodular	X				
LA 107	infiltrative	X				
MA 4BT	nodular	X				
MJ 120	micronodular	X			X	
MJ F26	infiltrative	X				
MM 596	nodular	X	X		X	X
MN 108	infiltrative	X				
NJ 646	morphoeic	X				
RP 201	nodular	X				
SL A01	nodular	X				
SP 430	nodular	X	X		X	X
SR 920	nodular / morphoeic					X
ST 002	nodular	X	X		X	X
SW M68	nodular	X				X
TT 686	nodular	X		X	X	X
WC M51b	nodular		X		X	X
WJ 140	nodular / micronodular	X			X	X
WS 922	nodular	X			X	X

4.2.2 Immunofluorescent staining of Normal Human Hair Bearing Skin with GLI1 (H-300) antibody

Frozen sections of normal human hairy skin obtained from an abdominoplasty (Fig 4.1 a, b) or a facelift surgery (Fig 4.2 a, b) were stained with the rabbit polyclonal antibody GLI1 H-300 (GLI1 H-300 sc-20687, Santa Cruz Biotechnology). This antibody has been raised against amino acids 781-1080 of GLI1 of human origin (C-terminus); these amino acids positions span a rather large region situated from the centre of the GLI1 protein to its carboxyl-terminal end (see Appendix III).

Consistent with previously published data (Ghali et al., 1999), GLI1 was found to be present in the outer root sheath of hair follicles and shows a predominantly cytoplasmic localization (Fig 4.1) with some perinuclear and nuclear staining observed in a few regions. In addition to the hair follicle, some positive staining was seen in the surrounding areas, which could be attributed to adjacent mesenchymal cells. This pattern of staining appears to be similar in both skin samples. The different intensity in the staining could be due to hair follicles being in different growing stages (Ghali et al., 1999). Of note, GLI1 staining is also present in the interfollicular epidermis, appearing to be stronger in the upper layers of the skin compared to the basal layer (Fig 4.1 b and Fig 4.2 a).

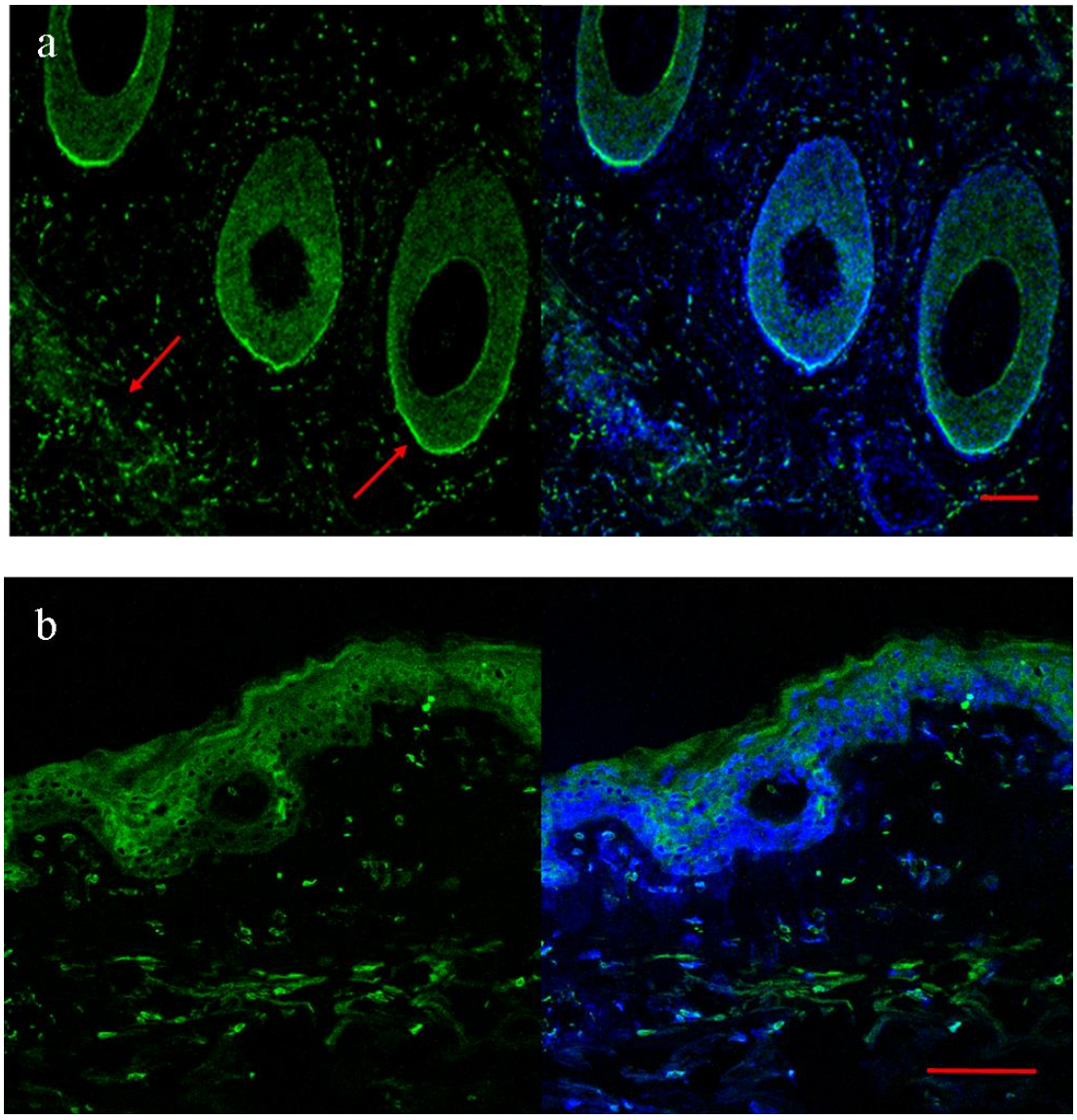

Figure 4.1: GLI1 expression in Normal Hair Bearing Human Skin derived from an abdominoplasty using GLI1 (H-300) antibody

Normal human hairy skin cryosections derived from an abdominoplasty (a, b) were stained with an antibody against a C-terminal epitope of GLI1; positive fluorescent signal is present in the epidermis and in outer root sheath of the hair follicle. GLI1 is predominantly cytoplasmic, with a few regions displaying nuclear localization. Some staining is also observed in the area surrounding the hair follicle, possibly due to the adjacent mesenchymal cells. Scale bar represents 50 µm.

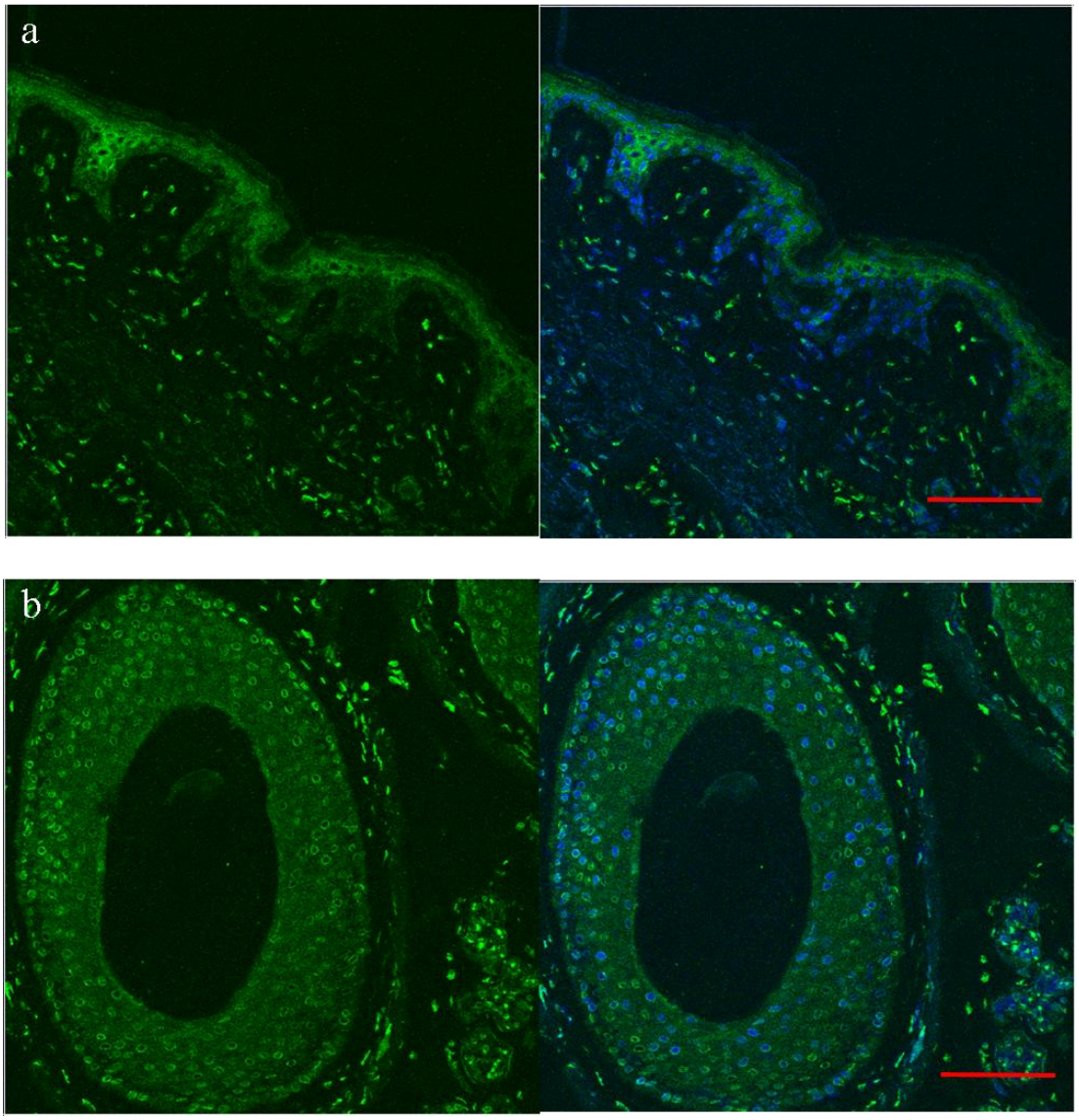

Figure 4.2: GLI1 expression in Normal Hair Bearing Human Skin derived from a facelift using GLI1 (H-300) antibody

Normal human hairy skin cryosections derived from a facelift surgery (a, b) were stained with an antibody against a C-terminal epitope of GLI1; positive staining is present in the epidermis and in outer root sheath of the hair follicle. GLI1 localization is predominantly cytoplasmic, with a few regions displaying nuclear localization. The staining pattern appears similar to the results observed in skin cryosections derived from an abdominoplasty (see Fig 4.1 a, b). Scale bar represents 50 µm.

4.2.3 Immunofluorescent staining of Basal Cell Carcinomas with GLI1 (H-300) antibody

A panel of 31 BCCs belonging to different subtypes (nodular (n=20), micronodular (n=1), morphoeic and infiltrative (n=5), superficial (n=3), nodular / micronodular (n=1), nodular / morphoeic (n=1)) was stained using the GLI1 H300 (Santa Cruz) antibody. Staining appears to be predominantly cytoplasmic with perinuclear or nuclear staining observed in some areas. Out of 31 BCCs analysed, 23 (belonging to different subtypes) showed GLI1 staining in the tumour and also in the adjacent stroma, with staining appearing to be higher in intensity in the stroma (Fig 4.3, 4.4, 4.5). In 8 BCCs GLI1 staining was mostly restricted to the epithelial component of the tumour, with GLI1 staining in the stroma absent or almost absent (Fig 4.6). There does not appear to be any correlation between the presence of GLI1 staining in the stroma and the BCC subtype, although since the vast majority of the samples belong to the nodular and micronodular subtypes (23 out of 31), no definitive conclusion could be reached (BCCs positive for stromal staining: nodular and micronodular n=15, nodular / morphoeic n=1, morphoeic n=2, infiltrative n=2, superficial n=3; BCCs negative for stromal staining, nodular and micronodular n=7, infiltrative n=1). Positive staining cells surrounding the neoplastic lesion are likely to be of mesenchymal origin as they stain with an antibody against vimentin (Fig 4.7). Vimentin is an intermediate filament protein generally found in cells of mesenchymal origin and was therefore used as a bona-fide marker to distinguish the epithelial and mesenchymal components of basal cell carcinomas. Figure 4.7 shows vimentin staining of a morpheaform BCC (JG 138); another section of the same tumour had previously been stained with GLI1 H300 (see Fig 4.5). Vimentin staining is located outside the dense tumour masses and appears to be superimposable to the GLI1 bright stained cells observed outside the BCC tightly packed tumour structures (Fig 4.5).

Out of 31 BCCs stained with GLI1 H-300 antibody, 8 (25%) showed weaker GLI1 staining in palisading cells compared to cells located at the centre of the tumour masses. Basal cell carcinoma samples in which the overlying epidermis was present were 13, and in 9 out of 13 (69%) GLI1 H-300 staining appeared to be weaker in the tumour compared to the epidermis

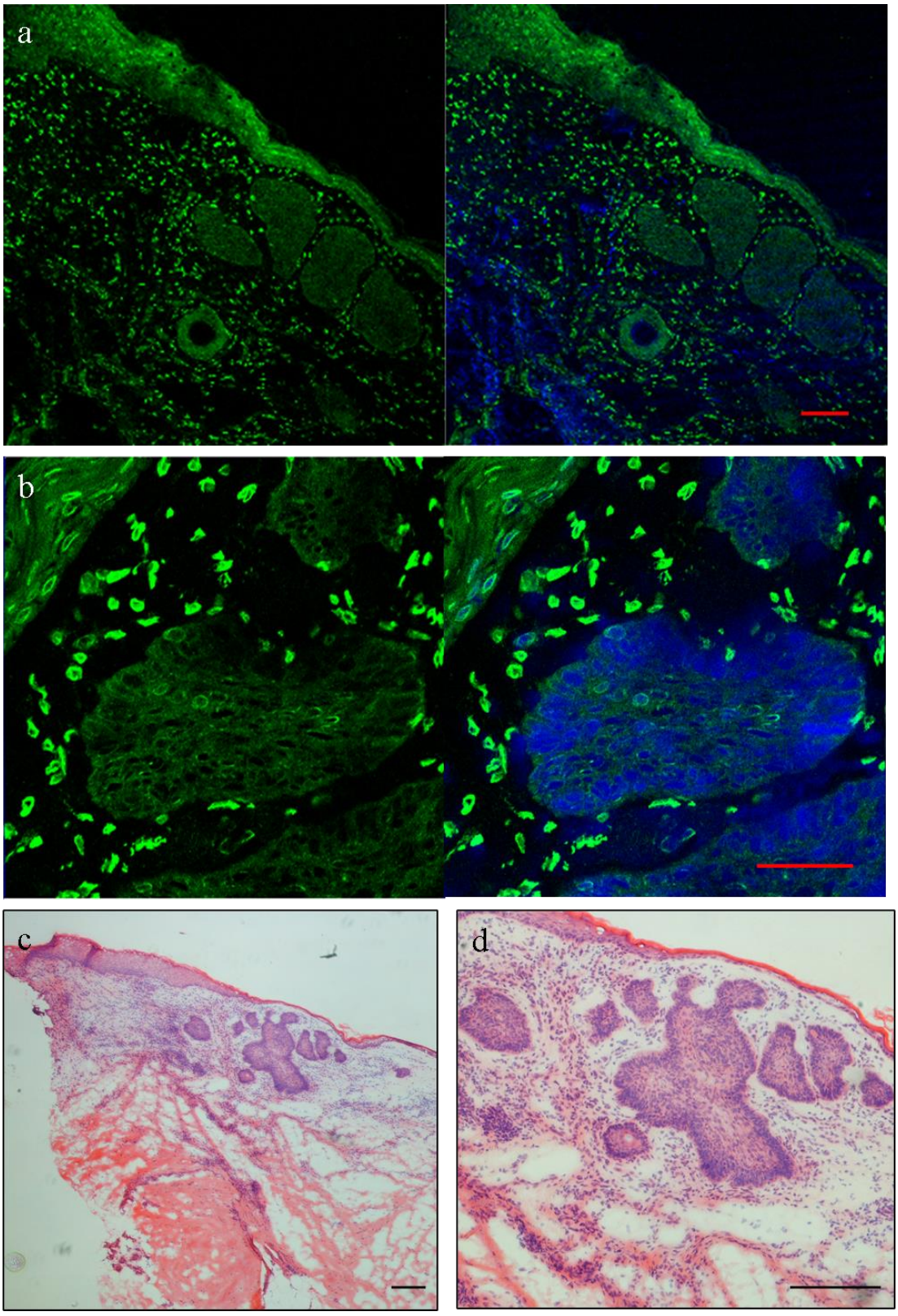

Please see figure legend on the next page

Figure 4.3: GLI1 H-300 antibody staining in a nodular Basal Cell Carcinoma and its surrounding stroma

Sections of BCCs belonging to different subtypes showing immunostaining for GLI1 in the epithelial and mesenchymal component of the tumour (Fig. 4.3, 4.4, 4.5, 4.6). Representative images are shown, with respective hematoxylin and eosin (H&E) staining of each tumour shown above the images. FP 200 – nodular BCC GLI1 staining (Fig 4.3 a, b) and H&E (Fig 4.3 c, d). Out of 31 BCCs analysed belonging to different subtypes, 23 (74%) showed positive GLI1 staining in the tumour and also in the stroma (representative images in Fig. 4.3, 4.4, 4.5). In 8 BCCs GLI1 staining appears to be restricted to the epithelial component (representative images in Fig. 4.6). Scale bar represents 50 µm in (a) and (b) and 200 µm in (c) and (d).

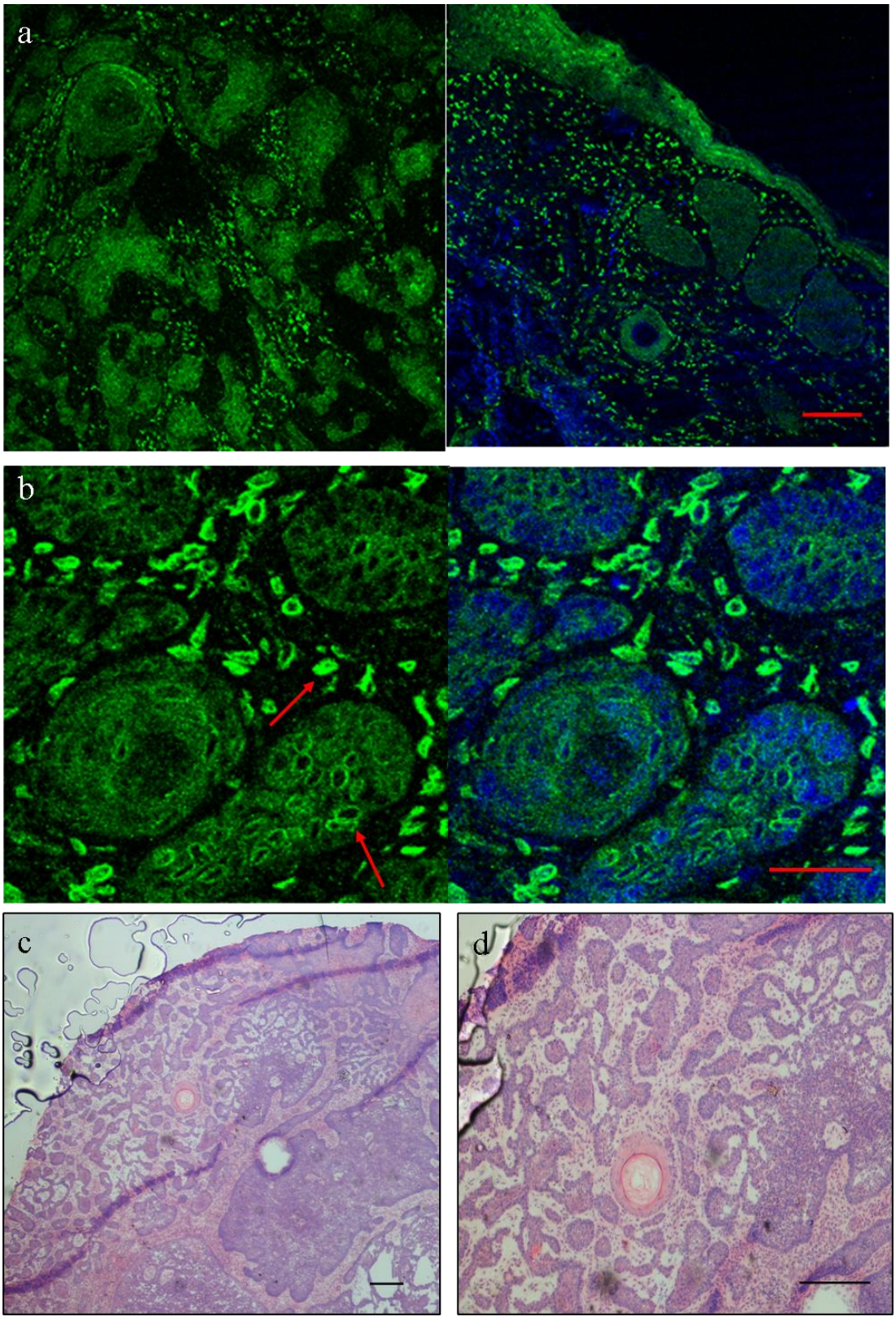

Please see figure legend on the next page

Figure 4.4: GLI1 H-300 antibody staining in a nodular/morpheaform Basal Cell Carcinoma and its surrounding stroma

Sections of a nodular/morpheaform BCC (JS 668) displaying immunostaining for GLI1 in the epithelial and mesenchymal component of the tumour. GLI1 staining (Fig. 4.4 a, b) and H&E staining (Fig. 4.4 c, d). Scale bar represents 50 µm in (a) and (b) and 200 µm in (c) and (d).

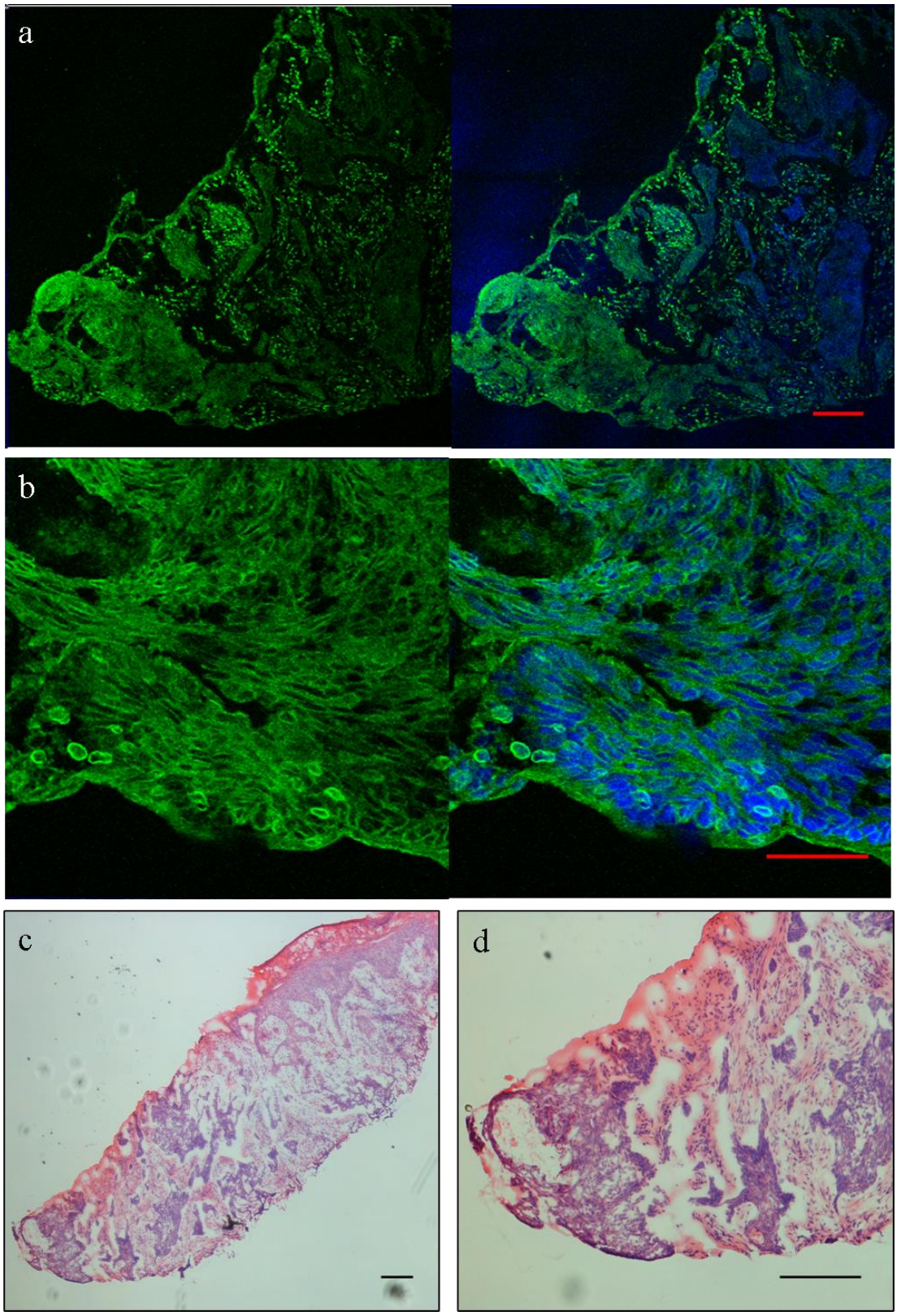

Please see figure legend on the next page

Figure 4.5: GLI1 H-300 antibody staining in a morphoeic Basal Cell Carcinoma and its surrounding stroma

Sections of a morphoeic BCC (JG 138) displaying immunostaining for GLI1 in the epithelial and mesenchymal component of the tumour. staining GLI1 staining (Fig. 4.5 a, b) and H&E staining (Fig. 4.5 c, d). Scale bar represents 50 µm in (a) and (b) and 200 µm in (c) and (d).

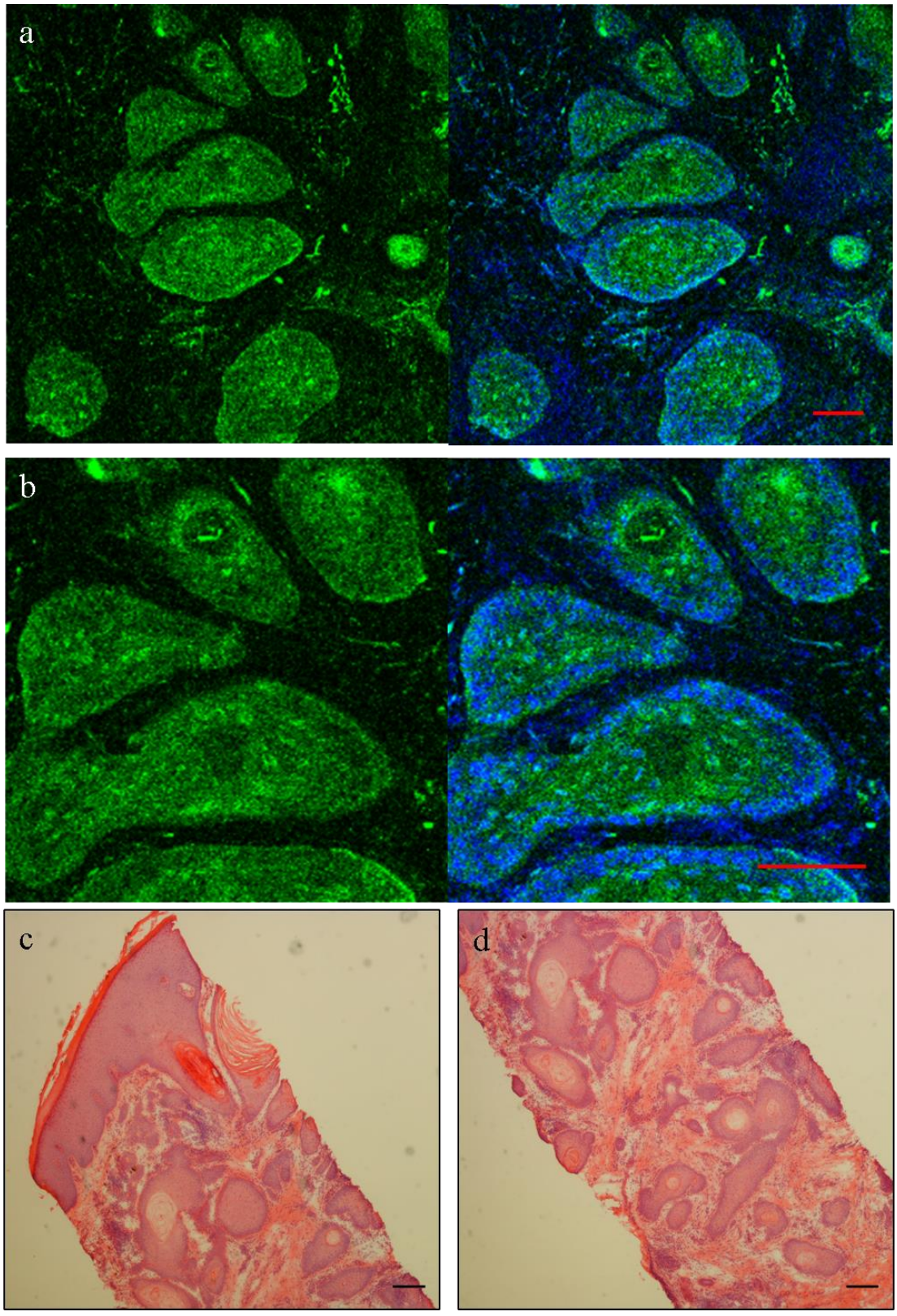

Please see figure legend on the next page

Figure 4.6: GLI1 (H-300) antibody staining in the epithelial component of a nodular Basal Cell Carcinoma

Sections of a nodular BCC (TT 686) displaying immunostaining for GLI1 restricted to the epithelial component of the tumour. GLI1 staining (Fig. 4.6 a, b) and H&E staining (Fig. 4.6 c, d). Scale bar represents 50 µm in (a) and (b) and 200 µm in (c) and (d).

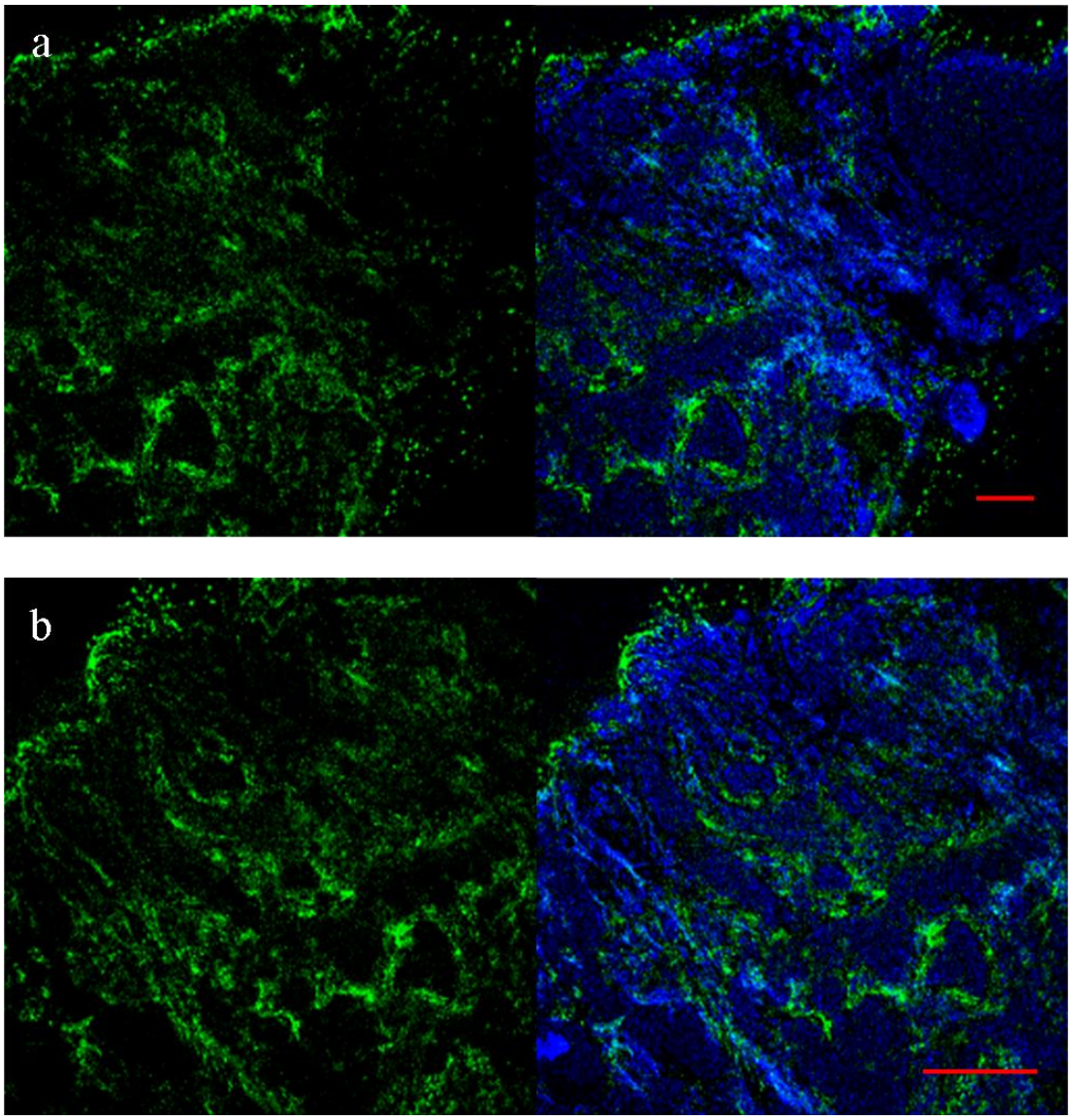

Figure 4.7: Vimentin staining in a morphoeic Basal Cell Carcinomas

Staining of a morphoeic BCC (JG 138) with an antibody against vimentin. Cells surrounding the tumour mass that show positive GLI1 immunostaining (see Fig. 4.5) were postulated to be of mesenchymal origin due to the expression of vimentin. Scale bar represents 50 µm.

4.2.4 Quantification of GLI1 (H-300) antibody staining in Basal Cell Carcinomas

Because of the brightness of GLI1 H-300 staining in the stroma of 23 out of 31 BCCs, we sought to quantify the intensity of the staining in the stroma compared to the tumour in these 23 samples.

Out of 23 samples, 17 were suitable for quantification purposes: the remaining 6 samples showed either similar staining intensity in the stroma and in the epithelia (n = 4) or the stromal component was difficult to highlight (n = 2) using the procedure described below.

The image processing software ImageJ allows quantification based on fluorescence intensity distribution: by setting threshold values, this method permits selection of the epithelial or the mesenchymal component of the tumour and determination of their specific intensities (Fig 4.8). To allow comparison between slides, each flourescence measurement was normalised against the black background. Analysis of the quantifiable 17 BCCs in which GLI1 is present in the mesenchyme as well as in the epithelia reveals a statistically significative difference ($P < 0.05$) between the two tumour components, with GLI1 fluorescence intensity in the stroma notably higher than in the tumour (Fig. 4.9) in the samples analysed. Student's t-Test (two-sample assuming unequal variance) was used for statistical analysis; the variance is assumed to be unequal as the tumours are derived from different individuals.

A possible explanation for this observation is the existence of a paracrine mechanism of HH signalling in BCCs. Paracrine activation of HH signalling in some types of cancer has recently been reported (Yauch *et al.*, 2008; Nolan-Stevaux *et al.*, 2009; Tian *et al.*, 2009) and has been shown to influence tumour growth. Alternatively, non-canonical activation of GLI transcription factors by transforming growth factor beta (TGFβ) has recently been described in human keratinocytes and fibroblasts (Dennler et al., 2007; Dennler et al., 2009); it could be responsible for the result observed and play a role in BCC tumorigenesis. To help distinguish between these two possibilities, BCCs samples were stained with an antibody against SHH (see section 4.2.11) to verify if SHH ligand was present in the tumour area and therefore could be responsible for paracrine HH signalling activation in the surrounding stromal cells.

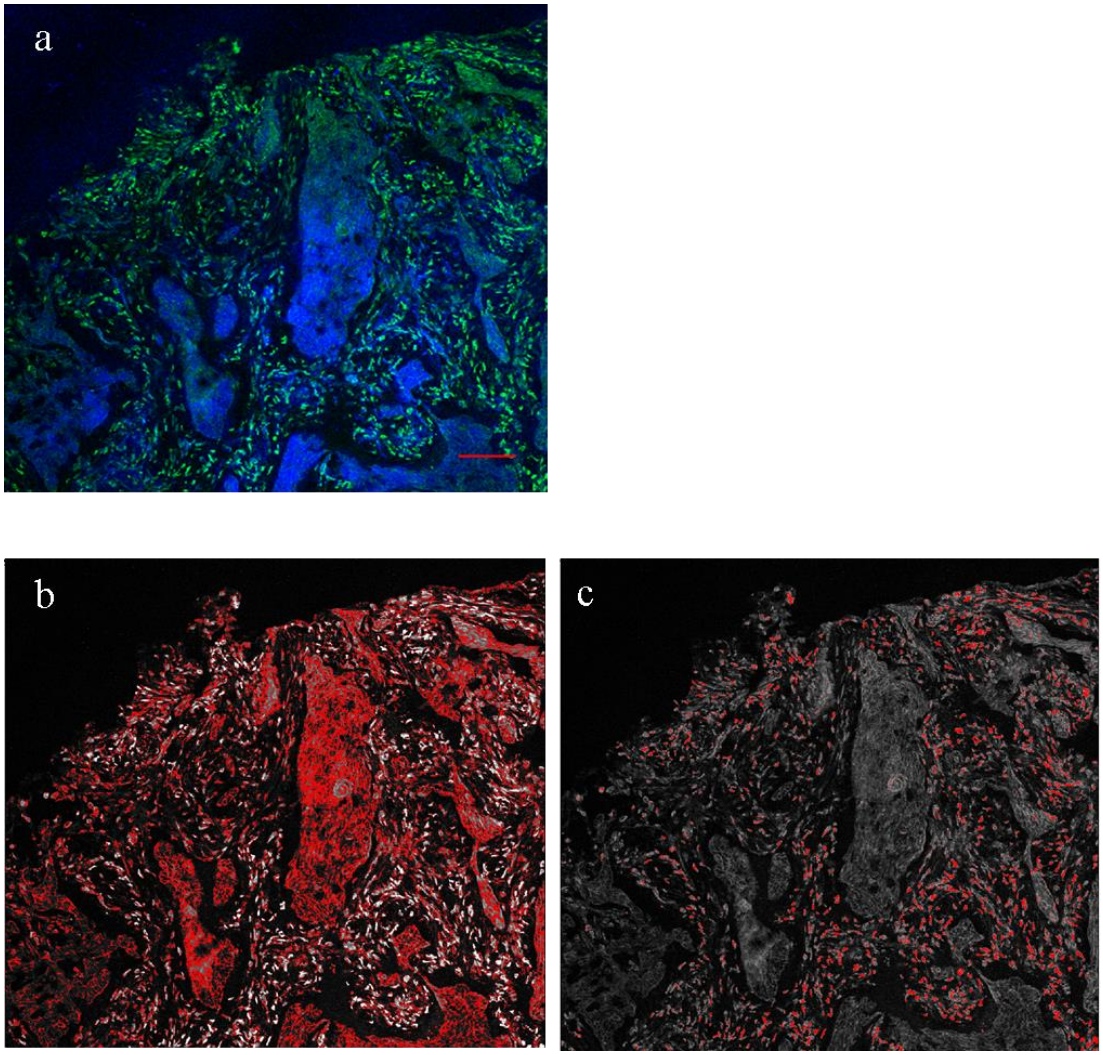

Figure 4.8: Measurement of GLI1 expression levels using the Image J software

Representative screenshots of the image processing software ImageJ highlighting either the epithelial (Fig. 4.8 b) or the mesenchymal (Fig. 4.8 c) component of the morphoeic BCC JG 138 stained with GLI1 H-300 (Fig. 4.8 a). Scale bar represents 50 µm.

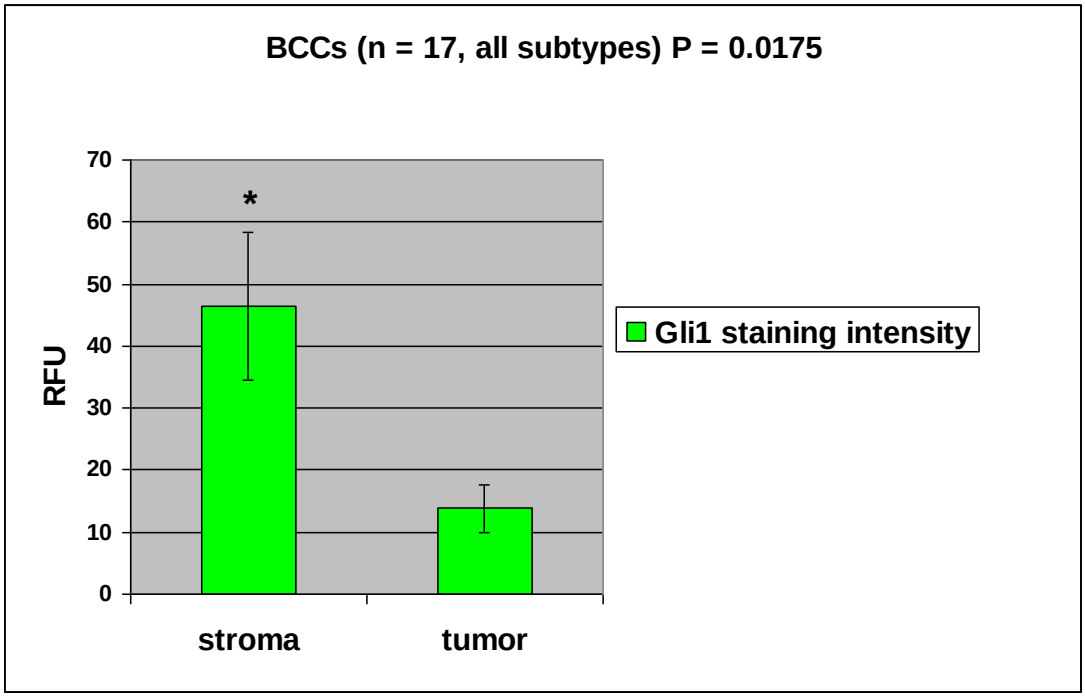

Figure 4.9: Quantification of GLI1 expression levels in a subset of 17 Basal Cell Carcinomas that showed positive staining in both stromal and epithelial components

Analysis of GLI1 fluorescence intensity in 17 BCC samples using the image processing software Image J reveals a statistically significative difference ($P < 0.05$) with staining intensity in the stroma notably higher compared to the tumour in the subset of samples analysed. Student's t-Test (two-sample assuming unequal variance) was used, data are expressed by means ± standard error (n=17). RFU = Relative Fluorescence Units.

4.2.5 Immunofluorescent staining of Normal Human Hair Bearing Skin with GLI1 (C-18) antibody

Frozen sections of normal hair bearing skin obtained from an abdominoplasty were stained with a different antibody against GLI1, GLI1 C-18 (GLI1 (C-18) sc-6152, Santa Cruz Biotechnology). GLI1 C-18 is a goat polyclonal antibody that maps within the range of amino acids 1056-1106 of GLI1 of human origin (C-terminus).
The epitope recognised is located within the last 50 amino acids of the human GLI1 protein. These 50 residues partly overlap with the longer amino acids sequence recognised by GLI1 H-300 (positions 781-1080, approximately 300 amino acids, for further details see Appendix III). Similarly to what has been observed with GLI1 H-300 antibody, positive staining is present in the different layers of the epidermis (Fig. 4.10 a) and also in the outer root sheath of the hair follicle (Fig. 4.10 b and also (Ghali *et al.*, 1999). However, staining of adjacent mesenchymal cells which was prominent with GLI1 H-300 appears to be almost non-existent with GLI1 C-18.
Further attempts to repeat staining with GLI1 C-18 gave inconclusive results, with widespread non-specific staining observed. Normal skin stained with a second batch of antibody showed positive green signal diffused throughout the epidermis and also into the dermis (Fig. 4.11 a, b). Figure 4.11 (a) and Figure 4.11 (b) show representative images of staining experiments performed on different days. A third batch of GLI1 C-18 was also tested and failed to give specific staining: green signal is faint and scattered through the dermis, with no staining present in the hair follicles (Figure 4.11 c). This inconsistency in staining results could be attributed to the high variability between batches of antibodies, even if purchased from the same company.

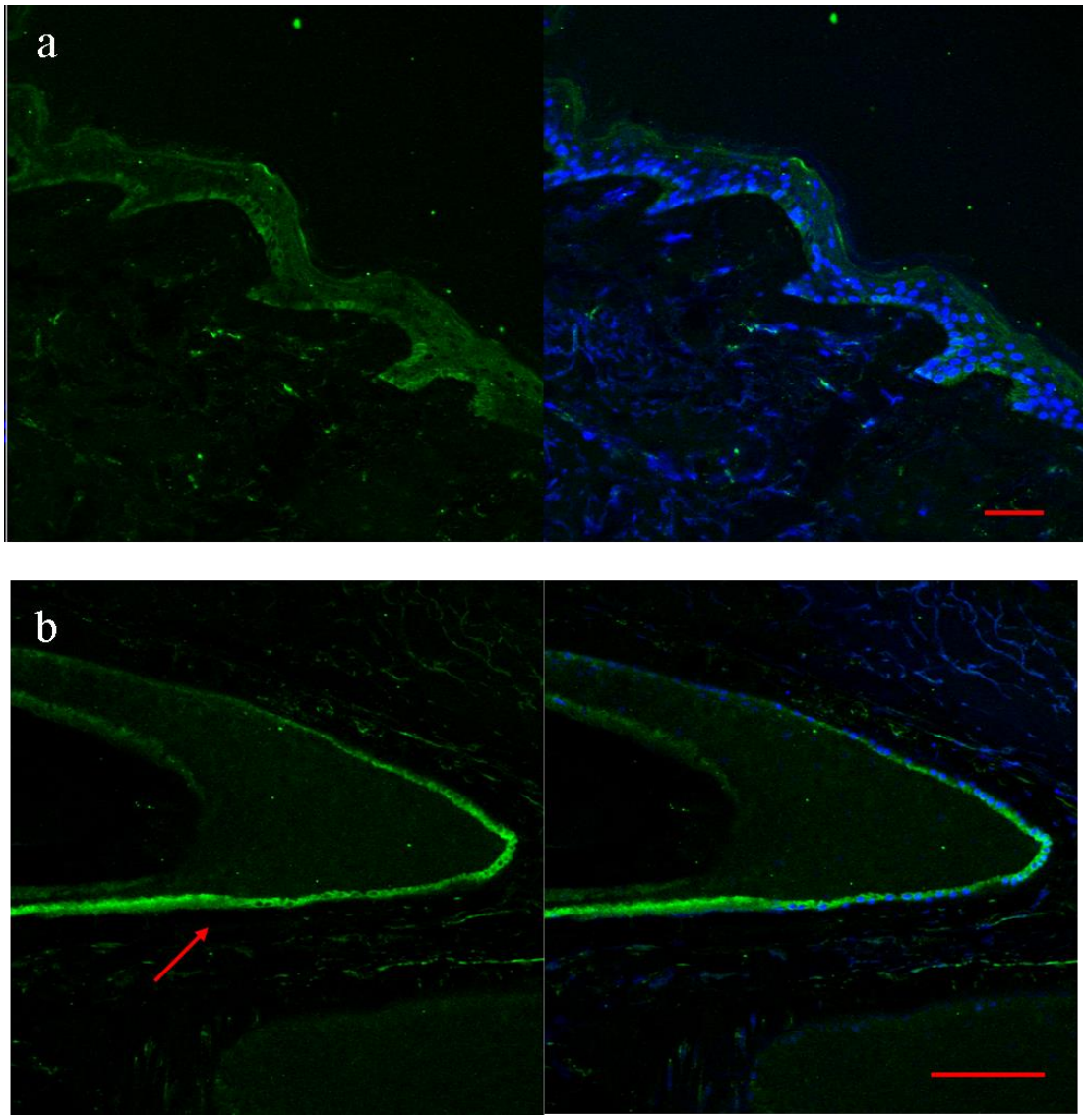

Figure 4.10: GLI1 expression in Normal Hair Bearing Human Skin using GLI1 (C-18) antibody (batch 1)

Normal human hairy skin cryosections were stained with GLI1 (C-18), an antibody that recognise the carboxyl-terminal end of the GLI1 protein; positive staining is present thorough the epidermis (a) and in the outer root sheath of the hair follicle (b). GLI1 localisation appears to be predominantly cytoplasmic. Skin was derived from an abdominoplasty surgery. Scale bar represents 50 µm.

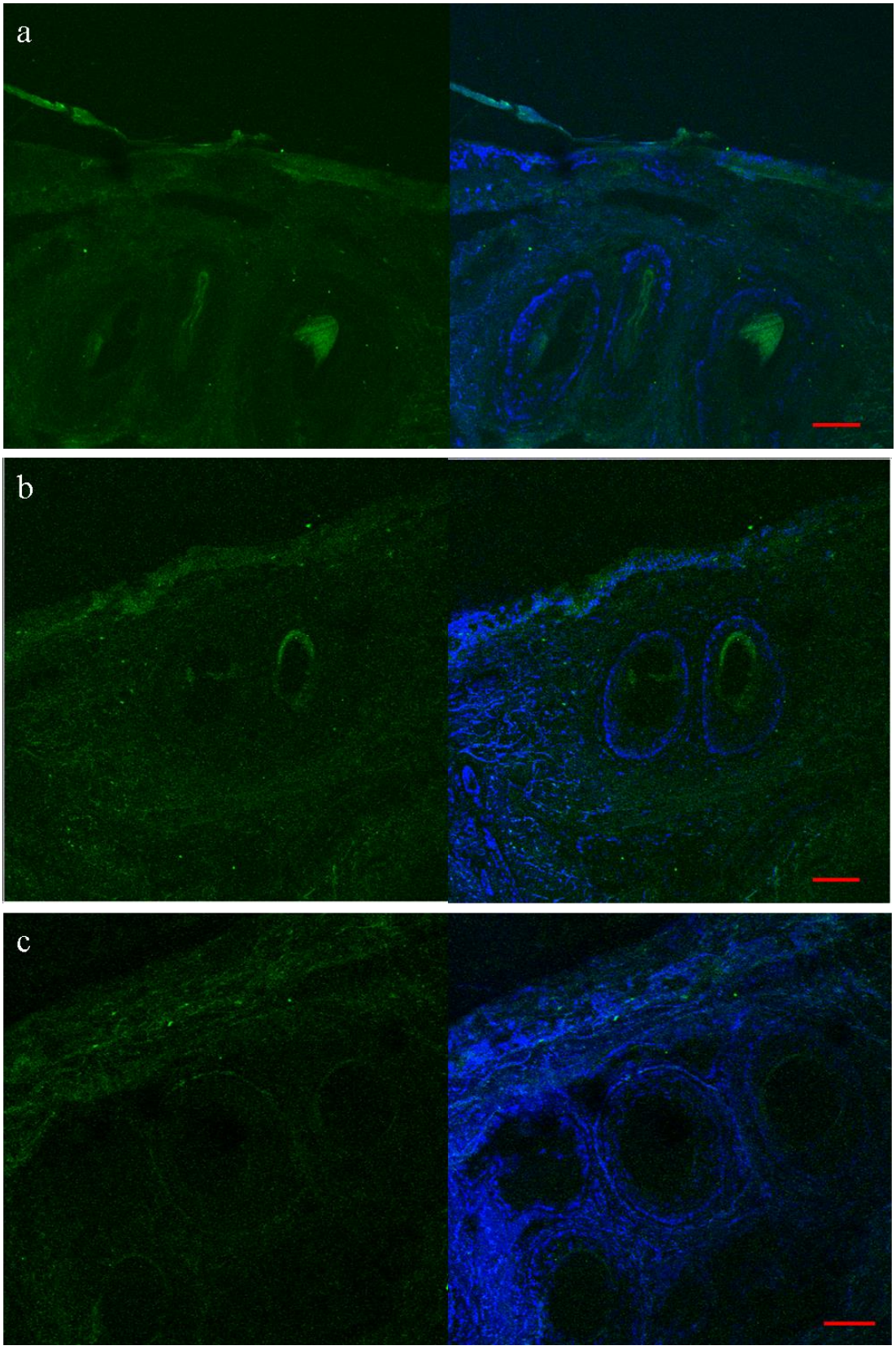

Please see figure legend on the next page

Figure 4.11: GLI1 expression in Normal Hair Bearing Human Skin using GLI1 (C-18) antibody (batch 2 and batch3)

Normal human hairy skin cryosections were stained with GLI1 (C-18), an antibody that recognise the carboxyl-terminal end of the GLI1 protein; two different batches of antibody were used, distinct from the one used for staining showed in Figure 4.10. No specific staining could be detected, with either batch 2 (Fig. 4.11 a, b) or batch 3 (Fig. 4.11 c). Figure (a) and (b) represent two different experiments using batch 2 and in both cases signal is diffused throughout the epidermis the dermis. Using batch 3 (Fig. 4.11 c), green signal is faint and no staining is present in the hair follicles. Skin was derived from a facelift surgery. Scale bar represents 50 µm.

4.2.6 Immunofluorescent staining of Normal Human Hair Bearing Skin with GLI1 (RD) antibody

Frozen sections of normal hair bearing skin obtained from an abdominoplasty were stained with a third antibody against GLI1. GLI1 RD (GLI1 MAB3324, R&D Systems) is a rat monoclonal antibody raised against amino acids 1-234 of GLI1 of human origin (N-terminus); contrary to the antibodies previously used (GLI1 H-300 and GLI1 C-18), GLI1 RD recognises the amino-terminal portion of human GLI1. GLI1 staining is present thorough the epidermis, although its intensity varies (Fig. 4.12 a); positive staining is also observed in the outer root sheath of the hair follicle (Fig. 4.12 b), similarly to the results obtained with GLI1 H-300 and GLI1 C-18. Staining appears to be predominantly cytoplasmic. GLI1 RD seemed not to be affected by problems of variability with different batches of antibodies and was therefore selected to perform double immunostaining experiments (see sections 4.2.10 – 4.2.11 and 4.2.15 – 4.2.16).

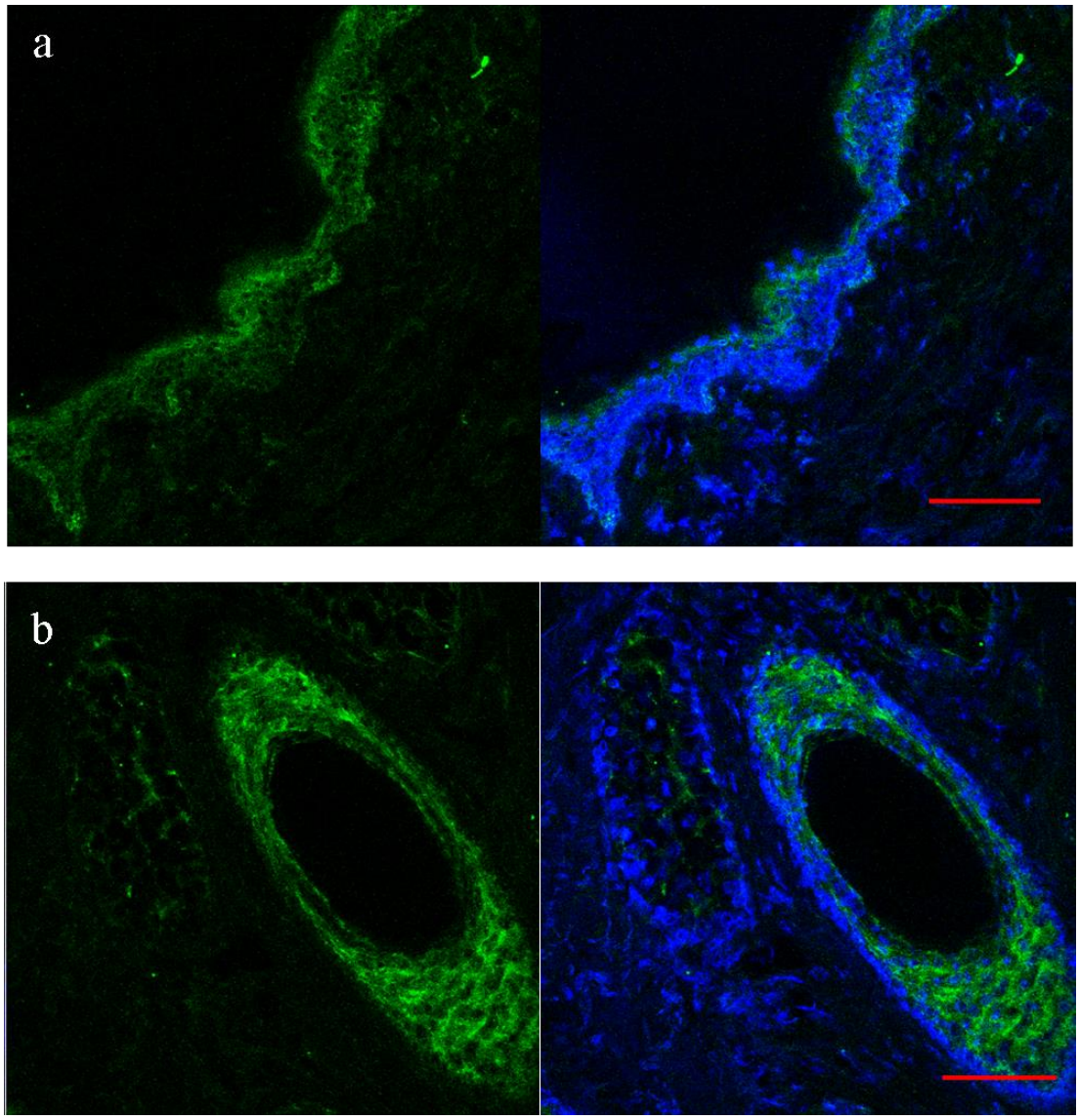

Figure 4.12: GLI1 expression in Normal Hair Bearing Human Skin using GLI1 (RD) antibody

Normal human hairy skin cryosections stained with GLI1 (RD), a monoclonal antibody raised against the amino-terminal end of GLI1. GLI1 staining is present in the different layers of the epidermis and diffuse throughout the root sheath of the hair follicles. GLI1 is mainly localised in the cytoplasm. Skin was derived from an abdominoplasty surgery. Scale bar represents 50 µm.

4.2.7 Immunofluorescent staining of Basal Cell Carcinomas with GLI1 (RD) antibody

Six Basal Cell Carcinoma samples, all belonging to the nodular subtype, were initially stained using the GLI1 RD antibody. Staining throughout the tumours appears to be predominantly cytoplasmic.

The GLI1 RD antibody was subsequently used to perform double immunostaining experiments with either Sonic Hedgehog (SHH) (see sections 4.2.10 and 4.2.11) or GLI2 (sections 4.2.15 and 4.2.16): taking into account those experiments a total of 20 BCCs were stained with GLI1 RD antibody. Of these 20 samples 4 (20%) showed weaker GLI1 staining in palisading cells (Fig. 4.13 b). The epidermis was present in 18 BCCs sections and in 9 of them (50%) GLI1 staining intensity appeared to be weaker in the tumour compared to the epidermis.

BCC samples that gave a stromal GLI1 immunofluorescence pattern with the GLI1 H-300 antibody were also analysed with GLI1 RD; contrary to what had been observed with GLI1 H-300, none of the 6 BCCs stained with GLI1 RD showed positive staining for GLI1 in the stroma.

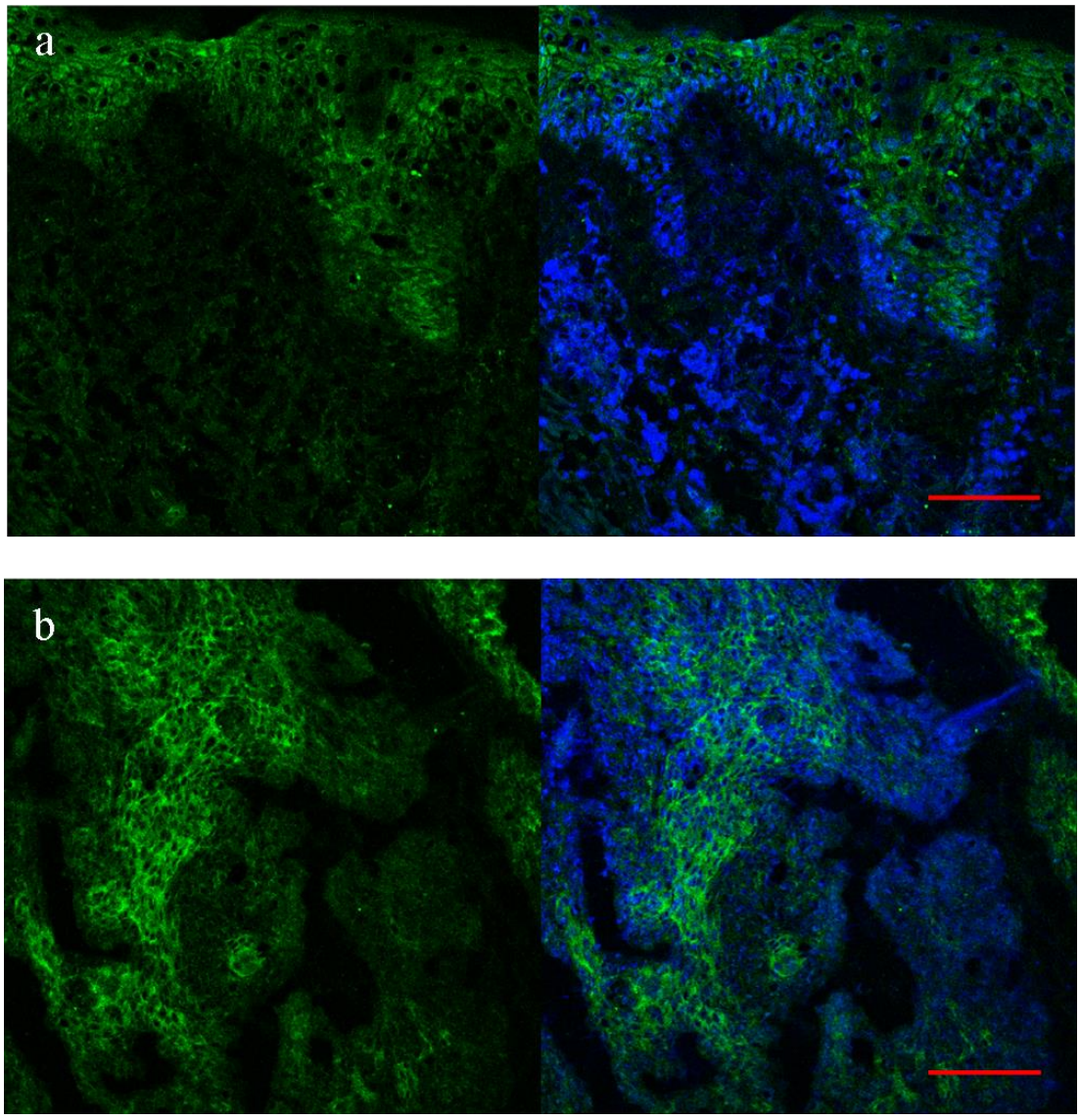

Figure 4.13: GLI1 (RD) antibody staining in Basal Cell Carcinomas

Sections of two BCCs stained with GLI1 RD antibody. Representative images are shown, (a) AK 674 and (b) DS 327, both nodular BCCs. GLI1 staining appears to be restricted to the epithelial component. Scale bar represents 50 µm.

4.2.8 DAB staining optimization of GLI1 and GLI2 antibodies on Normal wax-embedded Human Skin

Some of the GLI1 and GLI2 antibodies used for immunofluorescent staining were also tested and optimised to be used for DAB (3,3'-Diaminobenzidine tetrahydrochloride) staining on wax-embedded sections; this was done in order to take advantage of the large number of wax embedded BCCs conserved in the Pathology archive as well as eliminating logistic problems associated with working with frozen samples. DAB staining optimisation was carried out on wax-embedded normal skin sections.

In immunofluorescent immunohistochemistry the secondary antibody is linked with a fluorophore that allows the visualization of the antigenic sites in tissue sections, while in immunoperoxidase-based immunohistochemistry the secondary antibody is linked with the enzyme horseradish peroxidase (HRP). This enzyme catalyses hydrogen peroxide oxidation of the 3,3' Diaminobenzidine (DAB) substrate to yield a colored product which stains antigen-antibody sites brown (see also the Materials and Methods section).

Prior to wax-embedding, tissues are fixed in 4% (v/v) paraformaldehyde which results in cross-linking of the amino groups of proteins through the formation of methylene bridges. These methylene linkages need to be removed before staining as they could mask antigenic sites and therefore interfere with primary antibody binding. Antigen retrieval can be heat-mediated (using a waterbath or a microwave) or enzymatic. The composition and the pH of retrieval buffers in which the tissues are heated up could also be modified to obtain the best antigen retrieval conditions. Details of the antigen retrieval procedure are outlined in Table 2.4. Twelve different conditions were tested for each antibody, each consisting of a different combination of heating methods, time of incubation and pH variations in the retrieval buffer. Pictures of the conditions that gave the best results for each of the different antibodies are shown in Figures 4.14 - 4.17.

GLI1 H300, a polyclonal antibody that recognises the carboxyl-terminal end of human GLI1, gives a faint diffuse staining (both cytoplasmic and nuclear) thorough the epidermis which is best highlighted using condition 6 (Fig. 4.14 c); this condition was subsequently used to stain Basal Cell Carcinoma samples (see section 4.2.8).

GLI1 RD, a monoclonal antibody that recognises the amino terminal of human GLI1, also seems to work better using staining condition 6 (Fig. 4.15 b). This antibody gives a clearer staining which appears to be mainly nuclear and slightly stronger in the basal layer of the epidermis. GLI1 H300 and GLI1 RD antibodies were also used to stain wax-embedded Basal Cell Carcinoma samples using both fluorescence and DAB-based immunohistochemistry techniques (see section 4.2.8).

Two antibodies against GLI2 were also tested, GLI2 H-300 and GLI2 Abcam; GLI2 H300 recognise an epitope at the carboxyl-terminal end of human GLI2, while GLI2 Abcam epitope is located in the central region of the protein. For further details please see section Appendix III.

GLI2 H-300 staining is quite faint and mainly localised in the basal cell layer of the epidermis; this antibody seems to give similar results regardless of the condition used, though condition 4 seems to give a slightly clearer signal (Fig. 4.16 b).

GLI2 Abcam staining is stronger and more diffuse thorough the epidermis, with both nuclear and cytoplasmic localisation; condition 6 seems to combine good signal specificity and limited background stain (Fig. 4.17 c). GLI2 Abcam was also used in immunofluorescent staining experiments on frozen skin and Basal Cell Carcinomas samples (see section 4.3.8).

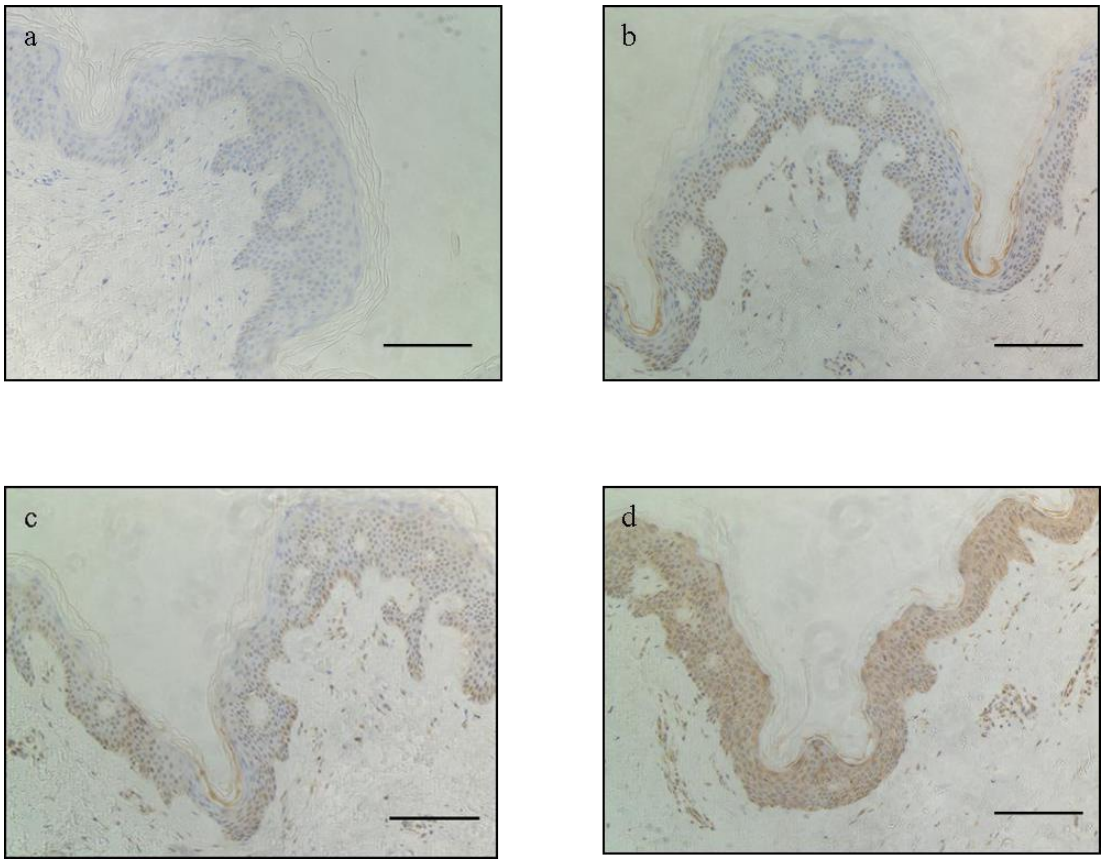

Figure 4.14: GLI1 (H-300) antibody DAB staining optimization on wax-embedded normal skin sections

DAB staining of normal wax-embedded skin sections with GLI1 (H-300) antibody. Representative images of 4 of the 12 conditions tested: (a) condition 2, (b) condition 4, (c) condition 6, (d) condition 10. Condition 6 (c) seems to combine good signal specificity with reduced level of background and was therefore subsequently used to stain Basal Cell Carcinomas samples. For details of staining conditions see Table 2.4. Scale bar represents 200 μm.

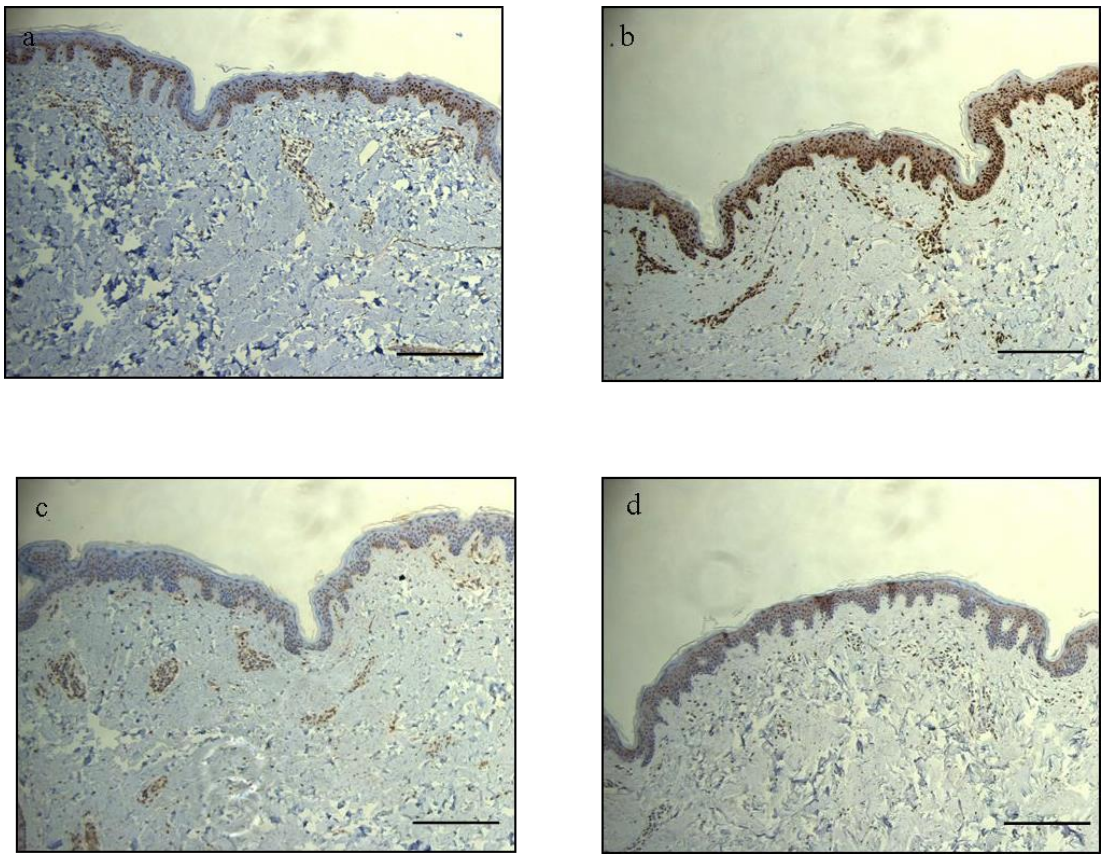

Figure 4.15: GLI1 (RD) antibody DAB staining optimisation on wax-embedded normal skin sections

DAB staining of normal wax-embedded skin sections with GLI1 (RD) antibody. Representative images of 4 of the 12 conditions tested: (a) condition 2, (b) condition 6, (c) condition 8, (d) condition 11. Condition 6 (b) seems to combine good signal specificity with reduced level of background and was therefore subsequently used to stain Basal Cell Carcinomas samples. For details of staining conditions see Table 2.4. Scale bar represents 200 µm.

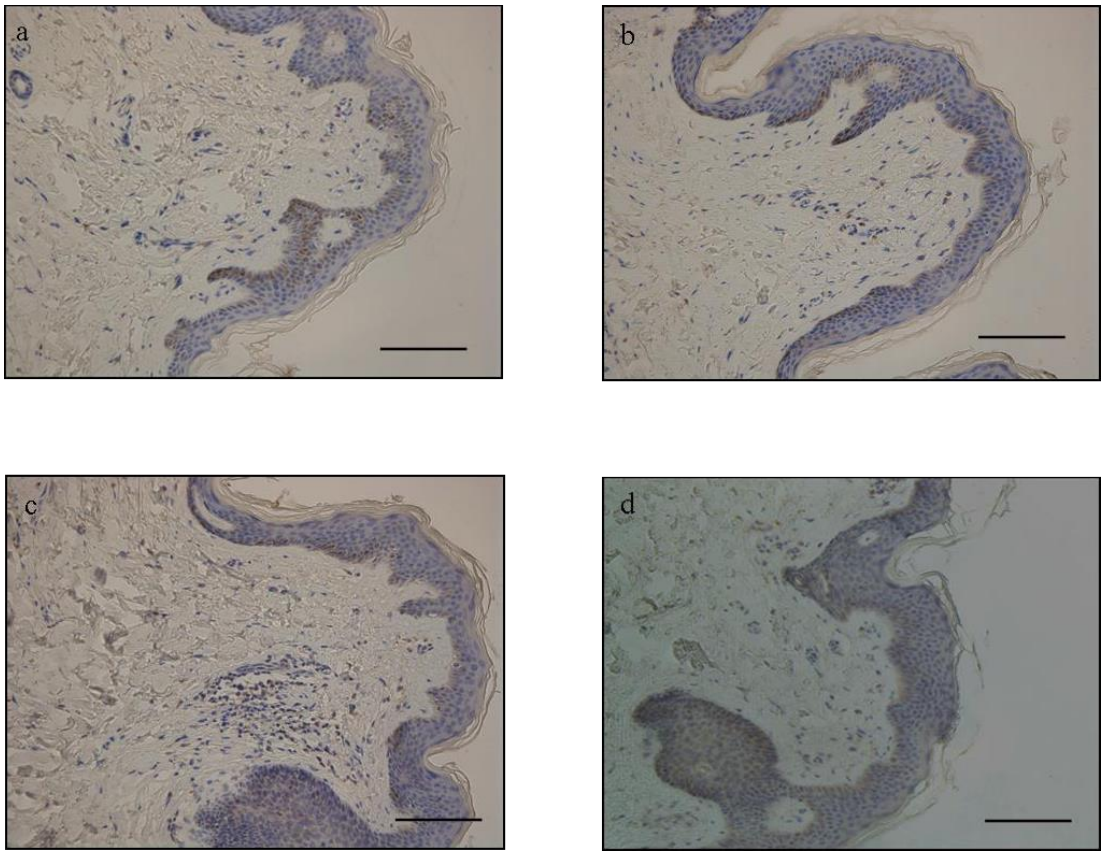

Figure 4.16: GLI2 (H-300) antibody DAB staining optimization on wax-embedded normal skin sections

DAB staining of normal wax-embedded skin sections with GLI2 (H300) antibody. Representative images of 4 of the 12 conditions tested: (a) condition 2, (b) condition 4, (c) condition 6, (d) condition 10. This antibody appears to work similarly in different conditions, though condition 4 (b) seems to give a slightly clearer signal. For details of staining conditions see Table 2.4. Scale bar represents 200 µm.

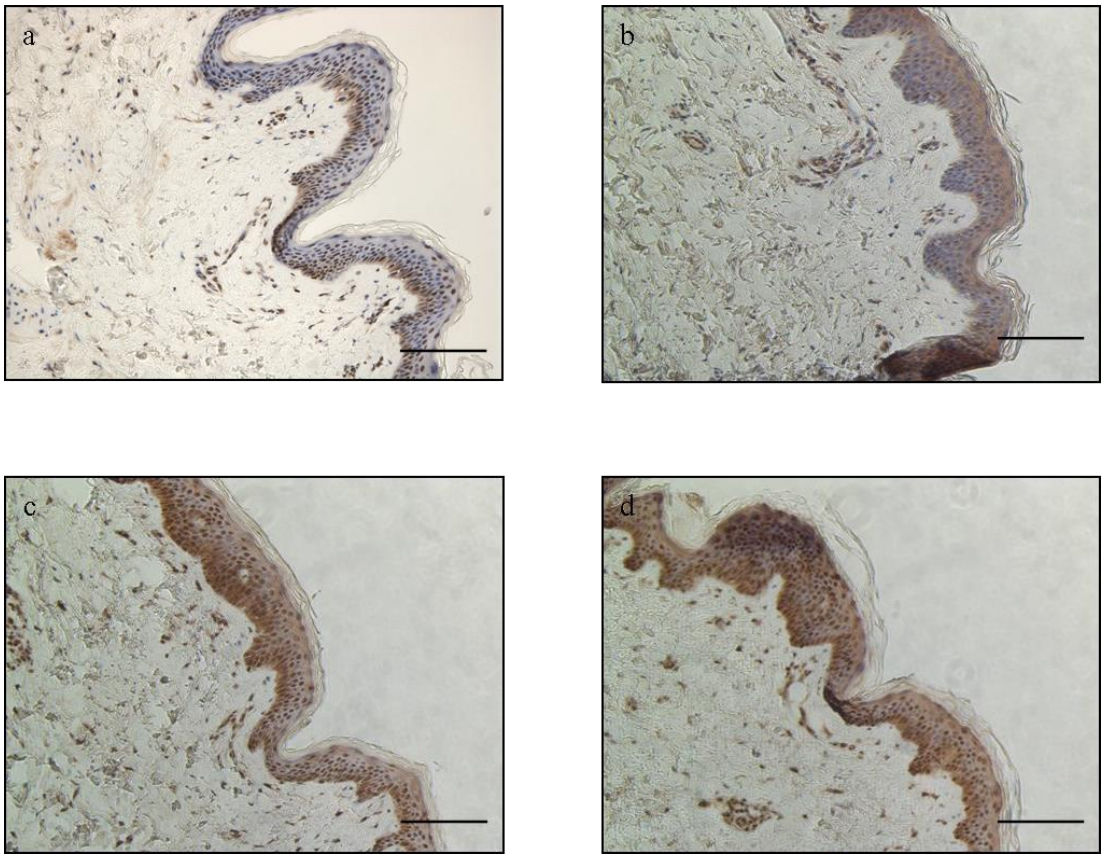

Figure 4.17: GLI2 (Abcam) antibody DAB staining optimisation on wax-embedded normal skin sections

DAB staining of normal wax-embedded skin sections with GLI2 Abcam antibody. Representative images of 4 of the 12 conditions tested: (a) condition 2, (b) condition 1, (c) condition 6, (d) condition 10 Condition 6 (c) seems to combine good signal specificity and a limited background stain. For details of staining conditions see Table 2.4. Scale bar represents 200 μm.

4.2.9 Comparison between immunofluorescent and DAB staining with GLI1 (H-300) and GLI1 (RD) antibodies using Basal Cell Carcinomas wax-embedded sections

Wax-embedded sections from two Basal Cell Carcinomas, one belonging to the nodular (8396A2) and one to the infiltrative (1759) subtype, were stained with either GLI1 H-300 (Fig. 4.18 and 4.19) or GLI1 RD antibody (Fig. 4.20, 4.21). For each antibody, both immunofluorescence and DAB-based immunohistochemistry were used. Two different batches of GLI1 RD antibody were tested to asses the impact of batch to batch variability, as this issue had arisen when other antibodies against GLI proteins were used. Pictures of immunofluorescence and DAB staining were taken of representative areas of both BCCs and overlying epidermis. Staining pattern appears to be overall similar with both techniques, though sometimes slightly fainter when DAB chemistry is used. No significative difference was observed using two different batches of GLI1 RD antibody. GLI1 H-300 is an antibody that recognises the carboxyl-terminal end of human GLI1, previously used for immunofluorescence on frozen sections and also optimised for use on wax-embedded section: condition 6 (see Table 2.4) was used to perform this staining experiment. With GLI1 H-300 antibody GLI1 staining is present in BCCs and also in all layers of epidermis, and its localisation appears diffuse in both the nucleus and the cytoplasm. GLI1 H-300 seems to work better in frozen sections, with staining on wax-embedded slides being overall fainter (Fig. 4.18 and 4.19 compared to Fig. 4.3 to 4.6). GLI1 RD, a monoclonal antibody that recognise the amino-terminal end of human GLI1, also used in immunofluorescence experiments, seems to work better on wax-embedded section using staining condition 6. GLI1 RD staining results are comparable using two different batches of antibody and overall similar to the staining pattern observed with GLI1 H-300, the only noticeable difference being the increased nuclear localisation with GLI1 RD (Fig. 4.20, 4.21). GLI1 staining is present in all layers of the epidermis and also in underlying BCCs tumour masses. GLI1 RD staining seems to be also present in the stroma when DAB chemistry is used, while this feature is not evident using immunofluorescence (Fig. 4.20, 4.21).

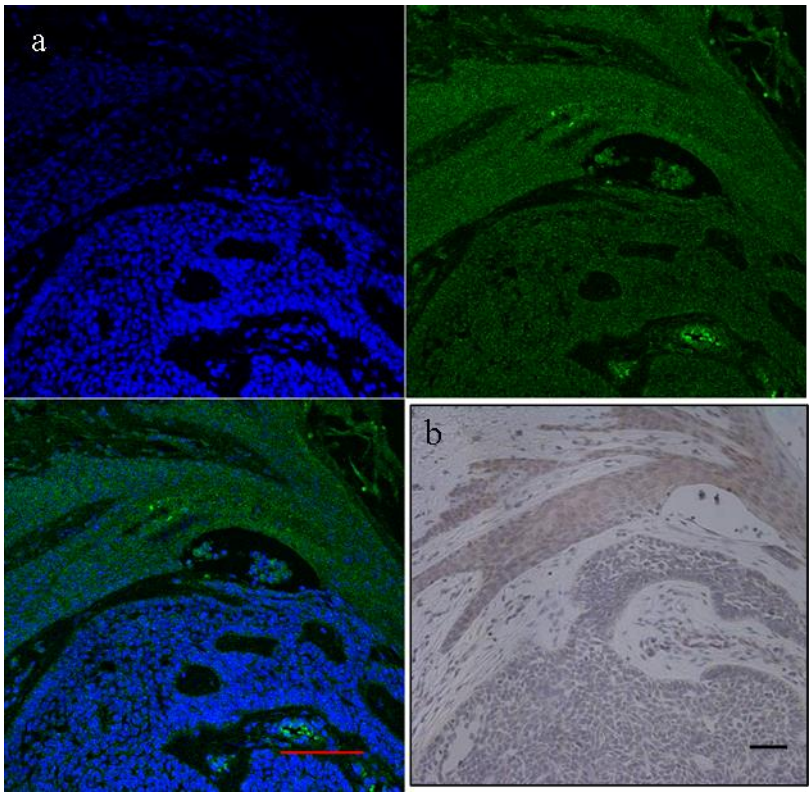
a
b

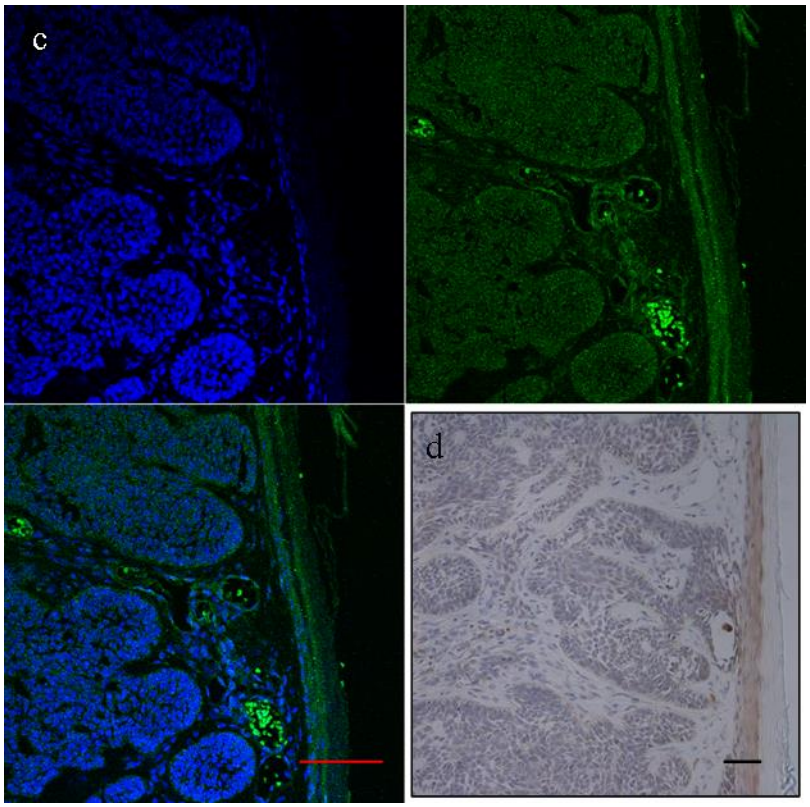
c
d

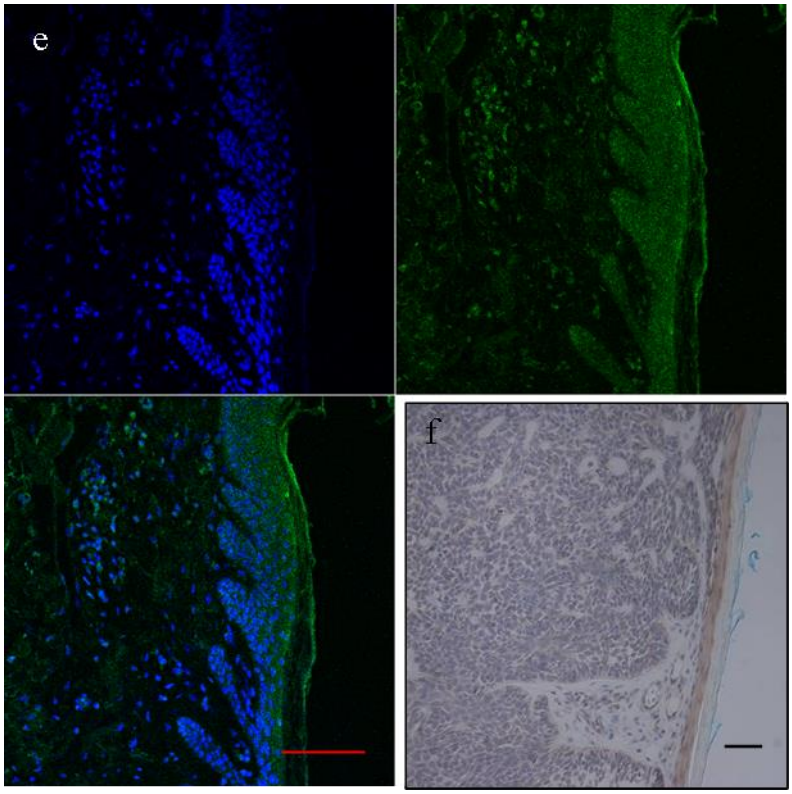

Figure 4.18: Staining of a nodular wax-embedded BCC using GLI1 (H-300) antibody

A nodular wax-embedded Basal Cell Carcinomas (8396A2) was stained using immunofluorescence (Fig. 4.18 a, c, e) or DAB-based immunohistochemistry (Fig. 4.18 b, d, f). Representative images of three different areas of the BCC are shown, with immunofluorescence staining juxtaposed to DAB staining (lower right panel). Staining pattern appears to be similar with both techniques, although slightly fainter when DAB chemistry is used. GLI1 staining is present in all layers of the epidermis and also in BCCs tumour masses, and its localisation seems to be diffused in both the nucleus and the cytoplasm. Scale bar represents 50 µm.

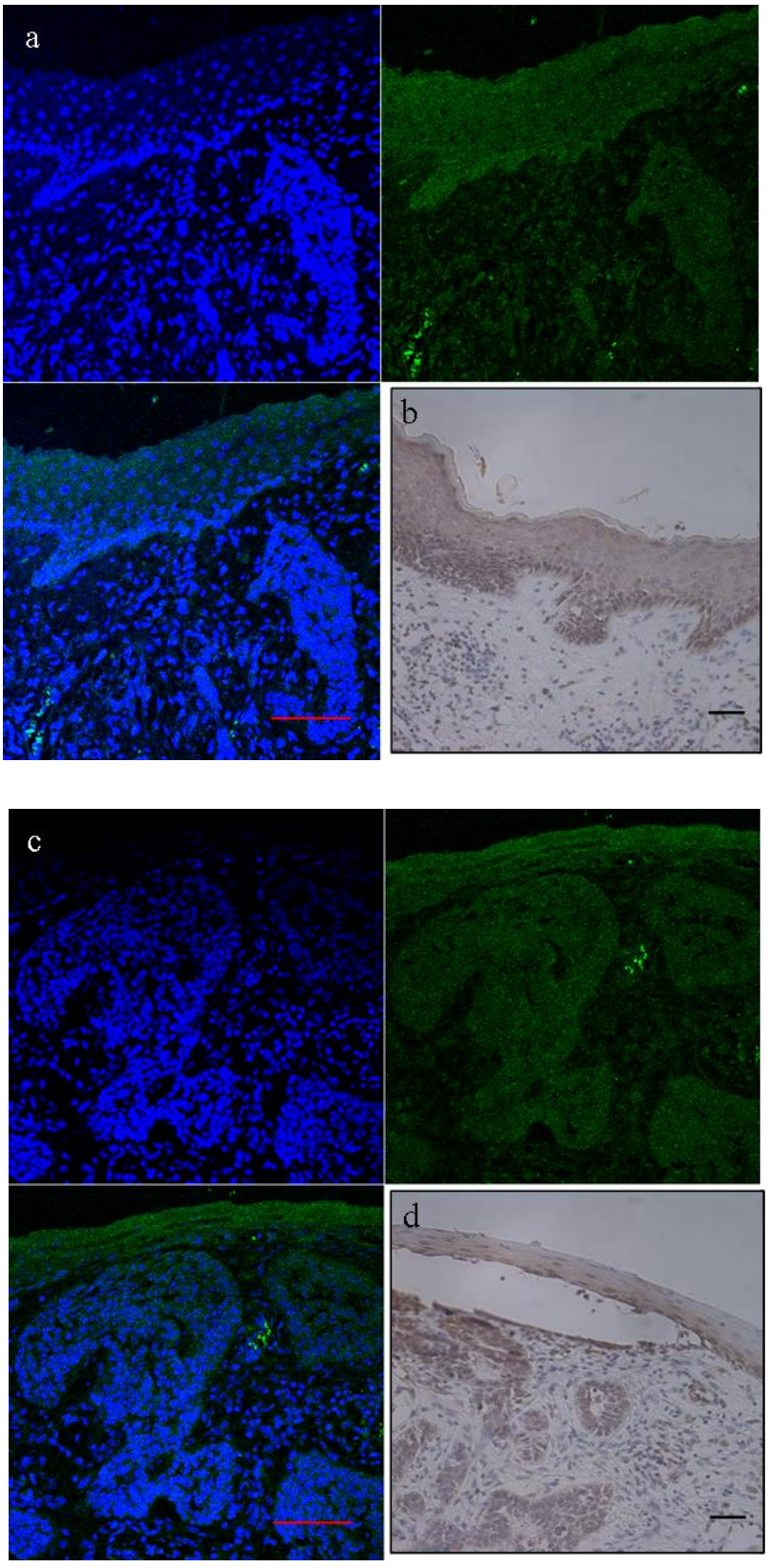
a
b
c
d

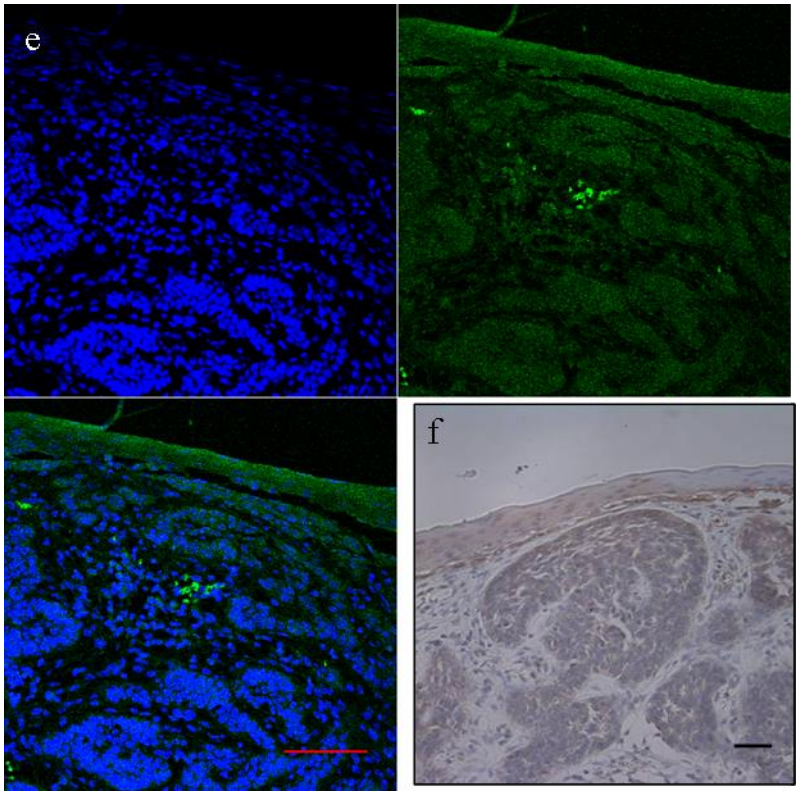

Figure 4.19: Staining of an infiltrative wax-embedded BCC using GLI1 (H-300) antibody

An infiltrative wax-embedded Basal Cell Carcinomas (1759) was stained using immunofluorescence (Fig. 4.19 a, c, e) or DAB-based immunohistochemistry (Fig. 4.19 b, d, f). Representative images of three different areas of the BCC are shown, with immunofluorescence staining juxtaposed to DAB staining (lower right panel). Staining pattern appears to be similar with both techniques, and GLI1 localisation is similar to what is observed in a nodular BCC (8396A2, Fig. 4.18 a-f). GLI1 staining is present in all layers of the epidermis and also in BCCs tumour mass and is diffused in both the nucleus and the cytoplasm. Scale bar represents 50 µm.

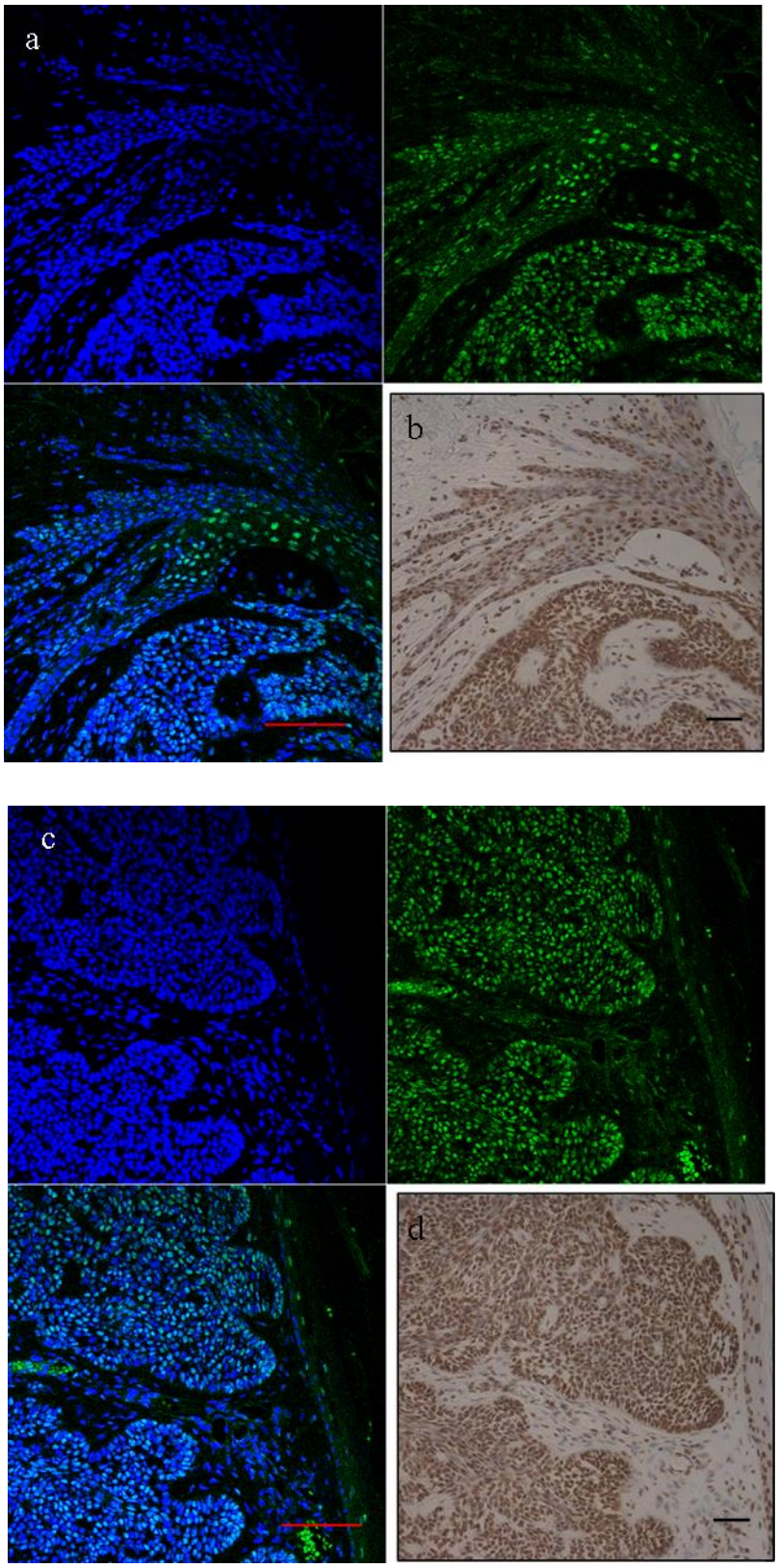
a
b
c
d

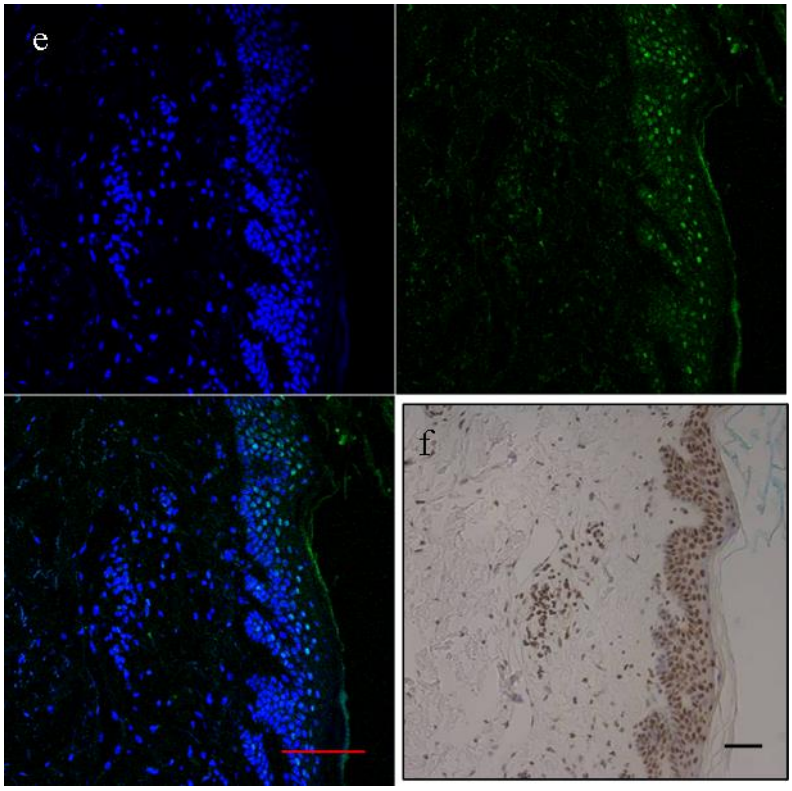

Figure 4.20 –continued

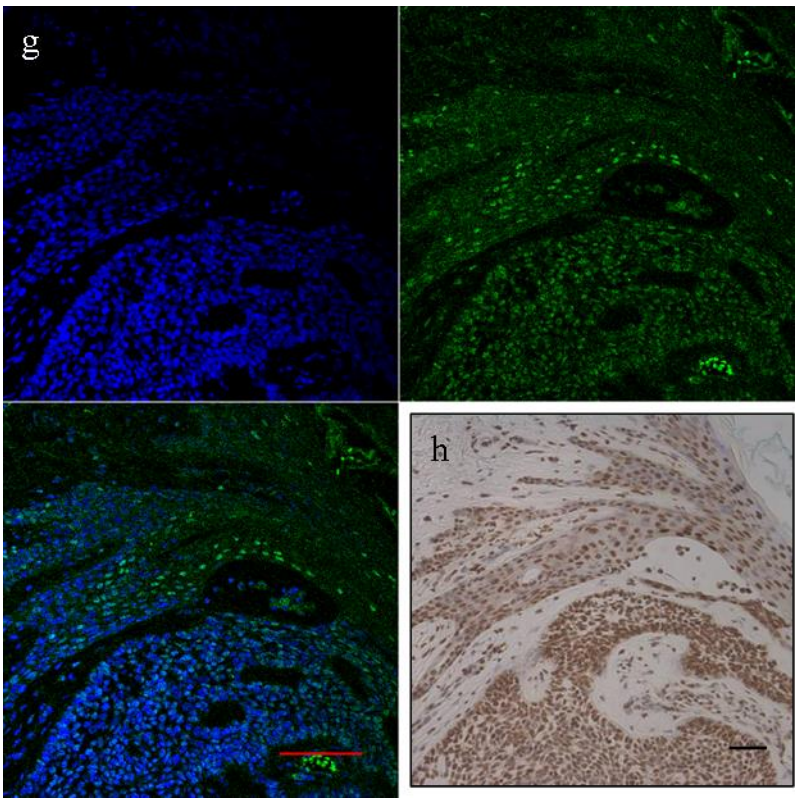
g
h

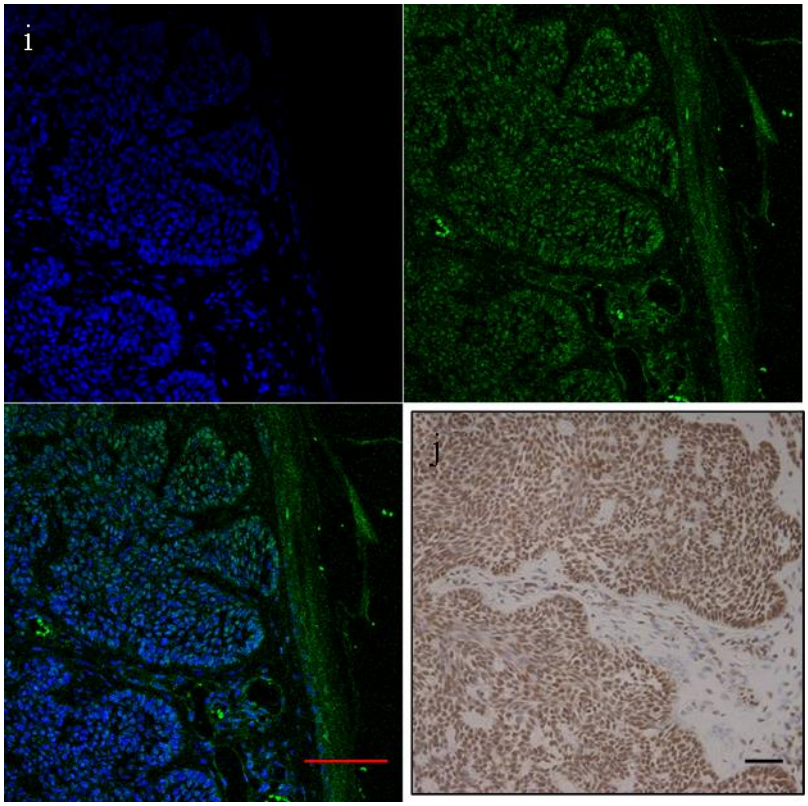
i
j

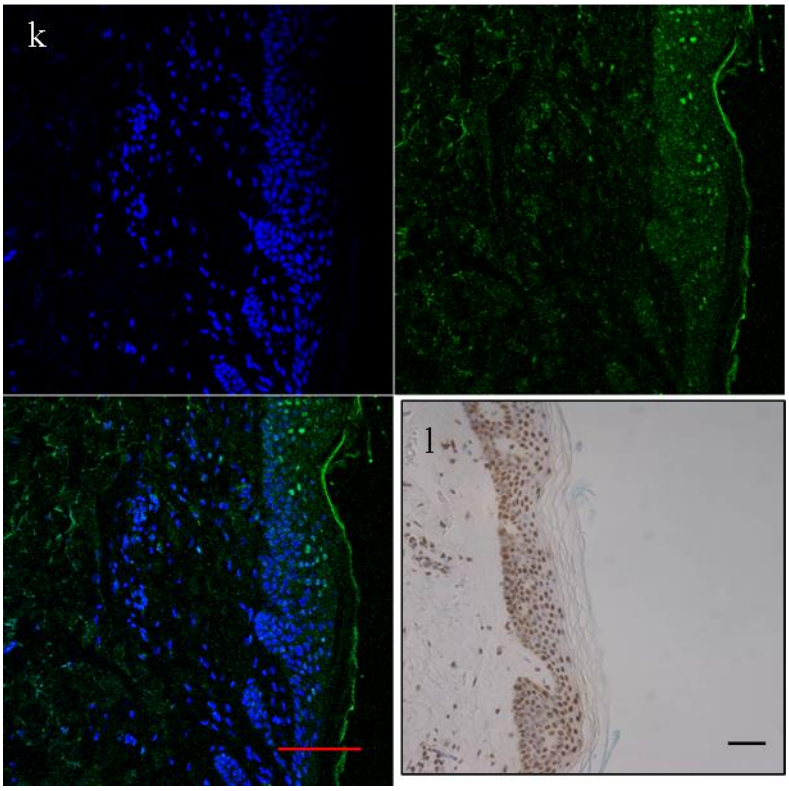

Figure 4.20: Staining of a nodular wax-embedded BCC using two different batches of GLI1 (RD) antibody

Two distinct batches of GLI1 RD antibody were tested to asses the impact of batch to batch variability (batch 1 Fig. 4.20 a-f, batch 2 Fig. 4.20 g-l). A nodular wax-embedded Basal Cell Carcinoma (8396A2) was stained using either immunofluorescence (Fig. 4.20 a, c, e and g, i, l) or DAB-based immunohistochemistry (Fig. 4.20 b, d, f and h, j, l). Staining pattern appears to be similar with both techniques, and no significative difference is present when the two batches of antibody are compared. GLI1 staining is present in the epidermis and also in underlying BCCs tumour masses. GLI1 localisation seems to be more nuclear with GLI1 RD if compared with staining results using the GLI1 H300 antibody (Fig. 4.19), but areas of cytoplasmic localisation are also present. Scale bar represents 50 µm.

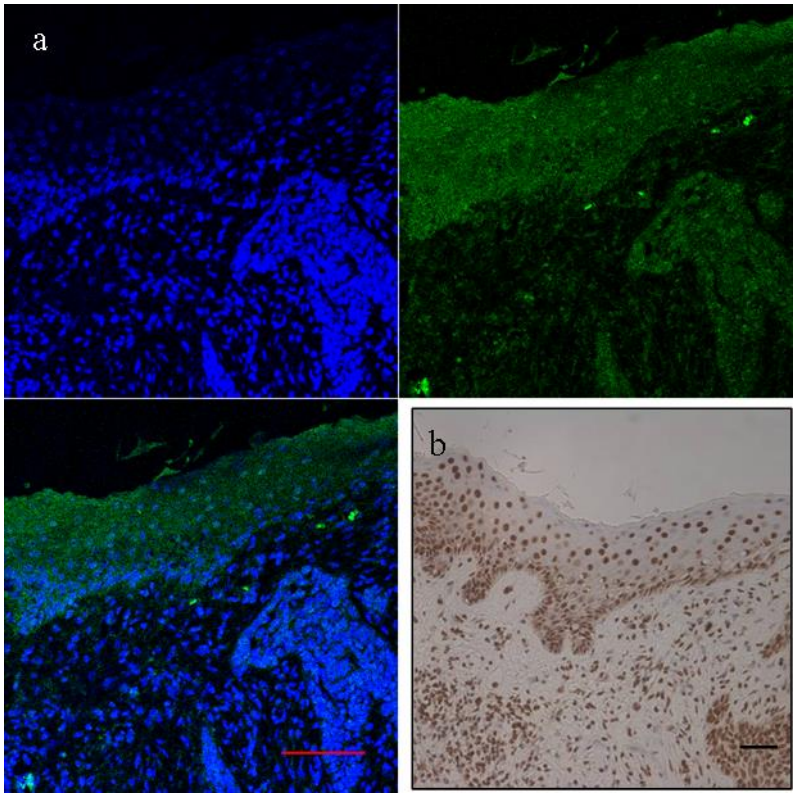
a
b

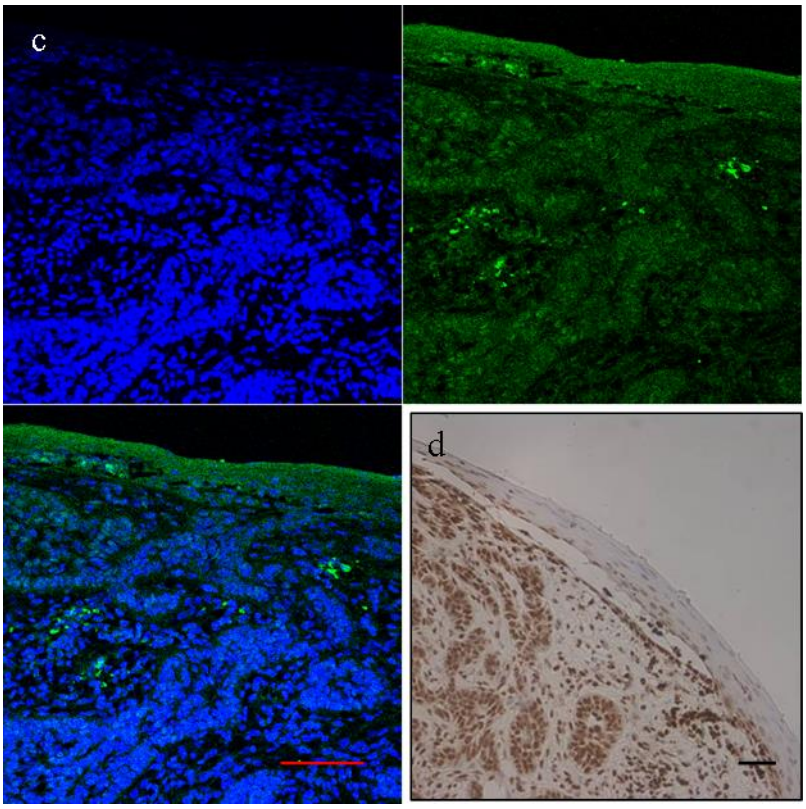
c
d

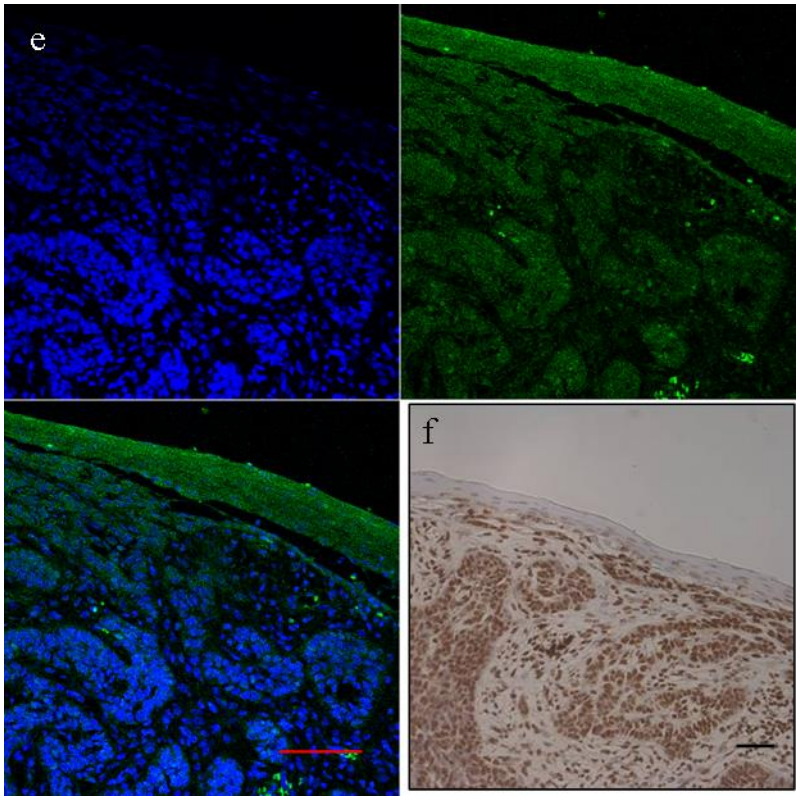

Figure 4.21 -continued

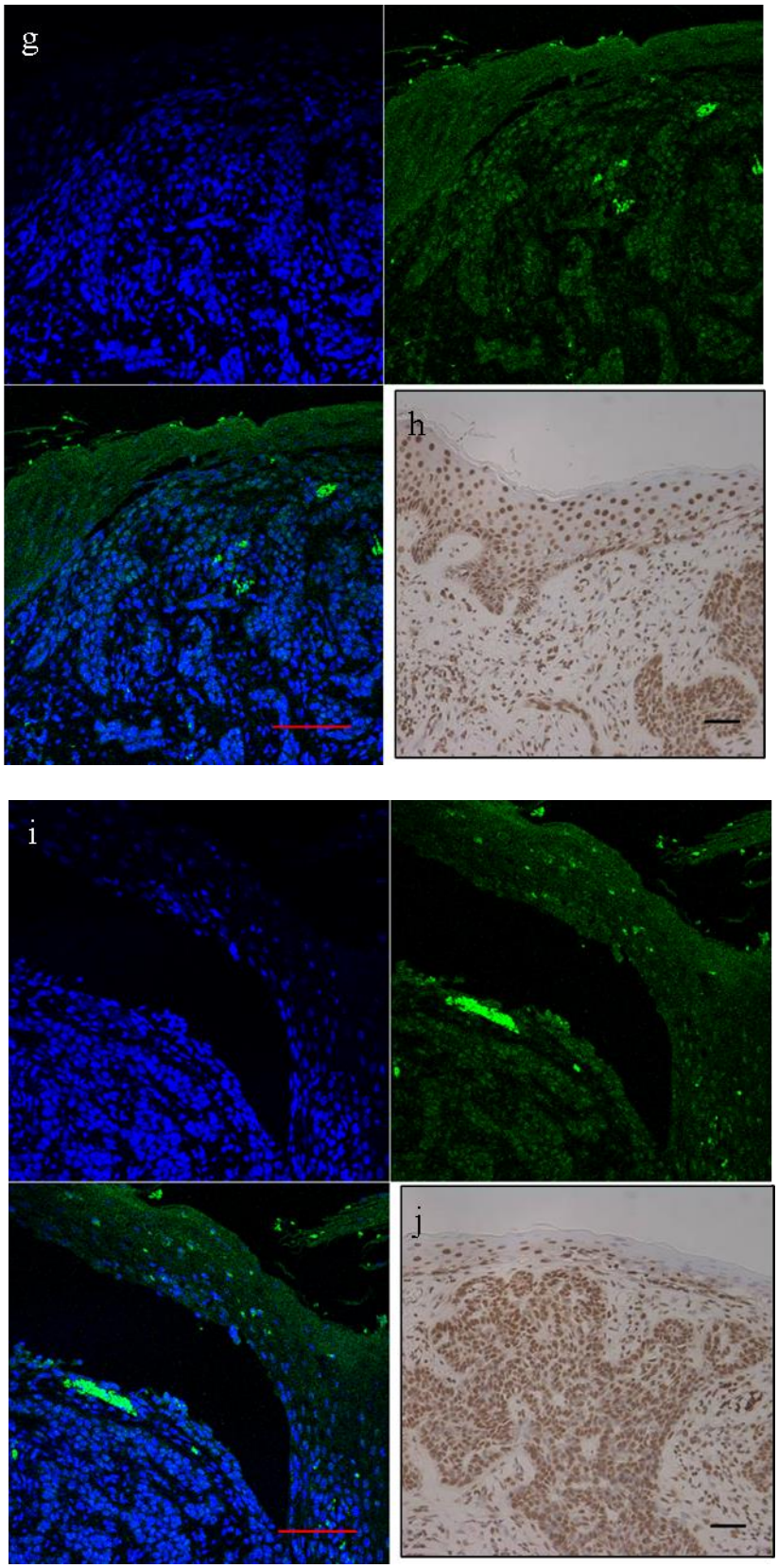
g
h
i
j

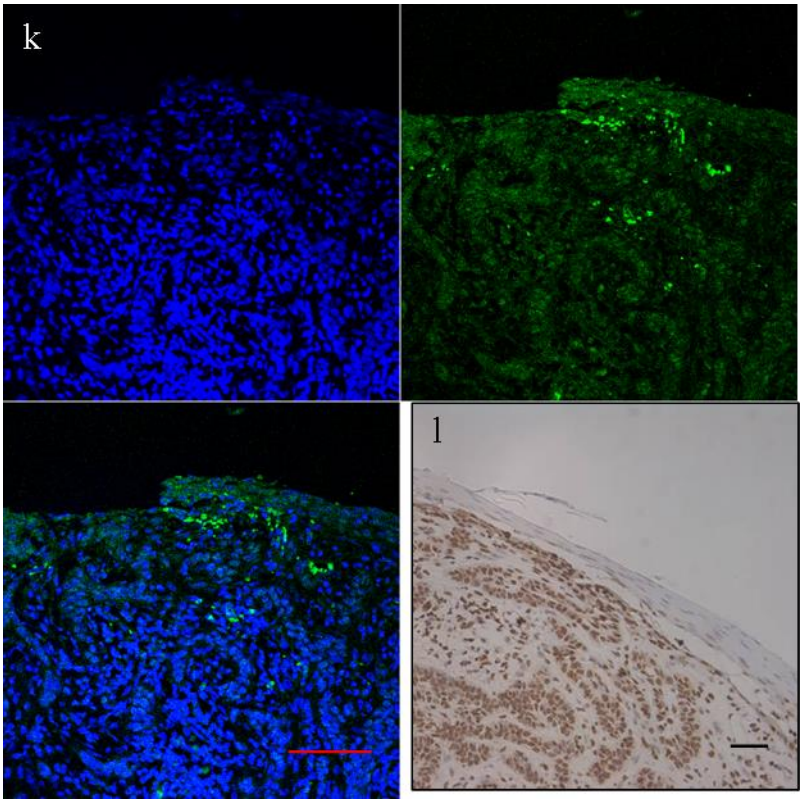

Figure 4.21: Staining of an infiltrative wax-embedded BCC using two different batches of GLI1 (RD) antibody

Two distinct batches of GLI1 RD antibody were tested to asses the impact of batch to batch variability (batch 1 Fig. 4.21 a-f, batch 2 Fig. 4.21 g-l). An infiltrative wax-embedded Basal Cell Carcinoma (1759) was stained using either immunofluorescence (Fig. 4.21 a, c, e and g, i, l) or DAB-based immunohistochemistry (Fig. 4.21 b, d, f and h, j, l). Staining results are similar with both techniques, and no significative difference is present when the two batches of antibody are compared. GLI1 staining is present in both the epidermis and in underlying BCCs tumour masses. GLI1 localisation seems to be more nuclear if compared with staining results using GLI1 H300 antibody (Fig. 4.19). Scale bar represents 50 µm.

4.2.10 Immunofluorescent staining of rat adrenal cortex with Sonic Hedgehog (AbCam) antibody

The Sonic Hedgehog ligand (SHH) is expressed in the outer murine adrenal cortex and is implicated in the adrenal gland development (King *et al.*, 2009). In order to test the specificity of a Sonic Hedgehog ligand antibody (SHH, ab19897, Abcam), frozen sections of rat adrenal cortex were stained. Positive staining is present in the outer region of the adrenal cortex (zona glomerulosa) (Fig. 4.22 a, b), in accordance to what has been previously published (King *et al.*, 2009).

This SHH antibody has subsequently been used to stain BCC samples to investigate the hypothesis of a paracrine mode of Hedgehog signalling activation in the stroma (see section 4.2.11).

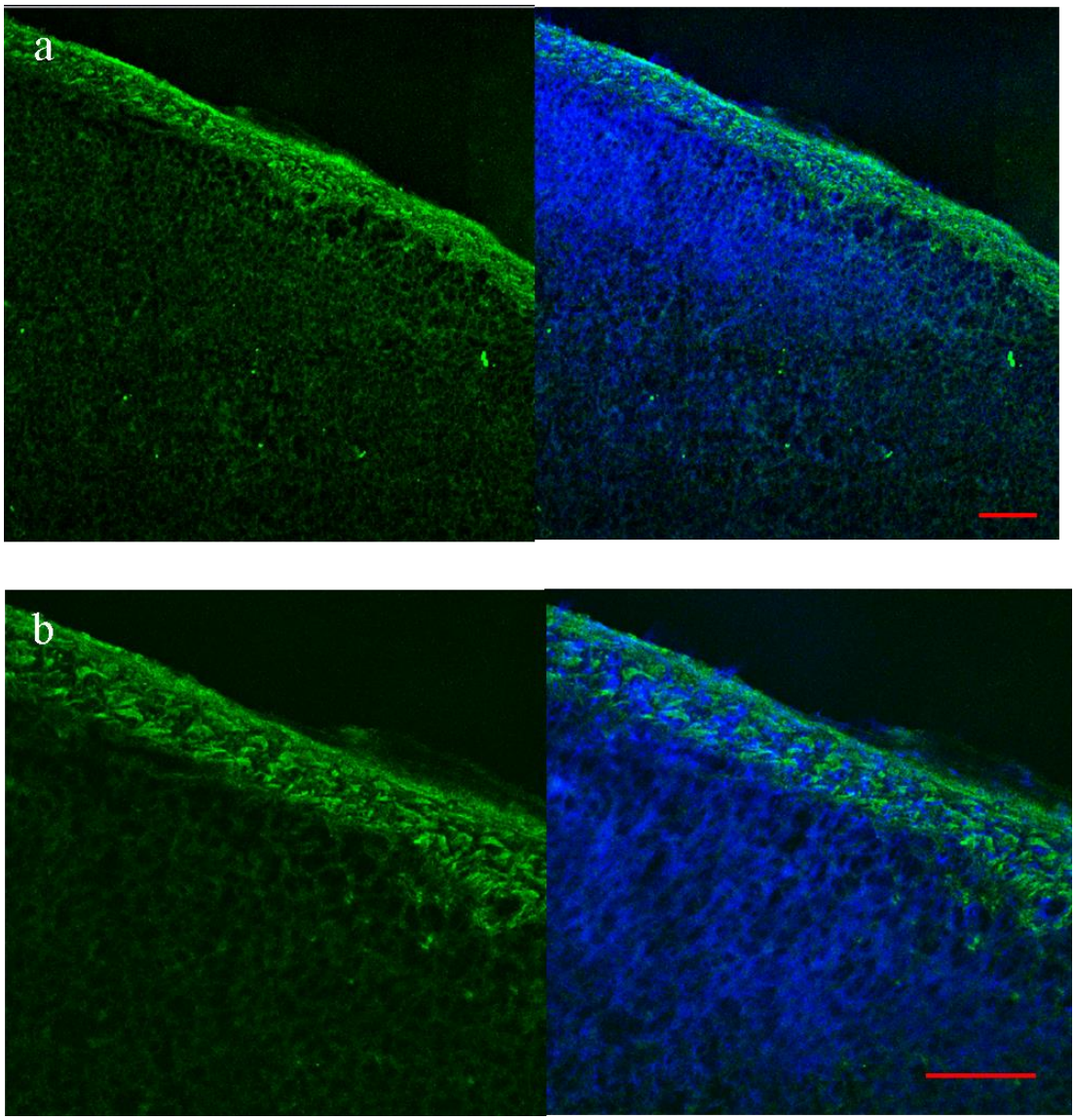

Figure 4.22: Sonic Hedgehog ligand (SHH) expression in rat adrenal cortex using SHH (Abcam) antibody

Rat adrenal cortex cryosections were stained with SHH (ab19897, Abcam), an antibody that recognise the amino terminal end of the Sonic Hedgehog peptide. Positive staining is present in the outer region of the adrenal cortex (zona glomerulosa). Scale bar represents 50 µm.

4.2.11 Double immunofluorescent staining of Normal Human Hair Bearing Skin with GLI1 (RD) and Sonic Hedgehog (AbCam) antibodies

A double immunofluorescence experiment was performed on a frozen section of normal hair bearing skin obtained from an abdominoplasty using GLI1 (RD), a rat monoclonal antibody against GLI1, and SHH (AbCam), a rabbit polyclonal antibody against Sonic Hedgehog. GLI1 is localised through the epidermis and in the outer root sheath of the hair follicle, while Sonic Hedgehog is present in the upper layers of the epidermis and in the inner root sheath of the hair follicle (Fig. 4.23 a, b), consistent with data that has been previously published (Oro and Higgins, 2003).

Of note, SHH staining was also observed in cutaneous nerve fibers, as recently reported by Brownell et al.; SHH action on bulge stem cells is necessary to maintain their ability to become epidermal stem cells and participate in epidermis regeneration after wounding (Brownell et al., 2011).

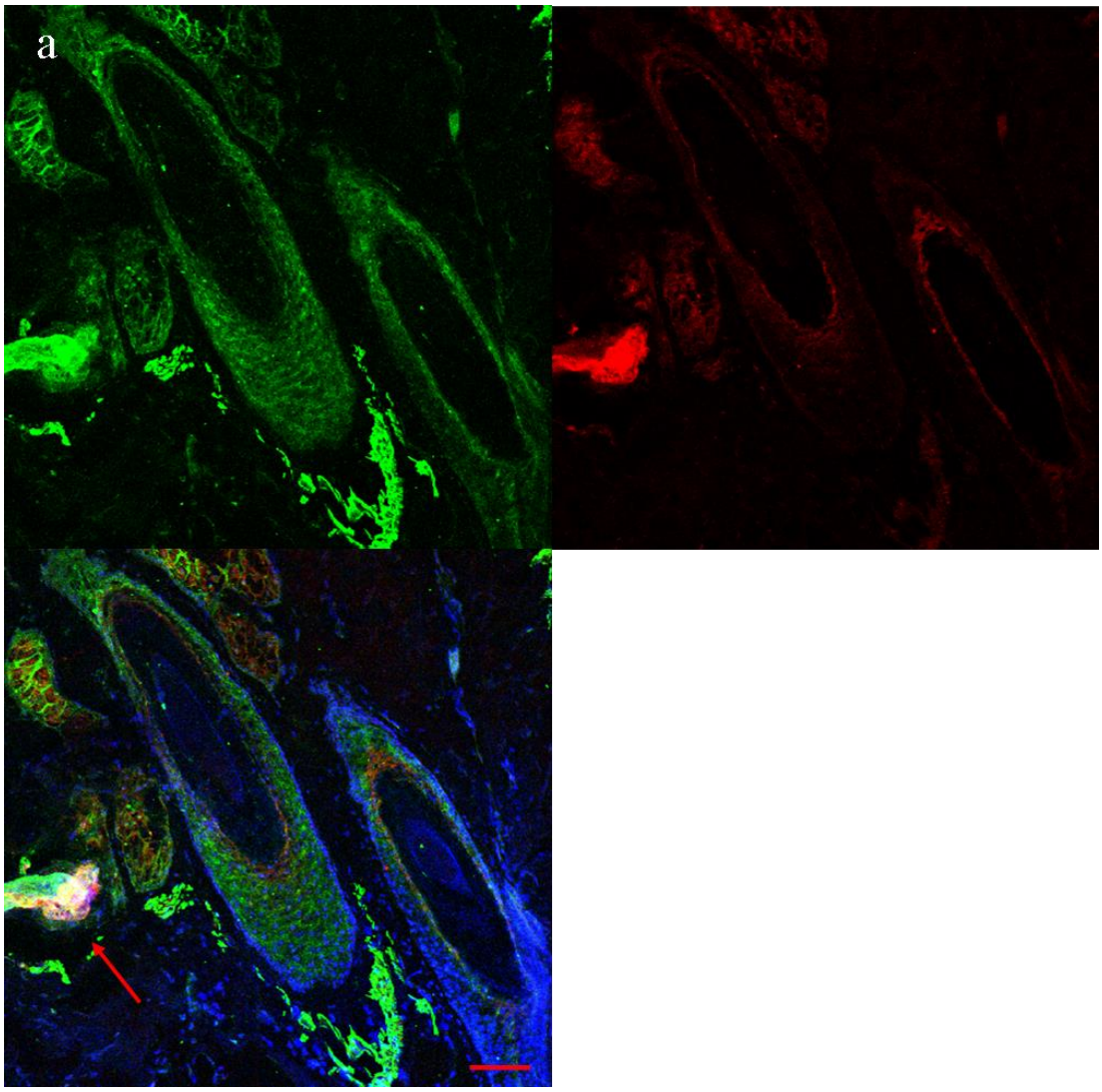

Please see figure legend on page 178

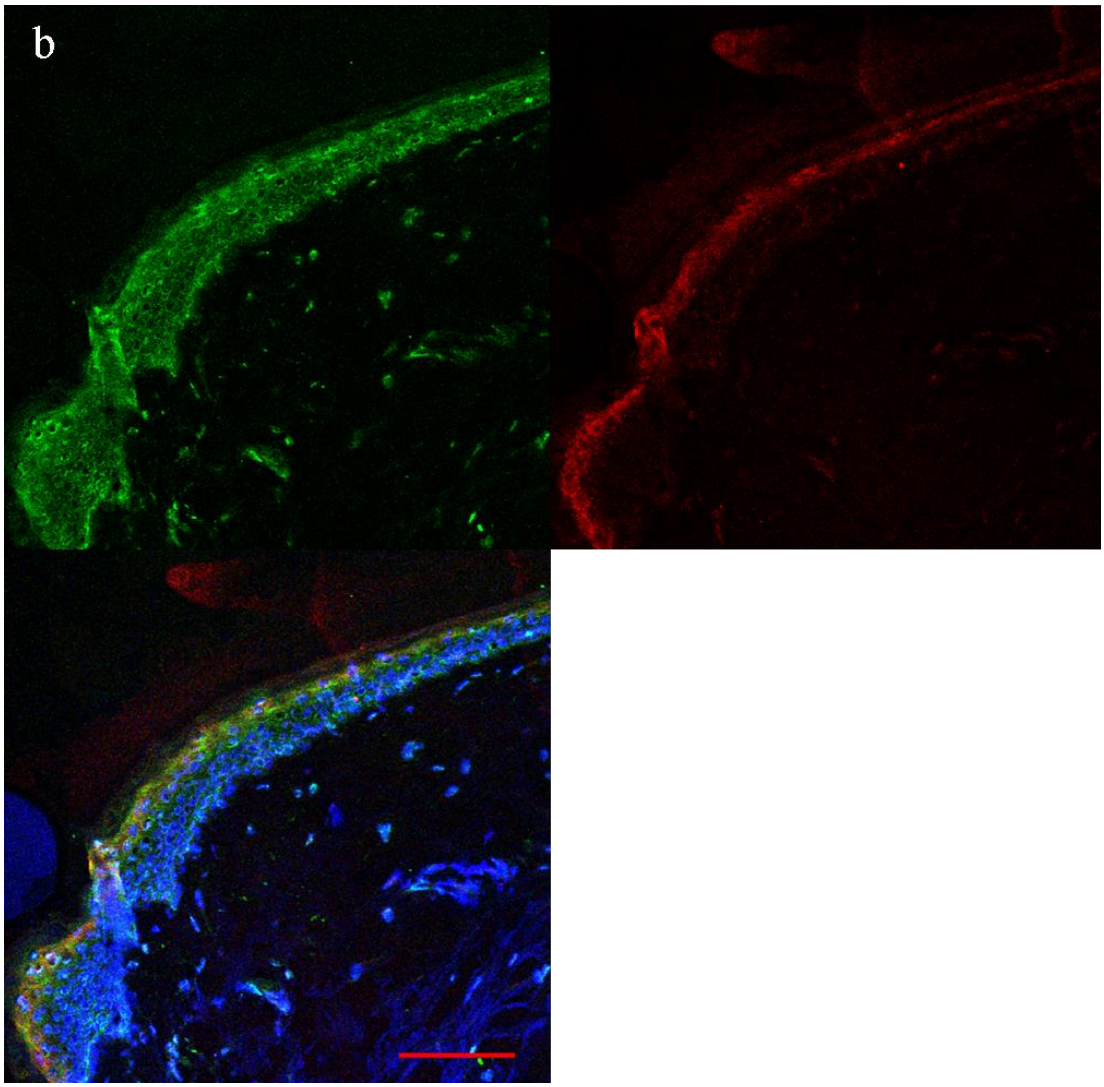

Figure 4.23: GLI1 and Sonic Hedgehog ligand expression in Normal Hair Bearing Human Skin using GLI1 (RD) and Sonic Hedgehog (AbCam) antibodies

A normal human hairy skin cryosection was double stained using GLI1 (RD) (green) and Sonic Hedgehog (AbCam) (red) antibodies. GLI1 positive staining is present thorough the epidermis and in the outer root sheath of the hair follicle. GLI1 localisation appears to be predominantly cytoplasmic. SHH staining is localised in the upper layers of the epidermis and in the inner root sheath of the hair follicle. SHH staining is also observed in cutaneous nerve fibers. Skin was derived from an abdominoplasty surgery. Scale bar represents 50 µm.

4.2.12 Double immunofluorescent staining of Basal Cell Carcinomas with GLI1 (RD) and Sonic Hedgehog (AbCam) antibodies

Double immunofluorescence experiments using GLI1 (RD) and SHH (AbCam) were also performed on frozen sections of Basal Cell Carcinomas. Because of the intensity of GLI1 staining in the stroma using GLI1 H-300 antibody (see section 4.2.2), SHH ligand expression levels in BCCs were analysed in order to test the hypothesis of a paracrine mode of Hedgehog signalling activation in the stromal compartment.

Although GLI1 stromal staining has been observed with GLI1 H300 and therefore it would have been ideal to double stain samples with GLI1 H300 and SHH, this could not be done as both are rabbit polyclonal antibodies. To perform double immunostaining experiments the two antibodies must have been raised in different species. GLI1 RD is a rat monoclonal antibody and was therefore chosen to double stain with SHH.

A panel of 13 BCCs belonging to different subtypes: nodular (n=10), superficial (n=1), nodular / micronodular (n=1), nodular / morphoeic (n=1) were stained (Fig. 4.24).

Out of 13 BCCs analysed, only 4 showed positive staining for Sonic Hedgehog: of note, in 2 of these 4 samples staining intensity was very weak (Table 4.4). This seems to argue against paracrine signalling in BCC.

Notably, GLI transcription factors have been recently reported to be activated by TGFβ (Dennler *et al.*, 2007; Nolan-Stevaux *et al.*, 2009), therefore TGFβ mediated non-canonical activation of GLI1 in the stroma may offer another possible explanation for the pattern of staining observed in human BCCs samples.

Table 4.3: List of all Basal Cell Carcinomas samples stained with GLI1 (RD) and SHH (Abcam) antibodies

BCC code	Histological subtype	Positive for SHH staining
AV 501	nodular	No
BD 641	nodular	No
EK F55	superficial	No
GJ 106	nodular	No
MM 596	nodular	No
SP 430	nodular	No
SR 920	nodular / morphoeic	No
ST 002	nodular	No
SW M68	nodular	No
TT 686	nodular	Yes (weak)
WC M51b	nodular	Yes
WJ 140	nodular / micronodular	Yes (weak)
WS 922	nodular	Yes

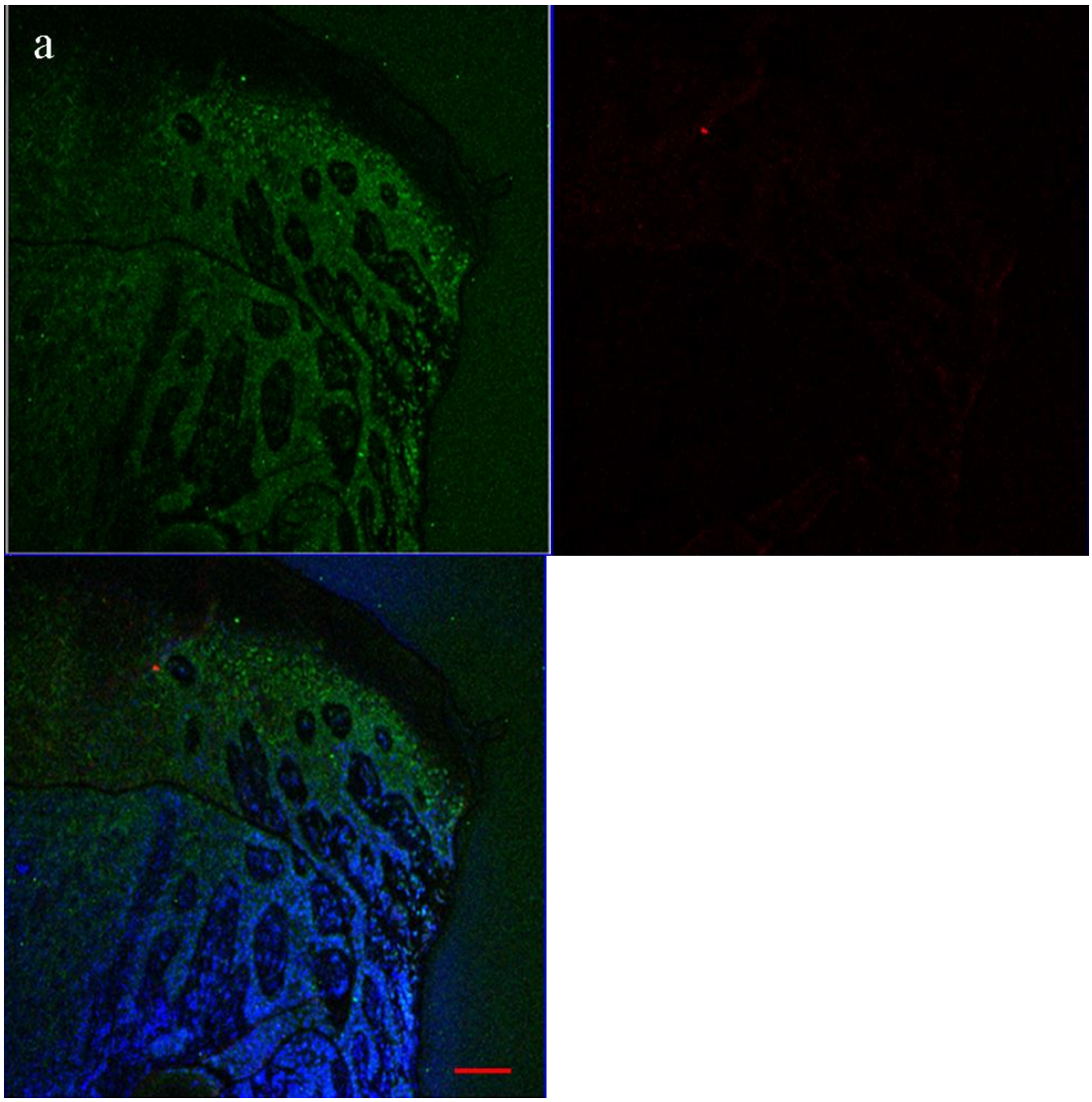

Please see figure legend on page 184

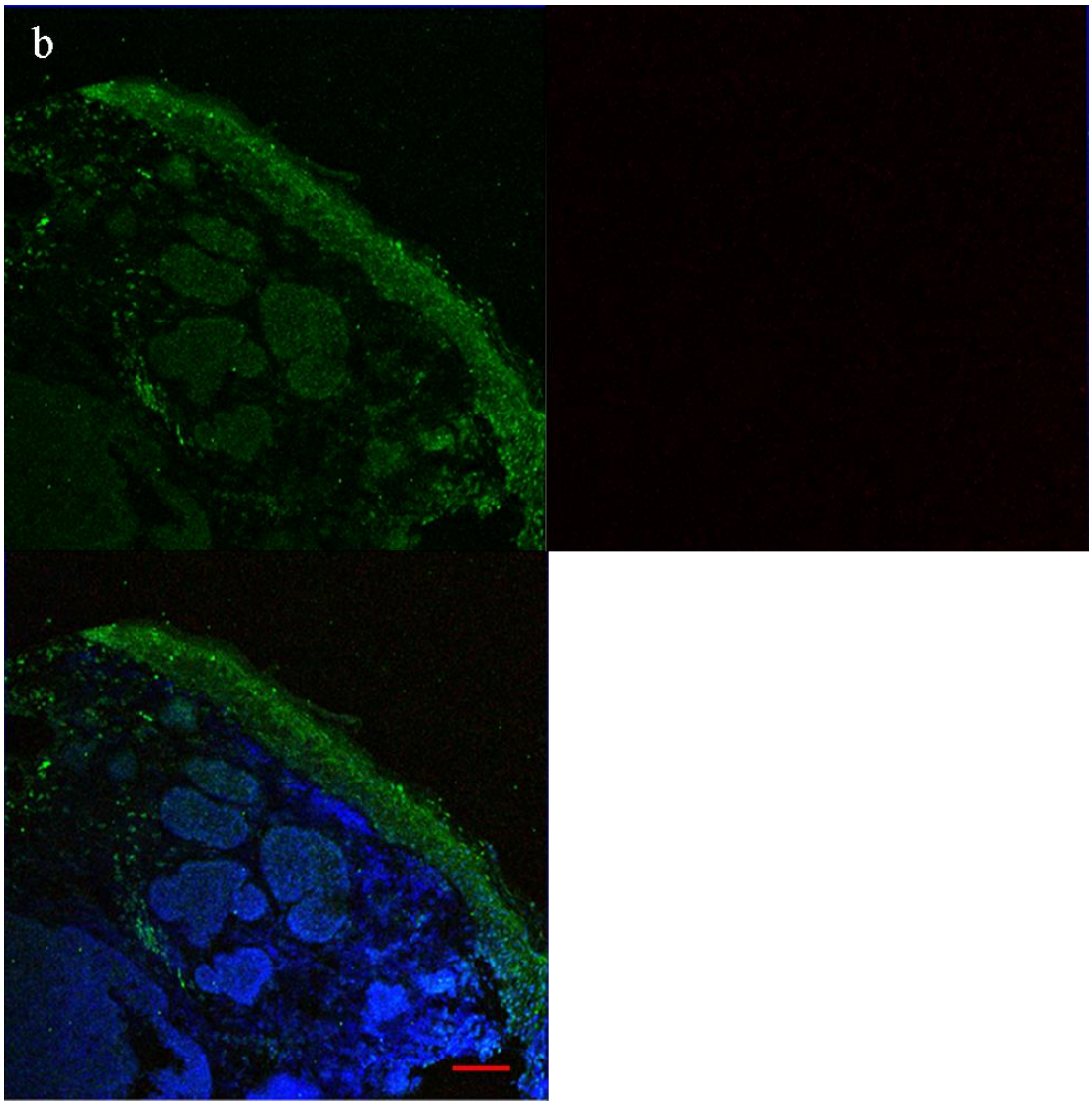

Please see figure legend on page 184

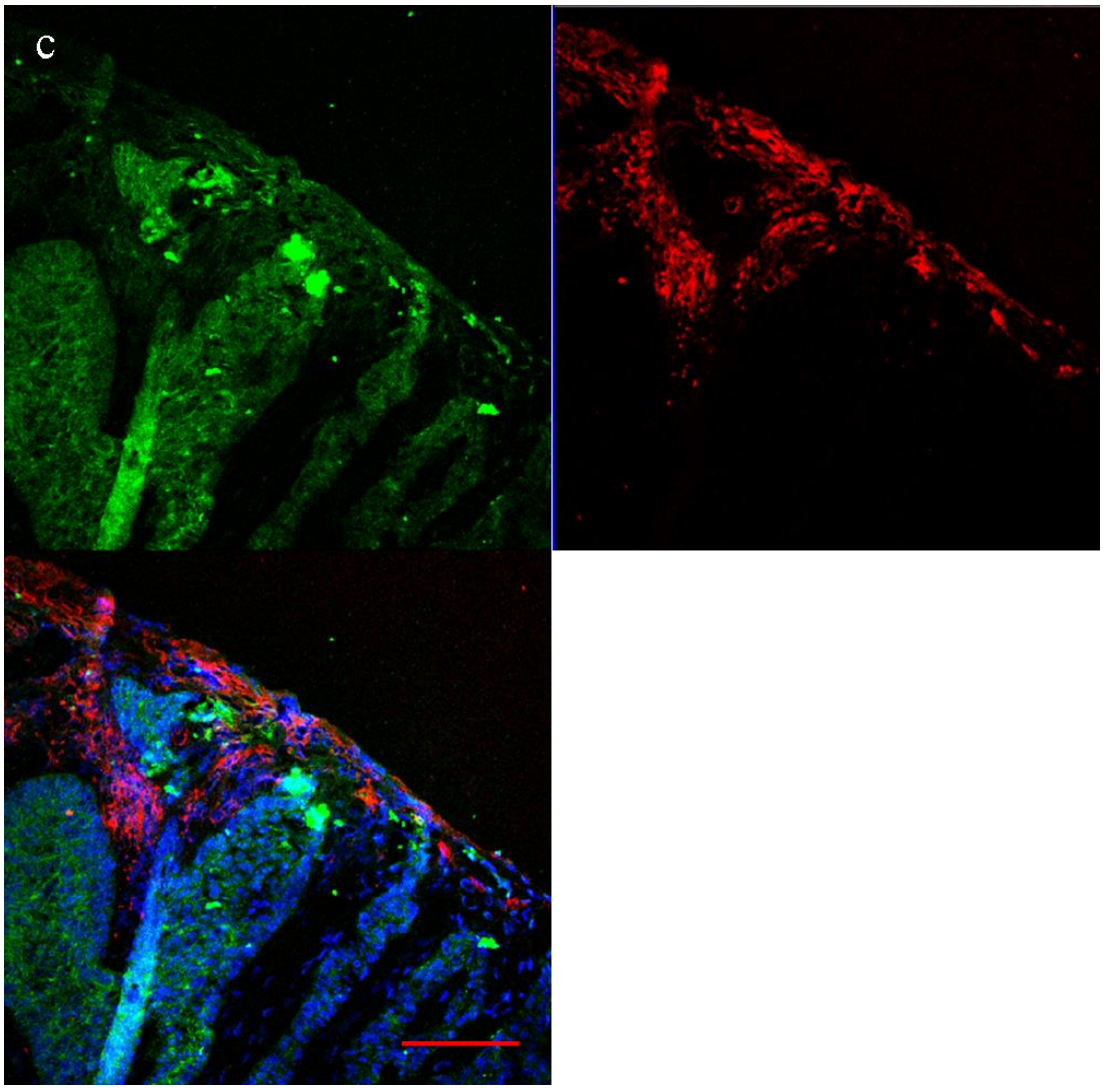

Please see figure legend on page 184

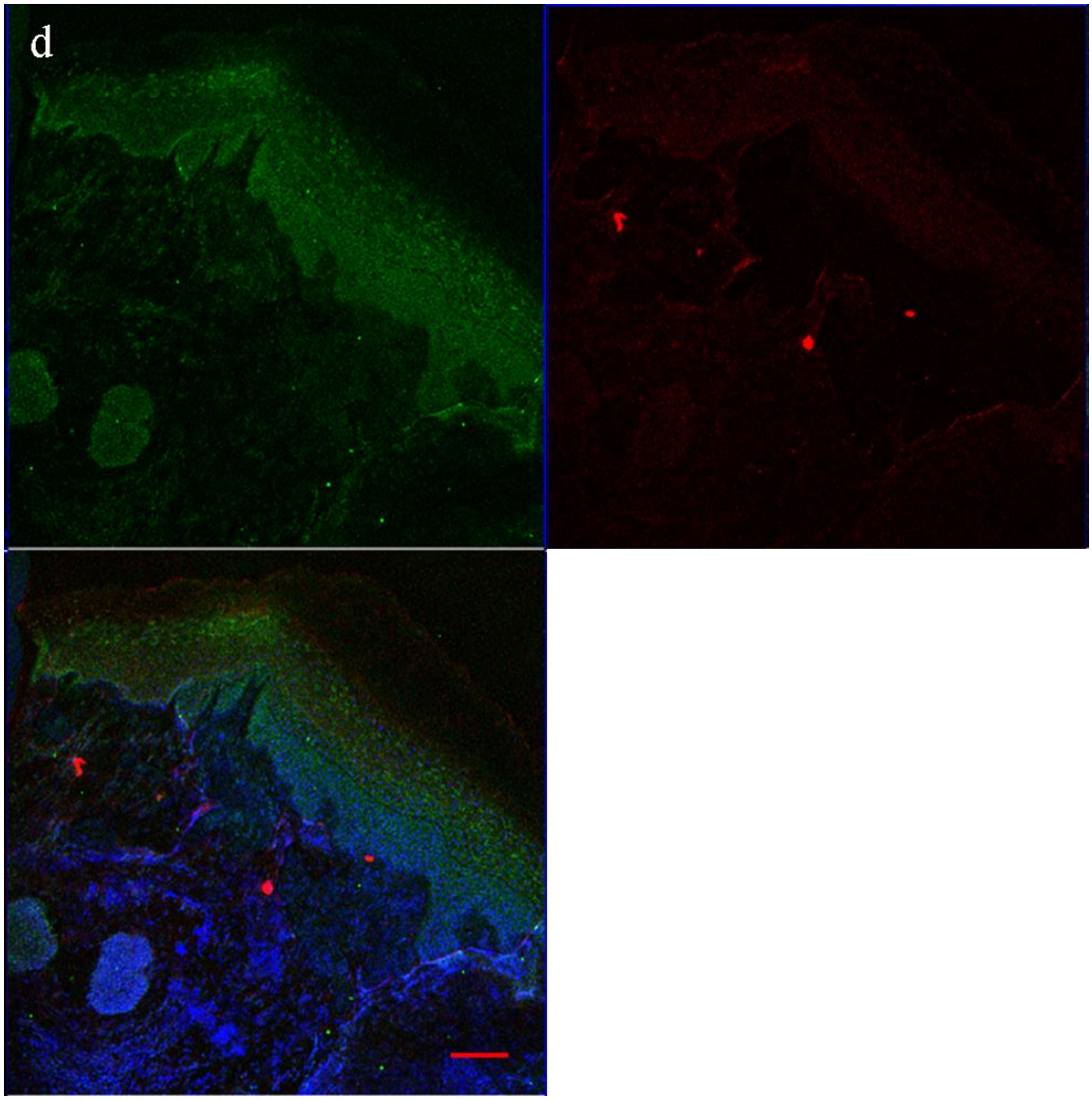

Figure 4.24: GLI1 and Sonic Hedgehog ligand expression in Basal Cell Carcinomas samples using GLI1 (RD) and SHH (Abcam) antibodies

Sections of BCCs showing double immunostaining for GLI1 (GLI1 RD, green) and Sonic Hedgehog (red). Representative images are shown. (a) AV 501– nodular BCC (b) BD 641- nodular BCC (c) WC 51b – nodular BCC (d) WJ 140- nodular / micronodular BCC.

Out of 13 BCCs analysed, belonging to different subtypes, only 4 (30%) showed positive SHH staining (Fig. 4.24 c); in 2 of these 4 samples SHH staining was very weak (Fig. 4.24 d). Scale bar represents 50 µm.

4.2.13 Immunofluorescent staining of Normal Human Hair Bearing Skin with GLI2 (H-300) antibody

GLI2 H-300 (GLI2 (H-300) sc-28674, Santa Cruz), a rabbit polyclonal antibody raised against amino acids 841-1140 mapping near the carboxyl-terminal of GLI2 of human origin, was used to stain frozen sections of normal human hairy skin obtained from an abdominoplasty. Positive staining is observed in all layers of epidermis and also in the outer root sheath of the hair follicles (Fig. 4.25 a, b). GLI2 localisation is diffuse, though slightly more cytoplasmic in the hair follicles.

When further staining was carried out with this GLI2 antibody widespread non-specificity was observed, possibly due to variability between batches of antibodies and similarly to what has been observed with the GLI1 C-18 antibody (see section 4.2.4).

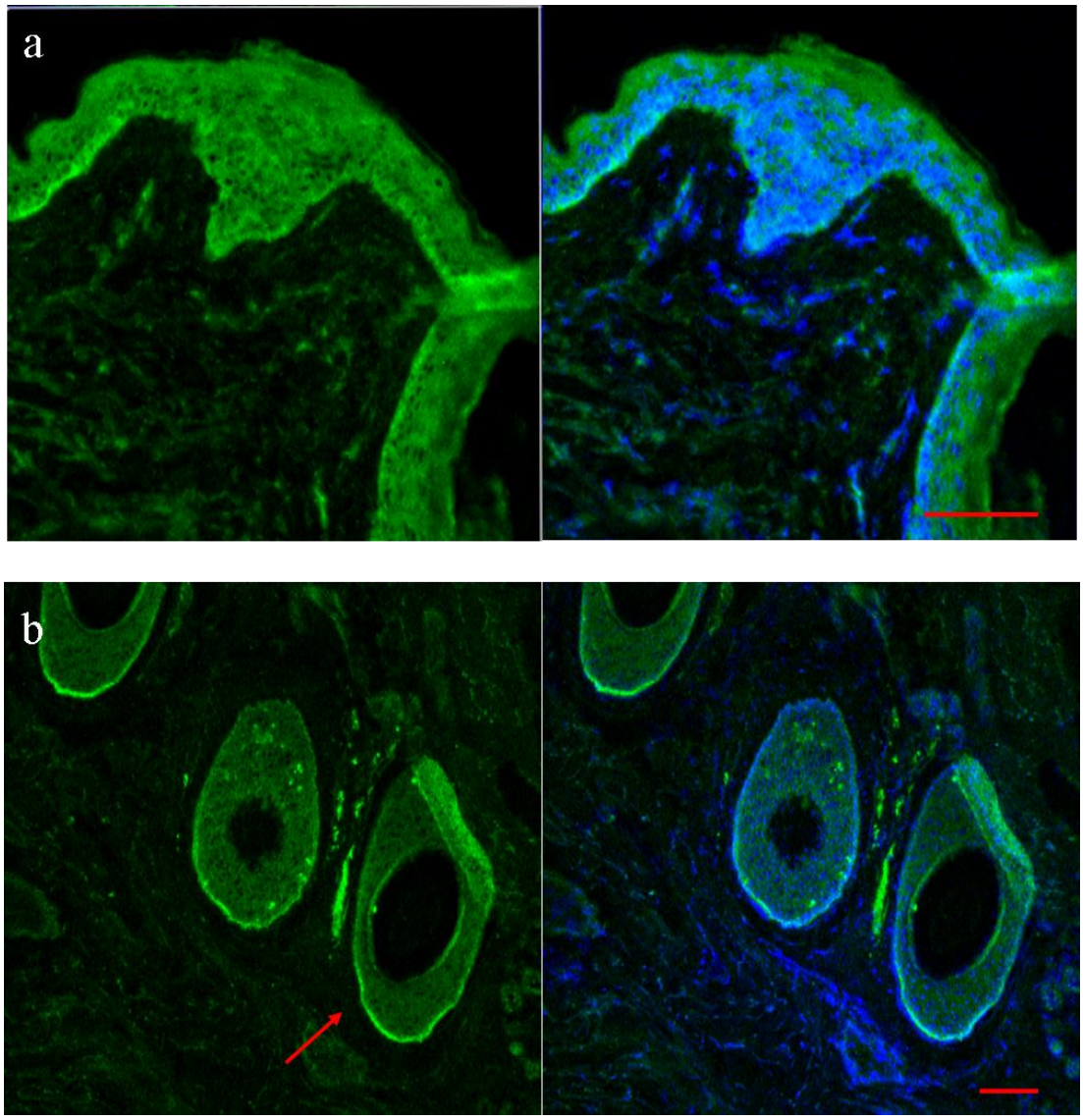

Figure 4.25: GLI2 expression in Normal Hair Bearing Human Skin using GLI2 (H-300) antibody

Normal human hairy skin cryosections were stained with GLI2 H-300, a polyclonal antibody raised against the carboxyl-terminal end of GLI2. Positive GLI2 staining is present in the different layers of the epidermis (a) and in the outer root sheath of the hair follicles (b). GLI2 localisation is both nuclear and cytoplasmic. Skin was derived from an abdominoplasty surgery. Scale bar represents 50 µm.

4.2.14 Immunofluorescent staining of Basal Cell Carcinomas with GLI2 (H-300) antibody

Two nodular Basal Cell Carcinomas AV 501 (Fig. 4.26 a) and TT686 (Fig. 4.26 b) were stained with GLI2 H300 antibody: this antibody recognises an epitope situated at the carboxyl-terminal of GLI2 of human origin. Staining is diffuse thorough the tumour, both in the nucleus and in the cytoplasm. Further staining with this antibody could not be carried out due to batch to batch variability.

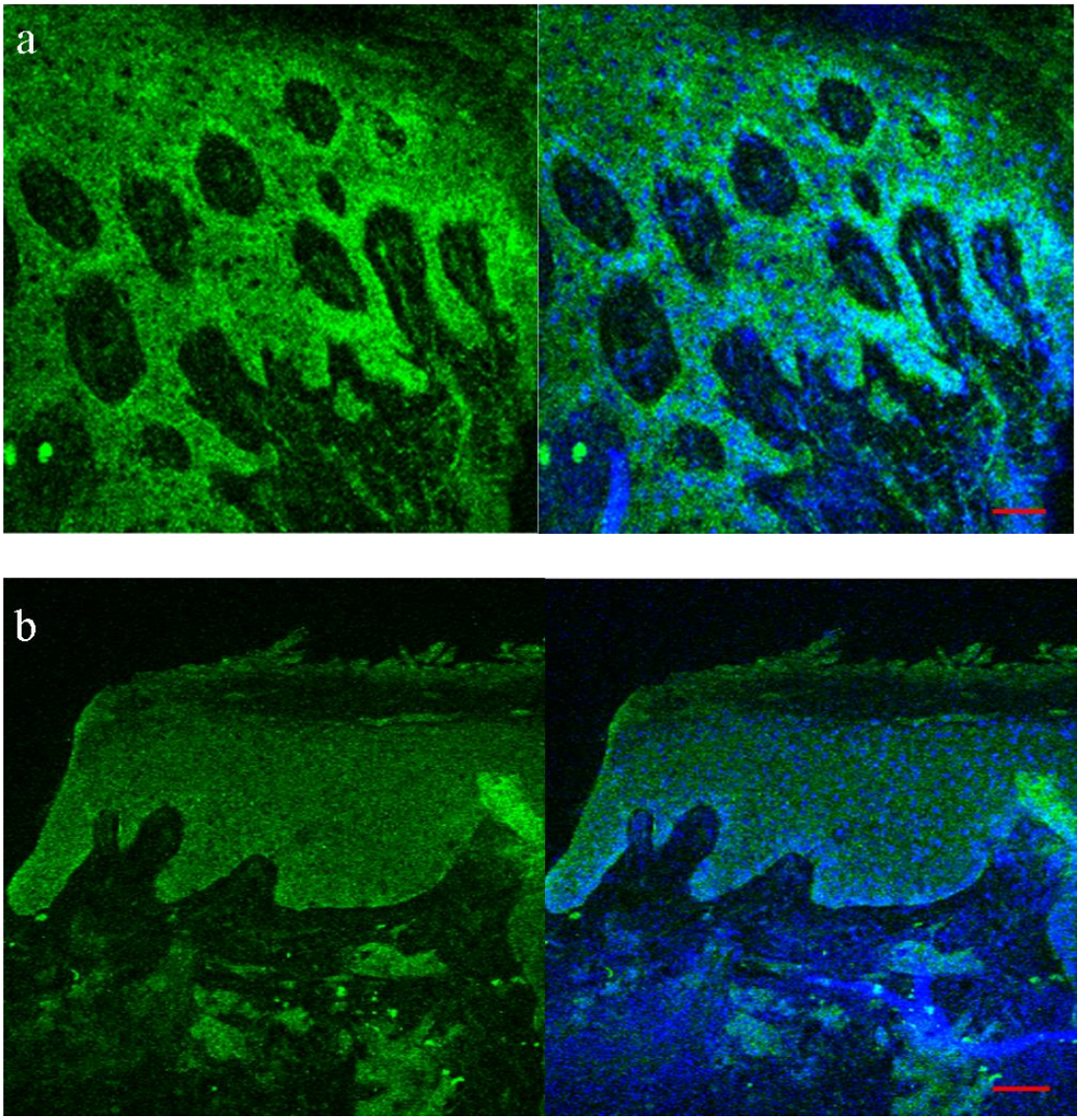

Figure 4.26: GLI2 expression in Basal Cell Carcinomas using GLI2 (H-300) antibody

Sections of BCCs stained with GLI2 (H-300) antibody, AV 501 (a) and TT686 (b), both nodular BCCs. GLI2 is present in the epithelial component of the tumour, showing both nuclear and cytoplasmic localisation. Scale bar represents 50 µm.

4.2.15 Immunofluorescent staining of Normal Human Hair Bearing Skin with GLI2 (AbCam) antibody

Frozen sections of normal human hairy skin obtained from either from an abdominoplasty were stained with a rabbit polyclonal antibody against GLI2 (GLI2 ab26056, Abcam). This antibody has been raised against amino acids 600 – 649 of GLI2 of human origin, located in the central region of the protein. GLI2 staining is present in all layers of epidermis (Fig. 4.27 a), appearing slightly stronger in the basal layer. GLI2 is also present in the outer root sheath of hair follicles (Fig. 4.27 b) and shows a predominantly cytoplasmic localization, with nuclear staining observed in a few regions.

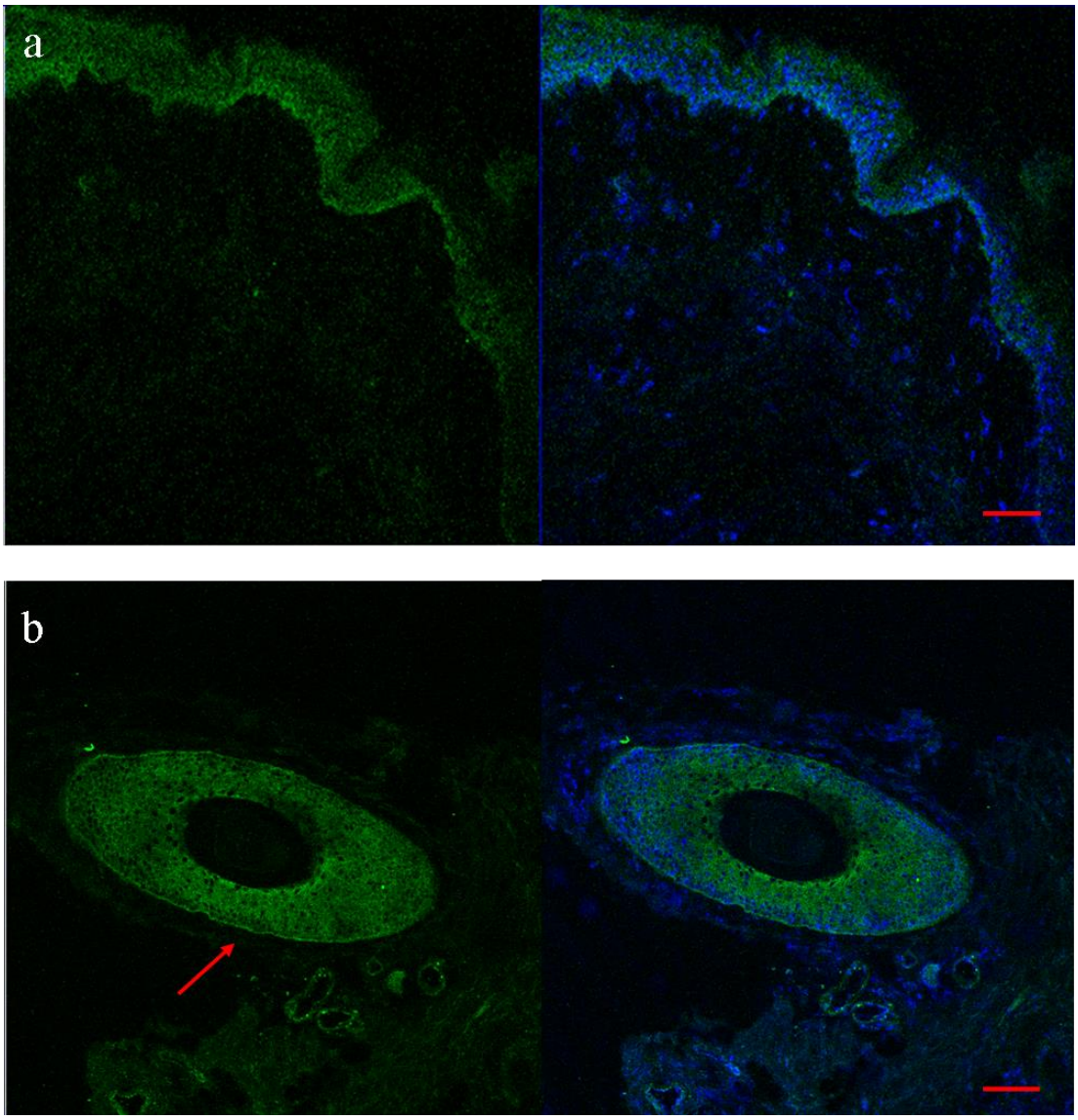

Figure 4.27: GLI2 expression in Normal Hair Bearing Human Skin using GLI2 (Abcam) antibody

Normal human hairy skin cryosections were stained with an antibody against an epitope located in the central region of the GLI2 protein; positive staining is present in all layers of the epidermis (a) and in the inner and outer root sheath of the hair follicle (b). GLI2 is mainly cytoplasmic, with nuclear localization present in some regions. Skin is derived from an abdominoplasty. Scale bar represents 50 µm.

4.2.16 Double immunofluorescent staining of Normal Human Hair Bearing Skin with GLI1 (RD) and GLI2 (AbCam) antibodies

A double immunofluorescence experiment was performed on frozen sections of normal hair bearing skin obtained from an abdominoplasty using GLI1 (RD), a rat monoclonal antibody against GLI1, and GLI2 (AbCam), a rabbit polyclonal antibody against GLI2. GLI1 RD is a rat monoclonal antibody raised against amino acids 1-234 of GLI1 of human origin (N-terminus) while GLI2 Abcam is a rabbit polyclonal antibody against an epitope in the central region of the GLI2 protein corresponding to amino acids 600 - 649. Both GLI1 and GLI2 staining is localised through the epidermis (Fig. 4.28 a) and in the outer root sheath of the hair follicle (Fig. 4.28 b). GLI2 staining seems to be slightly stronger in the basal cell layer of the epidermis (Fig. 4.28 a).

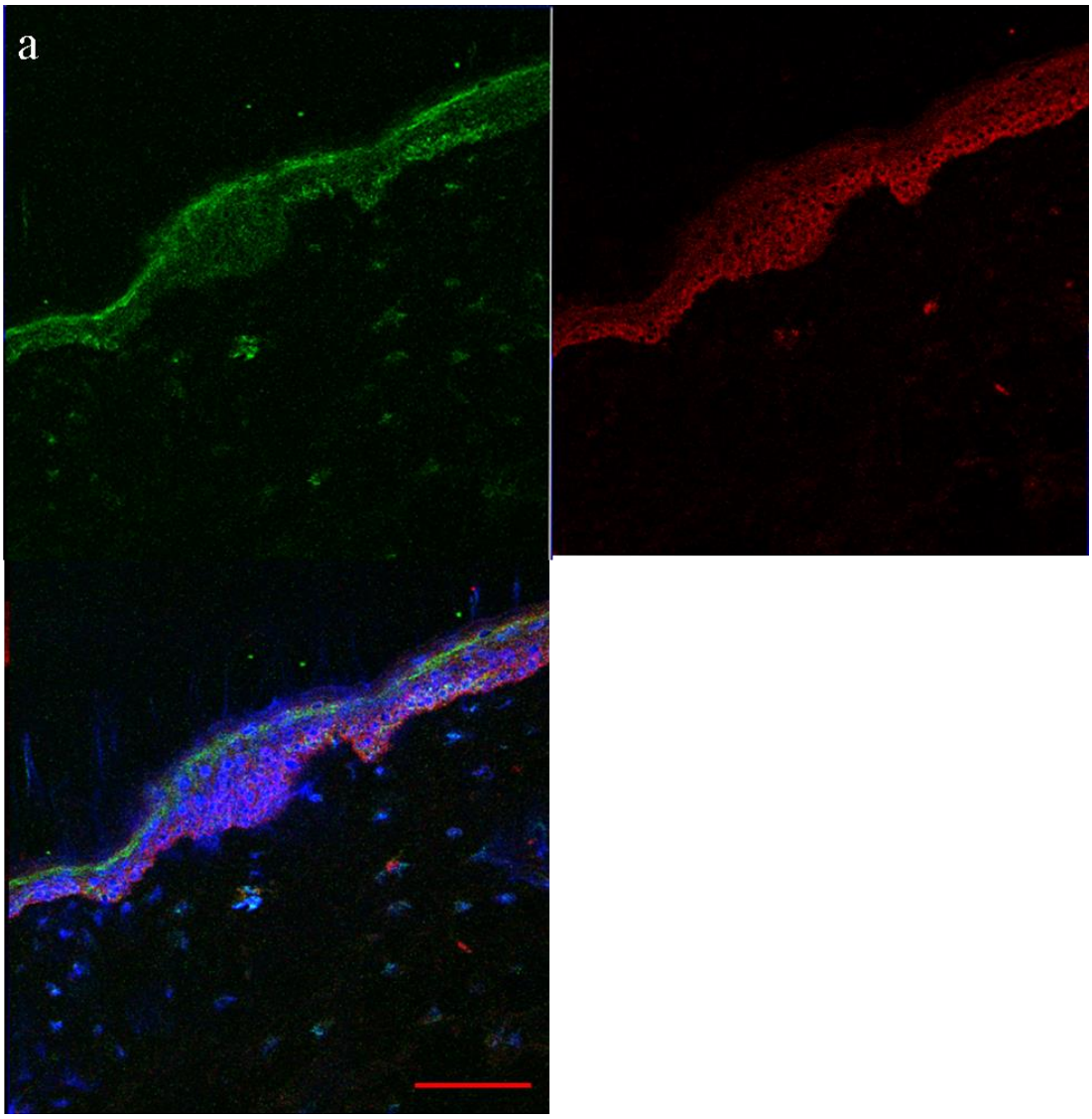

Please see figure legend on page 193

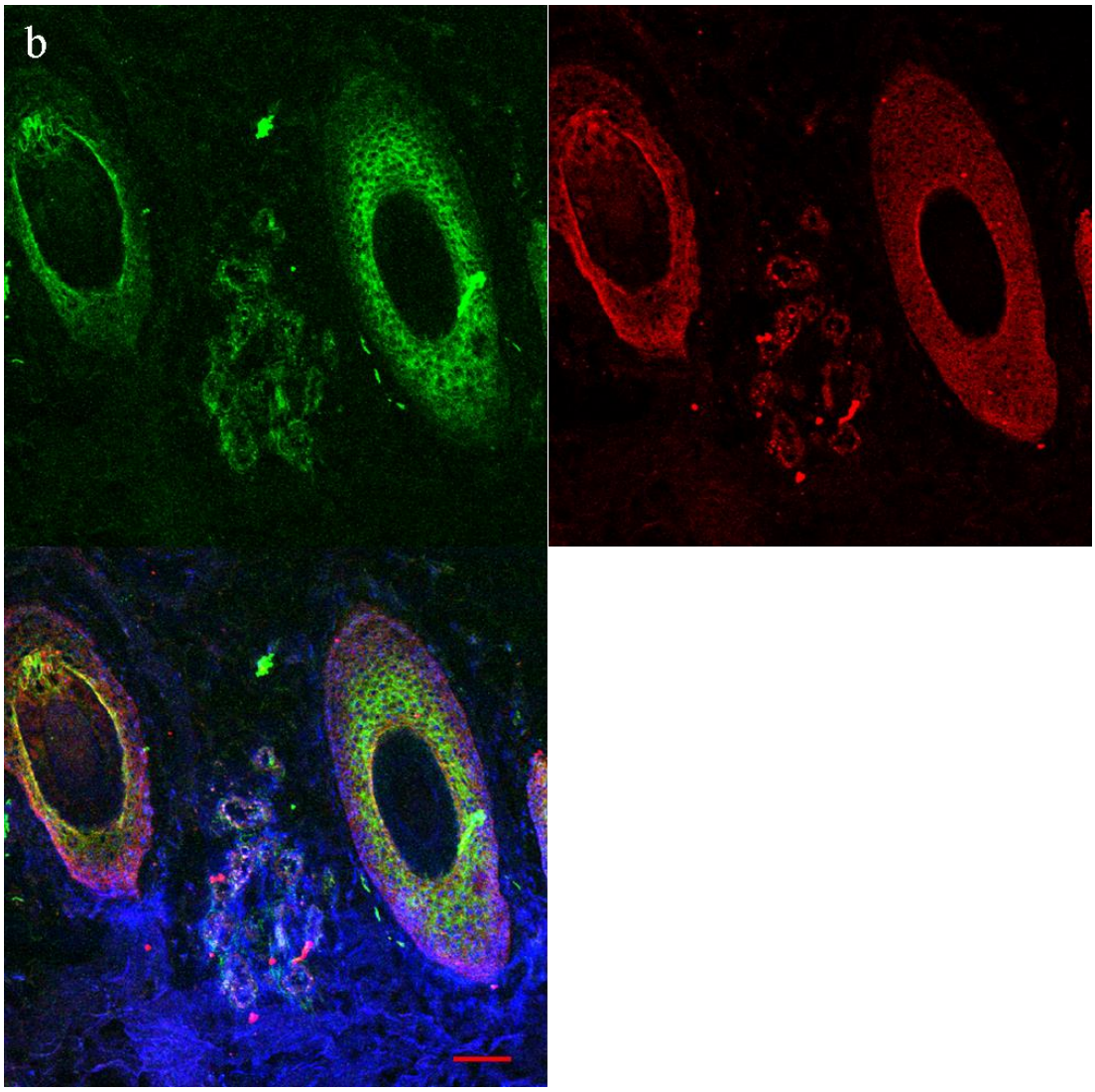

Figure 4.28: GLI1 and GLI2 expression in Normal Hair Bearing Human Skin using GLI1 (RD) and GLI2 (AbCam) antibodies

Normal human hairy skin cryosections were double stained using GLI1 (RD) (green) and GLI2 AbCam (red) antibodies. GLI1 positive staining (green) is present thorough the epidermis, GLI2 staining (red) is also scattered through the epidermis but appears slightly stronger in the basal layer (a). Both GLI1 and GLI2 staining are present in the outer root sheath of the hair follicle (b). Localisation of both proteins is mainly cytoplasmic. Skin was derived from an abdominoplasty surgery. Scale bar represents 50 µm.

4.2.17 Double Immunofluorescent staining of Basal Cell Carcinomas with GLI1 (RD) and GLI2 (AbCam) antibodies

Double immunofluorescence experiments using GLI1 (RD) and GLI2 (AbCam) were also performed on frozen sections of Basal Cell Carcinomas. A panel of 18 BCCs belonging to different subtypes: nodular (n=13), micronodular (n=1), superficial (n=3), nodular/micronodular (n=1) were stained. In most samples GLI1 and GLI2 show extensive areas of co-expression, as well of areas where one protein appears to be more abundant than the other (Fig. 4.29).

GLI1 staining appears to be diffused but sometime weaker at the invading front of the tumour (e.g. in the palisading cells) compared to the centre of the tumour masses (in about a fifth of the samples stained). It is sometimes difficult to distinguish between staining in the basal layer and staining in the BCC as some tumours appears as outgrowth from the epidermis into the dermis; it is hard to discriminate between normal and hyperplastic tissue. GLI2 on the other hand is sometime stronger and more defined in the basal layer. Some samples show areas in which GLI1 is clearly nuclear or perinuclear, especially in the epidermis, while a comparable pattern is absent for GLI2.

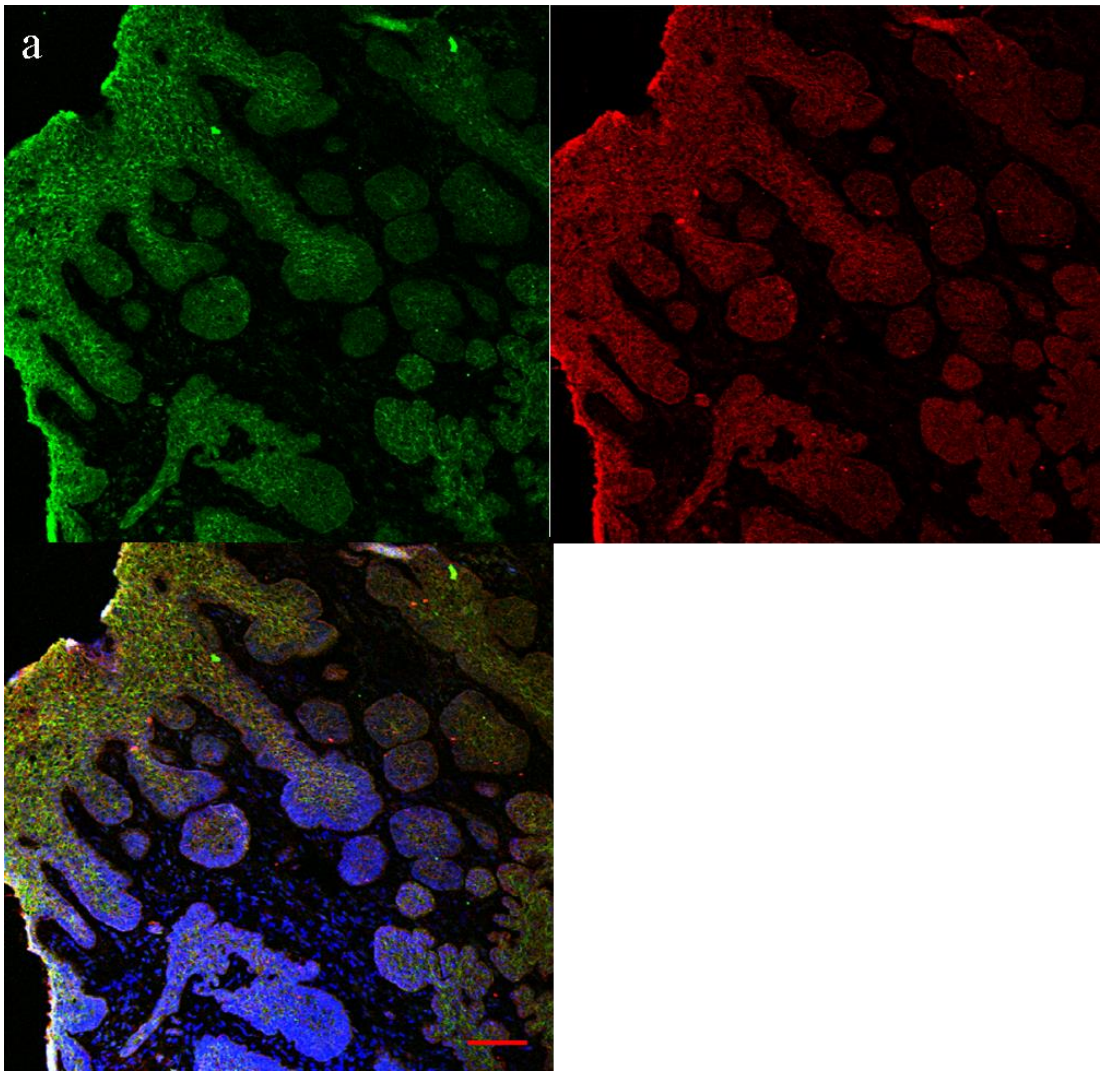

Please see figure legend on page 198

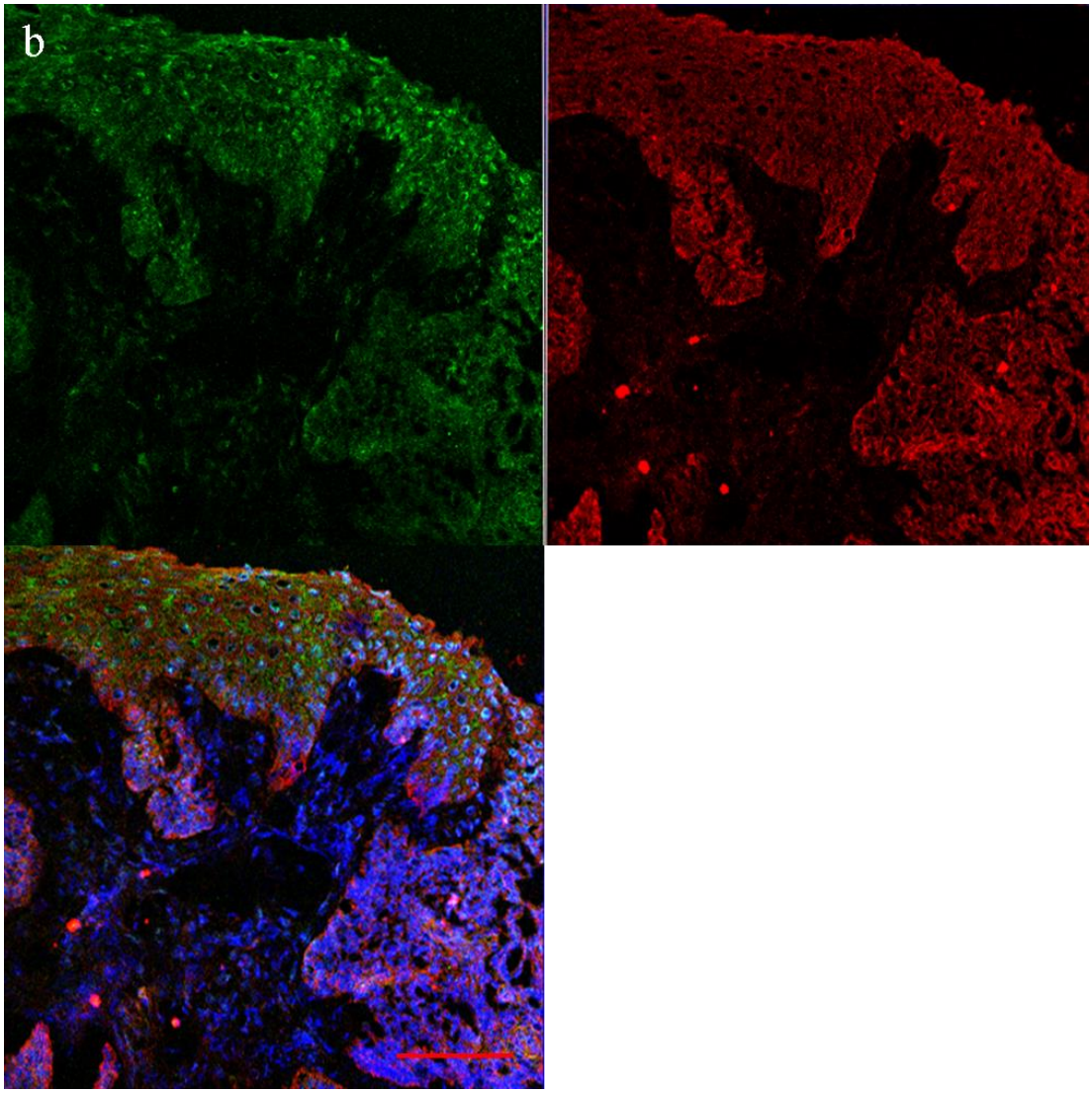

Please see figure legend on page 198

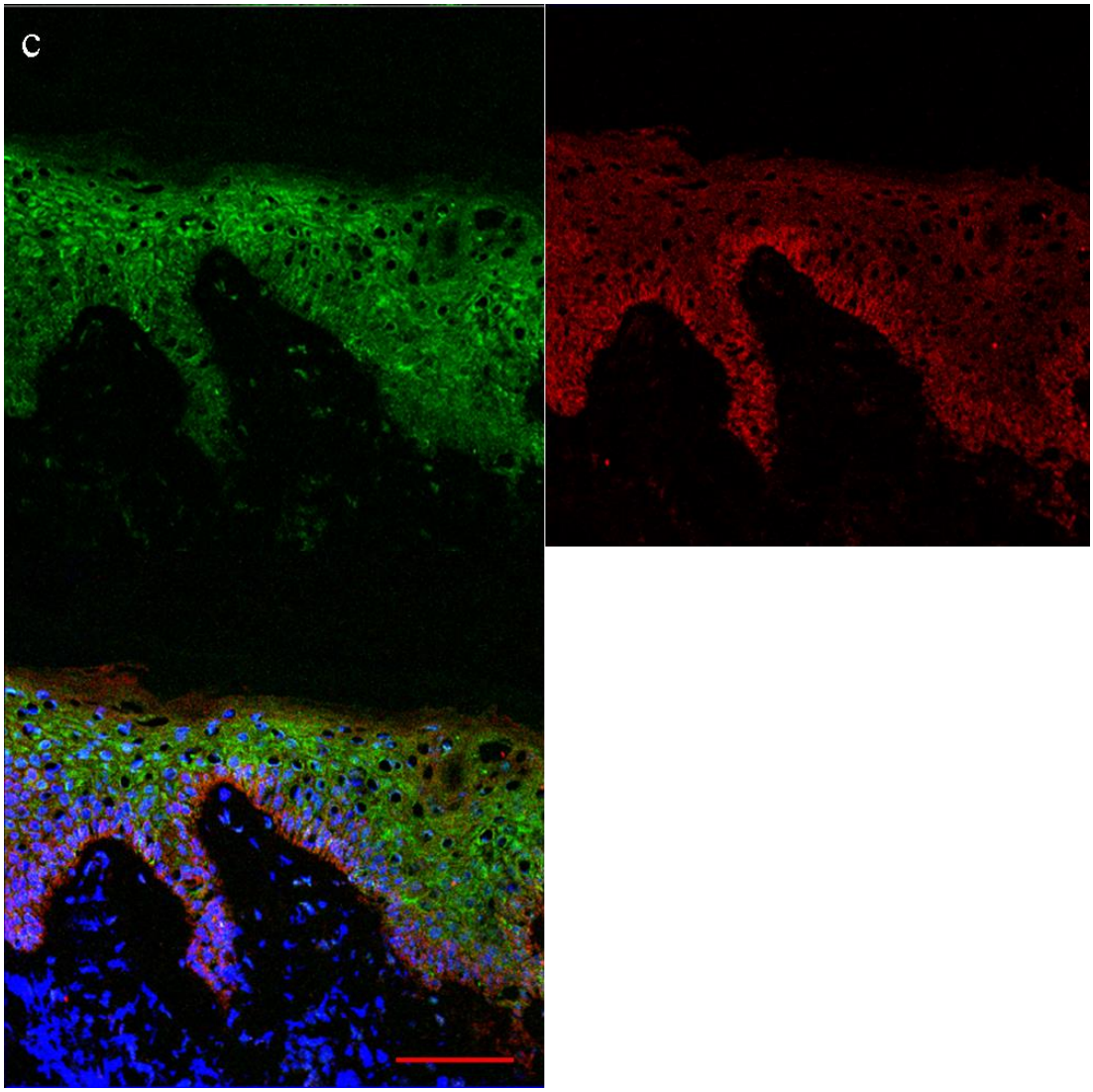

Please see figure legend on page 198

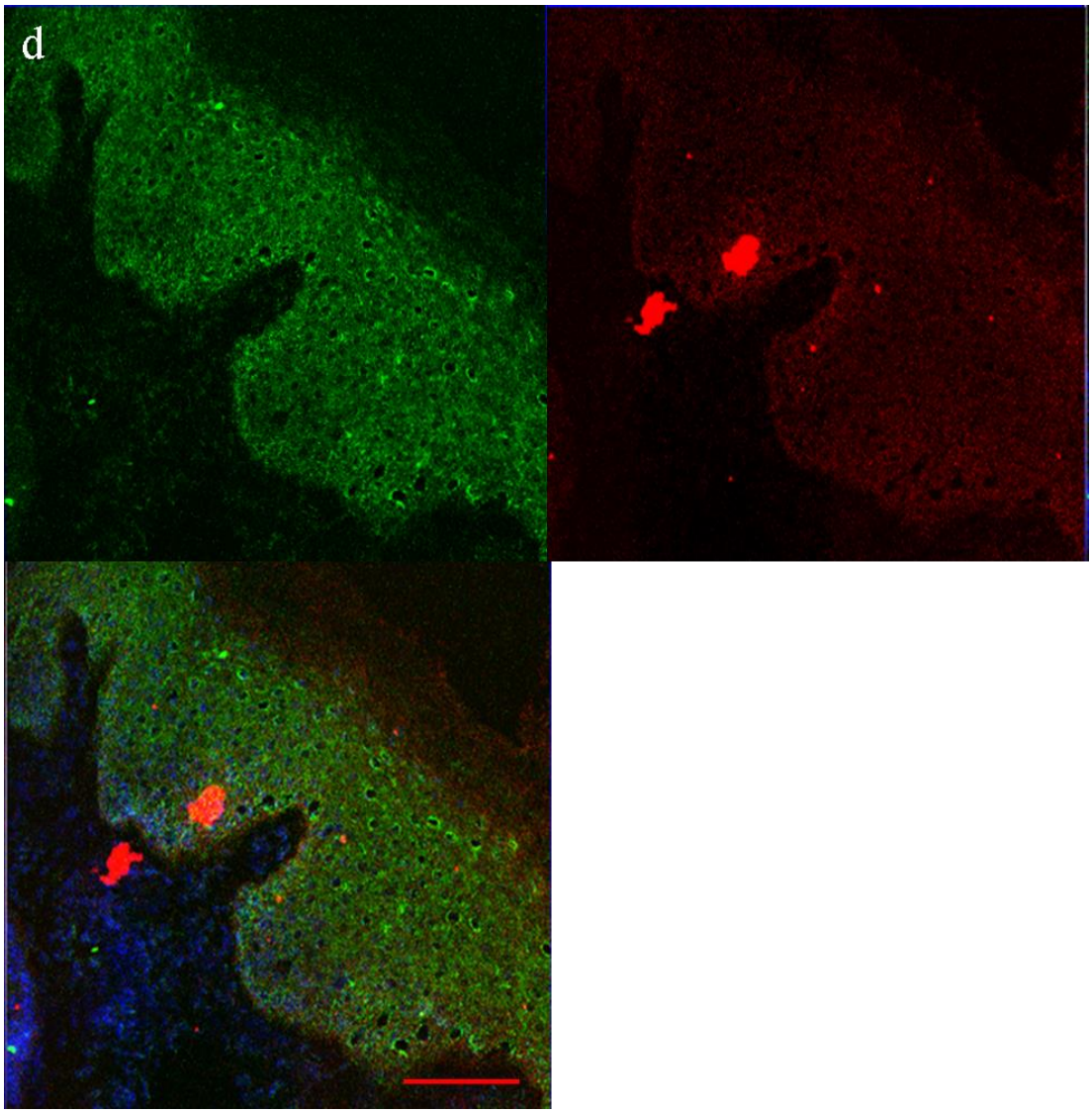

Figure 4.29: GLI1 and GLI2 expression in Basal Cell Carcinoma samples using GLI1 (RD) and GLI2 (AbCam) antibodies

Eighteen frozen sections of Basal Cell Carcinomas belonging to different subtypes were double stained using GLI1 (RD) (green) and GLI2 (AbCam) (red) antibodies. Representative BCCs are shown: WC51b – nodular (a), DS327 – nodular (b), AK674 nodular (c), WJ140 – nodular / micronodular (d). GLI1 and GLI2 staining is present thorough the epidermis and in the BCC tumour masses, showing areas of overlapping expression as well as areas where one protein appears to be more abundant than the other. Localisation of both proteins is overall mainly cytoplasmic. Scale bar represents 50 µm.

4.2.18 Analysis of antibodies specificity in cultured cell lines

4.2.18.1 Immunofluorescent analysis using SMO inhibitors

Antibodies against GLI1 and GLI2 have been made commercially available recently and therefore not thoroughly been tested for specificity; however, most of the antibodies I used for staining of tissue sections had been used in recent publications (see Appendix IV). Positive results indicating good antibody specificity for GLI1 H-300 and GLI1 C-18 have been obtained by other members of the group, as described in the following sections. Moreover, GLI2 H-300 has been validated in a recent publication (Bishop *et al.*, 2010).

Antibodies specificity was analysed by immunofluorescence using NEB1 keratinocytes exposed to SMO inhibitors KAAD-cyclopamine (KAAD-cyc) and SANT-1. NEB1 wild-type keratinocytes had been shown to express GLI1 (M. Rahman et al, unpublished results); NEB1 PTCH1 knockdown keratinocytes (shPTCH1 189A), in which GLI1 has been shown to be upregulated (M. Rahman et al, unpublished results), have also been tested. KAAD-cyclopamine is a cyclopamine derivative that has been shown to inhibit Hedgehog signaling in a mouse cultured cell assay (Taipale et al., 2000), while SANT-1 is a chemically synthesized Hedgehog pathway inhibitor identified in a high-throughput screening (Chen *et al.*, 2002); both molecules act as SMO antagonists.

Other work in the group has shown that exposure of NEB1 keratinocytes to either KAAD-cyc or SANT-1 100 nM for 24 hours suppresses GLI1 expression as shown by qPCR and immunofluorescence with the GLI1 H-300 and GLI1 C-18 antibodies (M. Rahman et al, unpublished data). Reciprocally, targeted suppression of PTCH1 with shRNA leads to an increase of GLI1 as shown by qPCR and immunofluorescence with GLI1 H-300 and GLI1 C-18 antibodies thus helping confirm their specificity. In NEB1 PTCH1 knockdown keratinocytes (shPTCH1 189A) GLI1 H-300 gives a nuclear pattern in whereas GLI1 C-18 gives a more diffuse cytoplasmic/nuclear pattern (M. Rahman et al, unpublished data). Using the conditions optimised by Mr Muhammad Rahman, I performed a preliminary experiment to validate GLI1 RD antibody specificity using GLI1 H-300 as a positive control. NEB1 keratinocytes were exposed to either KAAD-cyclopamine (100 nM),

SANT-1 (100 nM) or DMSO (negative control) for 24 hours, then fixed and stained with either GLI1 RD or GLI1 H300 antibody (Fig. 4.30); staining intensity was subsequently measured using the ImageJ software (Fig. 4.31).

No significative decrease in immunofluorescence was observed with either antibody in cells treated with SMO antagonists (as measured with the Image J software (Fig. 4.31)), but exposure to KAAD-cyc resulted in a partial loss of the nuclear immunofluorescent signal with the GLI1 H-300 (Fig. 4.30, panel e); this suggest GLI1 is inhibited from entering the nucleus which correlates with what is know about the mechanism of canonical HH signalling. The different results obtained in the experiment I did are possibly due to the fact a different batch of inhibitor was used, and this may not have been as effective (other people in the group have also noted batch to batch variation with SMO antagonists). I subsequently employed NEB1 shPTCH1 keratinocytes to determine if an increase in GLI1 fluorescence could be detected with the GLI1 RD antibody, similarly to what has been observed by Mr Muhammad Rahman with the GLI1 H-300 antibody; I included GLI1 H-300 antibody in this experiment a positive control.

NEB1 scramble control (shCON) or NEB1 PTCH1 knockdown keratinocytes (shPTCH1 189A) were fixed and then stained with either GLI1 RD or GLI1 H300 antibody (Fig. 4.32); staining intensity was measured using the ImageJ software (Fig. 4.33).

With GLI1 RD antibody there seems to be slightly an increase in GLI1 fluorescence in PTCH1 knockdown cells (shPTCH1 189A) compared to scramble control (shCON) (as measured with the Image J software (Fig. 4.33)), although this is not statistically significative. Surprisingly this is not observed with GLI1 H-300. GLI1 H-300 staining appears more nuclear in PTCH1 knockdown cells (shPTCH1 189A) (Fig 4.32), consistent with GLI1 nuclear translocation as a result of PTCH1 inactivation; this is not as clearly observed using the GLI1 RD antibody.

Since a decrease in GLI1 RD immunofluorescence was not observed using SMO antagonists, nor a clear GLI1 RD fluorescence increase in PTCH1 knockdown cells, we decided to use short interfering RNA (siRNA) technology to help validate antibody specificity.

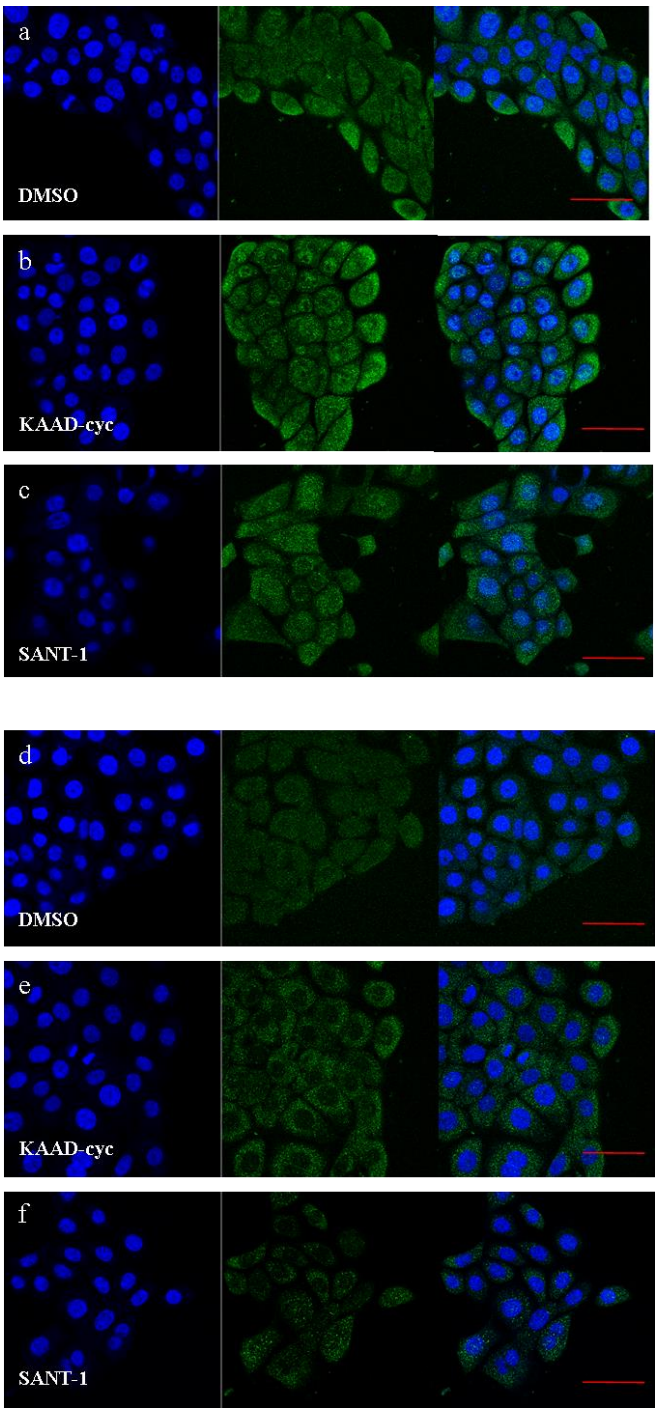

Figure 4.30: Immunofluorescent analysis of NEB1 keratinocytes treated with SMO inhibitors using GLI1 (RD) and GLI1 (H-300) antibodies

NEB 1 keratinocytes were treated with SMO inhibitors KAAD-cyclopamine or SANT-1 (both 100 nM) for 24 hours, fixed and stained with either GLI1 RD (panel a, b, c) or GLI1 H300 antibody (panel d, e, f). Control cells were treated with DMSO only (a, d). Quantification of staining intensity from these images is shown in Figure 4.31. Scale bar represents 20 µm.

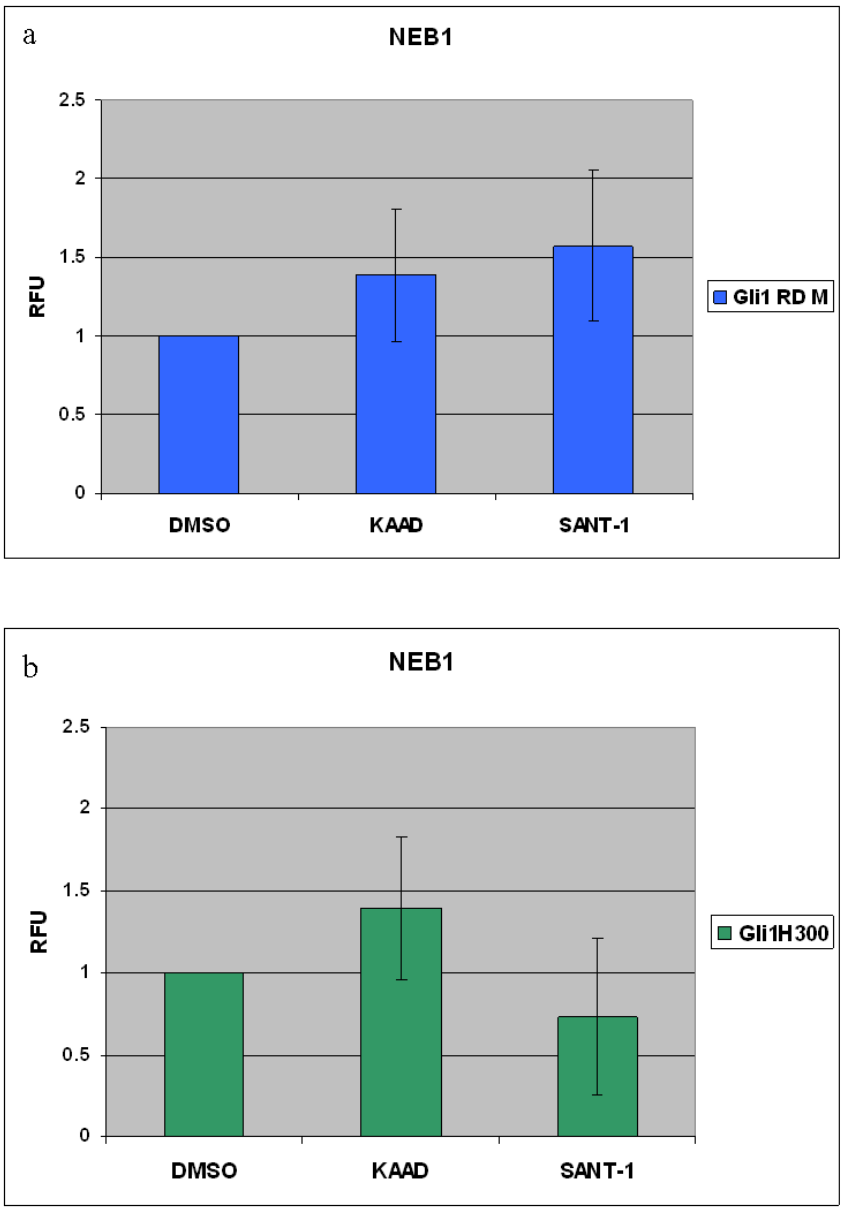

Figure 4.31: Quantification of immunofluorescent analysis of NEB1 keratinocytes treated with SMO inhibitors using GLI1 (RD) and GLI1 (H-300) antibodies

Quantification of GLI1 antibodies fluorescence intensity in NEB1 keratinocytes exposed to SMO inhibitors. Images displayed in Figure 4.30 were quantified using the image processing software Image J. (a) GLI1 RD antibody (b) GLI1 H300 antibody. Data are expressed as mean ± standard deviation. RFU, Relative Fluorescence Units.

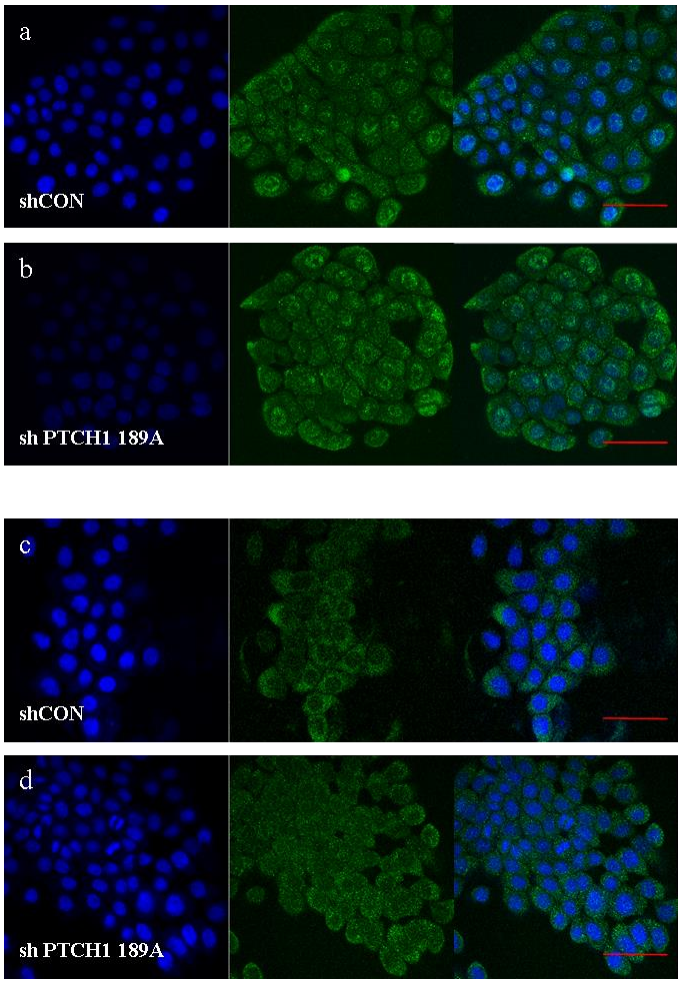

Figure 4.32: Immunofluorescent analysis of NEB1 PTCH1 knockdown keratinocytes using GLI1 (RD) and GLI1 (H-300) antibodies

NEB 1 scramble control (shCON) (a, c) or PTCH1 knockndown (sh PTCH1 189A) (b, d) keratinocytes were then fixed and stained with either GLI1 RD (a, b) or GLI1 H300 (c, d) antibody. Quantification of staining intensity from these images is shown in Figure 4.33. Scale bar represents 20 µm.

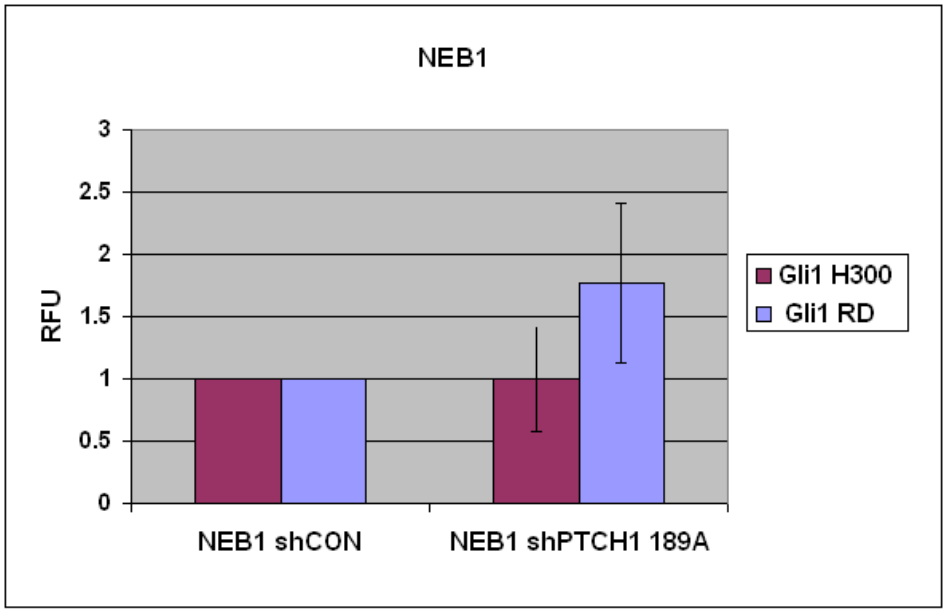

Figure 4.33: Quantification of NEB1 PTCH1 knockdown keratinocytes using GLI1 (RD) and GLI1 (H-300) antibodies

Quantification of GLI1 fluorescence intensity in NEB1 scramble control (shCON) or PTCH1 knockdown keratinocytes (189A) using GLI1 RD or GLI1 H300 antibody. Images displayed in Figure 4.32 were quantified using the image processing software ImageJ. Data are expressed as mean ± standard deviation. RFU, Relative Fluorescence Units.

4.2.18.2 GLI1 siRNA optimisation in NEB 1 keratinocytes

Short interfering RNA (siRNA) is a technique used to modulate the expression of a particular gene by interfering with the stability of its messenger RNA (mRNA). Short double stranded RNA molecules against a specific mRNA target are introduced into cells by transfection; once in the cytoplasm the RNA is unwound and processed, so that it can bind to complementary sequence found on the mRNA leading to its degradation. Conditions for GLI1 siRNA were optimised by Mr Sandeep Nadendla, who observed ectopic GLI1 was maximally suppressed in LNCaP-GLI1 prostate cancer cells 96 hours post-transfection by Western Blotting and qPCR (Nadendla *et al.*, 2011). He employed a commercially available siRNA against GLI1 (si5816, Ambion) at 30 nM concentration. Moreover, at 96 hours post-transfection levels of endogenous GLI1 mRNA were reduced in DU145 and PC-3 prostate cancer cells (Nadendla *et al.*, 2011)). Another positive results indicating good antibody specificity for GLI1 H-300 came from data obtained by Miss Jane Elliott. GLI1-expressing BCC-derived fibroblasts were transfected with siRNA si5816 using Lipofectamine: after 96 hours of transfection GLI1 H-300 fluorescence was almost completely abolished compared to the Lipofectamine only mock transfection (J. Elliott et al., unpublished results).

siGlo is a fluorescently labelled siRNA against Cyclophilin B which localises to the endoplasmic reticulum and is used to assess transfection efficiency. I therefore tested two different commercially available siRNAs (si5815 and si5816, Ambion, see Appendix II for details) against GLI1 in NEB 1 keratinocytes using the optimal 96 hours timepoint and 30 nM final concentration. siGLO Cyclophilin B siRNA was used as a control: siGLO Cyclophilin B are fluorescent double stranded siRNA against Cyclophilin B, a protein widely expressed in human cells whose silencing does not impact on cell viability. Cells were reverse-transfected with siRNAs, grown for 96 hours, then fixed and stained with GLI1 RD antibody (Fig. 4.34). If the siRNA had successfully downregulated GLI1 mRNA levels there should be a reduction in the amount of GLI1 protein present inside the cell and therefore a reduction in staining intensity. A lower level of fluorescence in cells silenced for GLI1 would suggest good antibody specificity. Similar validation could be carried out for GLI2 antibodies. There seem to be no significative reduction in staining intensity in GLI1

silenced cells compared to siGLO controls using GLI1 RD antibody (staining intensity was quantified using the ImageJ software) (Fig. 4.35). Lack of reduction in fluorescence levels in GLI1 siRNA cells could be due to inefficient silencing, therefore in the following experiment GLI1 mRNA levels were analysed before staining for GLI1. Since NEB1 keratinocytes have been shown to be quite difficult to transfect (M. Rahman et al., unpublished data), Hacat keratinocytes and more easily transfectable prostate cancer cell lines were used in subsequent experiments.

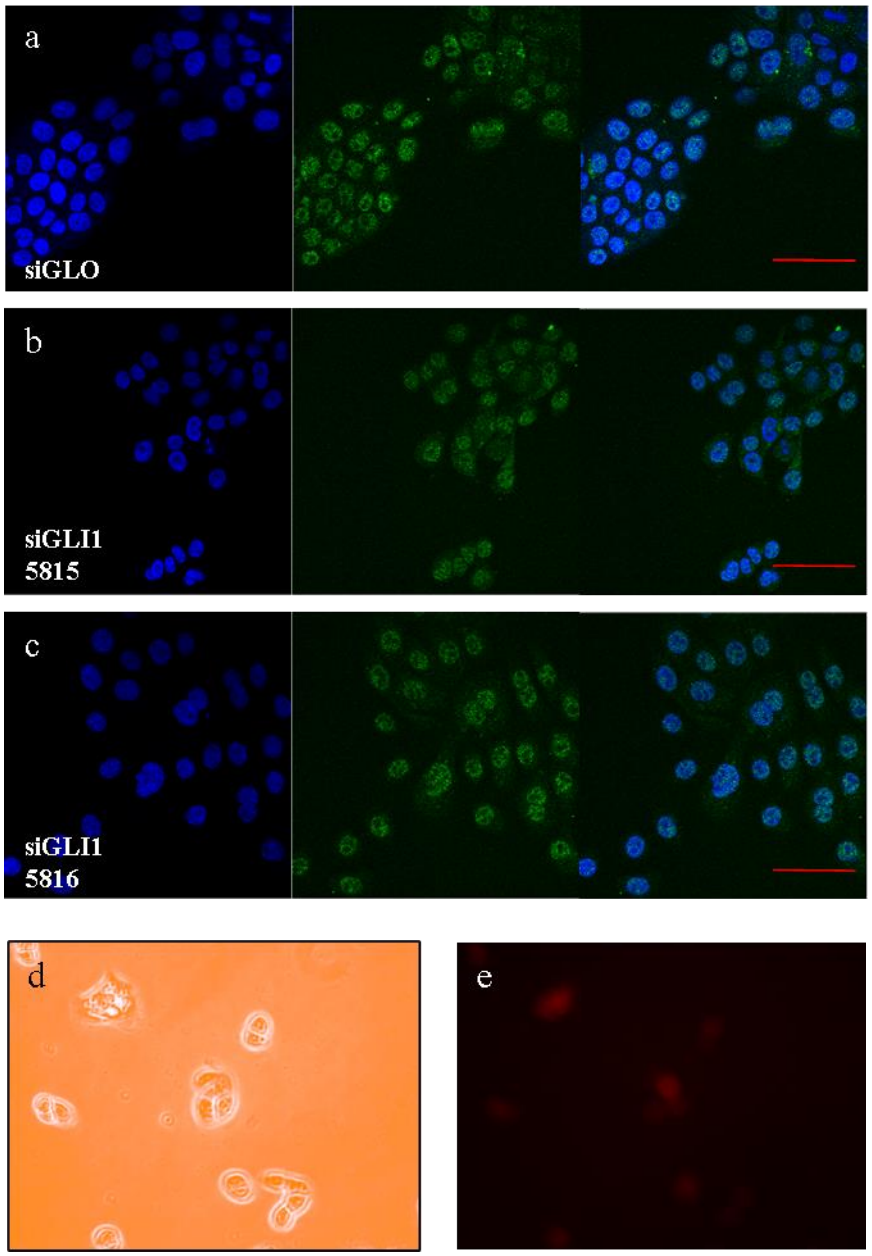

Figure 4.34: Immunofluorescent analysis of NEB1 GLI1 siRNA keratinocytes using GLI1 (RD) antibody

NEB 1 keratinocytes were treated with two different short interfering RNA (siGLI1 5815, panel b and siGLI1 5816, panel c) for 96 hours, then fixed and stained with GLI1 RD antibody. siGlo control (panel a). siGlo fluorescence in NEB1 keratinocytes: brightfield (d), siGlo (e). Scale bar represents 20 µm.

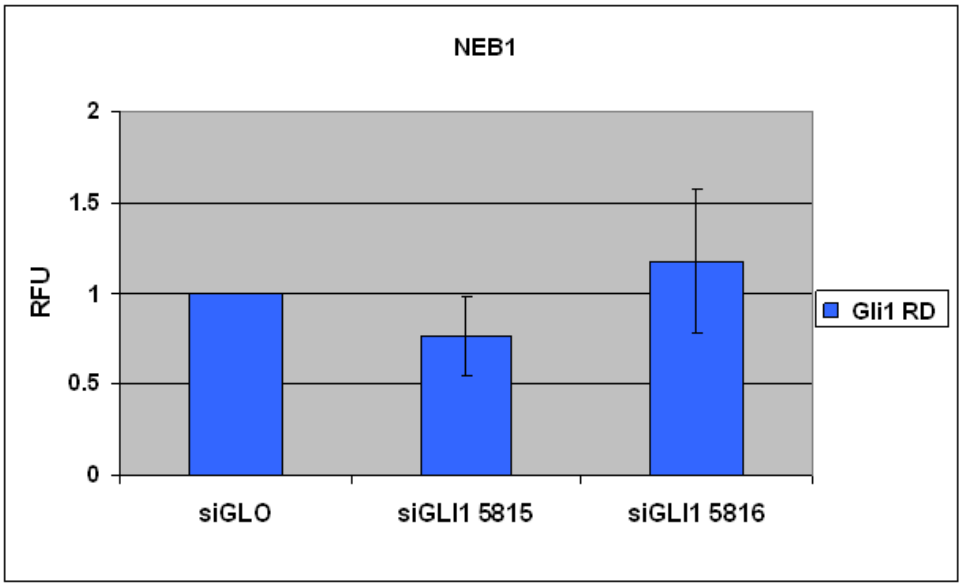

Figure 4.35: Quantification of immunofluorescent analysis of NEB1 GLI1 siRNA keratinocytes using GLI1 (RD) antibody

Quantification of GLI1 RD antibody fluorescence intensity in NEB1 keratinocytes treated with two different short interfering RNA (si5815, si5816); control cells were treated with siGlo. Images displayed in Figure 4.35 were quantified using the image processing software Image J. Data are expressed as mean ± standard deviation. RFU, Relative Fluorescence Units.

4.2.18.3 GLI1 siRNA optimisation in Hacat keratinocytes

Levels of messenger RNA (mRNA) for Cyclophilin B and for GLI1 were measured in Hacat cells transfected with two different commercially available siRNAs against GLI1 (si5815 and si5816, Ambion). Two control siRNAs were used: siGlo against Cyclophilin B (see section 4.2.17.2) and siAmb, a scramble non-fluorescent control from Ambion (Silencer Negative Control #1, Ambion, U.K.). Cyclophilin B is a protein expressed in most human cells and measuring the level of its mRNA in the siGLO Cyclophilin B siRNA transfected cells gives an indication of the efficiency of the transfection and a hint that successful silencing could be achieved with the conditions used (though siRNA against GLI1 could have a different efficiency as this is dependent on other factors, including the sequence used). Hacat keratinocytes were transfected with siRNAs and grown for 96 hours, then RNA was extracted using a commercially available kit (RNeasy Mini Kit, Qiagen, U.K.) and qPCR analysis was performed. Primers used for detection of GLI1 (Yauch et al., 2008) are designed against a region located in the middle of the human GLI1 mRNA transcript. Cyclophilin B mRNA levels appear to be reduced in Hacat siGLO cells, indicating successful transfection (Fig. 4.36, a). There seem to be a reduction in GLI1 mRNA levels with siRNA 5815 but levels are increased with siRNA 5816 (Fig. 4.36, b).

The results of these preliminary experiments are unexpected and further investigation would be needed in order to validate the GLI1 RD antibody.

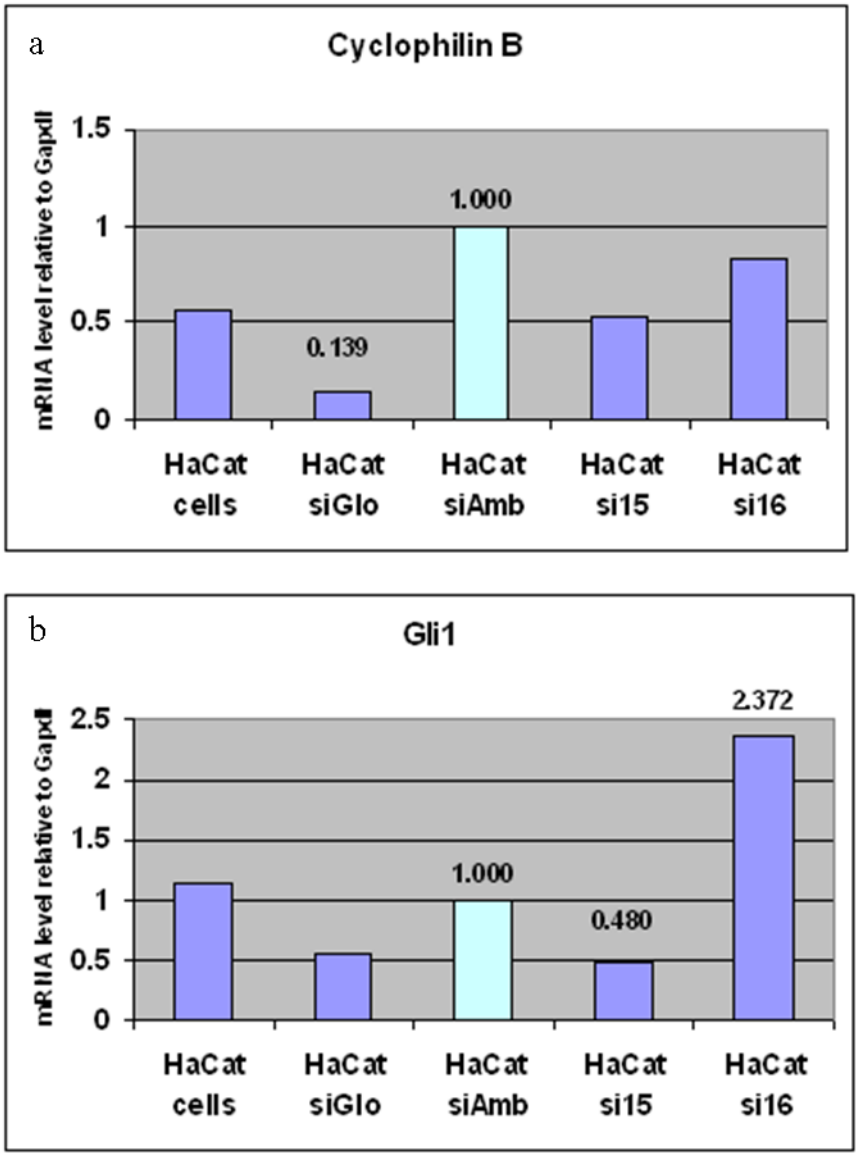

Figure 4.36: qPCR analysis for Cyclophilin B and for GLI1 of Hacat keratinocytes transfected with two different GLI1 siRNAs

qPCR measurements of mRNA levels of Cyclophilin B and of GLI1 in Hacat keratinocytes transfected with two different GLI1 siRNA (si5815 and si5816). All values are expressed relative to Hacat siAmb scramble control taken as 1.

4.2.18.4 GLI2 siRNA optimisation in Du145 cells and Hacat keratinocytes (experiment 1)

In order to validate the GLI2 Abcam antibody, siRNA experiments were carried out similar to what has been done for GLI1. Conditions for GLI2 siRNA were optimised by Mr Sandeep Nadendla, who observed a reduction in the levels of endogenous GLI2 mRNA at 96 hours post-transfection in DU145 and PC-3 prostate cancer cells (Nadendla *et al.*, 2011); he used a commercially available siRNA against GLI2 (si5817, Ambion) at 30 nM concentration. GLI2 H-300 has been validated for immunofluorescence in a recent publication (Bishop *et al.*, 2010) and was used as a positive control. I therefore tested GLI2 si5817 siRNA (using the optimal 96 hours timepoint and 30 nM final concentration) in Hacat (spontaneously transformed keratinocytes) and Du145 (prostate cancer cell line) cells as they are reported to be relatively easy to transfect; Du145 cells have also been shown to express high levels of GLI2 (Nadendla *et al.*, 2011). Cells were stained with either GLI2 H300 or GLI2 Abcam antibody (Fig. 4.37 - 4.38 and Fig. 4.40 - 4.41); staining intensity was subsequently measured using the ImageJ software (Fig. 4.39 and Fig 4.42). No significative differences in staining intensity were observed in knockdown cells compared to control with either antibody; this is true for both Du145 and Hacat cells. qPCR analysis reveals levels of Cyclophilin B are reduced approximately by half in both cell types tested (Du145, Fig. 4.43a and Hacat, Fig. 4.44a). In Du145 cells siRNA si17 seems to reduce GLI2 level by half, though only by about 15% in Hacat cells (Fig. 4.43b and 4.44b). As no difference was observed by immunofluorescence and because of the discrepancy with the qPCR data, Western Blotting analysis was also performed. GLI2 levels appear reduced with si17 by Western Blot using the GLI2 H300 antibody; however, GLI2 levels in the controls raise some concerns as they seem to vary in Du145 cells while in Hacat keratinocytes siGlo and siAmb GLI2 levels are very similar to si17 (Fig. 4.45). To try and understand the reason for these abnormalities, the experiment was repeated (see section 4.2.17.5).

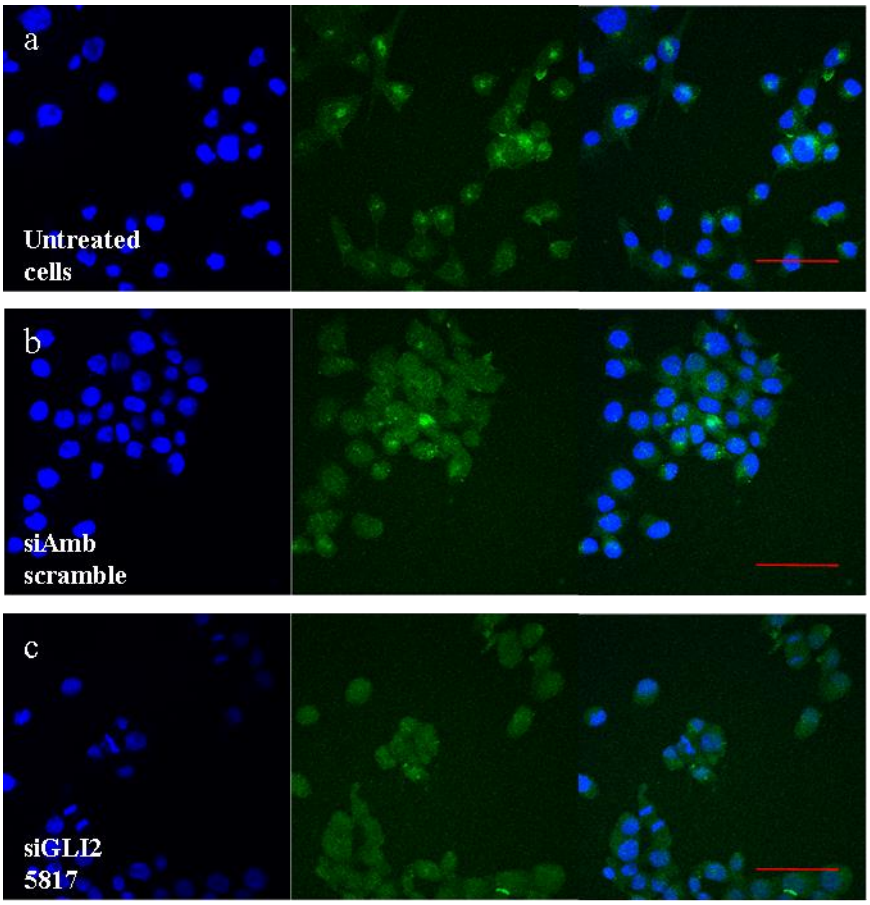

Figure 4.37: Immunofluorescent analysis of Du145 GLI2 siRNA cells using GLI2 (H-300) antibody

Du145 cells were treated with a short interfering RNA (siGLI2 5817) for 96 hours, then fixed and stained with GLI2 H300 antibody (c). Untreated cells (a), cells treated with siAmb scramble control (b). Scale bar represents 20 µm.

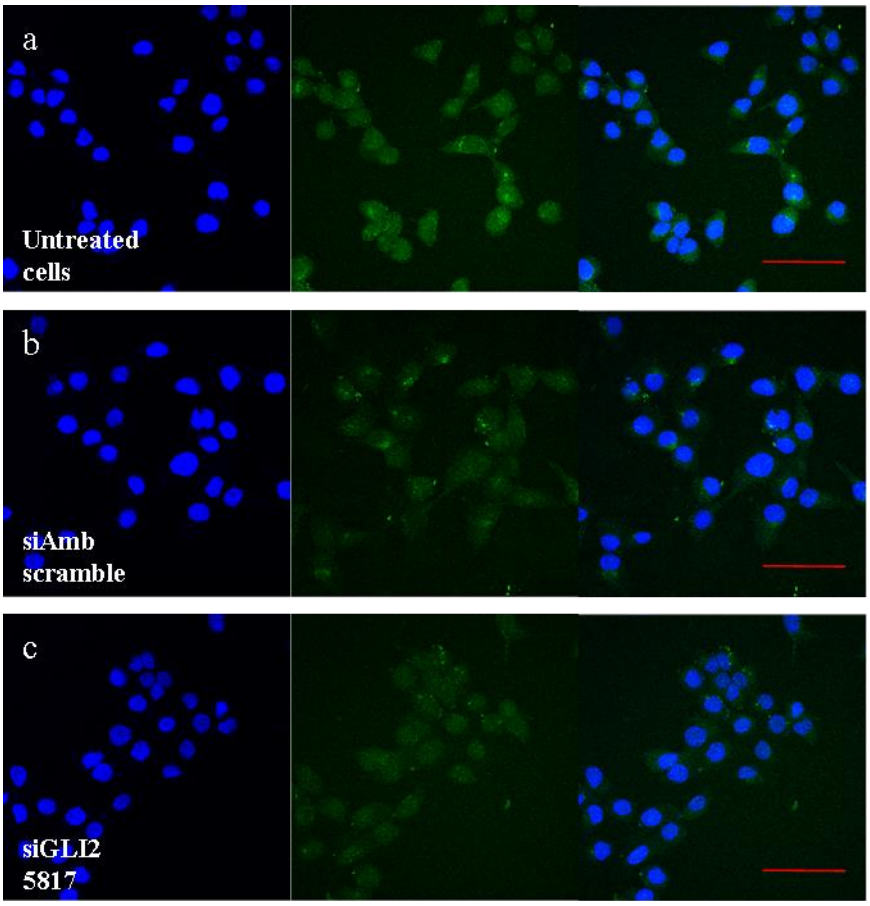

Figure 4.38: Immunofluorescent analysis of Du145 GLI2 siRNA cells using GLI2 (Abcam) antibody

Du145 cells were treated with a short interfering RNA (siGLI2 5817) for 96 hours, then fixed and stained with GLI2 Abcam antibody (c). Untreated cells (a), cells treated with siAmb scramble control (b). Scale bar represents 20 µm.

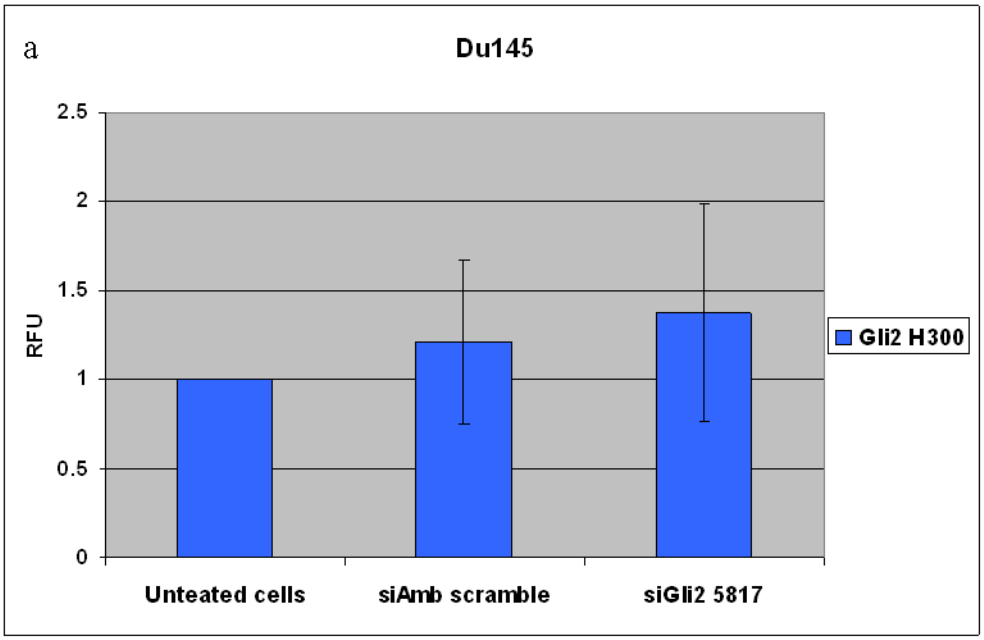

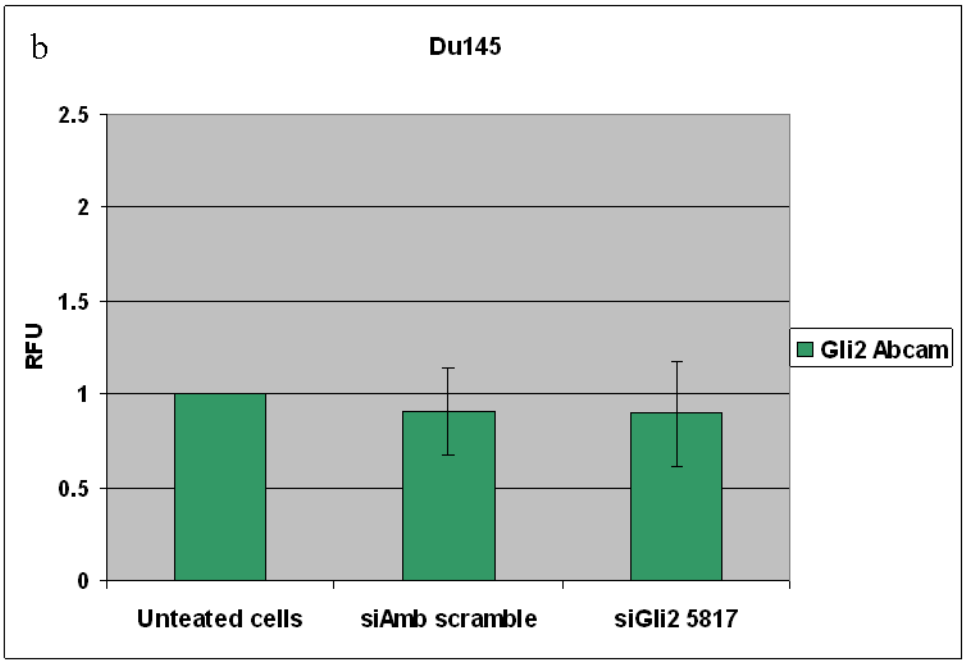

Figure 4.39: Quantification of immunofluorescent analysis of Du145 GLI2 siRNA cells using GLI2 (H-300) and GLI2 (Abcam) antibodies.

Quantification of GLI2 H-300 (a) and GLI2 Abcam (b) antibody fluorescence intensity in Du145 cells treated with short interfering RNA si5817. Images displayed in Fig. 4.38 - 4.39 were quantified using the image processing software Image J. Data are expressed as mean ± standard deviation. RFU, Relative Fluorescence Units.

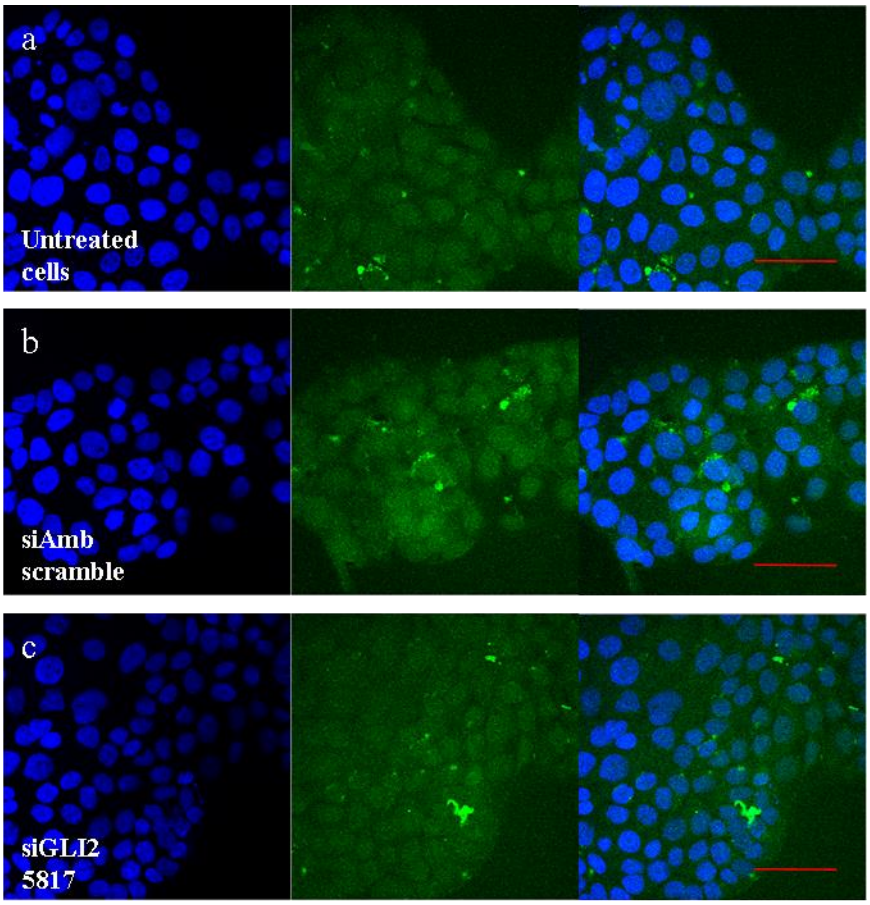

Figure 4.40: Immunofluorescent analysis of Hacat GLI2 siRNA keratinocytes using GLI2 (H-300) antibody

Hacat keratinocytes were treated with a short interfering RNA (siGLI2 5817) for 96 hours, then fixed and stained with GLI2 H300 antibody (c). Untreated cells (a), cells treated with siAmb scramble control (b). Scale bar represents 20 µm.

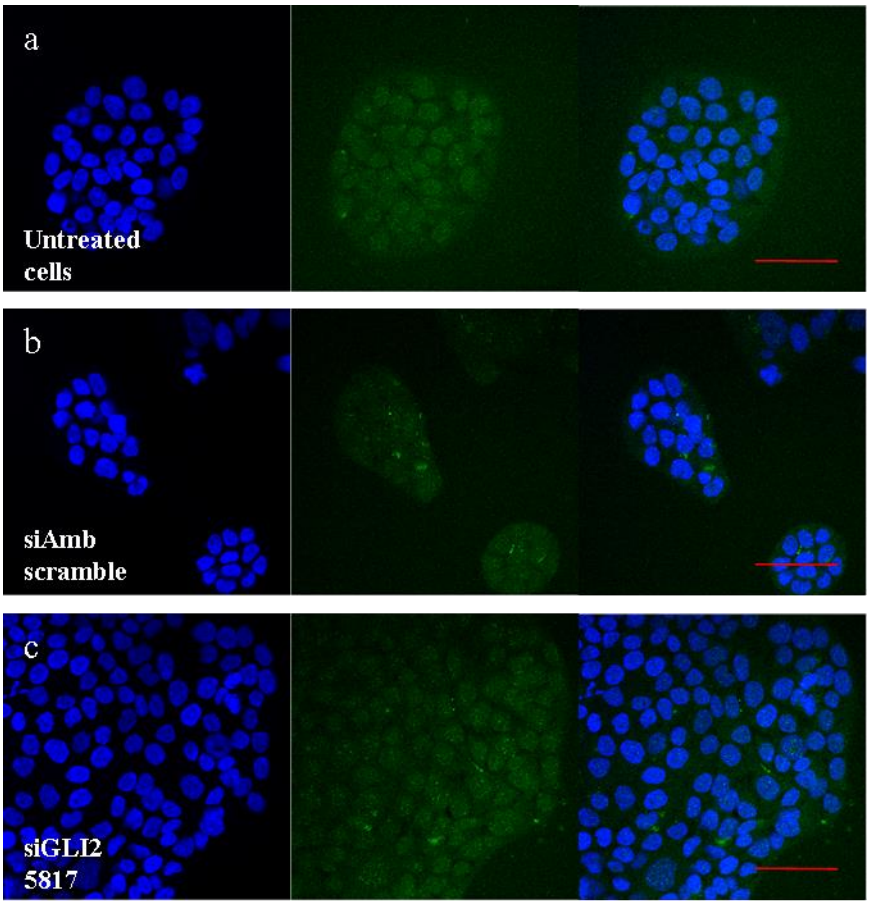

Figure 4.41: Immunofluorescent analysis of Hacat GLI2 siRNA keratinocytes using GLI2 (Abcam) antibody

Hacat keratinocytes were treated with a short interfering RNA (siGLI2 5817) for 96 hours, then fixed and stained with GLI2 Abcam antibody (c). Untreated cells (a), cells treated with siAmb scramble control (b). Scale bar represents 20 µm.

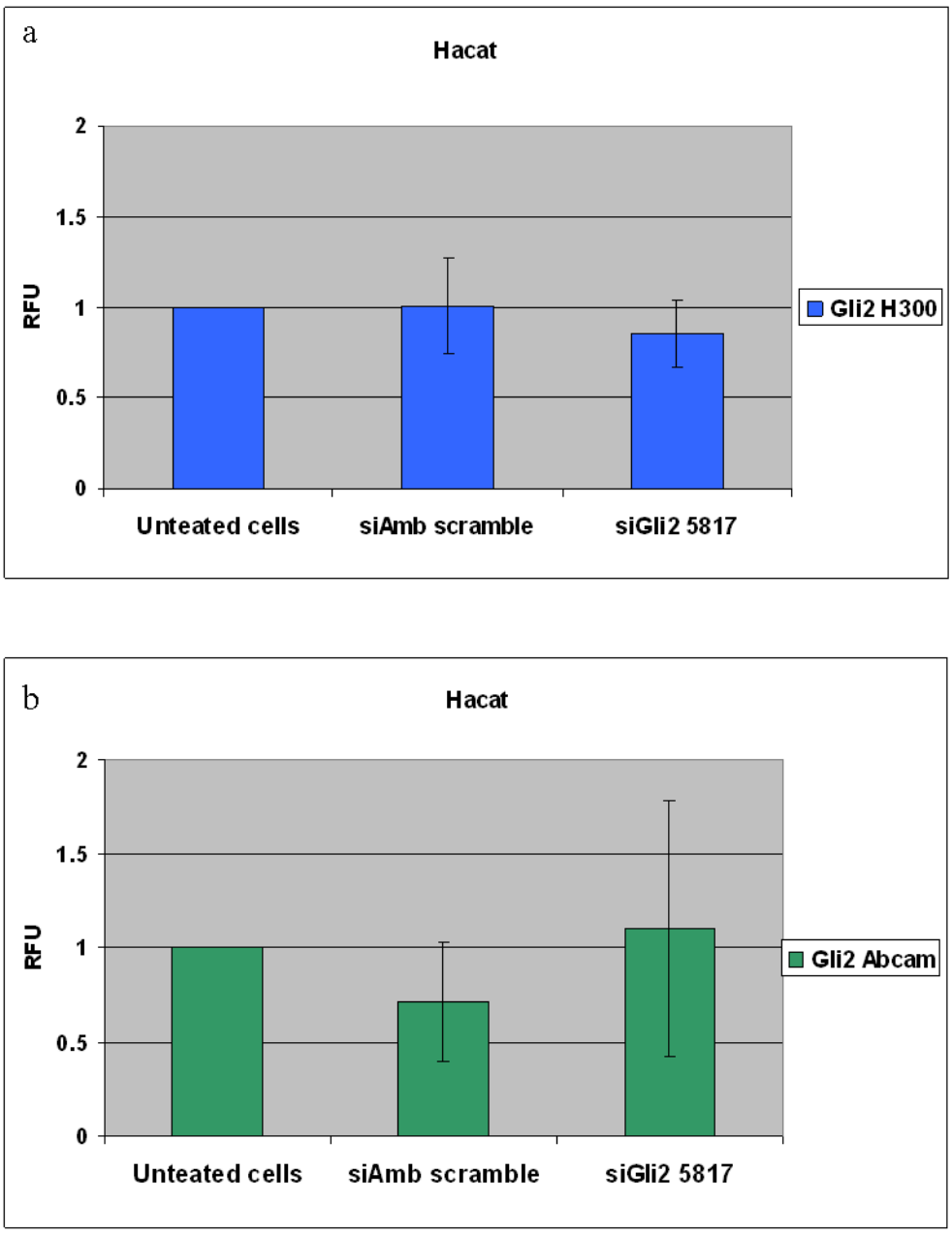

Figure 4.42: Quantification of immunofluorescent analysis of Hacat GLI2 siRNA keratinocytes using GLI2 (H-300) and GLI2 (Abcam) antibodies.

Quantification of GLI2 H-300 (a) and GLI2 Abcam (b) antibody fluorescence intensity in Hacat keratinocytes treated with short interfering RNA si5817. Images displayed in Fig. 4.41 - 4.42 were quantified using the image processing software Image J. Data are expressed as mean ± standard deviation. RFU, Relative Fluorescence Units.

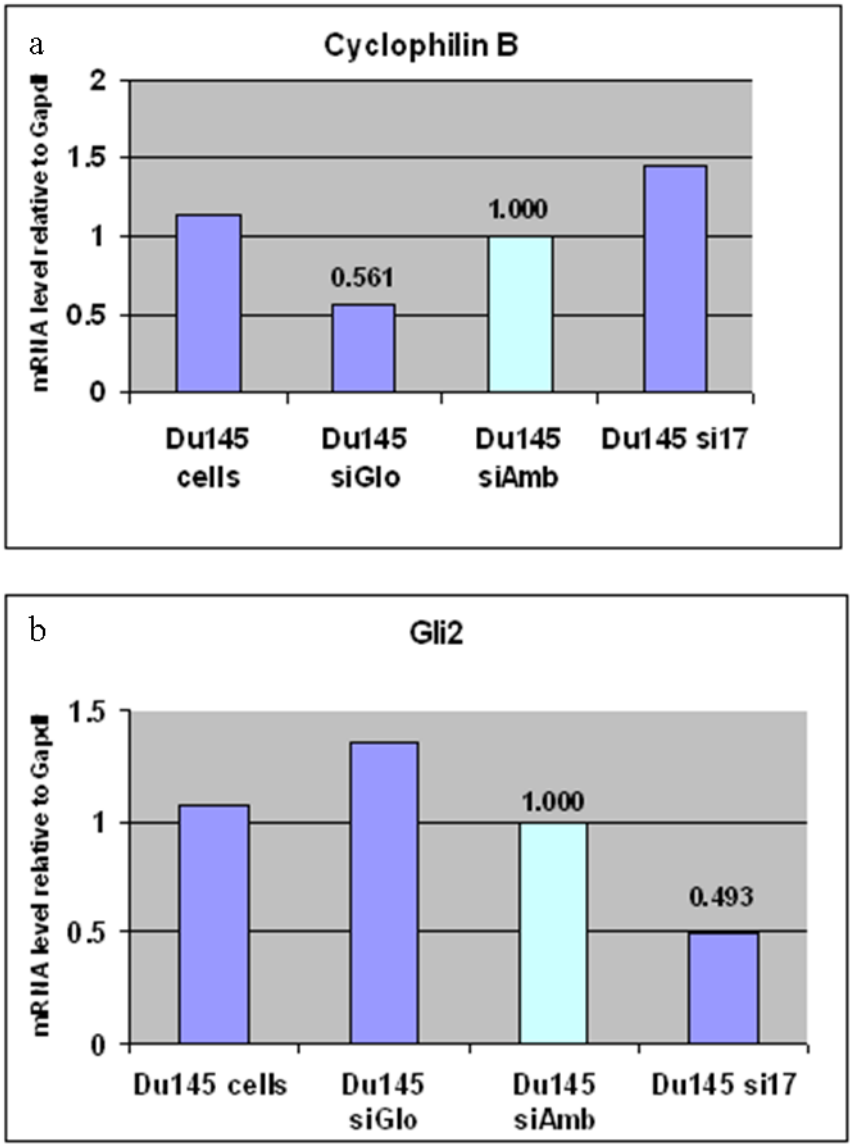

Figure 4.43: qPCR analysis for Cyclophilin B and for GLI2 of Du145 cells transfected with GLI2 siRNA

qPCR measurements of mRNA levels of Cyclophilin B and of GLI2 in Du145 cells transfected GLI2 siRNA (si5817). All values are expressed relative to Du145 siAmb scramble control taken as 1.

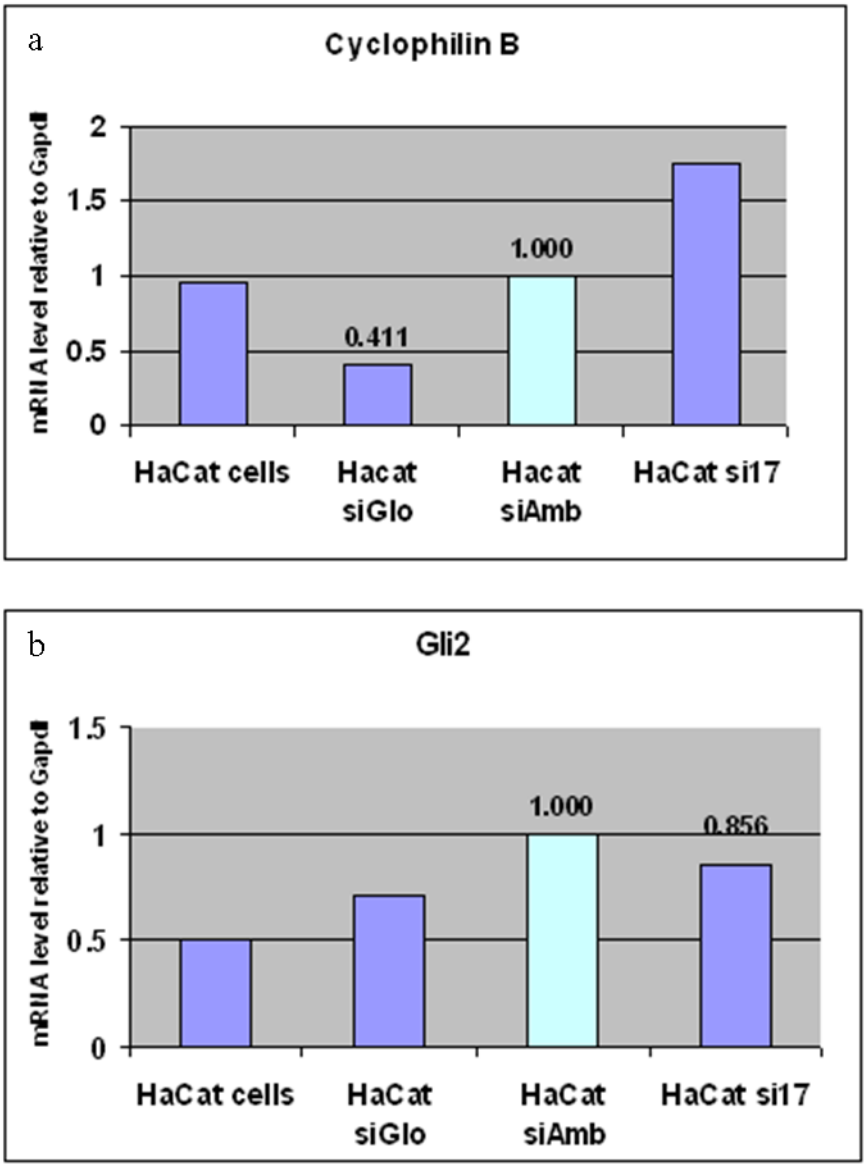

Figure 4.44: qPCR analysis for Cyclophilin B and for GLI2 of Hacat keratinocytes transfected with GLI2 siRNA

qPCR measurements of mRNA levels of Cyclophilin B and of GLI2 in Hacat keratinocytes transfected GLI2 siRNA (si5817). All values are expressed relative to Hacat siAmb scramble control taken as 1.

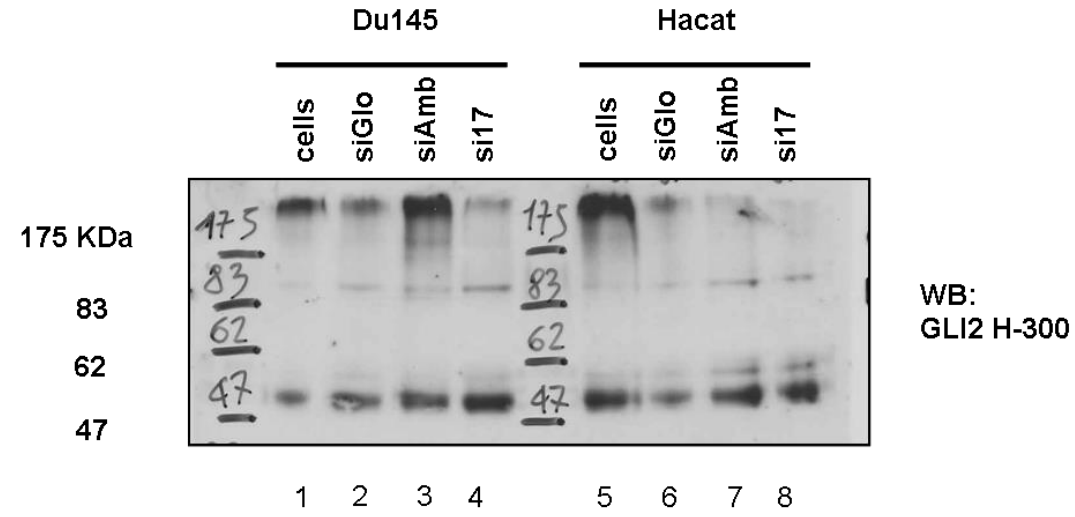

Figure 4.45: Western Blotting for GLI2 protein levels in Du145 cells and Hacat keratinocytes transfected with GLI12 siRNA (GLI2 H300 antibody)

Western Blot analysis of Du145 or Hacat cells with GLI2 H300 antibody. Cells, untreated cells; siAmb, scramble siRNA control; siGlo, Cyclophilin B siRNA fluorescent control, si17, GLI2 siRNA.

4.2.18.5 GLI2 siRNA optimisation in Du145 cells and Hacat keratinocytes (experiment 2)

A second GLI2 siRNA experiment was performed using two different GLI2 siRNAs, si17 (see section 4.2.17.4) and si44 (see Appendix II for details).

The transfection seem to have worked in all cell types judging by Cyclophilin B levels analysed by qPCR (Fig. 4.46a and Fig. 4.47a) but GLI2 interference looks effective

only in Du145, with si17 giving the best result. In Hacat keratinocytes GLI2 siRNA appears ineffective at reducing GLI2 levels (si44) or, paradoxically, seems to increase its levels (si17) (Fig. 4.46 b and Fig. 4.47 b). In Western Blotting analysis using the GLI2 H300 antibody no significative difference in GLI2 band intensity was observed between siRNA cells and controls in both Du145 and Hacat cells (Fig. 4.48). LnCap and PC3 (prostate cancer cell lines) cells were included for comparison. GLI2 expressed by these cells migrates at a slightly lower molecular weight, in line with the hypothesis that different isoforms or differently cleaved products of GLI2 are expressed by different cell types. In Western Blot analysis of Du145 cells using GLI2 Abcam antibody (Fig. 4.49) GLI2 was only picked up in LnCap cells included in the blot as a reference. Immunofluorescent analysis revealed an extremely faint staining with both GLI2 H-300 and GLI2 Abcam and no difference in intensity could be detected in GLI2 silenced cells (data not shown). Because of the anomalies observed in the analysis of GLI2 siRNA cells, the specificity of the GLI2 Abcam antibody cannot be confirmed with the data gathered so far and further experiments would be needed.

To help confirm the validity of the immunohistochemistry work previously described Laser Capture Microdissection could be used; preliminary experiments to optimise this technique are described in section 4.2.18.

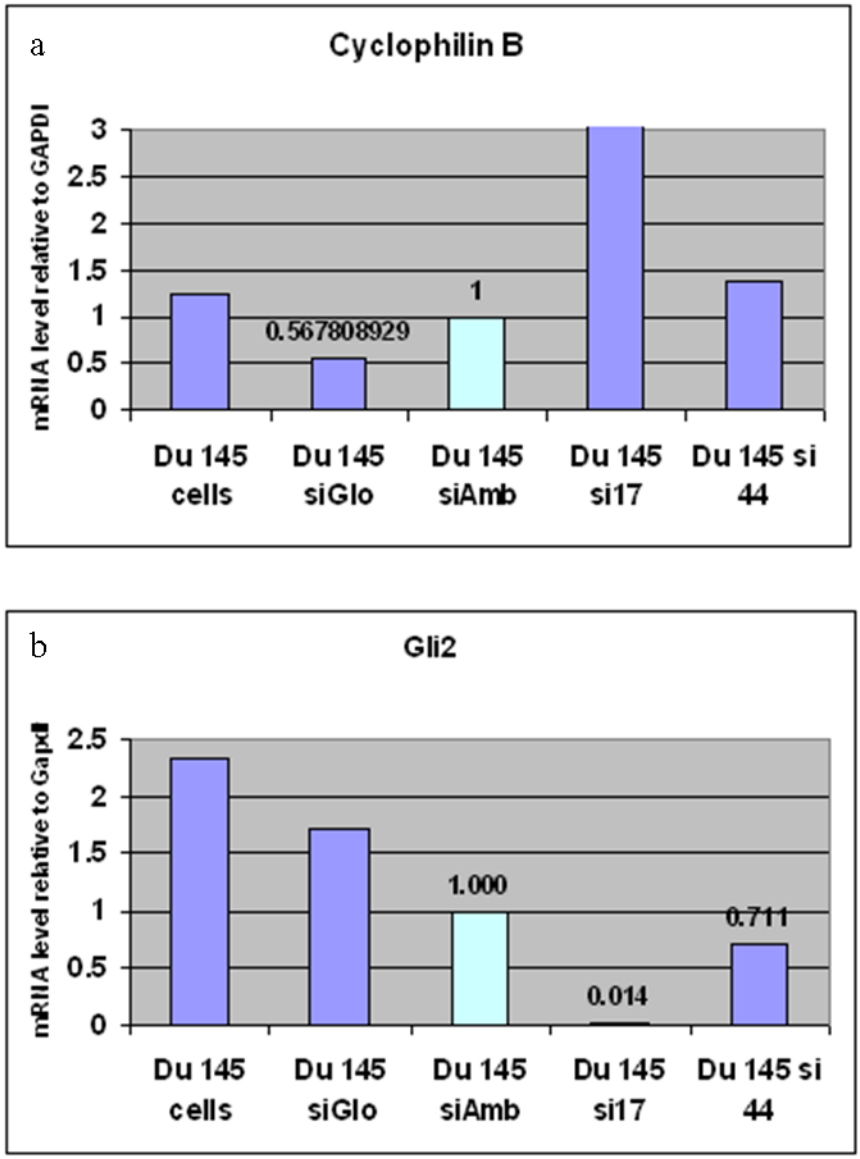

Figure 4.46: qPCR analysis for Cyclophilin B and for GLI2 of Du145 cells transfected with two different GLI2 siRNAs

qPCR measurements of mRNA levels of Cyclophilin B and of GLI2 in Du145 cells transfected with two different Gli2 siRNA (si17 and si44). All values are expressed relative to Du145 siAmb scramble control taken as 1.

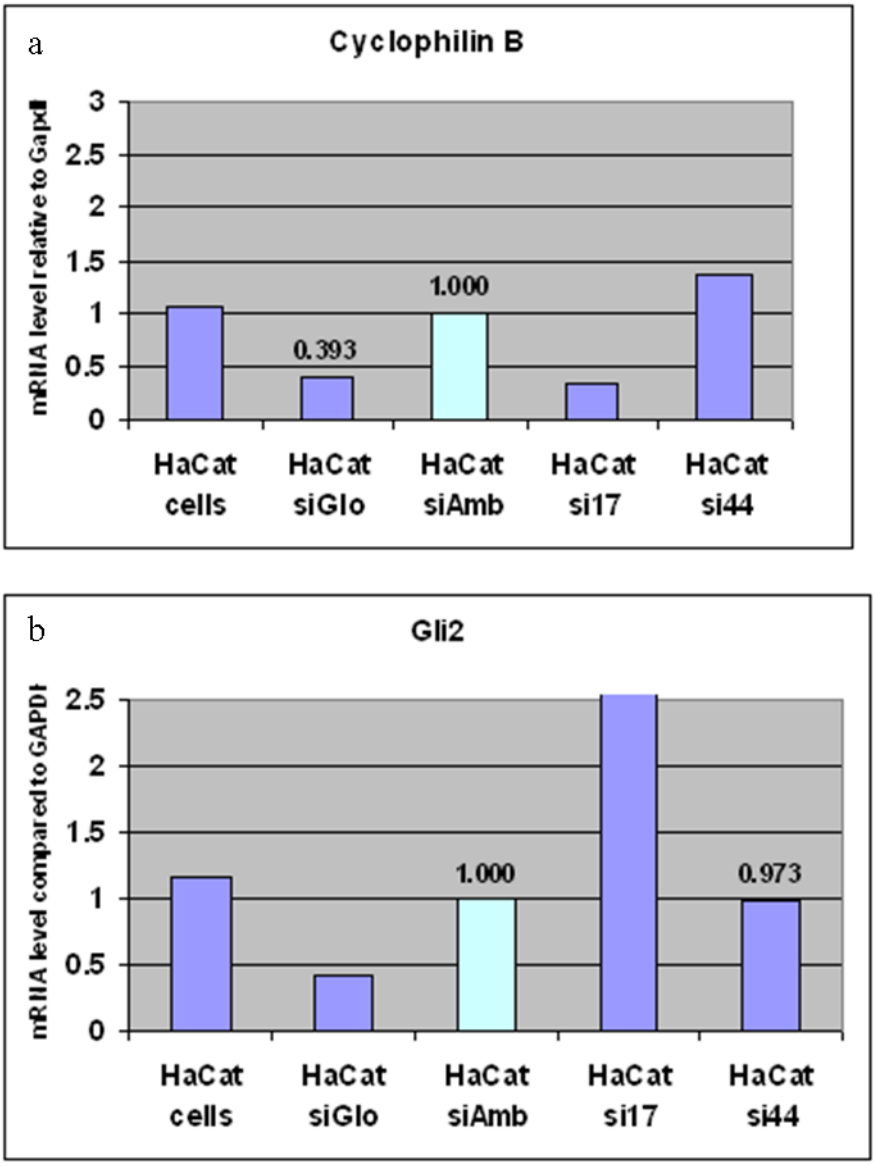

Figure 4.47: qPCR analysis for Cyclophilin B and for GLI2 of Hacat keratinocytes transfected with two different GLI2 siRNAs

qPCR measurements of mRNA levels of Cyclophilin B and of GLI2 in Hacat keratinocytes transfected with two different Gli2 siRNA (si17 and si44). All values are expressed relative to Hacat siAmb scramble control taken as 1.

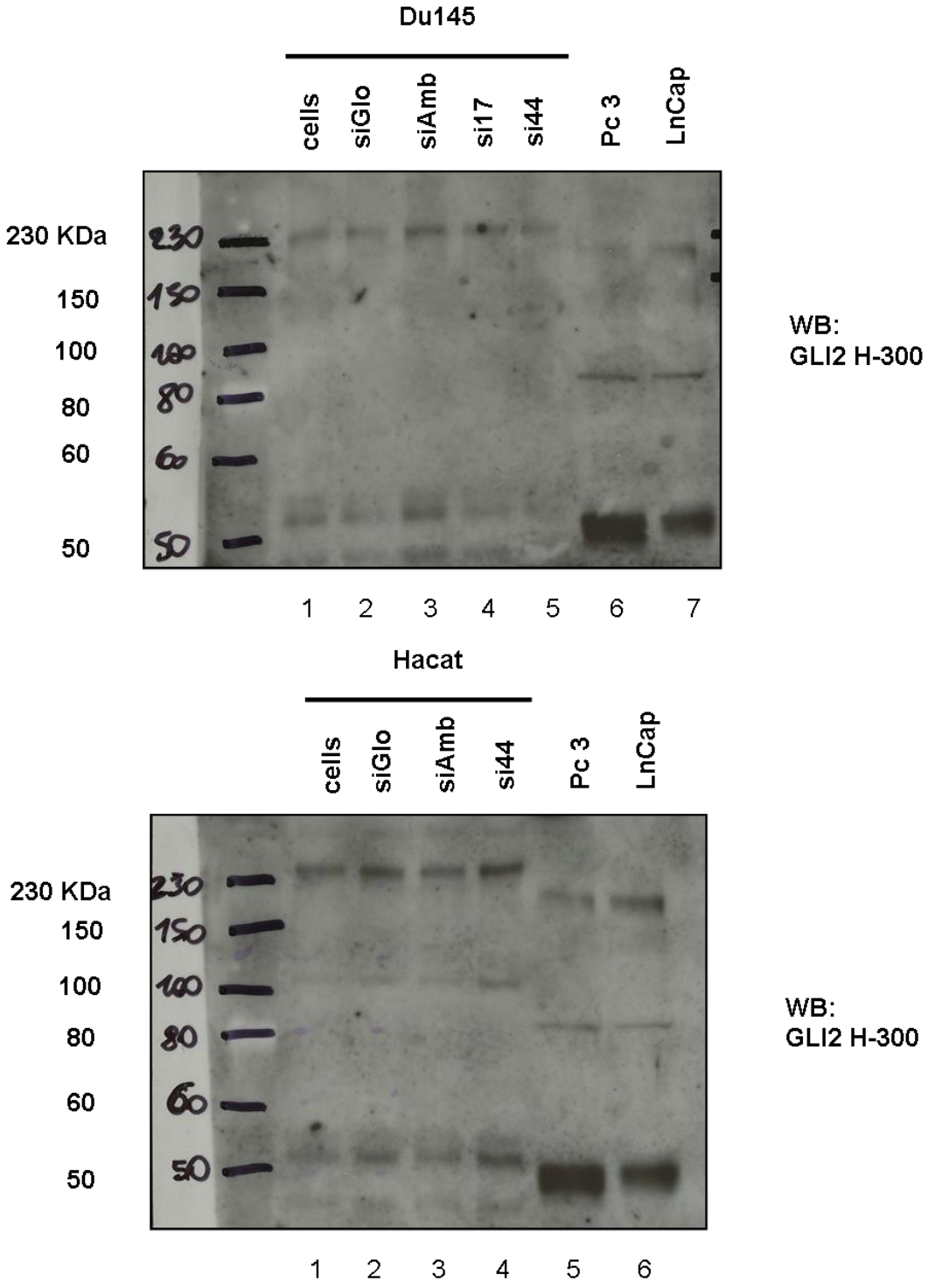

Figure 4.48: Western Blotting for GLI2 protein levels in Du145 cells and Hacat keratinocytes transfected with two different GLI2 siRNAs (GLI2 H300 antibody)

Western Blot analysis of Du145 or Hacat siGLI2 cells with GLI2 H300 antibody. Cells, untreated cells; siAmb, scramble siRNA control; siGlo, Cyclophilin B siRNA fluorescent control, si17 and si44, Gli2 siRNA.

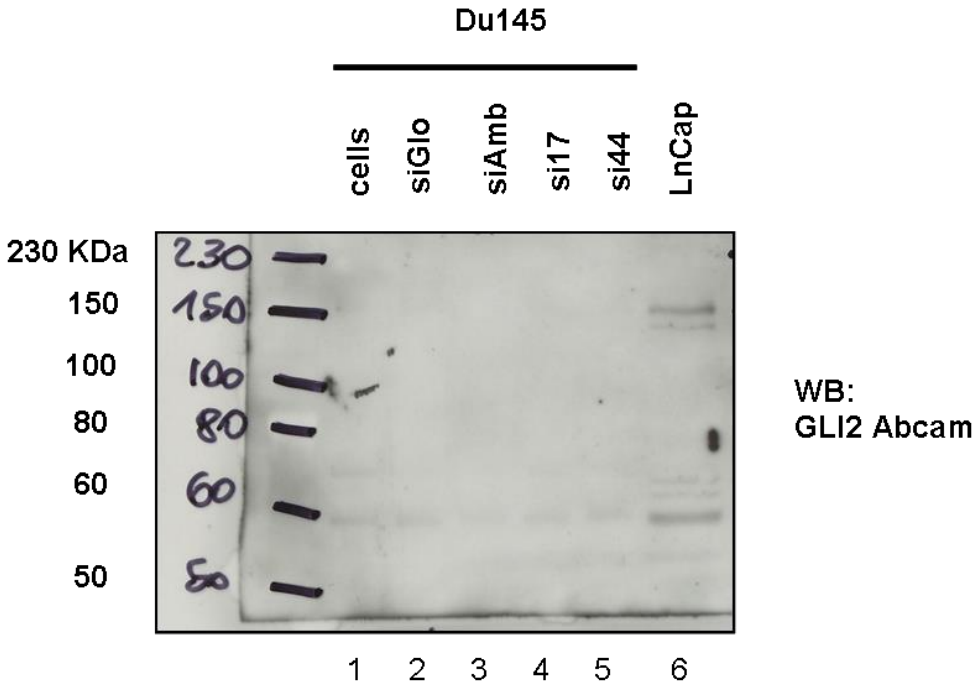

Figure 4.49: Western Blotting for GLI2 protein levels in Du145 cells transfected two different GLI12 siRNAs (GLI2 Abcam antibody)

Western Blot analysis of Du145 siGLI2 cells with GLI2 Abcam antibody. Cells, untreated cells; siAmb, scramble siRNA control; siGlo, Cyclophilin B siRNA fluorescent control, si17, si44, Gli2 siRNA.

4.2.19 Optimisation of total RNA extraction from small tissue samples

To confirm GLI1 expression in the stroma of Basal Cell Carcinomas samples which has been detected using immunohistochemistry (see section 4.2.2), as wells as analyzing GLI1 - GLI2 relative abundance and the potentially complex network of interactions that governs GLI expression (both canonical and non-canonical), we planned to use Laser Capture Microdissection (LCM) followed by RNA extraction and qPCR. Preliminary experiments were carried out to optimize RNA extraction from small samples, which is a known problem when performing LCM experiments.

LCM is a microscope-based dissection system that allows separation of specific cell populations from histological tissue sections. RNA can be subsequently extracted from these cells to analyse gene expression in the selected population by qPCR. A major drawback of this technique is the small starting amount of biological material, in which an extremely low amount of RNA is present (usually a few nanograms per section). Another problem is RNA stability: recovery from tissue that is frozen or wax-embedded is problematic as sample processing could lead to RNA degradation, therefore further reducing the amount of RNA available for analysis.

The feasibility of this approach was tested by extracting RNA from whole BCC samples in the first place, and then see if the process could be scaled down to tissue sections and to specific areas microdissected from a single section. So far successful RNA extraction was achieved from whole frozen tissue and from pooled frozen or wax-embedded sections.

RNA extracted from whole frozen BCC samples could also be used to quantify the amount of GLI1 and GLI2 by qPCR and therefore analyse the interplay of these two transcription factors ex vivo.

4.2.20 RNA extraction from whole frozen tissue

To avoid loss of precious samples, RNA extraction from whole frozen tissue was optimised using incompletely or badly labelled specimens. Samples were homogenized using a Tissue Rupture (Qiagen, U.K.) according to manufacture's instructions. Extraction of total RNA was subsequently achieved using the RNeasy Fibrous Tissue Mini Kit (Qiagen, U.K.); this kit is designed for purification of up to 100 µg total RNA from fiber-rich tissues, including skin. RNA purification from skin

is hindered by the presence of connective tissue and contractile proteins such as collagen: during the extraction process the sample is treated with proteinase K, so these proteins are degraded and can then removed by centrifugation.

RNA was extracted from three frozen tissue samples, one micronodular BCC (Sample 1) and two incompletely labelled samples, thought to be also BCCs but whose identity cannot be confirmed due to lack of information in the records. Total RNA yields varied from about 30 μg to 2 μg of RNA (Table 4.4). The ratio of absorbance at 260 nm and 280 nm is used to assess RNA purity; a ratio lower than 2.0 indicates the presence of protein or phenol contaminants; all ratio were above 2 and therefore acceptable. A 260/230 ratio was also measured as values appreciably lower than 2 denote contamination from carryover of reagents used in the extraction process: sample 1 could potentially be affected by reagents contamination.

Table 4.4: RNA yields from whole frozen tissues samples

Tissue	Code	Subtype	ng / μl	260 / 280	260 / 230	Total RNA amount (Vf = 40 μl)
Sample 1	SA 603	Micronodular BCC	58.5	2.13	1.09	2.34 μg
Sample 2	897	? badly labelled	732.1	2.06	2.14	29.28 μg
Sample 3	GT561	? badly labelled	127.8	2.11	1.73	5.11 μg

4.2.21 Preliminary qPCR experiments on RNA extracted from frozen tissue

1 μg of RNA from each of the frozen tissue samples was retrotranscribed into cDNA using the SuperScript III First-Strand Synthesis SuperMix (Invitrogen, U.K.) according to manufacturer's instructions. This kit is optimised for cDNA synthesis from a range of starting materials that goes from 0.1 pg to 5 μg of total RNA. qPCR experiments were performed using primers against PTCH1 as well as with two different primers against GLI1, one against a region in the mRNA that corresponds to the N-terminus of the protein (GLI1 RD) and another against a region located at the C-terminus of the protein (GLI1 H300)(Fig. 4.50). Sample 3 was arbitrarily chosen as a reference sample. In Sample 1 there is a clear upregulation of PTCH1, consistent with the fact this is the only sample who is a BCC, while this is not observed in Sample 2. The amount of GLI1 present in Sample1 seems to differ

slightly when two different primers are used, as it appears the amount of GLI1 mRNA in which the region corresponding to the C-terminus region is present is a bit higher compared to the amount detected used the primers against the N-terminus. This preliminary data need to be confirmed before it can be speculated if this difference has a biological significance.

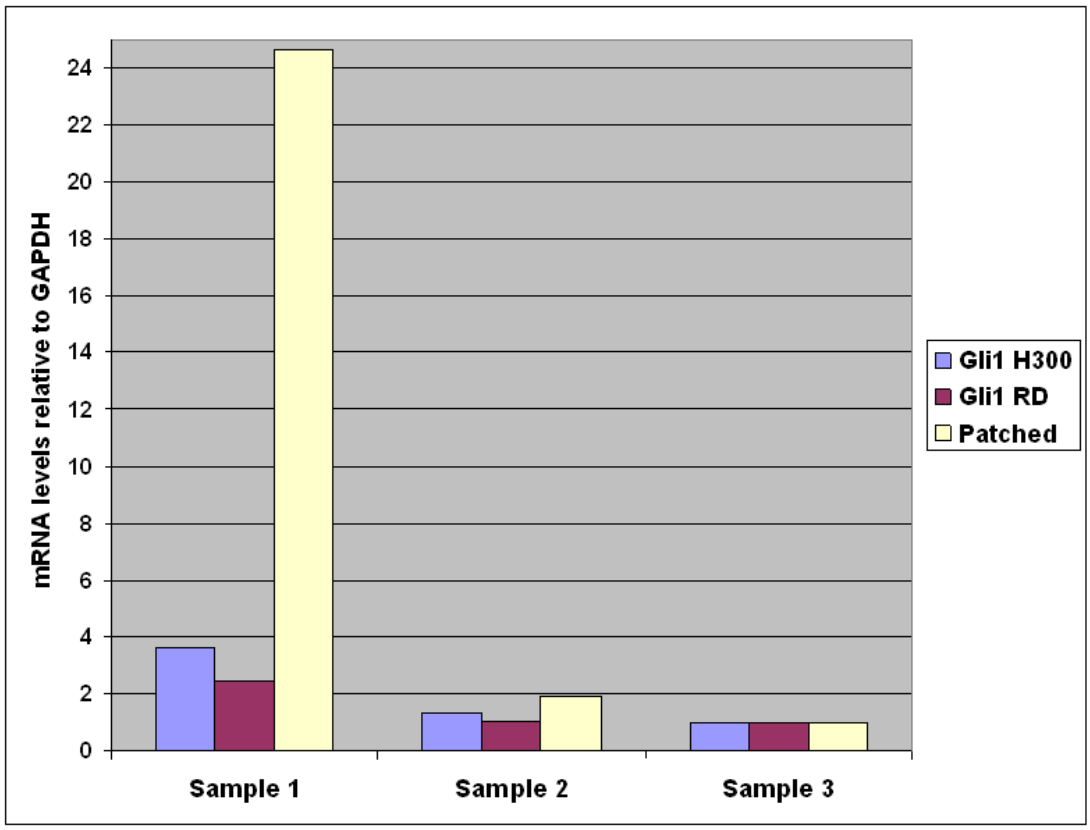

Figure 4.50: qPCR analysis for GLI1 and PTCH1 on whole frozen tissues

Two different pairs of primers were used for GLI1: GLI1 RD, targeting a region at the 5' end of the mRNA (corresponding to the N-terminus of the protein) and GLI1 H300, which targets a region at the 3' end of the mRNA (corresponding to the C-terminus of the protein). Results are expressed as fold induction using Sample 3 as a standard.

4.2.22 RNA extraction from sectioned frozen or wax-embedded tissue

RNA extraction optimisation was carried out on frozen or wax-embedded normal skin sections as these samples are more easily available and less precious than tumour tissue. Tissue was sectioned using a cryostat (frozen samples) or a microtome (wax-embedded samples).

Frozen normal human skin samples were sectioned using a cryostat and sections were placed into an eppendorf tube containing 100 μl lysis buffer from the RNeasy Micro Kit. Extraction of total RNA was subsequently achieved using the RNeasy Micro Kit (Qiagen, U.K.), following manufacture's instructions.

Wax-embedded normal human skin was sectioned using a microtome and sections were placed in an eppendorf tube containing 100 μl lysis buffer from the RNeasy FFPE Kit. Extraction of total RNA was subsequently achieved using the RNeasy FFPE Kit (Qiagen, U.K.). The RNA extraction procedure is similar to that employed for RNA extraction from cultured cells except for previous removal of paraffin by sequential addition of xylene and 100% ethanol, followed by centrifugation. Also, an additional digestion with proteinase K was performed before the ethanol precipitation step. Table 4.5 illustrates RNA yield from different amount of starting material (number of sections) for both frozen and wax samples; from this preliminary experiment it seems RNA yield increases using more sections in wax samples while it decrease in frozen samples. The issue of mRNA integrity needs also to be considered, as sample processing could lead to degradation and fragmentation of RNA. mRNA quality is usually assessed by electrophoresis of total RNA and visualization of the 28S and 18S ribosomal RNA (rRNA) bands. Ribosomal RNA makes up the majority (around 80%) of the total RNA samples, and is assumed rRNA quality reflects the underlying mRNA population (which cannot be detected even with the most sensitive of methods). RNA samples listed in Table 4.5 were run on agarose gel and visualized using SYBR Green II RNA Gel Stain (Invitrogen). SYBR Green II Stain was used as it is significantly more sensitive than Ethidium Bromide and can detect as little as 100 pg RNA. The 18S and 28S ribosomal RNA bands are visible, although faint, in frozen samples (Fig. 4.51b) and therefore good quality mRNA can be inferred while in wax samples RNA appears as a smear and is

therefore degraded (Fig. 4.51a). For this reason, frozen samples appear to be more suitable for LCM analysis.

It should be noted so far RNA has been extracted from the whole tissue present on the slides, while for LCM only a fraction of the tissue on the slide will be used. Since the average RNA yield per section in frozen slides is about 40 ng (Table 4.5) and assuming a tenth of the section will be used for LCM, the amount of RNA would be 400 pg in the best case scenario (40 ng / 10 = 0.4 ng = 400 pg). In order to extract RNA from such a tiny sample, different RNA extraction kits could be used in addition to the RNeasy Micro Kit (Qiagen), such as The PicoPure RNA Isolation Kit (Arcturus), which is optimized for use with cells acquired using Laser Capture Microdissection. Due to the low quantities of RNA extracted, a further RNA amplification step may be needed prior to the retrotranscription step; among all the commercial kits available the RNA-Amp kit (Epistem) has been reported to give the best result on LCM samples. Sections will need to be stained to reveal morphology in order to be cut using the Laser Capture Microdissection machine; as staining has been shown to affect RNA integrity (Wang *et al.*, 2006), different histological stains would need to be tested; a good starting point could be the HistoGene Stain (Arcturus).

These preliminary RNA extractions experiments highlight the feasibility of the Laser Capture Microdissection approach to address the heterogeneity of GLI protein expression in Basal Cell Carcinomas; however, further optimisation on all critical steps of the protocol would be needed.

Table 4.5: RNA yields from varying numbers of either wax or frozen sliced Human Skin Sections (NHS)

Tissue	Number of sections	ng / ml	260 / 280	Tot RNA amount (ng)	RNA / section (ng)
NHS wax (3W)	3	2.4	1.19	31.2	10.4
NHS wax (5W)	5	10.2	1.56	132.6	26.52
NHS wax (7W)	7	17.5	1.71	227.5	32.5
NHS frozen (3F)	3	10.2	1.79	132.6	44.2
NHS frozen (5F)	5	4.6	1.97	59.8	11.96
NHS frozen (7F)	7	6.4	1.77	83.2	11.88

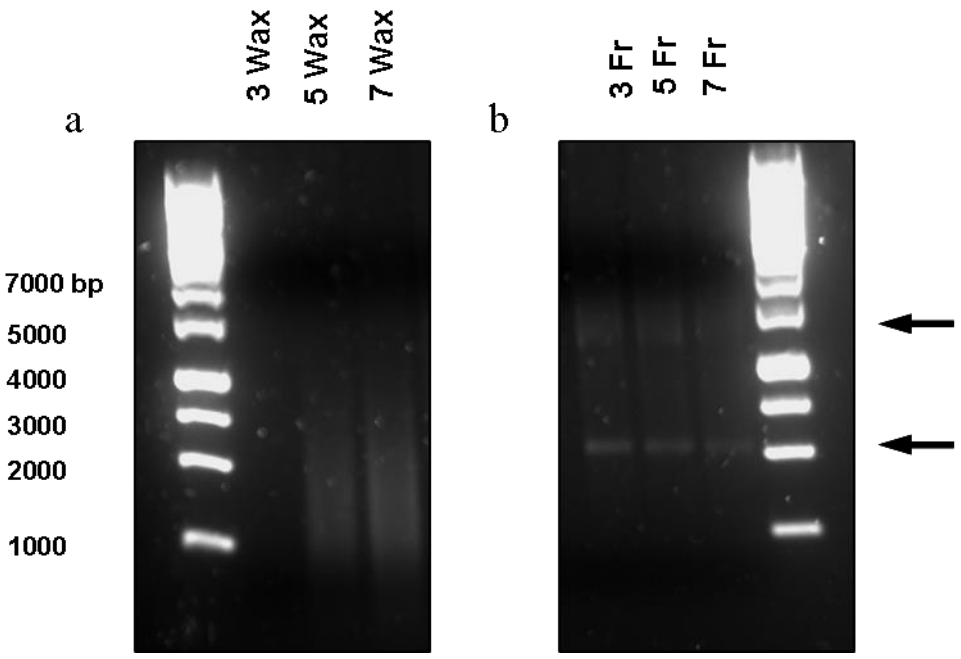

Figure 4.51: Integrity analysis of RNA samples

RNA samples listed on Table 3.5 were run on a 2% agarose gel containing SYBR Green II Stain (Invitrogen). RNA extracted from frozen tissues (b) seem to be of good quality while RNA from wax tissues is degraded (c).

4.3 Discussion

Different commercially available antibodies against GLI1 and GLI2 have been tested on human skin and Basal Cell Carcinoma samples. A widespread heterogeneity was observed in terms of staining patterns using different antibodies and staining techniques, which highlights the known complexity of the Hedgehog pathway and warrants further investigation. Some antibodies like GLI1 C-18 and GLI2 H-300 presented consistency issues, as subsequent staining performed with different aliquots showed widespread aspecificity, with a diffuse signal which sometimes extended into the underlying dermis. They were therefore abandoned and staining on BCC samples was performed with the other antibodies. A strategy for double immunofluorescent staining was also developed in order to analyse the presence of either GLI1 and Sonic Hedgehog ligand (SHH) or GLI1 and GLI2 in the same sample. The vast majority of the staining was performed on frozen samples as this allows for double staining using secondary antibodies coupled with different fluorochromes. However, some antibodies were also tested on wax-embedded BCCs to see if these samples could be used (they are easier to obtain as most Pathology departments routinely wax-embed specimen for diagnostic purposes).

I will first summarise the main results of my staining experiments and compare them with the existing literature and then analyse their significance in more details in the following sections. To date, GLI1 expression in BCCs has been analysed only in a few publications. Ghali et al. reported GLI1 expression in BCCs by DAB immunohistochemistry on wax-sections using two different antibodies, GLI1 C-18 (which recognises the carboxyl-terminal) or GLI1 N-16 (which binds to the N-terminus): staining was predominantly cytoplasmic. They observed stronger staining in BCCs using the C-terminal antibody (GLI1 C-18), and also staining of a subpopulation of mesenchymal cells (Ghali et al., 1999). In my experiments GLI1 C-18 did not work consistently by immunofluorescence on frozen section, though with GLI1 H-300, another antibody that recognises the C-terminus of human GLI1, frequent stromal staining was observed. Ghali et al. did not analyse GLI1 protein expression in normal skin, though they argue for its absence based on a previous study when they detected GLI1 mRNA by RT-PCR and in-situ hybridisation in BCCs but not in normal skin (Green *et al.*, 1998; Ghali *et al.*, 1999). Of note, GLI1

was rarely detected in hair follicles by in-situ (Green *et al.*, 1998; Ghali *et al.*, 1999), but found to be present in the outer root sheath (ORS) of hair follicles when immunohistochemistry was used (Ghali et al., 1999), thus highlighting the possible discrepancy in results using techniques that measure either mRNA level or protein abundance. Notably, they describe the staining in the ORS to be considerably more intense than the one seen in BCC islands in the same section. Though in the BCCs sections I have analysed no hair follicles were present, in many sections GLI1 intensity appeared to be stronger in the epidermis than in the BCCs, highlighting the possible variation in GLI1 levels between normal and neoplastic tissue.

In the work by Dahmane et al. (Dahmane et al., 1997) GLI1 was found to be expressed in 6 BCCs analysed by immunofluorescence using an in-house made antibody against the zinc finger domain of GLI1 (aa 255-408) but again no normal skin was analysed for comparison. GLI1 localisation was reported to be cytoplasmic in the BCCs but nuclear in COS cells transfected with a GLI1 construct probed with the same antibody (Dahmane et al., 1997); the significance of this observation is not discussed in the paper. In the BCCs I have stained GLI1 is mostly cytoplasmic with all antibodies used. Although the predominantly cytoplasmic localisation is surprising for a transcription factor, GLI1 is known to shuttle between the cytoplasm and the nucleus (Murone et al., 2000) and is bound to the cytoskeleton when inactive. Dahmane et al also detected GLI1 in 47 BCCs by in-situ hybridization, though the level of expression varied; furthermore, GLI1 mRNA was present in the basal cell layer adjacent the BCCs and in some cells surrounding the tumours, but not in normal epidermis distant from the tumour site. In the BCCs I stained I observed staining in both the epidermis and the tumour masses; though surprising, this difference could be attributed to the different technique used. It is also possible that GLI1 is subject to different post-transcriptional regulation in the epidermis compared to the tumour, so it could be hyphothesised that, although GLI1 mRNA levels may be low, GLI1 protein is expressed and stabilized in the epidermis.

SHH expression was also analysed by in-situ hybridisation by Dahmane et al; SHH ligand was detected at a much lower frequency compared to GLI1, which is consistent with what I have observed using immunofluorescent histochemistry. This

observation argues against a paracrine mode of Hedgehog signal in BCCs and suggests GLI1 expression may be regulated by other factors in the mesenchyme.

GLI2 mRNA was shown to be present in human BCCs and also in intefollicular skin and outer root sheath of hair follicles by in-situ hybridization and qPCR (Bonifas *et al.*, 2001; Ikram *et al.*, 2004). Four isoforms of GLI2 have so far been described, GLI2 α, β, γ, and δ (Tanimura et al., 1998): GLI2β isoform appear to be the most expressed isoform in BCCs by RT-PCR (Tojo et al., 2003). The result of the staining I did on normal skin and BCCs confirm GLI2 expression in the epidermis, ORS and BCCs; both antibody used (GLI2 H-300 and GLI2 Abcam) are predicted to recognise all GLI2 isoforms (see Appendix III).

4.3.1 GLI1 antibodies staining on Normal Human Hair Bearing Skin

Three different GLI1 antibodies were tested: GLI H-300 (sc-20687, Santa Cruz, polyclonal), GLI1 C-18 (sc-6152, Santa Cruz, polyclonal) and GLI1 RD (MAB3324, R&D Systems, monoclonal); the first two antibodies recognise an epitope located in a region in the C-terminal end of human GLI1, while the latter recognises a region at the N-terminal. For details please see Appendix III.

When used to stain frozen human hair bearing skin by immunofluorescence, all three GLI1 antibodies tested gave an overall similar staining pattern, with positive staining in the epidermis and in the outer root sheath of hair follicles. One novel feature observed was the presence of GLI1 in all layers of the epidermis, since GLI1 is thought to be predominantly expressed in the basal layer; however, antibody against GLI protein have been made commercially available only recently, and most of the previous studies relied on RT-PCR or in-situ hybridization, which may explain the difference. Of note, GLI1 staining appears to be weaker in the basal layer of the epidermis when GLI1 H-300 antibody is used; this is also true, although to a much lesser extent, with GLI1 RD in some regions. GLI protein expression has been shown to be influenced by other cellular pathway in addiction to Hedgehog signaling (Riobo *et al.*, 2006a; Lauth and Toftgard, 2007; Schnidar *et al.*, 2009) Dennler et al., 2007; Dennler et al., 2009), which may be differentially activated in normal or neoplastic skin and this could offer a possible explanation for this observation.

GLI1 localisation is mainly cytoplasmic with all the antibodies, though it appears perinuclear or nuclear in some regions with GLI1 H-300. The skin used for staining was derived for an abdominoplasty surgery; skin obtained from a facelift surgery was also used for GLI1 H-300 and the staining pattern appears similar regardless of the site of origin of the skin. Positive staining in the stroma as well as in the epithelia is a peculiar feature of GLI1 H-300, which is also observed in some BCC samples and discussed later.

4.3.2 GLI2 antibodies staining on Normal Human Hair Bearing Skin

For the detection of GLI2 two different antibodies were tested, GLI2 H-300 (sc-28674, Santa Cruz, polyclonal) and GLI2 Abcam (ab26056, Abcam, polyclonal); both antibodies recognise an epitope located in the central region of human GLI2. (see Appendix III). Both antibodies gave similar results on frozen section of normal hair bearing skin, with GLI2 staining present in the epidermis and in the outer root sheath of hair follicles, similar to what is known in the literature (Ikram et al., 2004). GLI2 staining intensity appears slightly stronger in the basal layer with GLI2 Abcam. GLI2 localisation is both cytoplasmic and nuclear with GLI2 H-300 and mainly cytoplasmic and sometimes nuclear in some areas with GLI2 Abcam.

GLI1 and GLI2 antibodies which yielded overall reproducible results on normal skin (GLI1 H-300, GLI1 RD, GLI2 Abcam) were subsequently used to stain BCC samples.

4.3.3 GLI1 (H300) antibody stromal staining in Basal Cell Carcinomas: quantitative analysis and possible explanations

GLI1 H-300 antibody was used to stain a panel of 31 BCCs; these tumours belonged to different subtypes, though about 2/3 of the samples were nodular BCCs, as this subtype is the most abundant (Crowson, 2006). GLI1 H-300 staining is present in the tumour masses and is predominantly cytoplasmic with perinuclear or nuclear staining observed in some areas. In 23 out of 31 BCCs GLI1 is also observed in the adjacent stroma and its intensity appears stronger than in the epithelia; in the remaining 8 BCCs GLI1 H-300 staining is restricted to the epithelial component of the tumour.

These observations led us to speculate about the biological significance of stromal GLI1. Since paracrine signalling has been implied the progression of different types of tumors (Yauch et al., 2008; Nolan-Stevaux et al., 2009; Tian et al., 2009), it could be hyphothesised BCCs in which stromal GLI is present may have a distinct fate compared to the ones who do not: consequently, the presence of stromal GLI1 may be a feature of the more aggressive subtype of BCC (morphoiec), while not being so evident in the more indolent subtype (nodular).

Though the number of BCCs positive for GLI1 was higher (n=23) than the number of BCCs which are negative (n=8), the majority of BCCs positive for stromal GLI1 were nodular (15 out of 23) and also the majority of BCCs negative for stromal GLI1 were nodular (7 out of 8). At the moment no strong correlation between the present of GLI1 staining in the stroma and BCCs subtypes can be detected, although since the vast majority of the samples belong to the nodular and micronodular subtypes (23 out of 31), no definitive conclusion could be reached (BCCs positive for stromal staining: nodular and micronodular n=15, nodular / morphoeic n=1, morphoeic n=2, infiltrative n=2, superficial n=3; BCCs negative for stromal staining, nodular and micronodular n=7, infiltrative n=1); more samples would be needed to examine possible variations between subtypes. Whether different BCC subtypes are distinct from each other or nodular BCCs evolve into morphoiec to become invasive is still an open question in the field. It is however possible activation of GLI1 in the stroma of nodular BCC is a step needed in the progression from an indolent to a more aggressive form (morphoeic). Alternatively, stromal GLI1 could be a factor that facilitates tumor recurrence: this hypothesis would be ideally addressed by follow-up of patients and comparing the status of GLI1 activation in the stroma in the primary and in the recurrent tumour. This could also be tested in vitro by taking advantage of the DED organotypic model (see section 5.1): keratinocytes could be grown on DED in the presence of normal fibroblasts or GLI1-overexpessing fibroblasts, to see if the latter would increase the invasiveness of the keratinocytes into the dermis (a feature associated with malignant tumor progression). Of note, in a mice model of pancreatic cancer, tumour-associated fibroblasts express GLI1 and are also positive for vascular endothelial growth factor (VEGF) (Bailey et al., 2009). The authors suggest HH pathway activation in the stroma promotes angiogenesis and metastasis.

Because of the brightness of GLI1 H-300 staining in the stroma, we sought to quantify its intensity compared to the staining in the epithelial tumour using the Image J software and a method based on fluorescence intensity distribution. Out of 23 samples, 17 were suitable for quantification purpose using this method: the remaining 6 samples showed either similar staining intensities in the stroma and in the epithelia (n = 4) or the stromal component was difficult to highlight (n = 2). In these 23 samples there seem to be a statistically significative difference ($P < 0.05$) between staining in the two tumour components, with GLI1 fluorescence intensity in the stroma notably higher than in the tumour.

GLI1 staining in the stroma could be explained by the existence of a paracrine mechanism of HH signalling (Yauch et al., 2008; Nolan-Stevaux et al., 2009; Tian et al., 2009); however, from the results of SHH staining in BCC (section 4.2.11), this hypothesis seems unlikely. Alternatively, this could be due to non-canonical activation of GLI1 in the stroma: notably, non-canonical activation of GLI proteins by transforming growth factor beta (TGFβ) has recently been described in human keratinocytes and fibroblasts (Dennler et al., 2007; Dennler et al., 2009).

4.3.4 Sonic Hedgehog ligand antibody staining

To further analyse the hypothesis that GLI1 H-300 antibody stromal staining could be due to paracrine Hedgehog signalling, Basal Cell Carcinoma samples were stained with an antibody against Sonic Hedgehog ligand (SHH). It would have been ideal to double immunostain the same BCC section with both GLI1 H-300 and SHH. However, this was not possible as all commercially available antibodies against SHH were raised in rabbit and GLI1 H-300 is also a polyclonal rabbit antibody; a prerequisite for double immunostaining is that the two antibodies are raised in two different species. This is necessary as secondary antibodies labelled with different fluorochromes must be able to recognise a specific primary antibody, e.g. a green fluorescent anti-mouse secondary against a mouse primary antibody in conjunction with a red fluorescent anti-rabbit secondary against a rabbit primary antibody. A viable combination for double immunostaining was GLI1 RD, a rat monoclonal antibody, used in conjunction with a rabbit polyclonal against SHH (ab19897, Abcam). This combination was first tested on a frozen section of normal human hair bearing skin: GLI1 was present in the epidermis and in the outer root sheath of hair

follicles and SHH in the upper layers of the epidermis and in the inner root sheath. Of note, SHH is also expressed in cutaneous nerve fibers, in accordance to what has been recently published by Brownell et al (Brownell et al., 2011). SHH from neurons signals in a paracrine manner to a subpopulation of responsive hair follicle bulge stem cells which as a result express GLI1; these cells are able to migrate into the epidermis upon wounding, become epidermal stem cells and contribute to wound healing. SHH signal from cutaneous neurons is essential to maintain bulge cells ability to become epidermal stem cells. This is particularly interesting as it has also been shown that introducing oncogenic mutations in HH pathway components in follicular stem cells promote the formation of BCCs after wounding (Kasper et al., 2011; Wong and Reiter, 2011). It can therefore be speculated that alterations of physiological SHH signalling from cutaneous nerve fibers could result in enhanced susceptibility to BCC development originating from hair follicle stem cells.

In the skin, SHH regulates the adult anagen hair cycle and controls the growth of multipotent progenitor cells. SHH was detected in one frozen section of normal human hair bearing skin used to test the antibody. Out of 13 BCC sections analysed, only 9 contained the epidermis: positive SHH staining was present in the epidermis of 5 out of these 9 BCCs. All BCCs which stained positive for SHH (n = 4) also presented SHH staining in the epidermis, one BCC was negative for SHH in the tumor mass but SHH was present in the overlying epidermis and four BCCs were negative for SHH in both the tumor and the epidermis. In the 9 skin-containing BCCs analysed, SHH presence in the epidermis seems to correlate with its presence in the tumor, though more samples would be needed to elaborate on the biological significance of this observation. Also, more normal skin samples should be analysed to better understand how SHH expression is regulated, which would help understand if SHH presence or absence in the epidermis of BCCs is related to the tumor.

In total, 13 BCCs samples were stained with GLI1 RD and SHH (this number includes samples with and without overlying epidermis); 9 of them had been previously stained with GLI1 H-300, 4 of them being positive for GLI1 staining in the stroma and 5 negative. Out of these 13 BCCs samples only 4 were positive for SHH, and in 2 of these 4 the staining for SHH was very weak. Considering the 4 BCCs samples previously found to be positive for GLI1 H-300 staining in the stroma, only one was positive for SHH. Although a bigger number of samples would

need to be stained to reach a definitive conclusion (especially ones displaying stromal GLI1 H300), it seems that the majority of BCCs analysed do not contain SHH ligand and therefore it is unlikely GLI1 is activated in the stroma in a paracrine manner.

An alternative explanation for the pattern of GLI1 staining in human BCC samples is TGFβ mediated non-canonical activation of GLI1 in the stroma. Non-canonical activation of GLI proteins has been reported in vitro in keratinocytes and fibroblasts cell line (Dennler *et al.*, 2007) and also been proposed to play a role in vivo in a murine model of pancreatic cancer (Nolan-Stevaux *et al.*, 2009). TGFβ signalling pathway components have been reported to be present in BCC epithelial (Schmid et al., 1996; Verhaegh et al., 1997; Gambichler et al., 2007) and stromal components (Schmid et al., 1996; Furue et al., 1997). TGFβ ligand presence in the stroma of the BCCs analysed and its correlation with GLI1 expression could be addressed by double fluorescent immunostaining or by taking advantage of the Laser Capture Microdissection (LCM) technique.

4.3.5 GLI1 (H-300), GLI1 (C-18) and GLI1 (RD) antibodies staining similarities and differences

20 Basal Cell Carcinoma samples belonging to different subtypes were stained with GLI1 RD antibody; this number includes both samples stained with GLI1 RD alone or GLI1 RD in conjunction with SHH Abcam or GLI2 Abcam. Surprisingly, stromal staining was only present in 2 out of 20 BCCs using the GLI1 RD antibody, and appears to be rather weak. Of those 20 samples, 16 have also been previously stained with GLI1 H-300; considering these 16 samples, 10 were positive and 6 negative for stromal staining with GLI1 H-300 while only one was positive and the remaining 15 negative when GLI1 RD was used; possible explanations for this observation are discussed further on. It should be noted both antibodies stained the tumour masses and the cellular localisation was similar: mainly cytoplasmic, with GLI1 H-300 sometimes more perinuclear. Moreover, in normal human hair bearing skin the staining pattern is also similar using both antibodies, with GLI1 present in the outer root sheath of hair follicles and the epidermis, appearing slightly weaker in the basal layer. These observations argue for staining specificity as a similar pattern is

observed with two different antibodies, GLI1 H-300 and GLI1 RD; this is also similar to observation made in normal human bearing skin with the GLI1 C-18 antibody.

Although the mainly cytoplasmic localisation of GLI1 observed with different antibodies could be surprising considering the fact GLI1 is a transcription factor, GLI proteins are known to shuttle between the cytoplasm and the nucleus (Murone et al., 2000). Moreover, cytoplasmic GLI1 localisation has been previously reported in BCCs using immunohistochemistry (Ghali *et al.*, 1999).

Both GLI1 H-300 and GLI1 C-18 recognise an epitope located in a region in the carboxyl-terminal end of human GLI1, while GLI1 RD recognises an epitope in a region of about 230 amino acids located at the amino-terminal end. The sequences against which GLI1 H-300 and GLI1 C-18 were raised partially overlaps; GLI1 H-300 had been raised against a much longer sequence compared to GLI1 C-18 (300 amino acids compared to about 50) (see Appendix III). GLI1 C-18 antibody presented consistency issues when different aliquots were used, and was therefore abandoned. Concerning GLI1 H-300, the technical support services at Santa Cruz stated this antibody was raised against a recombinant protein corresponding to amino acids 781-1080 of GLI1 of human origin and, since the epitope was not mapped, this amino acid range could not be further restricted. In terms of manufacturing methods, the main difference between GLI1 H-300 and GLI1 RD is that the former is a rabbit polyclonal antibody, while the latter is a rat monoclonal one.

Polyclonal antibodies are purified from animal serum and derived from different B cells; as a result they are a combination of immunoglobulin molecules secreted against a specific antigen, each identifying a different epitope.

To produce monoclonal antibodies, B cells are removed from the immunized animal and fused with tumour cells to become hybridomas; the antibody producing hybridomas are cloned by isolation and cultivated, so antibodies secreted by the cells into the culture media can be harvested. Monoclonal antibodies are monospecific antibodies that are identical since they are derived from a single hybridoma clone (usually selected by an affinity purification procedure); these antibodies detect only one epitope on the selected antigen. GLI1 H-300 antigen is about 300 amino acids long (position 781-1080 of GLI1 of human origin, corresponding to the proline-rich

domain – activation domain); since the maximum epitope length is 20 amino acids in length, even if we assume no overlapping between their sequences, GLI1 H-300 is potentially composed by a mixture of at least 15 different antibodies that recognise 15 different epitopes (300 amino acids (antigen length) / 20 amino acids (maximum epitope length) = 15). GLI1 RD antigen is 234 amino acids long (positions 1 – 234 of GLI1 of human origin, which include Sufu binding domain) but, since it is a monoclonal antibody, the epitope recognise will be only one and about 20 amino acids long; the exact sequence is not known as R&D Systems technical service was not able to disclose it.

To date, different GLI1 isoforms have been described: GLI1ΔN, generated by skipping exons 2 and 3 and encoding an N-terminal truncated protein (Shimokawa *et al.*, 2008), and tGLI1, an in-frame deletion spanning the entire exon 3 and part of exon 4 (Lo *et al.*, 2009). GLI1ΔN present a deletion of 128 amino acids and is a less potent transcriptional activator compared to full-length GLI1; the expression ratios of the two GLI1 isoforms are greatly variable in tumour cell lines. tGLI1 results in an in-frame deletion of 41 amino acids, it is express in human glioblastoma multiforme and confers enhanced migratory properties to cells. Both GLI1ΔN and tGLI1 deletions are located between amino acids positions 1 – 234 of human GLI1, which corresponds to the antigen against which the GLI1 RD antibody was generated (for details please see Appendix III). Since the exact position of the epitope is unknown, it cannot be excluded that it falls in one of the region which differs between isoforms; nevertheless, if these isoforms are expressed at the same time it is not possible to assess their relative abundance using just one antibody; this could be done by qPCR using isoform-specific primers.

Using the GLI1 H-300 antibody positive staining is present in the stroma of some BCCs samples, while this feature is not detected with GLI1 RD; the reason of this discrepancy is still unclear. Of note, positive staining was detected in cultured Basal Cell Carcinoma derived fibroblasts using GLI1 H-300 (J. Elliott et al., unpublished results), which confirms the observation made on BCCs sections.

One possible explanation for the discrepancy observed in stromal staining is to postulate the existence of a novel GLI1 isoform (C-terminal deleted isoform B) that differs in its carboxyl-terminal end from the full-length GLI1 (here named isoform

A) and assume these two variants are differentially expressed in the epithelia and in the stroma, as illustrate in Figure 4.52. Continuous line represents strong expression while dotted line symbolizes weak expression, GLI1 isoform B is postulated to be weakly expressed in the stroma. Since GLI1 H-300 epitope is located in a large antigen at the carboxyl-terminal end, it should be assumed this portion in deleted in the putative isoform B which therefore cannot be detected by this antibody. GLI1 RD binds to an epitope located at the amino-terminal end and therefore will detect both full length isoform A and carboxyl-terminal deleted isoform B. If this would be the case GLI1 H-300 would show fluorescent staining in both epithelia and stroma, while GLI1 RD signal would be present and strong in the epithelia but weaker and possibly below detection in the stroma. One possible way to test this hypothesis would be to stain the same section with both GLI1 H-300 and GLI1 RD and analyse the relative fluorescence intensities. However, since staining intensity could be influence by multiple factors (e.g. affinity of primary antibody for the epitope, type of fluorochrome associated with secondary antibody etc.), a better approach would be to design primers specific for the different isoforms and analyse their relative abundance in the epithelia and in the stroma using Laser Capture Microdissection. Another question to be considered is the function of this novel isoform: the fact that it would be not recognised by GLI1 H-300 implies the amino acids 781-1080 are missing, and therefore most of GLI1 activation domain is ablated. How this could reflect on the transcriptional activity of GLI1, possibly switching its function from an activator to a repressor of transcription, is another issue that would need further investigation.

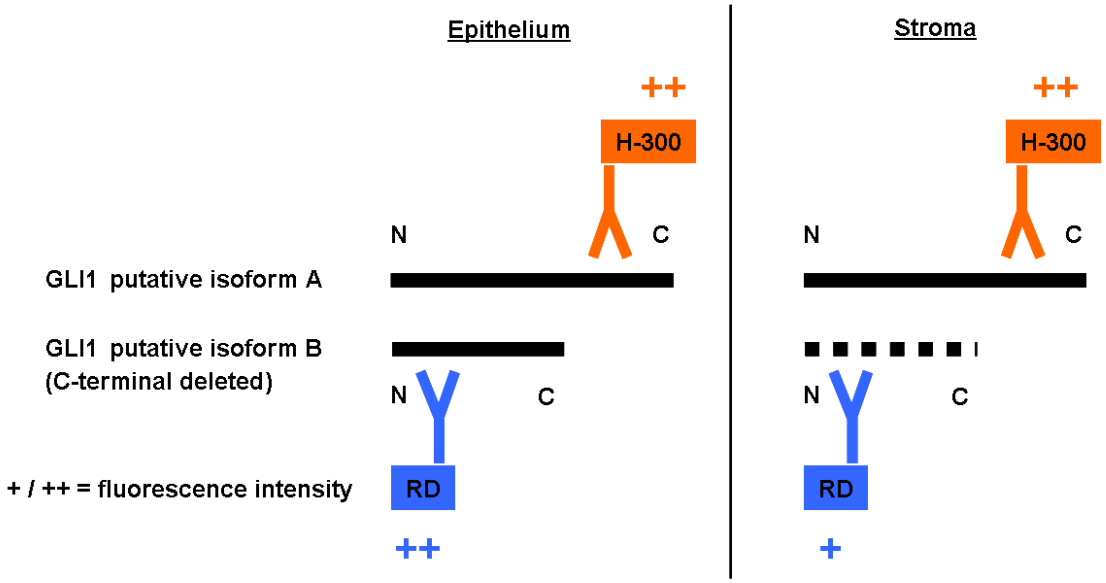

Figure 4.52: Diagram illustrating a possible explanation for GLI1 (H-300) and GLI1 (RD) antibodies staining pattern in the epithelia and in the stroma of Basal Cell Carcinomas

– please see text for details

However, in support of this hypothesis, two novel GLI1 isoform have been described by transfecting full length myc-tagged GLI1 into U251 glioma cells (Altaba, 1999; Stecca and Ruiz i Altaba, 2009), one deleted at the amino-terminal (positions 1 – 231) and the other missing a large portion at the carboxyl-terminal (position 515 to the end of the protein); the latter would not be recognised by the GLI1 H-300 antibody and could therefore support the model highlighted in Figure 4.53. In the publication by Stecca et al. the author discriminate between the three GLI1 variants (full length, amino-terminal deleted, carboxyl-terminal deleted) by Western Blotting taking advantage of three GLI1 antibodies that they generated in-house (not commercially available): one against the N-terminus, the second against a sequence adjacent the zinc-finger region at the centre of the protein, and the third against the C-terminus.

If we postulate the heterogeneous staining pattern observed in my staining experiments is due to these isoforms an antibody against the central region of GLI1 would be essential in addition to one for the N-terminus and another for the C-terminus. Assuming not only two GLI1 isoforms (full-length and C-terminal-deleted,

(as outlined in Figure 4.52) but three different variant are expressed (full-length, C-terminal-deleted, N-terminal-deleted), their discrimination by immunofluorescent would be extremely laborious in term of elaboration of a staining strategy, quantification of staining intensity would be approximate due to problems intrinsic to the methodology (e.g. affinity of primary antibody for the epitope, type of fluorochrome associated with secondary antibody etc.) and further complicated by the relative abundance of each isoform.

Nonetheless, the availability of three different antibodies could allow the discrimination of the three variants by Western Blotting (on cells or on tissues), as in this technique one can rely on separation based on protein size to distinguish between them, while in immunofluorescent staining the antibody will bind to the epitope (if present) and give the same signal regardless of protein length. For these reason, analysis of isoform expression in Basal Cell Carcinoma sections could be better address by designing specific primers and using Laser Capture Microdissection followed by qPCR.

Three different antibodies could be used to analyse isoform expression in keratinocyte cell lines upon GLI1 ectopic expression. In this case though, only GLI1 C-18 could be used for binding at the C-terminus as both GLI1 H-300 and GLI RD have been shown not to be suited for Western Blot analysis, the former giving a wide array of different bands in GLI1 overexpressing keratinocytes while the latter is unable to pick up ectopic GLI1 in NEB1 or prostate cells (results by Mr Sandeep Nadendla, data not shown). Two new GLI1 antibodies for Western Blotting would therefore be needed in addition to GLI1 C-18, one binding at the amino-terminal, and another raised against the central region of GLI1. Figure 4.53 illustrates a schematic representation of GLI1 isoforms described so far, other possible combinations between the different deletions are theoretically possible but have been omitted for clarity.

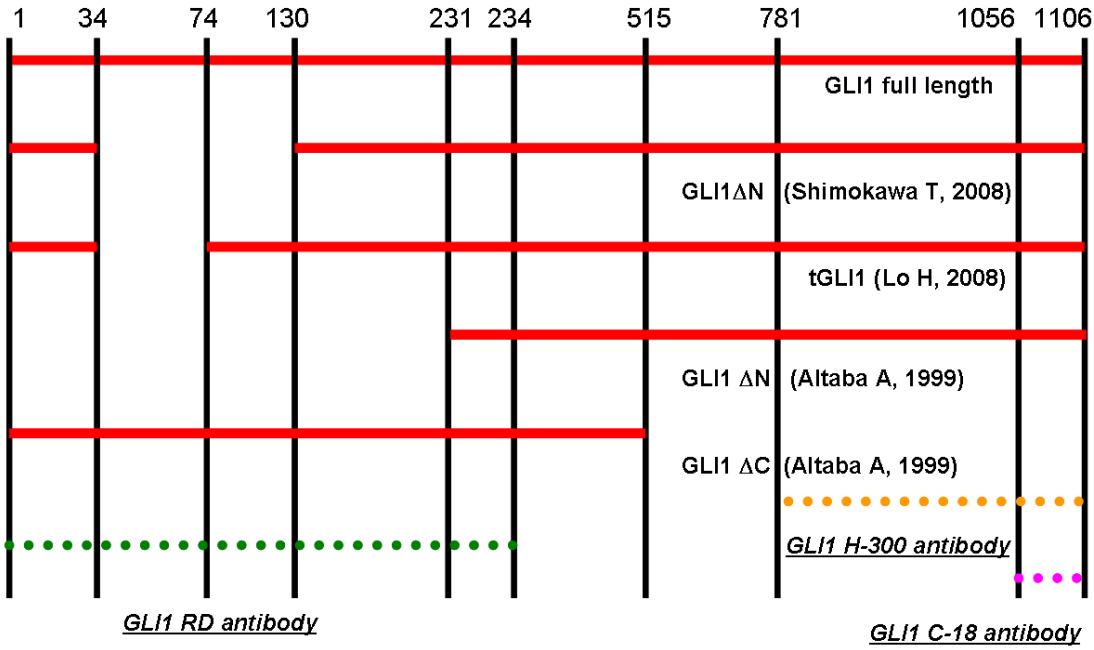

Figure 4.53: Diagram illustrating different known GLI1 isoforms and relative amino acids positions

Antigens recognised by GLI1 antibodies used for staining are also highlighted – please see text for details

Since GLI1 H300 it is a polyclonal antibody and the sequence against which it was generated is quite long it cannot be excluded this antibody is recognizing other proteins in addition to GLI1. To address this issue, inhibitors and siRNA experiments were carried out to validate the antibody. These experiments are at the moment not conclusive, although work carried out by other members of the lab supports the hypothesis of good antibody specificity (please see section "Analysis of antibodies specificity"). It should however be noted GLI antibodies described here have already been already used in a number of publications, which are listed in Appendix IV.

4.3.6 Heterogeneity in staining intensity with GLI1 antibodies

Another peculiar feature observed with both GLI1 antibodies (H-300 and RD) on Basal Cell Carcinoma samples is the variation in staining intensity. GLI1 staining appears to be weaker in the tumour compared to the overlying epidermis in about 50% of the samples with GLI1 RD (9 out of 18) and 69% of the samples with GLI1

H300 (9 out of 13 – it should be noted here the total number of samples is lower). It is important to note it is sometimes difficult to distinguish between staining in the basal layer and staining in the BCC as some tumours appears as outgrowth from the epidermis into the dermis. Also, not all BCC samples contain overlying epidermis as this is dependent on the surgical technique used for removal (e.g. it is very scarce in punch biopsies) and on the fact that half of the BCC must be collected for diagnostic purpose and is usually wax-embedded; the remaining half of the BCC is collected and frozen for research purpose, and sometime this second half contains little or no epidermis. This means BCCs with epidermis are only a subset of all BCCs stained.

Although this may appear counterintuitive as GLI1 deregulation is commonly associated with malignancy, this observation appears similar using two different antibodies and suggest further investigation to analyse its significance. Of note, a reduction in the level of GLI1 may be necessary to overcome GLI-promoted cell to cell adhesion, which has been recently described in an in vitro model of BCC based on GLI1-overexpressing keratinocytes (Neill *et al.*, 2008). Moreover, downregulation of GLI2-responsive genes in Hacat cells appears to be required for invasion in a skin organotypic model (Snijders et al., 2009) and silencing of GLI2 in a breast cancer mouse xenograft model is associated with a more invasive tumour phenotype (Hu *et al.*, 2008). All these observations suggest a complex modulation of HH-GLI signalling during cancer progression.

GLI1 staining also appears in be weaker in palisading cells compared to the centre of the tumour in about 20% of the samples with GLI1 RD (4 out of 20) and 25% of the samples with GLI1 H300 (8 out of 31 – again, different number of samples stained). Please note for GLI1 RD all BCCs stained have been considered, regardless if they were stained with GLI1 RD alone or in conjunction with either SHH or GLI2 Abcam antibodies (for a complete list, please see Table 4.2).

A recent paper reported an increase in the cell cycle inhibitor p16 and a decrease in phosphorylated Retinoblastoma protein (Rb) in the palisading cells of BCCs (Svensson *et al.*, 2003), suggesting a change from proliferation to invasion at the edge of the tumour; it would be therefore interesting to analyse if there is a correlation between a reduction in GLI1 levels and the acquisition of a more invasive phenotype.

4.3.7 Comparison between immunofluorescent and DAB staining in wax-embedded samples using GLI1 (H-300) and GLI1 (RD) antibodies

In order to take advantage of the large number of wax embedded Basal Cell Carcinomas conserved in the Pathology archive, which would address the problem of increasing the numbers of samples belonging to the rarer superficial and morphoeic subtypes, as well as eliminating logistic problems associated with working with frozen samples, GLI antibodies were also tested on wax-embedded BCCs using the DAB technique.

Optimisation of the conditions for antigen retrieval was carried out on normal skin; both GLI1 H-300 and GLI1 RD show diffuse staining in the epidermis, but while GLI1 H-300 is mainly cytoplasmic with a little nuclear staining, GLI1 RD nuclear staining is more pronounced. GLI2 H-300 and GLI2 Abcam were also tested: GLI2 H-300 staining is extremely faint, nuclear and localised in the basal layer, while GLI2 Abcam is stronger, diffused across the epidermis and both nuclear and cytoplasmic.

GLI1 staining pattern on two wax-embedded BCCs (one nodular and one infiltrative) was compared using either immunofluorescence or DAB staining with either GLI1 H-300 (carboxyl-terminal epitope) or GLI1 RD (amino-terminal epitope); staining pattern appears to be overall similar with both techniques. Furthermore, there seem not to be significative differences between the two BCCs analysed, which belonged to two different subtypes (nodular and infiltrative).

GLI1 H-300 staining is diffused throughout the epidermis and the BCCs, in both nucleus and cytoplasm; DAB staining appears fainter compared to immunofluorescence. GLI1 H-300 immunofluorescent staining intensity on wax sections appears weaker when compared to immunofluorescent staining on frozen sections. Stromal GLI1 H-300 staining which is diffuse and very bright in most BCC frozen sections by immunofluorescence is very limited in wax BCC sections, either by immunofluorescence or by DAB staining (although it should be noted only two wax-embedded BCCs were analysed, and it is possible these two BCCs do not express stromal GLI1).

GLI1 RD staining is present in the BCCs and in the overlying epidermis, although with this antibody localisation appears mostly nuclear; it is also present in the stroma when DAB chemistry is used, while this is not so evident using immunofluorescence. Conversely, in frozen sections GLI1 RD staining was restricted to the epithelia in nearly all samples analysed (it should be noted however only two wax-embedded BCCs were stained compared to 20 frozen BCCs and this could be the reason of the discrepancy). The reason why GLI1 RD is more nuclear in wax sections (DAB and immunofluorescence) compared to frozen ones (immunofluorescence) is not clear; it may be GLI1 is predominantly nuclear in the wax sections analysed (one normal skin and two BCCs) or this could be due to the different techniques used. It should be noted for wax sections an antigen retrieval step is required to remove the cross-linking of the amino groups of proteins that result from fixing with paraformaldehyde: it may be antigen retrieval treatment allows recognition of the epitope also in the nucleus. This is counterintuitive as amino groups in frozen sections are not subject to modification (fixing and permeabilization is achieved with acetone) and therefore there is supposed to be no hindrance to epitope recognition. However, it is possible this treatment is not suited for the recognition of the epitope also in the nucleus; moreover, it is not known how the thawing process required for staining frozen sections affects protein conformation and stability. Conceding the fact that nuclear GLI1 may be underestimated when immunofluorescence in frozen sections is used, it should be stressed this is a comparison between two different techniques and therefore the reason could be due to the different methods employed.

4.3.8 GLI1 and GLI2 antibodies double immunofluorescent staining

To analyse GLI1 - GLI2 interplay a strategy for double immunofluorescent staining was developed. Antibodies that gave inconsistent results depending on the batch used (GLI1 C-18, GLI2 H-300) were excluded; although GLI1 H-300 antibody has been used to stain the vast majority of Basal Cell Carcinoma samples, it is a rabbit polyclonal antibody like GLI2 Abcam and for this reason the two cannot be used together. Therefore, the only viable combination was GLI RD (rat monoclonal) with GLI2 Abcam (rabbit polyclonal). In a sample of normal human hair bearing skin, GLI1 and GLI2 staining is present throughout the epidermis and in the outer root

sheath of the hair follicle; GLI2 staining appears slightly stronger in the basal cell layer.

A panel of 18 BCCs, mostly belonging to the nodular subtype, was also stained with GLI1 RD in combination with GLI2 Abcam. In most samples GLI1 and GLI2 show extensive areas of co-expression, as well of areas where one protein appears to be more abundant than the other. As previously discussed (section 4.3.6), GLI1 RD staining appears to be diffuse but sometime weaker and at the invading front of the tumour (palisading cells) and also in some samples weaker in the tumour compared to the overlying epidermis. GLI2 on the other hand is stronger and more defined in the basal layer in 5 out of 17 BCCs (30%) in which the epidermis is present, though it should be noted this is sometime hyperplastic skin. In 4 out of these 5 samples GLI1 staining appears uniform throughout the epidermis. Although a positive feedback loop at mRNA level between GLI1 and GLI2 has been described human keratinocytes (Regl et al., 2002) and therefore one would expect GLI1 and GLI2 staining to be superimposable, double immunofluorescent staining for GLI1 and GLI2 in BCCs samples reveal areas of co-expression as well as areas when one or the other protein is more abundant; this highlights how the GLI1 - GLI2 interplay could be more complex that previously hyphothesised and is consistent with the putative inhibitory effect of ectopic GLI1 on GLI2 expression described in Chapter 3. GLI1 and GLI2 relative abundance could be further and more quantitatively analysed by using Laser Capture Microdissection (LCM) followed by qPCR.

4.3.9 Analysis of antibodies specificity in cultured cell lines

Due to the heterogeneity of the staining results observed, we decided to try and validate the GLI antibodies. It should be noted, however, that the GLI antibodies used for staining in this thesis have already been employed in a number of publications, which are listed in Appendix IV. Antibody specificity was analysed by immunofluorescence using NEB1 keratinocytes exposed to SMO inhibitors KAAD-cyclopamine (KAAD-cyc) and SANT-1. Exposure of keratinocytes to SMO antagonists should decrease GLI1 expression and a corresponding reduction in GLI1 fluorescence would support the notion of good antibody specificity. Previous work in the lab performed by Mr Muhammad Rahman had shown that GLI1 H-300 fluorescence is reduced upon 24 hours treatment with KAAD-cyc and SANT-1 in

NEB1 keratinocytes; this is concomitant with a reduction of about 50% in GLI1 mRNA by qPCR (M. Rahman et al., unpublished results). I repeated the experiment on NEB1 wild-type keratinocytes which had been shown to express GLI1 (M. Rahman et al, unpublished results) and also analysed NEB1 PTCH1 knockdown keratinocytes, in which GLI1 has been shown to be upregulated (M. Rahman et al, unpublished results). NEB1 keratinocytes were exposed to either KAAD-cyclopamine (100 nm) or SANT-1 (100 nm) for 24 hours then fixed and stained with either GLI1 RD or GLI1 H-300 antibody; staining intensity was then measured using the ImageJ software. No significative difference in fluorescence intensity was observed upon treatment with SMO inhibitors; this could be due to the fact different aliquots of inhibitors were used as it had also been noted by other group members that some batches did not suppress GLI expression as efficiently as others.

Because of the unexpected results of these two experiments, we decide to try and address GLI antibody specificity by using short interfering RNA (siRNA). Conditions for GLI1 siRNA were optimised by Mr Sandeep Nadendla, who observed ectopic GLI1 mRNA was maximally suppressed in LNCaP-GLI1 prostate cancer cells 96 hours post-transfection and, similarly, endogenous GLI1 mRNA levels were reduced in DU145 and PC-3 prostate cancer cells at 96 hours post-transfection (Nadendla *et al.*, 2011). I therefore tested two different commercially available siRNAs (si5815 and si5816, Ambion) against GLI1 in NEB 1 keratinocytes using a 96 hours timepoint and 30 nM final concentration as a starting point. Cells were transfected, grown for 96 hours, fixed and stained with GLI1 RD antibody; no significative reduction in staining intensity with either antibody was observed in GLI1 silenced cells. Lack of reduction in fluorescence levels in GLI1 siRNA cells could be due to inefficient silencing, therefore in the subsequent experiments GLI1 mRNA and protein levels were analysed before staining for GLI1. Since NEB1 keratinocytes have been shown to be quite difficult to transfect (M. Rahman et al., unpublished data), Hacat keratinocytes and more easily transfectable prostate cancer cell lines were used. Levels of messenger RNA (mRNA) for Cyclophilin B and for GLI1 were measured in Hacat transfected cells. Cyclophilin B mRNA levels are reduced, indicating successful transfection; GLI1 mRNA levels appear reduced with siRNA 5815 but are increased with siRNA 5816. This preliminary result is unexpected and need to be further investigated to assess its reproducibility; in the

following experiments it would be useful to also analyse GLI1 silenced cells by immunofluorescence.

In parallel to this work, similar validation was carried out to validate GLI2 Abcam antibody using two commercially available siRNA against GLI2, si5817 (Ambion) and si44 (Qiagen) (please see Materials and Methods sections for details). Conditions for GLI2 siRNA were optimised by Mr Sandeep Nadendla, who observed a reduction in the levels of endogenous GLI2 mRNA at 96 hours post-transfection in DU145 and PC-3 prostate cancer cells (Nadendla *et al.*, 2011); he used a commercially available siRNA against GLI2 (si5817, Ambion) at 30 nM concentration. Du145 prostate cancer cells or Hacat keratinocytes were transfected with siRNAs at 30 nM final concentration and after 96 hours cells were harvested and analysed. GLI2 H-300 has been validated for immunofluorescence in a recent publication (Bishop *et al.*, 2010) and was used as a positive control. Although Cyclophilin B mRNA levels appear decreased in both cell types, GLI2 levels are reduced by half in Du145 but only by about 15% in Hacat cells. Western Blot using the GLI2 H300 antibody revealed a decrease in GLI2 levels using si17, though GLI2 levels in the controls raise some concerns as they seem to vary in Du145 cells, while in Hacat keratinocytes GLI2 levels in siGlo and siAmb are very similar to si17. No significative differences in staining intensity were observed by immunofluorescence in knockdown cells compared to control with either GLI2 H300 or GLI2 Abcam antibody. The experiment was repeated using a second siRNA against GLI2, si44, in addition to si17. Though Cyclophilin B mRNA levels are reduced in all cell types, GLI2 silencing looks effective only in Du145, with si17 giving the best results; in Hacat keratinocytes GLI2 mRNA levels are not decrease with si17 and paradoxically increased by si44. No significative difference was detected by Western Blotting using the GLI2 H-300 antibody in either cell line. The lower molecular band detected in the LnCap and PC3 prostate cancer cell lines (included for comparison) is consistent with the hypothesis that different isoforms or differently cleaved products of GLI2 may be expressed by different cell types. No significative difference in staining intensity was observed with either antibody in silenced cells compared to controls.

In conclusion, although the transfection protocol seem to be working judging by the reduction in Cyclophilin B levels, it is difficult to see a correlation between qPCR, Western Blotting and staining data when cells are silenced for either GLI1 or GLI2.

One possible explanation is the conditions used (30 nM concentration, 96 hours timepoint) has been shown to be optimal for prostate cells but may be not be ideal for skin cells, in which different concentrations and timepoints would need to be tested. From the data obtained so far, it cannot be concluded GLI1 RD and GLI2 Abcam antibodies are 100% specific as the siRNA results are inconclusive and no clear reduction of GLI expression could be consistently detected.

4.3.10 Conclusions

Previous studies that analysed either GLI1 or GLI2 levels in human BCC relied almost exclusively on measurement of messenger RNA: this is based on the assumption mRNA is always translated to yield a functional protein, not taking into account possible post-transcriptional regulation mechanisms. Moreover, in situ hybridization does not allow co-expression studies (in situ co-hybridization is not a widely used and established technique). Immunohistochemical double-staining was therefore chosen as a feasible approach to characterise GLI1 and GLI2 expression pattern at the protein level in a panel of human BCC samples.

Antibodies against the GLI proteins have been made commercially available only recently; some of them presented reproducibility issues, as described in the previous sections, and were therefore dismissed. The GLI antibodies that worked consistently highlighted a widespread heterogeneity in the pattern of GLI1 and GLI2 expression: this result could be related to non-canonical activation of GLI proteins. In addition to that, difference in staining pattern using different GLI1 antibodies was observed: the different patterns could be due to different isoforms; an antibody will bind to a GLI1 isoform only if the epitope is present (Fig 4.53). GLI1 isoforms had been described in vitro (by transfecting full length GLI1 into glioma cells) (Altaba, 1999; Stecca and Ruiz i Altaba, 2009), but not until very recently they have been reported in human tissues (including lung, kidney, pancreas, and ovary) (Shimokawa et al., 2008) and in human glioblastoma multiforme samples (Lo et al., 2009). As such, these isoforms were not taken into account when commercially available antibodies were designed,

and this could in part account for the heterogeneity and discrepancies observed in the BCC staining results. Based on currently available information, to detect all the known GLI1 isoforms, an antibody should be generated against an epitope between amino-acids position 231 – 515 (Fig 4.53), and none of the antibodies used in this thesis satisfy this condition. To take into account this unexpected novel complexity of the HH-GLI signalling, highlighted by the staining results, GLI1 isoforms expression pattern in BCC are to be identified using LCM at mRNA level, then isoform-specific antibodies could be generated to see if this is reflected in GLI1 – GLI2 protein expression. Given these assumption, it is difficult to say which antibody is the best or more specific one for BCC staining. GLI antibodies used for staining in this thesis have already been employed in a number of publications, listed in Appendix IV. However, due to the heterogeneity of the staining results observed, (see section 4.3.9), we tried to validate the antibodies by using SMO inhibitors and subsequently by siRNA technology. Unfortunately, from the data obtained so far, it cannot be concluded that GLI1 RD and GLI2 Abcam antibodies are unequivocally specific as the results have been inconclusive and further troubleshooting could not be carried out due to time constraints. The reason for incorporating these inconclusive results is that they represent the starting point for further validation work. Since the lack of difference in fluorescence intensity observed upon treatment with SMO inhibitors could be due to the different aliquots of inhibitors used, a positive control for testing the efficacy of the inhibitors is needed. An ideal solution would be a cell line incorporating a GLI luciferase reporter, similar to the one employed by Taipale et al. (Taipale et al., 2000); if treatment of cells with cyclopamine significantly reduces GLI reporter activity we could be confident about the effectiveness of those inhibitors. An alternative approach for validating the antibodies is the use of short interfering RNA (siRNA) technology. We tested the cells by qPCR and by Western Blotting as methods to check siRNA efficacy in parallel with immunofluorescent cytochemistry analysis. No clear correlation between qPCR, Western Blotting and fluorescent staining data was observed, and further optimisation is needed, specifically testing different siRNA concentrations and timepoints for harvesting. Results obtained by other PhD students in the lab (J. Elliott et al. and M. Rahman et al., unpublished data) support GLI1 H-300

specificity, while GLI2 H-300 was validated for use in immunofluorescence in a recent publication by Bishop et al. (Bishop et al., 2010).

The majority of the immunochemistry work described in this thesis was carried out using frozen specimens and immunofluorescent detection. When immunofluorescence is used the structure of the tissue stained is not readily evident, for the purpose of clearly identifying tissue morphology histochemical staining (DAB) is a better technique. Immunofluorescent staining using GLI1 H-300 antibody revealed positive staining the stroma of some BCC samples: we speculated DAB staining would be more informative in trying to identify the location and cell type that stained positive for GLI1. In addition to this, we thought it was useful to test how these GLI antibodies performed in DAB staining (limited data was available in the literature as they had been made commercially available only recently). DAB staining is most widely used on wax-embedded tissues: we also could have taken advantage of the large number of wax embedded BCCs conserved in the Pathology archive and therefore address the problem of increasing the numbers of samples belonging to the rarer superficial and morphoeic BCC subtypes.

GLI2 antibodies (GLI2 H-300 and GLI2 Abcam) gave similar staining patterns in normal skin using wax sections and DAB detection and frozen sections and immunofluorescent detection, while GLI1 antibodies presented some differences. GLI1 RD is more nuclear in wax sections (DAB and immunofluorescence) compared to frozen ones (immunofluorescence) though the reason for this is not clear; it may be GLI1 is predominantly nuclear in the wax sections analysed (one normal skin and two BCCs) or this could be due to the different techniques used. GLI1 H-300 staining intensity is weaker in BCC wax sections (both by DAB and by immunofluorescence) when compared to immunofluorescent staining on frozen sections. Unfortunately GLI1 H-300 stromal staining was not evident in wax-embedded BCCs, either by DAB or by immunofluorescence (two BCCs analysed); this could be due to the fact an antigen-retrieval step is required. We decided to continue with immunofluorescent staining in frozen BCC sections in parallel with experiments aimed at validating the antibodies used. The main advantage of immunofluorescence is the possibility of performing double staining for two different proteins using different fluorochromes. This peculiarity was exploited in

double staining for GLI1 and SHH, aimed at investigating a possible paracrine mechanism of HH signalling and in double staining for GLI1 and GLI2, to analyse their pattern of expression. Paracrine HH signalling has been described in different kind of cancers (Yauch et al., 2008; Nolan-Stevaux et al., 2009; Tian et al., 2009) and has been linked to tumor progression, possibly by secretion of chemokines and growth-promoting factors. This was an attractive hypothesis to explain GLI1 staining in the stroma and could explain why BCC explants are difficult to culture in vitro once they are separated from the mesenchyme (Asada et al., 1992; Grando et al., 1996). However, since only a very small minority of BCC samples were positive for SHH staining (section 4.2.11), this seems unlikely. An alternative hypothesis is non-canonical activation of GLI proteins in the stroma by transforming growth factor beta (TGFβ) (Dennler et al., 2007; Dennler et al., 2009), which could be tested by staining or by using laser capture microdissection (LCM).

Several studies have shown that the GLI1 and GLI2 transcription factors are frequently upregulated in Basal Cell Carcinoma and this is linked with inappropriate Hedgehog pathway activation (Dahmane et al., 1997; Green et al., 1998; Ghali et al., 1999; Bonifas et al., 2001; Ikram et al., 2004; Hatta et al., 2005) However, the data presented here suggests the expression of GLI1 and GLI2 is considerably more complex than previously documented. For example, by specifically assessing protein expression using immunohistochemistry, it is apparent that there is a great deal of heterogeneity with regard to the level and pattern of GLI1 and GLI2 in human BCC. This is compounded by the fact that other research in the group has demonstrated that PTCH1 suppression (by siRNA) leads to an increase of GLI1 but not GLI2 mRNA expression in human keratinocyte cell lines (M. Rahman et al., unpublished data). As such, it is not possible to state that BCCs have a uniform increase in epithelial GLI expression as a result of ligand-independent HH signalling that stems from a loss of PTCH1 function or a gain of SMO function. Therefore, the role of the GLI transcription factors in BCC biology requires further evaluation. Moreover, preliminary data also question the presence of a positive GLI1-GLI2 feedback loop in cultured keratinocytes, although how this relates to Basal Cell Carcinoma development requires further investigation.

Chapter 5

5 Effect of over expression of constitutively active GLI2 in organotypics models

5.1 Introduction

Cells are usually grown completely submerged by culture media on treated plastic dishes or flasks. While this approach is suitable for the vast majority of cell types, a different type of culture condition has been found to be useful in studying cellular process that are peculiar to keratinocytes. The epidermis is composed of keratinocytes, and these cells are normally exposed to the air as they give rise to the upper layer of the skin; keratinocytes grown in submerged culture show signs of differentiation though they cannot fully differentiate, probably due to conditions that are quite different to an in vivo setting. Different models of skin equivalents in which cells are grown at the liquid-air interface have been proposed (Prunieras *et al.*, 1983): the most widely used are de-epidermalised dermis (DED) and collagen or collagen-matrigel gels. These models are useful in studying keratinocytes differentiation and also processes in which cell-extracellular matrix interactions are involved, such as migration and invasion.

GLI2ΔN is a constitutively active form of GLI2 lacking the amino-terminal repressor domain (Roessler et al., 2005). This truncated form of GLI2 (previously thought to be the whole protein) has been shown to be a more potent activator than the full-length GLI2, and has been previously used in cancer studies. A stable-expressing GLI2ΔN cell line has been previously generated and characterised in the lab (E. Pantazi et al., unpublished results): this has been achieved by transducing a GLI2ΔN overexpression vector into the immortalized human keratinocytes cell line N/Tert-1 as a GFP fusion protein. Human telomerase (h/TERT)-immortalised N/Tert-1 keratinocytes have functional p53/p21$^{WAF1/CIP1}$ and have been shown to retain normal epidermal keratinocyte differentiation in organotypic cultures (Dickson et al., 2000).

Cross talk between the Hedgehog and WNT pathways has been suggested to be implicated in Basal Cell Carcinoma pathogenesis. In a mouse model of skin cancer, WNT signalling is necessary for the development of follicular hamartomas, a type of benign tumour associated with deregulated HH signalling (Yang et al., 2008).

Intriguingly, this suggests HH-WNT cross-talk could also be important for BCC development. Notably, upregulation of WNT-family proteins WNT5a, WNT7a and WNT11 has been detected in GLI2ΔN cell line by qPCR (Pantazi E. et al, unpublished data). WNT5a, WNT7a and WNT11 are secreted ligands and had been shown to play a role in cell migration (Weeraratna et al., 2002; Ouko et al., 2004; Lyu and Joo, 2005; Kurayoshi et al., 2006; Pukrop et al., 2006). The aim of this chapter is to test if GLI2ΔN keratinocytes have enhanced migratory and/or invasive properties as a consequence of upregulation of specific WNT proteins. We used two different organotypic model of human skin, de-epidermalised dermis (DED) and collagen-matrigel gels; both these models have been previously used to assess invasion (Akgul et al., 2005; Nystrom et al., 2005). BCCs are slow growing tumors, and it is not clear how they switch from being indolent to a more aggressive and metastatic phenotype: upregulation of migratory WNT proteins could be a possible mechanism that contributes to this transition. Would this proven to be true, the use of antagonists of WNT pathways may be investigated as a treatment for aggressive BCCs.

5.2 Results

5.2.1 De-epidermalised dermis (DED) organotypic model

5.2.1.1 N/Tert-1 GLI2ΔN keratinocytes grown on De-epidermalised dermis (DED) organotypic model (first experiment)

N/Tert-1, N/Tert-1 GFP or N/Tert-1 GLI2ΔN keratinocytes were plated on the papillary surface of DEDs containing human dermal fibroblasts on its reticular surface. These organotypic cultures were grown on a stainless-steel grid and supplied with medium from below for 18 days; the tissue was then fixed and processed as detailed in the Materials and Methods section.

Hematoxylin and eosin staining of organotypic sections show how keratinocytes were able to attach and grown on the DED surface (Fig. 5.1 - 5.3). The staining of sections also highlighted how N/Tert-1 GLI2ΔN keratinocytes invade into the dermis (Fig. 5.3), a characteristic feature not observed in N/Tert-1and N/Tert-1 GFP keratinocytes (Fig. 5.1 and 5.2). Keratinocytes seem to invade in small groups, sometimes resembling string-like structures; it is interesting to note this feature is also characteristic of Basal Cell Carcinomas belonging to the infiltrative / morphoeic subtype, which often present thin strands of basaloid cells extending into the underlying dermis.

GLI2ΔN keratinocytes also display a peculiar morphology and appear to be less differentiated than their N/Tert-1 and N/Tert-1 GFP counterparts as denoted by the lack of a visible cornified layer and, more generally, by the apparent lack of stratified organisation (Fig. 5.3). This observation is consistent with a previous report that shows how GLI2ΔN overexpression is associated with repression of epidermal differentiation markers in vitro (Regl et al., 2004a). As a negative control N/Tert-1 cells were seeded on a DED lacking fibroblasts on the reticular side; here keratinocytes seem to have attached but not able to fully differentiate (Fig. 5.4).

These data suggest GLI2ΔN overexpression in keratinocytes promotes invasion and disorganised differentiation in a DED organotypic model system. We therefore planned to confirm this data and further analyse the phenotypes observed in GLI2ΔN cells.

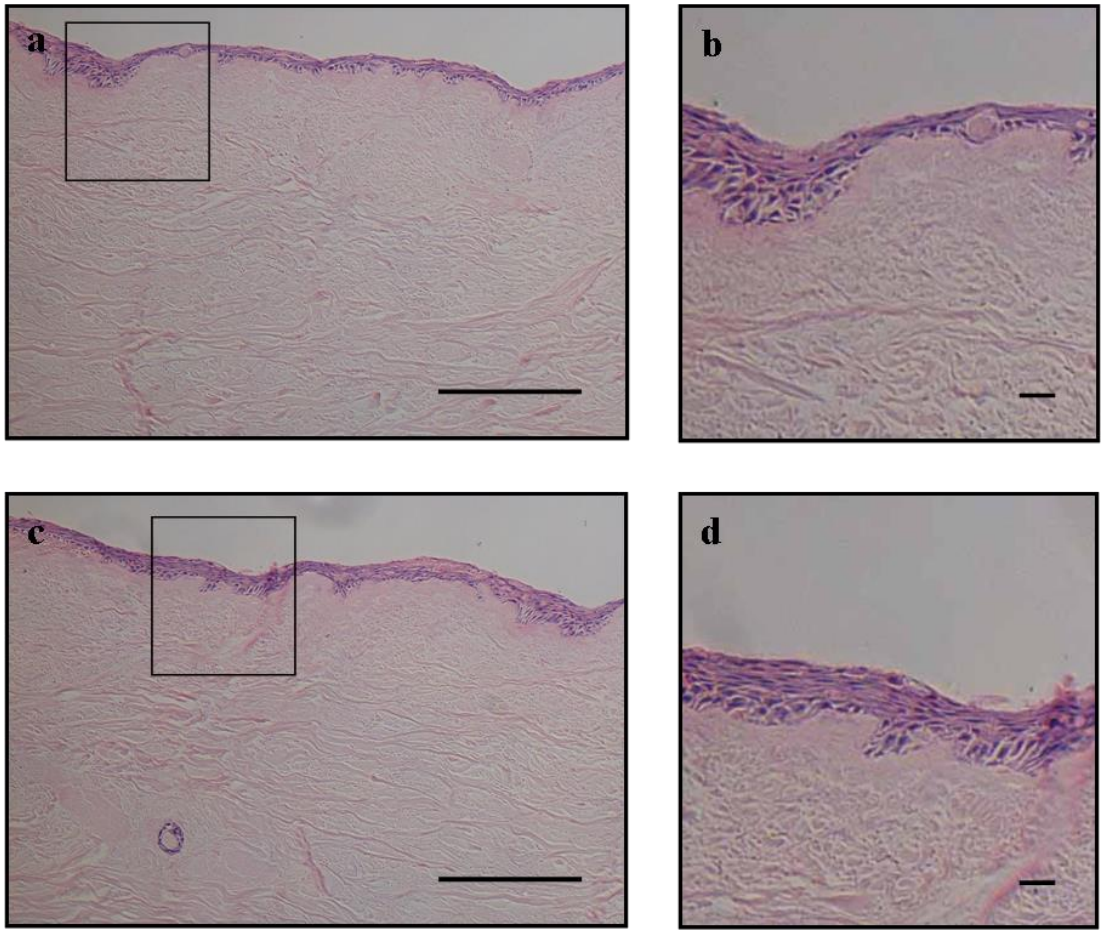

Figure 5.1: N/Tert-1 keratinocytes organotypic raft cultures

Haematoxylin and eosin stained transverse section of organotypic cultures of keratinocytes on De-Epidermalized Dermis (DED). N/Tert-1 keratinocytes were plated on top of DED and grown at the air-liquid interface for 18 days. Representative images are shown (a, c), with respective higher magnification pictures shown on the right (b, d). Scale bar represents 200 µm in (a) and (c) and 50 µm in (b) and (d).

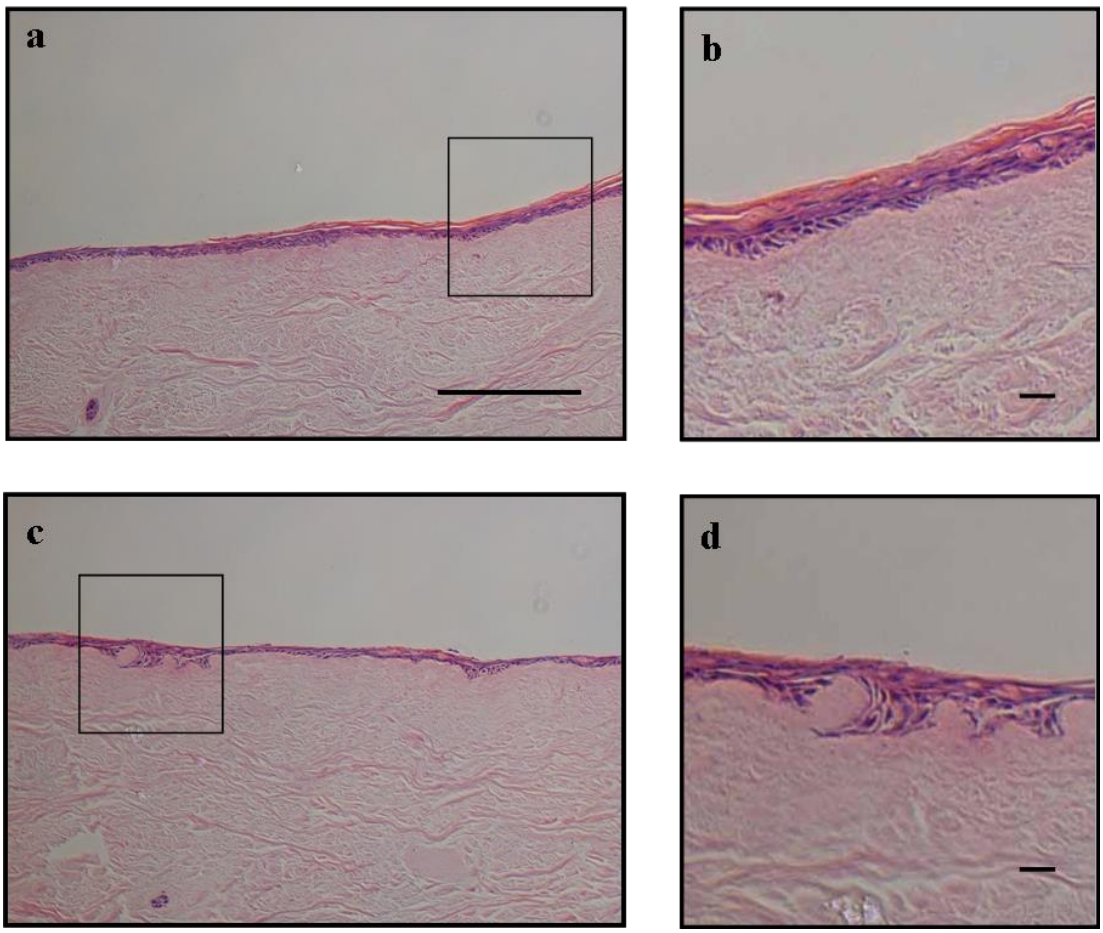

Figure 5.2: N/Tert-1 GFP keratinocytes organotypic raft cultures

Haematoxylin and eosin stained transverse section of organotypic cultures of keratinocytes on De-Epidermalized Dermis (DED). N/Tert-1 GFP keratinocytes were plated on top of DED and grown at the air-liquid interface for 18 days. Representative images are shown (a, c), with respective higher magnification pictures shown on the right (b, d). Scale bar represents 200 μm in (a) and (c) and 50 μm in (b) and (d).

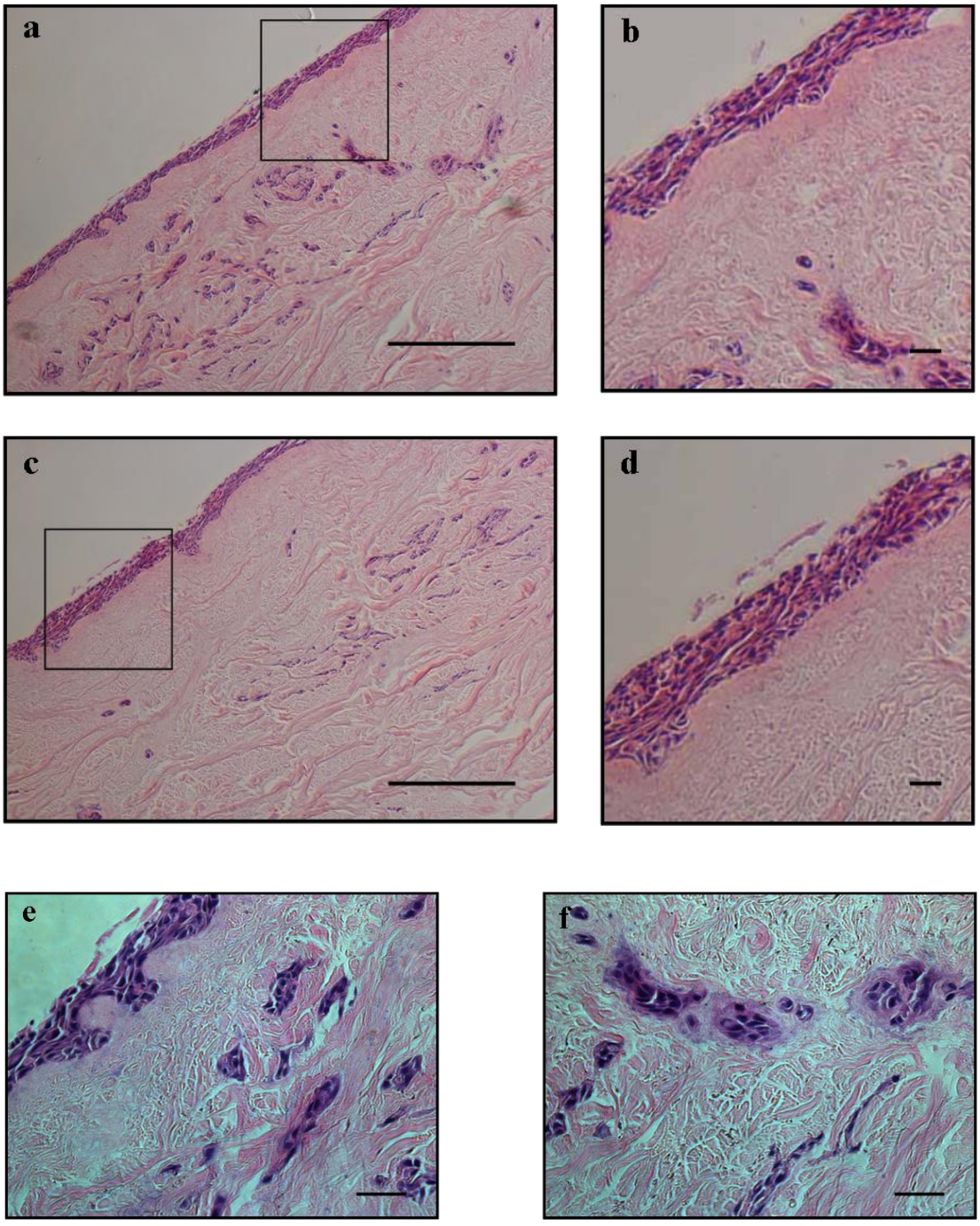

Figure 5.3: N/Tert-1 GLI2ΔN keratinocytes organotypic raft cultures

Haematoxylin and eosin stained transverse section of organotypic cultures of keratinocytes on De-Epidermalized Dermis (DED). N/Tert-1 GLI2ΔN keratinocytes were plated on top of DED and grown at the air-liquid interface for 18 days. Representative images are shown (a, c), with respective higher magnification pictures shown on the right (b, d). Invading cells display a peculiar string-like morphology (e, f). Scale bar represents 200 µm in (a, c,) and 50 µm in (b, d, e, f).

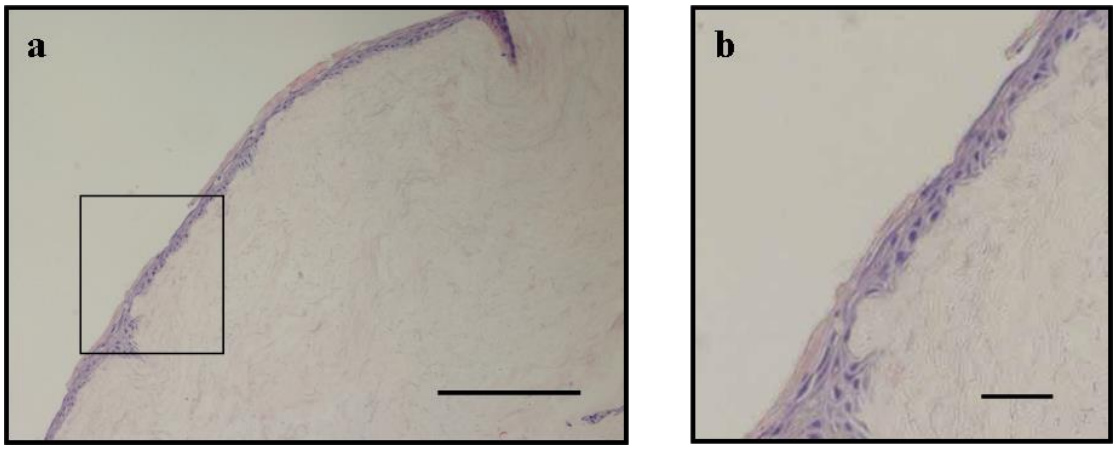

Figure 5.4: N/Tert-1 keratinocytes organotypic raft cultures grown in the absence of fibroblasts (negative control)

Haematoxylin and eosin stained transverse section of organotypic cultures of keratinocytes on De-Epidermalized Dermis (DED). N/Tert-1 keratinocytes were plated on top of DED and grown at the air-liquid interface for 18 days. As a negative control, no fibroblasts had been seeded in the reticular side of the de-epidermalised human skin (see text for details). Representative images are shown (a), with respective higher magnification pictures shown on the right (b). Scale bar represents 200 µm in (a) and 50 µm in (b).

5.2.1.2 N/Tert-1 GLI2ΔN keratinocytes grown on De-epidermalised dermis organotypic model (second experiment)

N/Tert-1, N/Tert-1 GFP or N/Tert-1 GLI2ΔN keratinocytes were plated on the papillary surface of DEDs containing human dermal fibroblasts on its reticular surface. These organotypic cultures were grown on a stainless-steel grid and fed with medium from below for 10 days; the tissue was then fixed and processed as detailed in the Materials and Methods. Hematoxylin and eosin staining of organotypic sections revealed how keratinocytes were able to attach and grown on the DED surface (Fig. 5.5); a thicker layer of epidermis was formed compared to the one observed in the previous experiment (Fig. 5.1 - 5.3): this could be due to a better ability to attach and / or proliferate.

N/Tert-1 and N/Tert-1 GFP keratinocytes appear to have at least partly differentiated on DEDs (Fig. 5.5 a, b, c, d), while this feature seems less pronounced in the N/Tert-1 GLI2ΔN DED (Fig. 5.5 e, f). GLI2ΔN keratinocytes also seem to have a more cuboidal shape compared to the more rounded N/Tert-1 and N/Tert-1 GFP; moreover, they seem to be less able to adhere to each other as judged by the wide crack-like gaps present in the epidermis structure (Fig. 5.5 e, f).

No overt invasion into the underlying dermis was seen in the GLI2ΔN keratinocytes DEDs, contrary to what was observed in the previous experiment. GLI2ΔN keratinocytes may, however, have invasive potential that could be revealed by staining for component of the basement membrane. Enzymatic breakdown of the basement membrane is necessary for keratinocytes invasion into the underlying dermis. Collagen type IV and collagen type VII are primarily expressed in the basement zone underlying epithelia; if an aberrant pattern expression of these proteins would be seen in the GLI2ΔN DEDs this would support the notion of a more invasive capacity. Of note, Hacat GLI2ΔN collagen organotypics has been previously reported to show reduced epithelial differentiation and an abnormal basement membrane zone (Regl *et al.*, 2004a; Regl *et al.*, 2004b; Kump *et al.*, 2008; Marsh *et al.*, 2008; Snijders *et al.*, 2009).

Overexpression of GLI2ΔN has also been associated with repression of epidermal differentiation markers in vitro (Regl et al., 2004a), and in both DEDs experiments

N/Tert-1 GLI2ΔN keratinocytes appear morphologically less differentiated than their N/Tert-1 and N/Tert-1 GFP counterparts. To further extend this observation, DEDs sections have been stained with markers of epithelial differentiation (see section 5.2.1.3).

As a negative control N/Tert-1 GFP and N/Tert-1 GLI2ΔN cells were also seeded on a DED lacking fibroblasts on the reticular side; surprisingly cells seem to have attached even in the absence of fibroblast, though keratinocytes seem to be less compact and gaps between cells are seen not only in the N/Tert-1 GLI2ΔN DED but also in the N/Tert-1 GFP DED (Fig. 5.6 a, b, c, d).

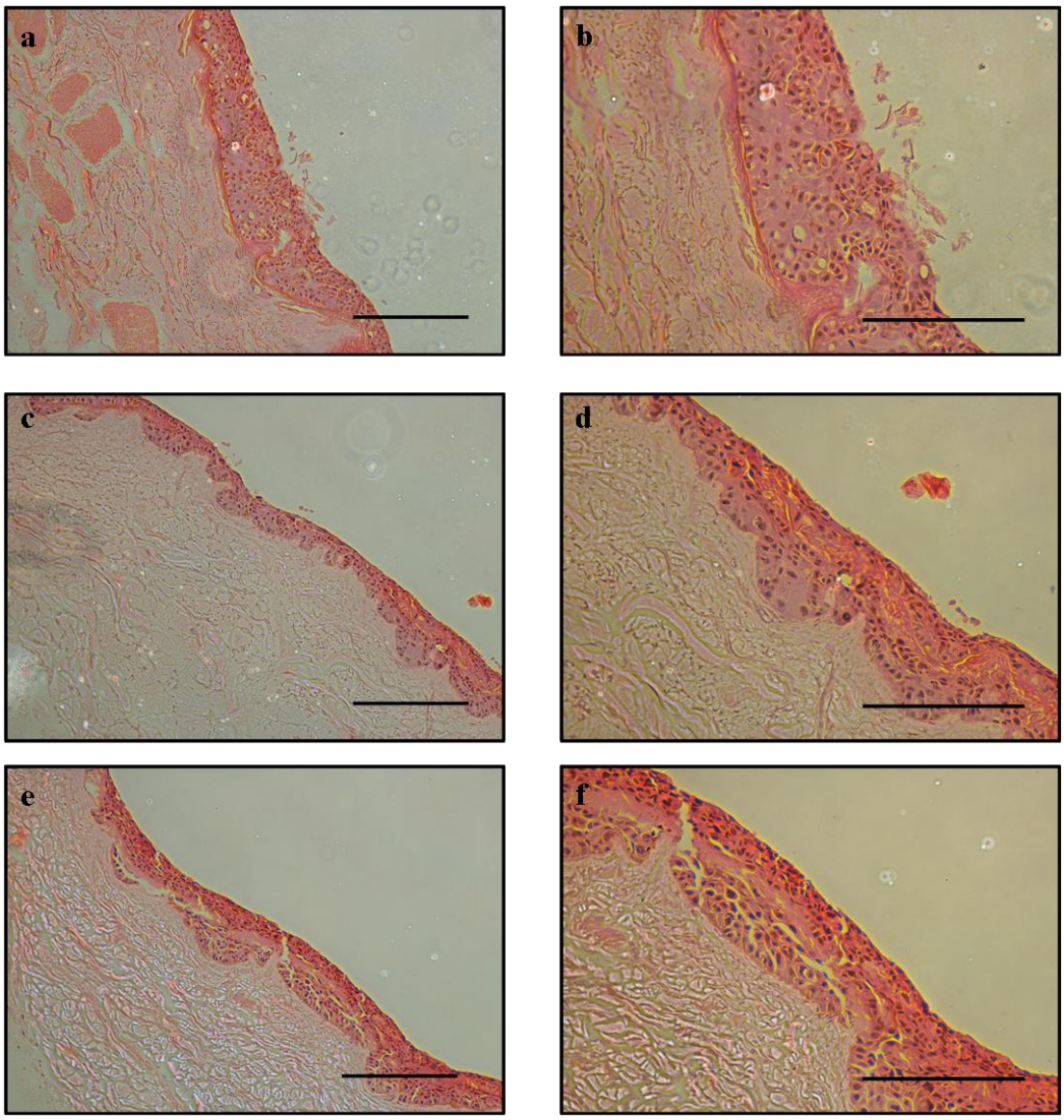

Figure 5.5: N-Tert-1, N/Tert-1 GFP and N/Tert-1 GLI2ΔN keratinocytes in organotypic raft cultures

Haematoxylin and eosin stained transverse section of organotypic cultures of keratinocytes on De-Epidermalized Dermis (DED). N-Tert-1 (a, b), N/Tert-1 GFP (c, d) or N/Tert-1 GLI2ΔN keratinocytes (e, f) were plated on top of DED and grown at the air-liquid interface for 10 days. Representative images are shown (a, c, e), with respective higher magnification pictures shown on the right (b, d, f). Scale bar represents 200 µm.

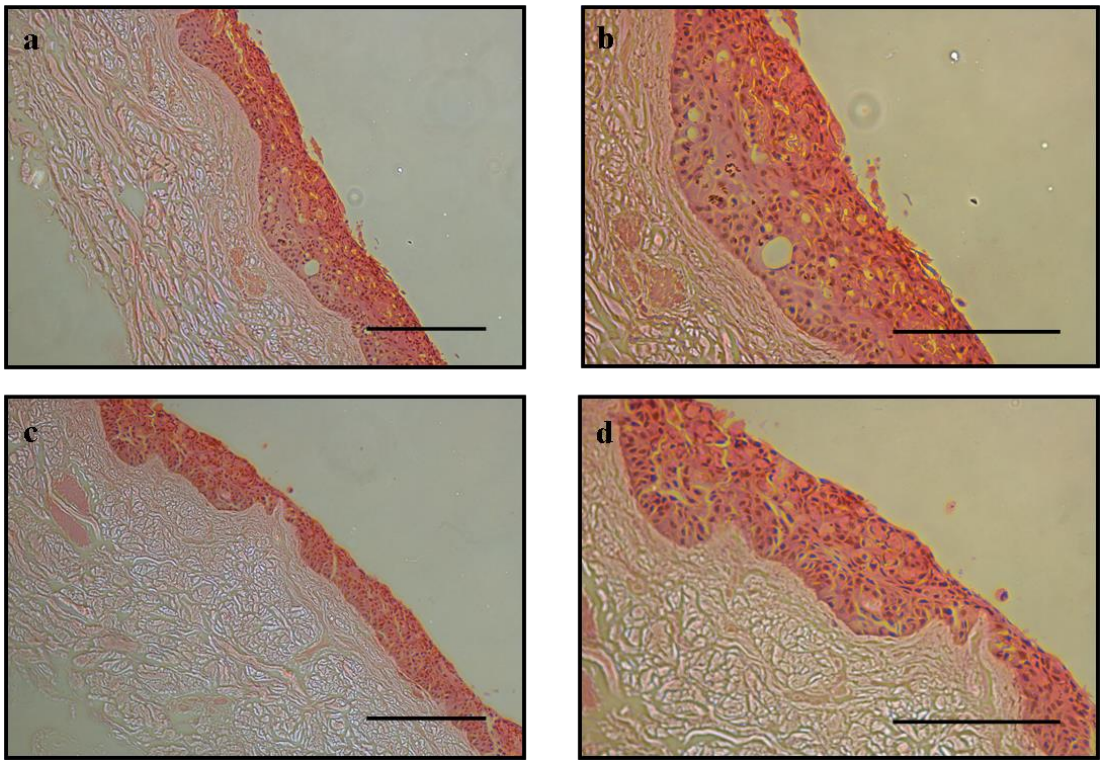

Figure 5.6: N/Tert-1 GFP and N/Tert-1 GLI2ΔN keratinocytes organotypic raft cultures grown in the absence of fibroblasts (negative control).

Haematoxylin and eosin stained transverse section of organotypic cultures of keratinocytes on De-Epidermalized Dermis (DED). N/Tert-1 GFP (a, b) or N/Tert-1 GLI2ΔN (c, d) keratinocytes were plated on top of DED and grown at the air-liquid interface for 10 days. As a negative control, no fibroblasts had been seeded in the reticular side of the de-epidermalised human skin. Representative images are shown (a, c), with respective higher magnification pictures shown on the right (b, d). Scale bar represents 200 µm.

5.2.1.3 Keratin 1, Involucrin, Loricrin and E-cadherin expression pattern in N-Tert-1, N/Tert-1 GFP and N/Tert-1 GLI2ΔN De-epidermalised dermis (DED) organotypic model

To analyse the effect of GLI2ΔN overexpression on differentiation and adhesion, N/Tert-1, N/Tert-1 GFP and N/Tert-1 GLI2ΔN wax-embedded DED sections were stained were stained with differentiation markers Keratin 1, Involucrin (two different antibodies), Loricrin and with an antibody against E-cadherin.

N/Tert-1 and N/Tert-1 GFP DEDs were positive for Keratin 1 filaments (a marker of the spinous layer), while they appear to be absent in the N/Tert-1 GLI2ΔN DED (Fig. 5.7). Involucrin and Loricrin expression, both markers of keratinocyte terminal differentiation, are normally expressed in the suprabasal layers of stratified epithelia.

Involucrin staining is observed in the upper layers of both N-Tert-1 and N/Tert-1 GFP DEDs using antibody SY7 (Fig 5.8), while a similar pattern is absent in the N/Tert-1 GLI2ΔN DED; the same result is obtained using a second Involucrin antibody (SY5)(Fig 5.9). Strong Loricrin staining is present in N/Tert-1 and also, albeit slightly less evident, in N/Tert-1 GFP DED, while it is rarely present in N/Tert-1 GLI2ΔN DED (Fig 5.10).. E-cadherin is a component of adherence junctions which plays a crucial role in epithelial cell-cell adhesion; down-regulation of E-cadherin expression is linked with increased invasive potential of epithelial carcinomas. There seem to be no significative difference in E-cadherin expression in N/Tert-1 GLI2ΔN DED compared to N/Tert-1 and N/Tert-1 GFP DEDs (Fig 5.11).

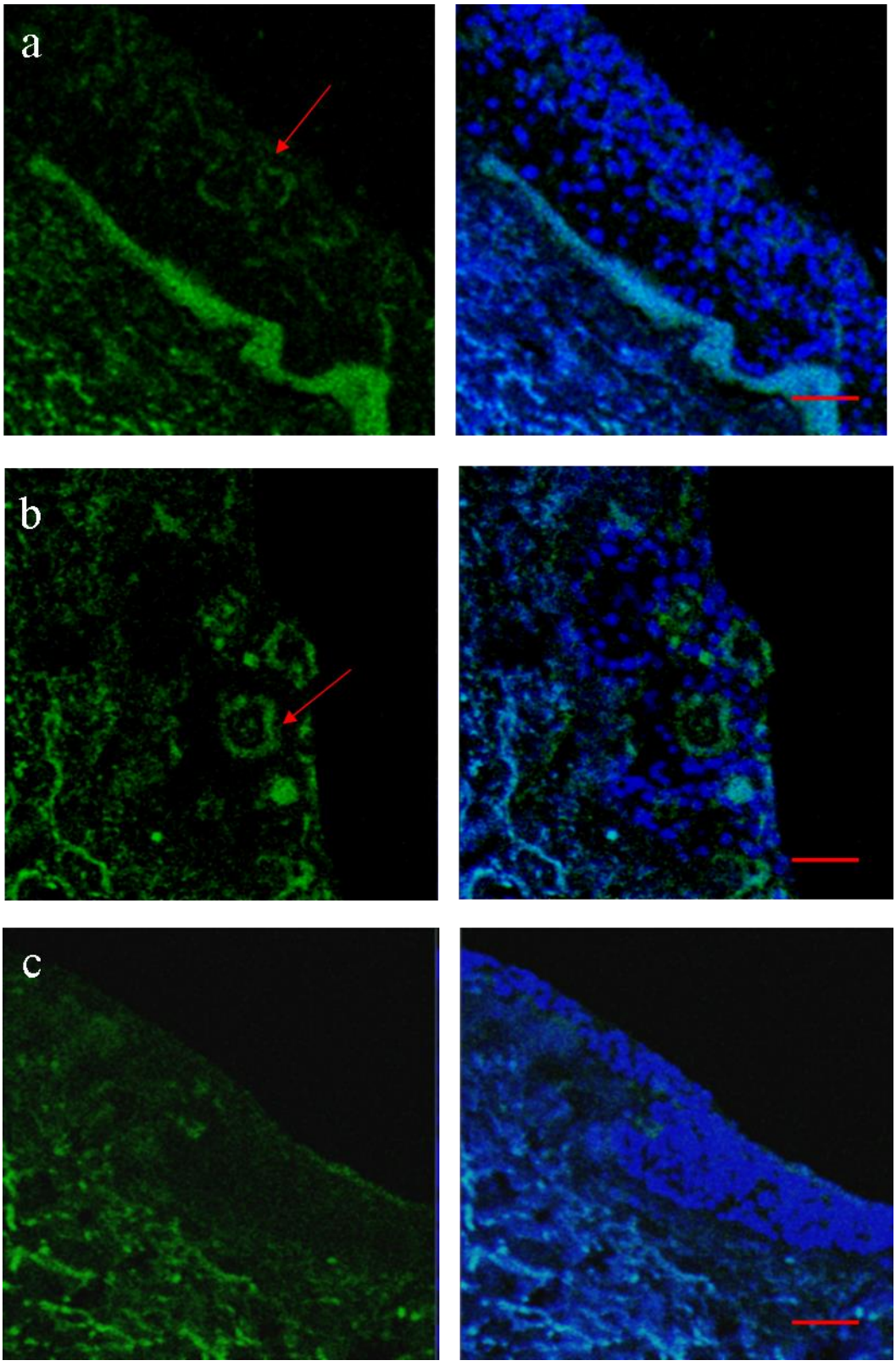

Figure 5.7: Keratin 1 staining of N-Tert-1, N/Tert-1 GFP and N/Tert-1 GLI2ΔN keratinocytes in organotypic raft cultures

N-Tert-1 (a), N/Tert-1 GFP (b) or N/Tert-1 GLI2ΔN keratinocytes (c) wax-embedded DED sections were stained with an antibody against Keratin 1. Scale bar represents 50 µm.

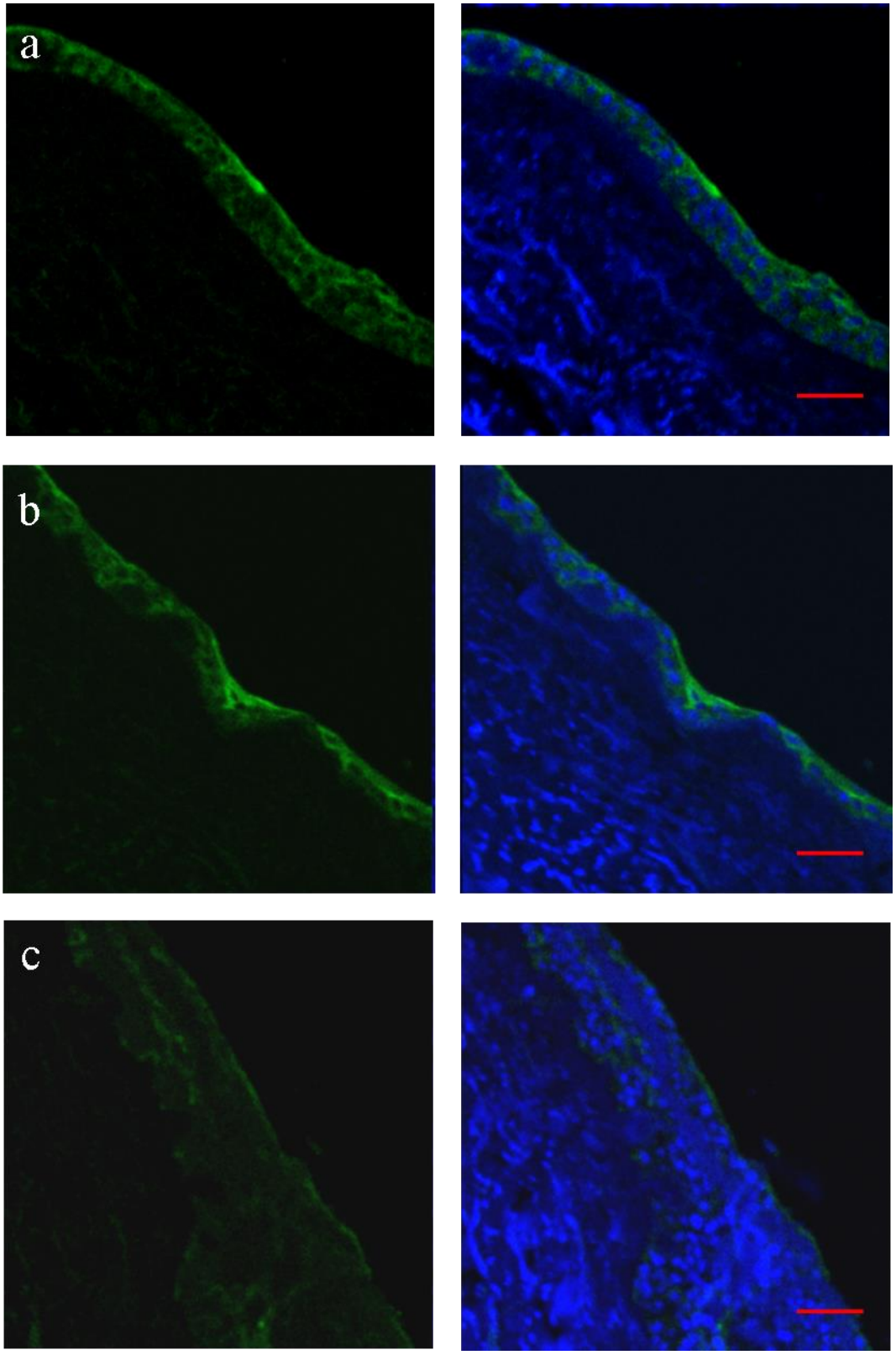

Figure 5.8: Involucrin (SY7) staining of N-Tert-1, N/Tert-1 GFP and N/Tert-1 GLI2ΔN keratinocytes in organotypic raft cultures

N-Tert-1 (a), N/Tert-1 GFP (b) or N/Tert-1 GLI2ΔN keratinocytes (c) wax-embedded DED sections were stained with an antibody against Involucrin (SY7). Scale bar represents 50 µm.

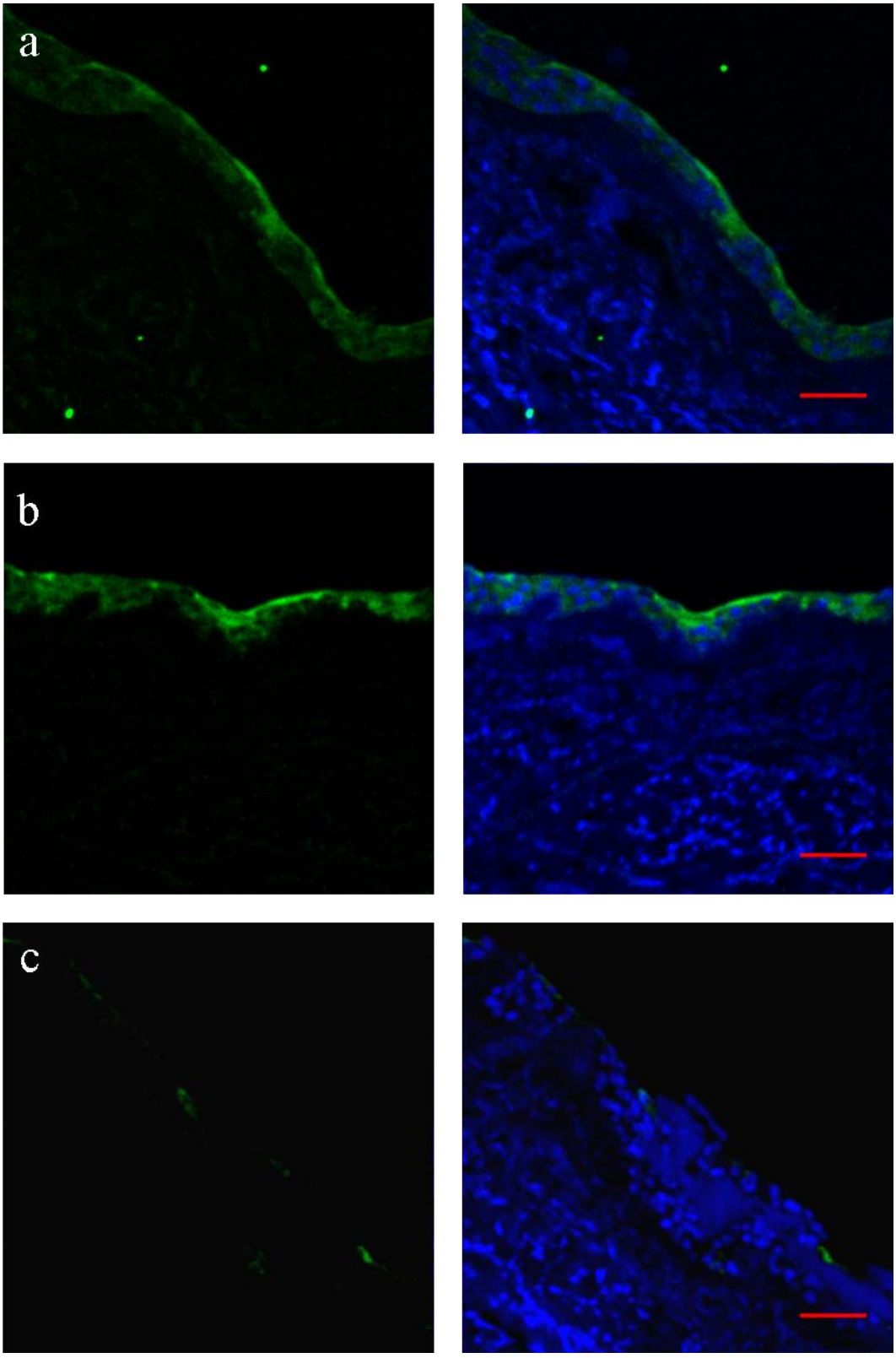

Figure 5.9: Involucrin (SY5) staining of N-Tert-1, N/Tert-1 GFP and N/Tert-1 GLI2ΔN keratinocytes in organotypic raft cultures

N-Tert-1 (a), N/Tert-1 GFP (b) or N/Tert-1 GLI2ΔN keratinocytes (c) wax-embedded DED sections were stained with an antibody against Involucrin (SY5). Scale bar represents 50 µm.

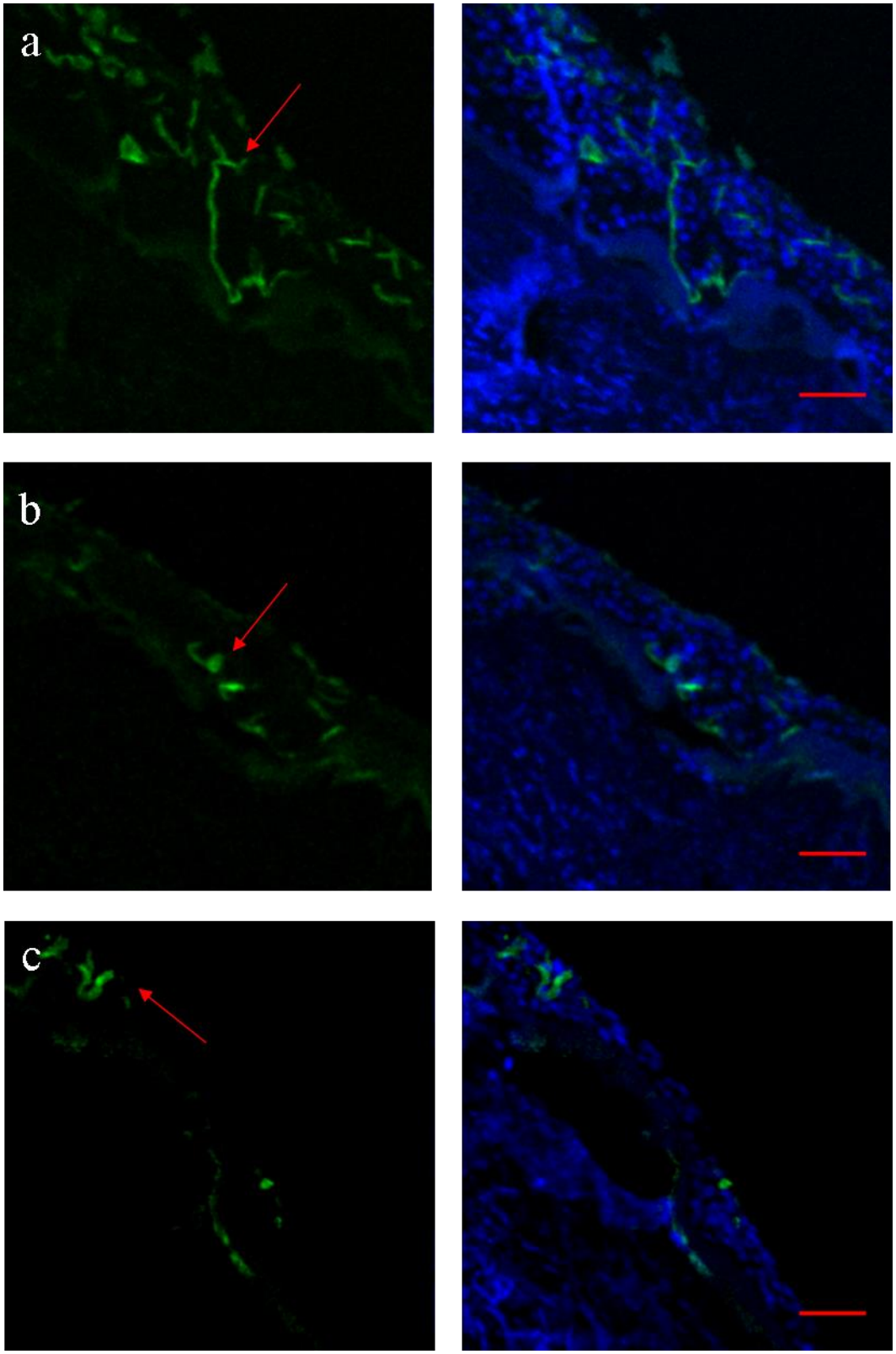

Figure 5.10: Loricrin staining of N-Tert-1, N/Tert-1 GFP and N/Tert-1 GLI2ΔN keratinocytes in organotypic raft cultures

N-Tert-1 (a), N/Tert-1 GFP (b) or N/Tert-1 GLI2ΔN keratinocytes (c) wax-embedded DED sections were stained with an antibody against Loricrin. Scale bar represents 50 µm.

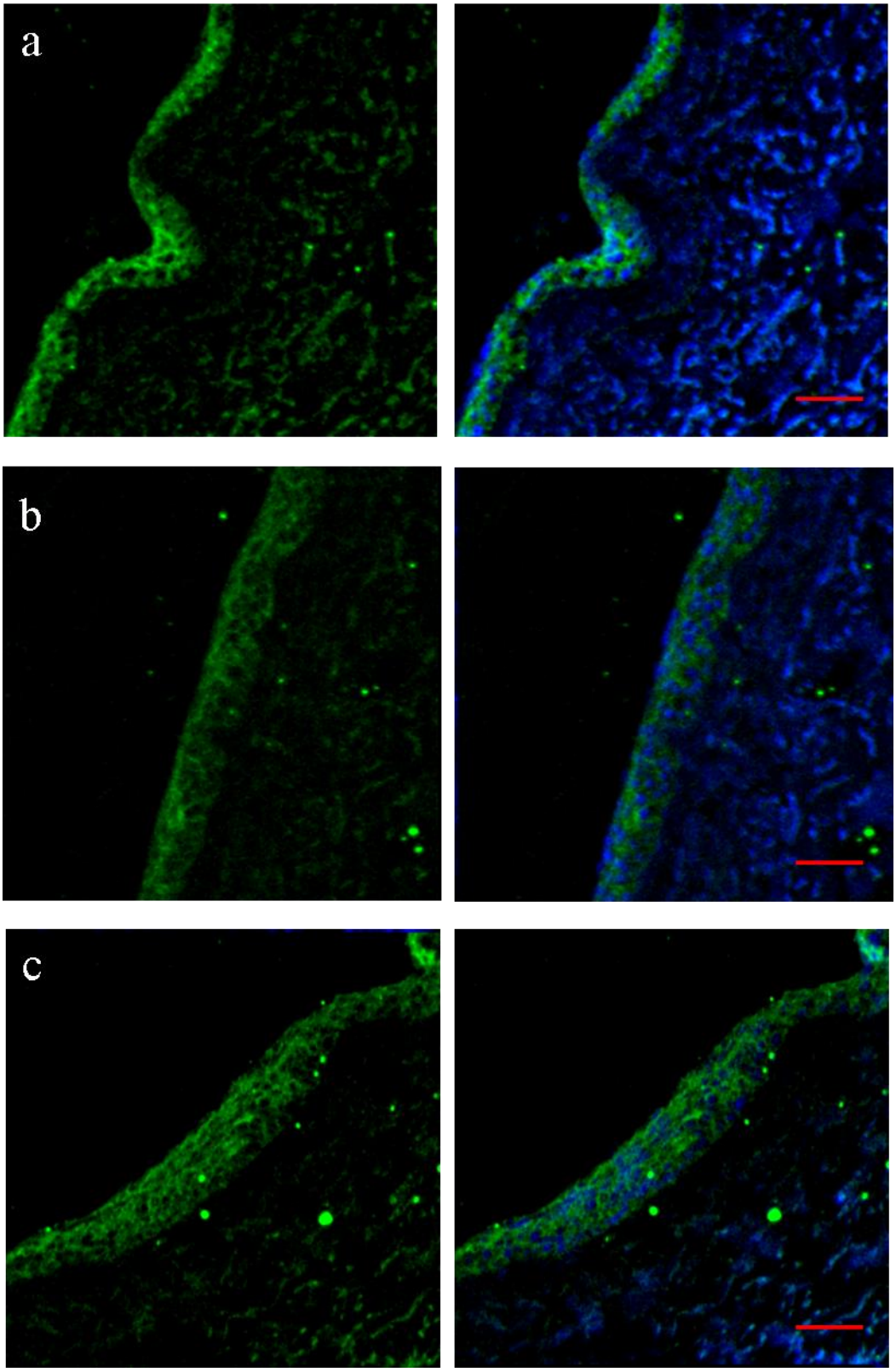

Figure 5.11: E-cadherin staining of N-Tert-1, N/Tert-1 GFP and N/Tert-1 GLI2ΔN keratinocytes in organotypic raft cultures

N-Tert-1 (a), N/Tert-1 GFP (b) or N/Tert-1 GLI2ΔN keratinocytes (c) wax-embedded DED sections were stained with an antibody against E-cadherin. Scale bar represents 50 µm.

5.2.2 Collagen-matrigel gels organotypic model

The dermis is composed for more than 70% of collagen, which is synthetised and organised by dermal fibroblasts; collagen or collagen-matrigel gels embedded with fibroblasts are widely used as a skin substitute to investigate cell invasion ((Akgul *et al.*, 2005; Nystrom *et al.*, 2005). Matrigel is an extracellular matrix preparation derived from a mouse sarcoma; this mixture includes high levels of collagen IV and laminin, as well as different growth factors, which make this composition more similar to the physiological in vivo setting.

To test if GLI2ΔN overexpression in N/Tert-1 keratinocytes has an effect on cell invasion, in N/Tert-1, N/Tert-1 GFP or N/Tert-1 GLI2ΔN keratinocytes (5×10^5 cells for each type) were plated on top of collagen-matrigel gels (50%-50%) with incorporated fibroblasts (5×10^5 fibroblasts per gel). Organotypic cultures were grown on a stainless-steel grid and fed with medium from below for 14 days; the tissue was then fixed and processed (see Materials and Methods). Although these gels seem to present some technical issues (which it is reflected in their histology) probably due to the fact they tend to lose compactness during culture and are therefore difficult to separate from the grids in order to be processed, cells appear to have been able to attach and proliferate (Fig. 5.17). GLI2ΔN keratinocytes seem to display increased invasion into the gel compared to N/Tert-1 and N/Tert-1 GFP keratinocytes, as shown by hematoxylin and eosin staining of organotypic sections (Fig. 5.17 c). This is similar to what we observed using the DED organotypic model, and consistent with data previously generated in the lab (Bahta A. et al., unpublished results). Notably, similar results have been recently obtained in the lab by Miss Eleni Pantazi using collagen-matrigel organotypics gels kept in culture for 13 days (E. Pantazi et al., unpublished results). This peculiar behavior of GLI2ΔN keratinocytes in organotypic cultures is consistent with the hypothesis that GLI2 could activate pathways involved in the regulation of cell migration and invasion, such as the WNT pathway.

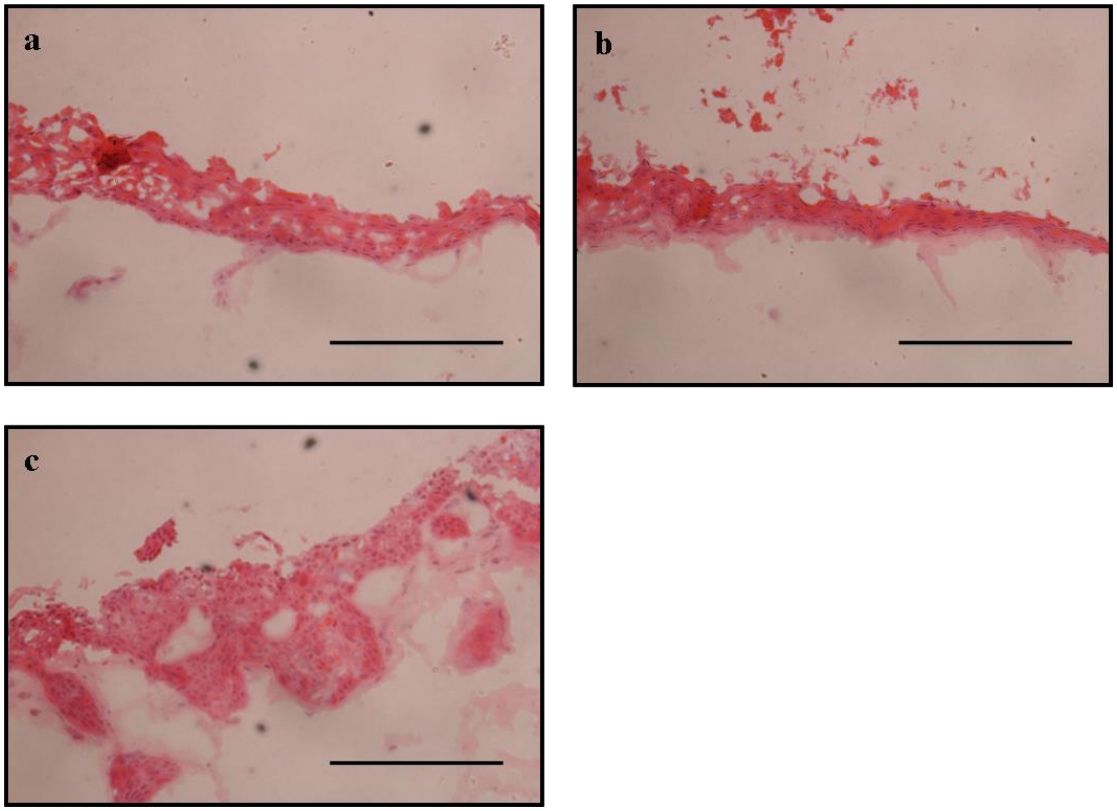

Figure 5.12: GLI2ΔN overexpression in N/Tert-1 keratinocytes increases invasion in collagen-matrigel organotypic cultures

Haematoxylin and eosin stained transverse section of organotypic cultures of keratinocytes on collagen-matrigel gels. N/Tert-1, N/Tert-1 GFP or N/Tert-1 GLI2ΔN keratinocytes were plated on collagen-matrigel gels with incorporated fibroblasts and grown at the air-liquid interface for 14 days. (a) N/Tert-1 organotypic gel (b) N/Tert-1 GFP organotypic gel (c) N/Tert-1 GLI2ΔN organotypic gel. Scale bar represents 200 µm.

5.2.3 Effect of over expression of constitutively active GLI2 in adhesion and migration assays

As organotypics models take a long time to establish we tried to find a faster and more reproducible assay, and decided to investigate GLI2ΔN invasive properties using adhesion and transwell migration assays. With these assays it is possible to test the effect of specific matrix macromolecules on cell migratory behavior and also to investigate effects of gene silencing using siRNA as well as drug treatment of cells. Collagen is the major constituent of the extracellular matrix, while fibronectin is a matrix glycoprotein involved in many cellular processes, including wound repair, cell migration and cell adhesion. For the cell adhesion assay serum-starved cells were plated in 96 wells pre-coated with either type I collagen (100 μg / ml) or fibronectin (10 μg / ml) and cultured for different amounts of time (1, 15, 30 or 45 minutes). Adherent cells were stained with crystal violet and then washed with SDS which leads to dye elution from stained cells into the supernatant. Cell adhesion can be quantified using a spectrophotometer by reading absorbance at 550 nm: the amount of dye is directly proportional to the number of cells. For the cell migration assay serum-starved cells were placed in the upper chamber of a transwell, on top of a permeable membrane pre-coated with either type I collagen (100 μg / ml) or fibronectin (10 μg / ml). After 4 hours cells that had not migrated were removed while migrated cells were fixed, stained with crystal violet and counted.

N/Tert-1 GLI2ΔN keratinocytes appear to be more adhesive compared to N/Tert-1 GFP on collagen substrate (Fig. 5.13), while this difference is not so evident when fibronectin is used as a substrate (Fig. 5.14). No difference in adhesion is seen as expected in the BSA negative control (Fig. 5.15).

In transwell assays more N/Tert-1 GFP cells migrate toward collagen compared to N/Tert-1 GLI2ΔN cells (Fig. 5.16); this is also true for migration on fibronectin substrate (Fig. 5.17). Collagen appears to be in general a more attractive substrate as about double the number of cells are able to migrate toward collagen compared to fibronectin. As we initially hyphothesised N/Tert-1 GLI2ΔN keratinocytes may be more migratory and therefore possibly less adhesive compared to N/Tert-1 GFP this was unexpected. Since GLI1 has been shown to enhanced cell–cell adhesion (Neill *et*

al., 2008), this could also potentially be true for GLI2ΔN. Another possibility is this result is due to the fact these assays offer a quick but oversimplified way to test cells invasive properties compared to organotypics models; specifically, keratinocytes are seeded on artificial plastic substrates and left in culture for a short period of time. The invasive phenotype of keratinocytes observed in organotypics models could be due to complex paracrine interactions between the keratinocytes and the surrounding mesenchyme that cannot be recreated using these assays.

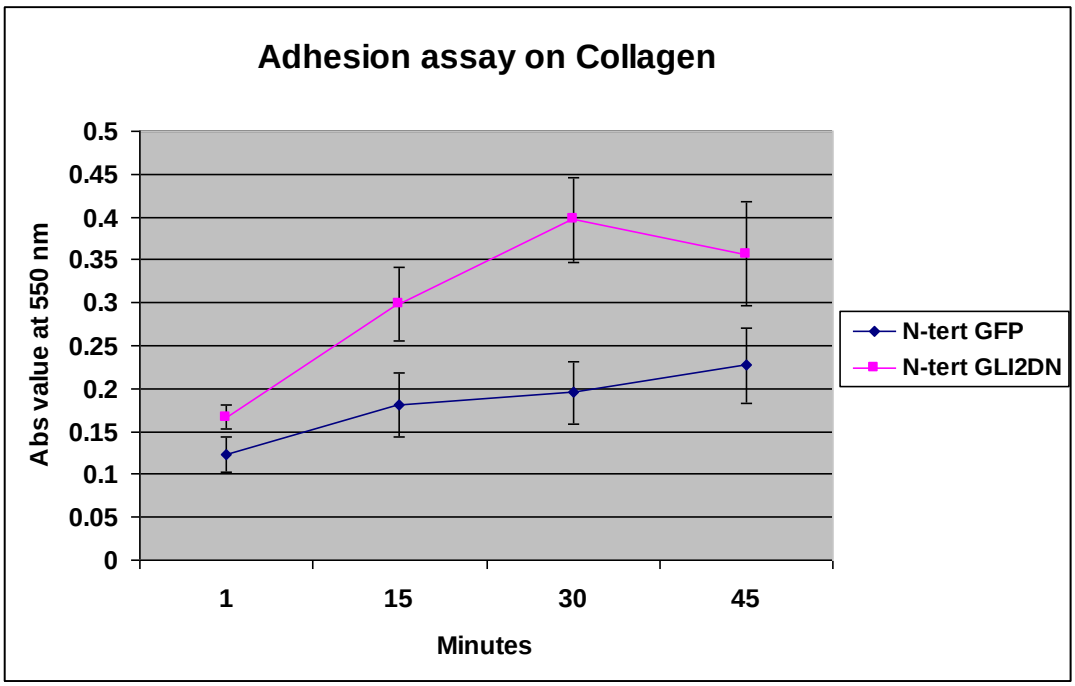

Figure 5.13: Adhesion assay of N/Tert-1 GFP and N/Tert-1 GLIΔN keratinocytes in the presence of collagen substrate

Cell adhesion assay performed on N/Tert-1 GFP and N/Tert-1 GLI2ΔN keratinocytes. 10000 cells were seeded on 96-well plates coated with collagen (100 μg / ml) and incubated for 1, 15, 30 or 45 minutes. The amount of adherent cells was determined by staining cells with crystal violet and measurements of absorbance values at 550 nm. Data are expressed as mean ± standard error, representative of four independent experiments performed in triplicate.

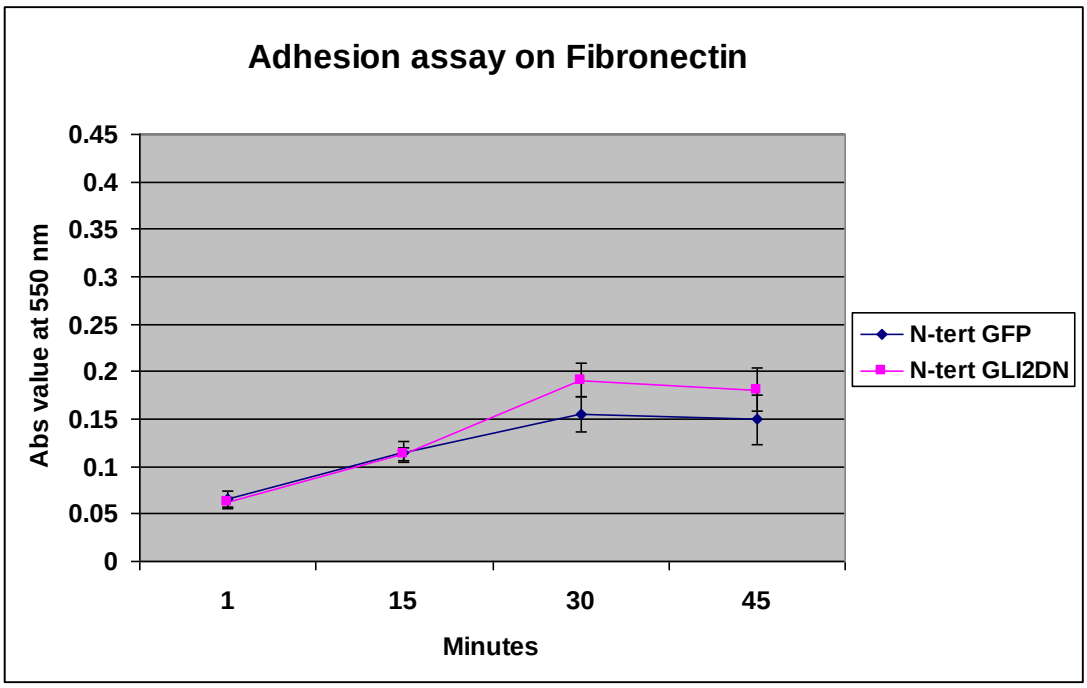

Figure 5.14: Adhesion assay of N/Tert-1 GFP and N/Tert-1 GLIΔN keratinocytes in the presence of fibronectin substrate

Cell adhesion assay performed on N/Tert-1 GFP and N/Tert-1 GLI2ΔN keratinocytes. 10000 cells were seeded on 96-well plates coated with fibronectin (10 µg / ml) and incubated for 1, 15, 30 or 45 minutes. The amount of adherent cells was determined by staining cells with crystal violet and measurements of absorbance values at 550 nm. Data are expressed as mean ± standard error, representative of four independent experiments performed in triplicate.

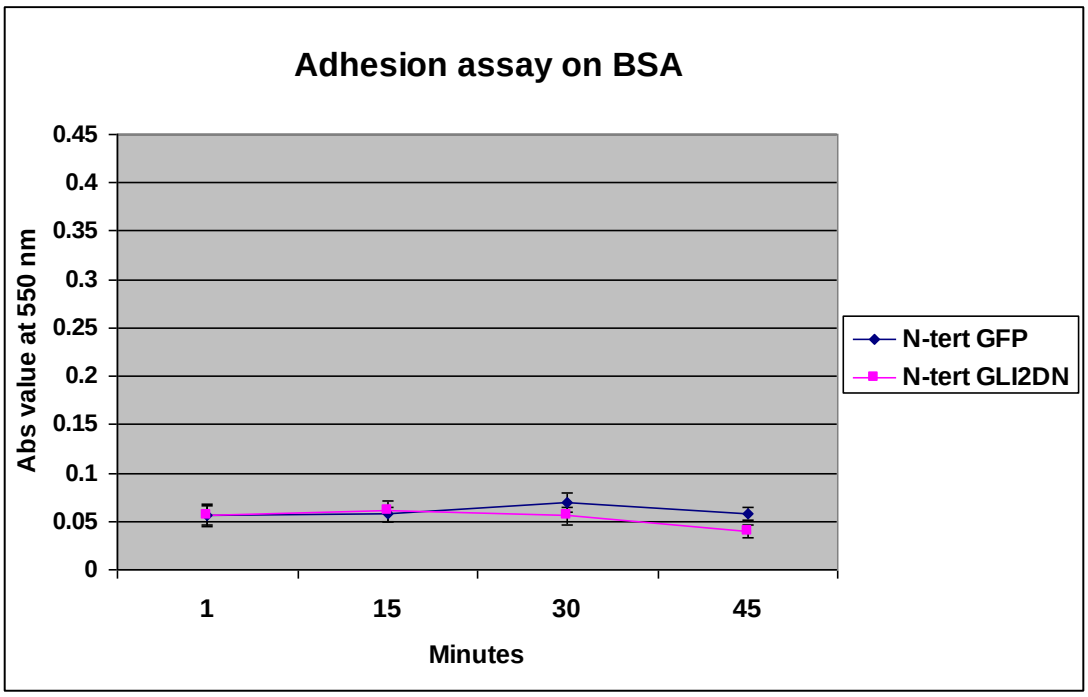

.

Figure 5.15: Adhesion assay of N/Tert-1 GFP and N/Tert-1 GLIΔN keratinocytes in the presence of BSA (negative control)

Cell adhesion assay performed on N/Tert-1 GFP and N/Tert-1 GLI2ΔN keratinocytes. 10000 cells were seeded on 96-well plates coated with BSA (Bovine Serum Albumin) as a negative control and incubated for 1, 15, 30 or 45 minutes. The amount of adherent cells was determined by staining cells with crystal violet and measurements of absorbance values at 550 nm. Data are expressed as mean ± standard error, representative of four independent experiments performed in triplicate.

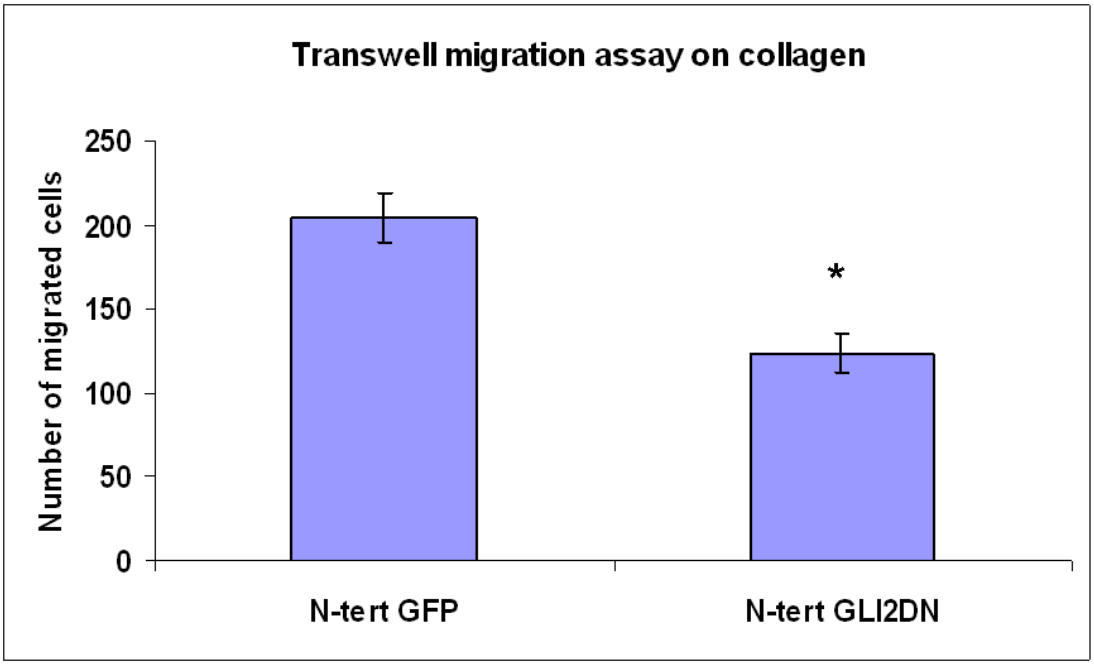

Figure 5.16: Migration assay of N/Tert-1 GFP and N/Tert-1 GLIΔN keratinocytes in the presence of collagen substrate

Transwell migration assay performed on N/Tert-1 GFP and N/Tert-1 GLI2ΔN keratinocytes. Cells were tested for their ability to migrate in a transwell assay in response to collagen (100 μg / ml) after being serum starved overnight (30000 cells per well). After 4 hours migrated cells were fixed, stained with crystal violet and counted. A statistically significative difference ($P < 0.05$) is present, with N/Tert-1 GLI2ΔN cells less migratory than N/Tert-1 GFP. Student's t-Test (two-sample assuming equal variance) was used, data are expressed as mean ± standard error, pooling together data of four independent experiments ($n = 40$).

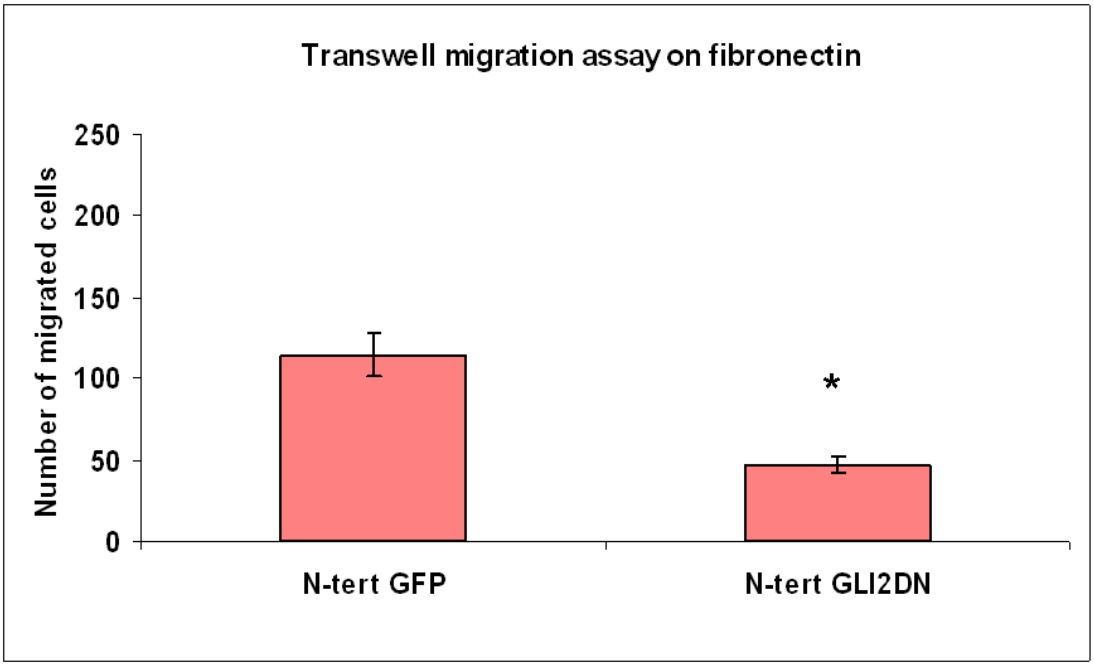

Figure 5.17: Migration assay of N/Tert-1 GFP and N/Tert-1 GLIΔN keratinocytes in the presence of fibronectin substrate

Transwell migration assay performed on N/Tert-1 GFP and N/Tert-1 GLI2ΔN keratinocytes. Cells were tested for their ability to migrate in a transwell assay in response to fibronectin (10 μg / ml) after being serum starved overnight (30000 cells per well). After 4 hours migrated cells were fixed, stained with crystal violet and counted. A statistically significative difference ($P < 0.05$) is present, with N/Tert-1 GLI2ΔN cells less migratory than N/Tert-1 GFP. Student's t-Test (two-sample assuming equal variance) was used, data are expressed as mean ± standard error, pooling together data of four independent experiments (n = 40).

5.3 Discussion

Keratinocytes are routinely grown in submerged cultures on plastic substrates; although these conditions are fine for most biochemical studies, a more physiological relevant model is represented by organotypic skin cultures, in which keratinocytes are grown on dermal equivalents in a three-dimensional state. Exposure to air permits keratinocytes differentiation and culture with dermal components (e.g. fibroblasts) allows the study of epidermal - dermal interactions which are not possible in monolayer cell culture models. Organotypics models are also a useful tool in cancer studies as the process of cell invasion is a hallmark of malignancy.

The two most widely used organotypic model of human skin are de-epidermalised dermis (DED) and collagen-matrigel gels. The DED method is based on the reconstruction of the epidermis using cadaveric skin in which keratinocytes are removed and replaced with the keratinocytes of interest; collagen or collagen-matrigel gels are mixtures of dermal components on top of which keratinocytes are seeded; both models have been used to asses invasion (Akgul *et al.*, 2005; Nystrom *et al.*, 2005; Martins *et al.*, 2009). The two major differences between these methods are fibroblasts location and the presence of an intact basement membrane. In DEDs fibroblasts are seeded on the reticular surface of the skin and lay at the bottom of the skin preparation, while in collagen-based preparations fibroblasts are embedded into the gel. In DEDs the original keratinocytes that compose the epidermis are removed but the underlying basement membrane is supposed to be kept intact: this is relevant as basement membrane breakdown is required in vivo for cells to invade into the dermis and this event is characteristic of malignant tumour behavior (Hagedorn *et al.*, 1998). In collagen gels there is not a specific barrier to be crossed for cells to invade, although different basal membrane and extracellular matrix components such as laminin, collagen IV, proteoglycans and various growth factors are present in the preparation.

Because of the cost and technical difficulties associated with the production of organotypic skin models, cell migration and invasion is also sometime studied using artificial substrates, such as Transwells. The Transwell chamber (or Boyden chamber) consists of two compartments separated by a membrane which the cells need to cross to move from the upper to the lower compartment. Cells seeded in the

top chamber migrate towards a chemotactic stimulus present in the lower chamber; the porous membrane can also be coated with Matrigel or with specific extracellular matrix components. After an appropriate incubation time the cells that have crossed the membrane can be fixed and counted. Transwell assays are often performed in conjunction with adhesion assay to investigate the adhesive properties of cells. In an adhesion assay cells are plated in wells coated with an extracellular protein of choice and incubated for different amounts of time. The amount of cells bound to the substrate is then evaluated by colorimetric measurement using crystal violet staining (see Materials and Methods).

The invasive properties of N/Tert-1 keratinocytes expressing a constitutively active form of GLI2 (GLI2ΔN) were tested using DEDs, collagen-matrigel gels and Transwell assay. Upregulation of WNT-family members proteins WNT5a, WNT7a and WNT11 has been detected by qPCR in GLI2ΔN cell line (Pantazi E. et al, unpublished data). These secreted WNT proteins had been shown to play a role in cell migration; moreover, cross talk between the Hedgehog and WNT pathways has been suggested to be implicated in BCC pathogenesis (Yang et al., 2008). For these reasons, N/Tert-1 GLI2ΔN keratinocytes behavior was tested in organotypics models.

To determine the best conditions for keratinocytes growth on DEDs the epidermis was removed by either enzymatic treatment (Dispase) or by PBS soaking; additionally, the DEDs where fed using media with or without the RM+ supplement (please see section 2.2.1.1 'DED optimisation' in Materials and Methods). Primary human keratinocytes were used in this experiment, and four different DEDs were generated. Primary keratinocytes attached to the dermis and a stratum corneum is clearly visible when epidermis removed with PBS soaking and DED is fed with RM+ media (Fig. 2.1 d). When Dispase treatment was used no cell attachment was observed (Fig. 2.1 a, b); although it cannot be excluded further optimisation of enzyme concentration or time of incubation may give better results. Dispase, a bacterial neutral protease, is widely used to separate epidermis from the dermis as it cleaves fibronectin, type IV collagen and, to a lesser extent, type I collagen (Stenn *et al.*, 1989); it is possible the condition used were too harsh and led to excessive degradation of these molecules on the dermis surface, impairing keratinocytes

attachment. The effect of growth supplement media was also tested: some of the DEDs were fed with RM+ supplemented media (see Appendix I for details), while the others were fed with the same media but lacking the RM+ supplement. The RM+ supplement contains epidermal growth factor (EGF) and cholera toxin, which had been shown to stimulate the growth of human epidermal cells in culture but also to inhibit their terminal differentiation (Jensen et al., 1985). In the absence of RM+ supplement cells were not able to grow on a DEDs; as primary keratinocytes fully differentiate when the DED was fed with RM+ containing media (Fig. 2.1 d), concerns about terminal differentiation inhibition were dismissed. We therefore decided to use PBS soaking as the method for epidermis removal and feeding with RM+ media in the following experiments with N/Tert-1 cells; primary keratinocytes were also included as a positive control, to check if the conditions of the experiment would allow for stratification.

DEDs experiments were characterised by a certain amount of variability in the results. In the first experiment N/Tert-1 GLI2ΔN keratinocytes appear less differentiated and more invasive compared to N/Tert-1 GFP and untransduced N/Tert-1 (Fig. 5.1-5.3).

The appearance of well defined clear stratum corneum is not observed when N/Tert-1 keratinocytes were used, although they display some evidence of stratification; therefore they are able to differentiate, albeit to a lesser extent compared to primary keratinocytes. N/Tert-1 cells are human epidermal keratinocytes immortalised by ectopic expression of the telomerase catalytic subunit hTERT (Dickson et al., 2000); it could he hyphothesised this alters the balance between proliferation and differentiation which is needed for the formation of a stratified epithelia.

The less differentiated phenotype of GLI2ΔN cells (Fig. 5.3) is consistent with GLI2 role in repressing genes associated with epidermal differentiation (Regl et al., 2004a) and has also been observed in collagen-based organotypic models using an inducible GLI2 Hacat cell line (Snijders A. et al., 2009).

Subsequent DEDs experiments were hindered by yeast contaminations or by lack or incomplete adhesion of keratinocytes to the dermal substrate (data not shown).

A further DEDs experiment was then performed using the optimised conditions, namely epidermis removal by PBS soaking and DED feeding with RM+ media. In order to avoid possible contamination problems these DEDs were kept in culture for a shorter amount of time (10 days compared to 18; the right time to harvest was determined by observing the appearance of the stratum corneum on the primary keratinocytes DEDs as it can be usually seen by naked eye).

Keratinocytes were able to attach to the DED surface and generated a thicker layer of epidermis compared to the one observed in the previous successful experiment (Fig. 5.5). Though no clear stratum corneum was observed, N/Tert-1 and N/Tert-1 GFP keratinocytes appear to have at least partly differentiated on DEDs (Fig. 5.5 a, b, c, d), while this feature is almost absent in the N/Tert-1 GLI2ΔN DED (Fig. 5.5 e, f). In addition to that, GLI2ΔN keratinocytes are not able to adhere properly to each other, as highlighted by the cracks and gaps present in the epidermis structure (Fig. 5.5 e, f). The cuboidal morphology of GLI2ΔN cells also suggest they may be less differentiated, which is in accordance with previously published studies (Regl et al., 2004a); this seems to confirmed by the fact markers of epithelial differentiation appear to be lacking in the N/Tert-1 GLI2ΔN DED compared to N/Tert-1 and N/Tert-1 GFP DEDs (Fig 5.7 – 5.10).

Although no overt invasion into the underlying dermis was seen in the GLI2ΔN keratinocytes DEDs (contrary to what was observed in the previous experiment), it cannot be excluded GLI2ΔN may have invasive potential. No difference in E-cadherin staining was observed in N/Tert-1 GLI2ΔN DED compared to N/Tert-1 and N/Tert-1 GFP DEDs (Fig 5.11), which seems to argue against this hypothesis. Since GLI1 has been shown to enhanced cell–cell adhesion (Neill et al., 2008), this could also potentially be true for GLI2ΔN. Analysis of more invasion more markers will be required to ascern the impact of this event on GLI2ΔN cells invasive potential, as well as further confirmation of the invasive phenotype in future DEDs experiments.

In the paper published by Snijders et al., collagen organotypics models of Hacat GLI2ΔN keratinocytes were also shown to display an altered basement zone with abnormal expression of adhesion proteins, like integrin β4, which normally anchor the epithelia to the underlying dermis. To investigate this possibility, DEDs sections

could be stained for markers of the basement membrane. Keratinocytes are linked to each other via the desmosomes and basal keratinocytes are anchored to the basement membrane and extracellular matrix through hemidesmosomes. In hemidesmosomes the α6β4 integrin receptor expressed on basal keratinocytes interacts with laminin 5 and fibronectin present in the basement membrane. During malignant tumour progression cells begin to invade the surrounding tissues; keratinocytes acquire the ability to cross the basement membrane barrier by promoting extracellular matrix degradation and activating cell motility mechanisms (Liotta and Kohn, 2001). Degradation of basement membranes components is achieved by secretion of matrix metalloproteinase (MMP), while extracellular-matrix signals cause cytoskeletal changes that favour migratory movement. Abnormal distribution of collagen type IV and collagen type VII, primarily expressed in the basement zone, or an aberrant pattern of integrin and laminin expression would support the notion of GLI2ΔN keratinocytes more invasive capacity.

To further investigate invasion I also used a collagen-matrigel assay. In a preliminary experiment, GLI2ΔN keratinocytes appeared to be more invasive compared to empty vector and untransduced controls in collagen-matrigel gel (Fig. 5.12), in line with data previously generated in the lab (Bahta A. et al., unpublished results) and recently confirmed by Miss Eleni Pantazi (E. Pantazi et al., unpublished results).

The adhesive and migratory properties of N/Tert-1 GLI2ΔN were also tested using adhesion and Transwell assays, respectively. Collagen and fibronectin were chosen as ligands for coating as interaction between these extracellular matrix components and integrins present on the cell surface is known to regulate adhesion between the basal keratinocytes and the dermis; these interactions are altered during cancer progression resulting in invasion into the underlying dermis.

N/Tert-1 GLI2ΔN keratinocytes seem to be more adhesive compared to N/Tert-1 GFP on collagen substrate (Fig. 5.13), while this difference is not so evident on fibronectin (Fig. 5.14). No difference in adhesion is seen as expected in the BSA negative control (Fig. 5.15). On collagen substrate, the difference in adhesion between GLI2ΔN and GFP control cells is most evident after 30 minutes, where GLI2ΔN keratinocytes appear to be roughly 50% more adhesive compared to GFP. At 45 minutes this difference in adhesion is reduced; to determine if enhanced GLI2

adhesion is a transient effect it would be useful to repeat the experiment including also later timepoints.

For Transwell assay, keratinocytes were serum-starved for 24 hours and then seeded in the upper chamber of Transwells whose porous membranes had been previously coated with either collagen or fibronectin; the lower chamber was filled with serum-containing media as a chemoattractant. This system investigates the ability of cells to migrate toward serum and helps determine if a specific stimulus (e.g. collagen or fibronectin) facilitate this process. This migration assay differs from an invasion assay where the porous membrane is coated with Matrigel, assessing the ability of cells to degrade Matrigel components in order to access into the lower chamber. Since only a minor fraction of the cells seeded were able to migrate into the lower chamber in migration assays, invasion assays were not performed because they are characterised by more stringent conditions.

In transwell migration N/Tert-1 GLI2ΔN keratinocytes appear less migratory than N/Tert-1 GFP on both collagen and fibronectin substrate (Fig. 5.16 - 5.17). Specifically, N/Tert-1 GLI2ΔN keratinocytes are about 40% less migratory than N/Tert-1 GFP on collagen and about 60% less migratory on fibronectin. Collagen seems to be a more attractive substrate as about double the number of keratinocytes are able to migrate toward collagen compared to fibronectin.

In the initial hypothesis, N/Tert-1 GLI2ΔN keratinocytes were postulated to be more migratory and consequently less adhesive compared to N/Tert-1 GFP: therefore the results of adhesive and Transwell migration assays were unexpected. However, it should be noted these assays are conducted on a short timescale (45 minutes for adhesion and 4 hours for Transwells) compared to organotypics models, and they rely on artificial plastic-based substrates. These assays offer a quick but possibly oversimplified way to test cells migratory behavior compared to organotypics models. The invasive phenotype of keratinocytes observed in organotypics models (should it be confirmed by staining with components of the basement membrane) could be due to complex paracrine interactions between the keratinocytes and the surrounding mesenchyme that cannot be recreated using these assays. In conclusion, judging by their morphology and by staining with differentiation markers antibodies, GLI2ΔN keratinocytes appear de-differentiated compared to controls; the invasive

phenotype of GLI2ΔN keratinocytes, on the other hand, is less reproducible. Both observations will require a more in-depth analysis for validation. DEDs and collagen-matrigel organotypics sections could be stained for markers of cell invasion such as MMPs, and the expression of collagen type IV and collagen type VII could be analysed to validate the hypothesis of GLI2ΔN keratinocytes more invasive capacity. Preliminary experiments with differentiation markers antibodies suggest GLI2ΔN keratinocytes are impaired in their ability to differentiate.

Organotypic skin cultures allow the study of differentiation, cell-matrix interactions and keratinocyte-fibroblast paracrine communications; all of these processes are relevant for cancer studies. Basal cell carcinoma are often composed of a large amount of undifferentiated cells (Miller, 1995) and GLI2 overexpression has been shown to repress genes involved in epidermal differentiation (Regl et al., 2004a), which appears to be confirmed from the organotypic experiments described in this thesis. Invasion is a hallmark of malignancy, and organotypics models could be useful in understanding the molecular mechanisms that are responsible for the conversion of BCCs, which are usually indolent tumours, into metastatic ones. Should the invasive phenotype of GLI2 keratinocytes be confirmed, it could be analysed if cell invasion is dependent on WNT pathway activation by treating the organotypics with WNT pathway inhibitors (e.g. Dkk1, which inhibits canonical WNT pathway, or sFRPs which inhibit both WNT canonical and non-canonical pathways). Alternatively, siRNA technology could be employed to silence specific WNTs in GLI2 keratinocytes before they are seeded onto the organotypic rafts, to see if this is sufficient to abolish the invasive phenotype. The results of these experiments could lead to the use of antagonists of WNT pathways as a treatment for BCCs. GLI1 expression has been detected by immunofluorescence in a number of BCC samples using the GLI1 H-300 antibody (see section 4.2.2) and also in BCC fibroblasts derived from tumour explants (J. Elliott et al., unpublished results). Although it is not yet clear whether GLI1 activation in the stroma occurs via a canonical or non-canonical mechanism, it could be hyphothesised this event has an influence on the tumour development. GLI1 overexpressing fibroblasts could be compared to normal dermal fibroblasts in organotypic models to see if mesenchymal GLI1 expression promotes keratinocytes invasion into the dermis (e.g. via

modification of the extracellular matrix or by secreting factors that promotes tumor growth).

Chapter 6

6 Discussion and future research

The transcription factors GLI1 and GLI2 have been proposed to be part of a positive feedback mechanism in BCC, although the exact sequence of Gli gene activation is not clear (Regl et al., 2002). It should be noted the complete GLI2 mRNA sequence was only discovered in 2005 (Roessler et al., 2005) and these experiments rely on an amino-terminal deleted version of GLI2 (GLI2ΔN) which has been shown to be a more potent transcriptional activator than full-length GLI2. Based upon the kinetics of transcript expression compared to the induction of PTCH1 mRNA, GLI1 is thought to be a direct transcriptional target of GLI2ΔN in human keratinocytes; moreover GLI2ΔN binds to the human GLI1 promoter (Bonifas *et al.*, 2001; Ikram *et al.*, 2004). On the other hand, GLI2 appears to be an indirect target of GLI1 (Regl et al., 2002). In contrast to these studies based on mRNA levels, previous work in the lab and my preliminary experiments suggest that endogenous GLI2 protein is suppressed by ectopic GLI1 in both prostate cells and immortalised keratinocytes. Moreover, another project in the group (M. Rahman et al., unpublished results) has shown that PTCH1 suppression in NEB1 human keratinocytes leads to an increase of GLI1 but not GLI2 mRNA

In order to address the biological relevance of these results, expression of GLI1 and GLI2 was analysed ex-vivo by immunostaining of normal human skin and Basal Cell Carcinoma samples. Immunohistochemical analysis of BCCs revealed areas of co-expression of GLI factors as well as areas where one protein appears to be more abundant than the other. A great deal of heterogeneity in the expression pattern of GLI1 and GLI2 in human BCCs was observed, which questions the presence of a positive GLI1-GLI2 feedback loop. This also seems to question the hypothesis that BCCs have a uniform increase in epithelial GLI expression as a result of ligand-independent HH signalling and other factors should be taking into account, including the recently described negative feedback loop of PTCH1 on GLI1 (Rahnama *et al.*, 2006) and the role played by non-canonical activation of GLI factors such as TGFβ and activated K-Ras (Dennler et al., 2007; Dennler et al., 2009; (Nolan-Stevaux *et al.*, 2009).

Rahnama et al. co-transfection experiments in HEK-293 cells have shown how GLI1 activation of a luciferase reporter construct is inhibited by PTCH1: this effect is observed with amounts of PTCH1 at least three times higher than that of GLI1. GLI1 expression is also inhibited by PTCH1 in transfection experiments using 3T3 cells: this effect is observed even in the presence of cyclopamine and moreover PTCH1 C-terminal region (proposed to play a role in HH/SMO signalling) is dispensable for this inhibition (Rahnama *et al.*, 2006). It can therefore be hypothesized mutated PTCH1 has lost its ability to repress SMO (resulting in GLI factor activation) but has retained its SMO-independent ability to inhibit GLI1.

A possible model to describe the complex network of interactions that governs GLI expression (both canonical and non-canonical) in vivo and how this could be modeled in vitro is outlined in Figure 6.1. For simplicity, it is assumed all positive and negative inputs that regulate GLI expression assume the same importance; it is however likely that some may have stronger effects than others.

When PTCH1 is mutated in vivo (Fig. 6.1 a), GLI1 is positively upregulated via SMO, the GLI2 positive feedback and potentially non-canonical signalling (e.g. via TGFβ or KRAS) and negatively regulated by PTCH1; similarly, GLI2 is upregulated via SMO and non-canonical signalling and downregulated by GLI1.

On the other hand, when PTCH1 is wild-type in vivo (Fig. 6.1 c), GLI1 is upregulated only by GLI2 and non-canonical signalling and downregulated by PTCH1; GLI2 is activated via non-canonical signalling and downregulated by GLI1. This could help explain the different intensities and heterogeneity observed in immunohistochemistry staining for GLI factors (see Chapter 4), as they would be the sum of canonical and non-canonical induction if PTCH1 is mutated but only due to non-canonical signalling if PTCH1 were wild-type. To further explore this hypothesis in future studies it would be useful to determine PTCH1 mutational status of the BCC before immunohistochemical analysis to see if there is a correlation between PTCH1 status and GLI proteins expression.

GLI1 overexpression in N/Tert-1 human keratinocytes has been used as an in vitro model of BCCs (Fig. 6.1 b); it should be noted in this system levels of GLI1 may be significantly different from physiological levels. From the literature it is known how transfection of 3T3 cells with ectopic GLI1 induces endogenous expression of the

GLI1 mRNA, though this event is inhibited when GLI1 is co-transfected with PTCH1. This highlights how PTCH1 could also affect GLI1 endogenous gene expression (Rahnama *et al.*, 2006). Therefore, it is conceivable ectopic GLI1 may lead to a significative increase of PTCH1 levels that in turn would reduce endogenous GLI1 expression.

Ectopic GLI2ΔN overexpression in vitro (Fig. 6.1 d) may also suppress endogenous GLI1 due to high levels of PTCH1 induction but this is counteracted by the fact that GLI2ΔN directly activates GLI1; it remains to be determined if the putative new GLI2 isoforms / degradation products (see Chapter 3) are also able to induce GLI1. To explore this possibility, they would need to be first isolated, cloned and then overexpressed in human keratinocytes.

A more relevant model of BCCs development could be the NEB1 PTCH1 knockdown cell line which has been recently created in the lab by Mr Muhammad Rahman (Fig. 6.1 e). In this system, GLI1 mRNA expression is increased but this is not associated with an increase of GLI2 expression. This further supports the hypothesis that GLI2 may be activated by HH-independent mechanisms in BCC. In addition, the role of SMO in regulating GLI1 expression is unclear and currently under investigation by Mr Muhammad Rahman.

Regulation of GLI factor expression appears to be more complex than previously thought. Laser Capture Microdissection technology could be used to assess the mRNA levels of GLI and their isoforms in BCCs samples. To help dissect the contribution of canonical vs. non-canonical signalling on GLI factors expression PTCH1 knockdown cells could be exposed to TGFβ or treated with SMO inhibitors.

GLI1 staining intensity appeared sometime reduced in the BCCs compared to the overlying epidermis; in some samples its intensity is also reduced in palisading cells compared to the centre of the tumour (see Chapter 4). Although this could be surprising as GLI deregulation is commonly associated with malignancy, a reduction in the level of GLI1 may be necessary to overcome GLI-promoted cell to cell adhesion and the acquisition of invasive properties (Neill *et al.*, 2008). Furthermore, GLI2-responsive genes downregulation appears to be required for invasion of Hacat cells in a skin organotypic model (Snijders et al., 2009). Also stemming from this observation it would be interesting to confirm the invasive phenotype of N/Tert-1

GLI2ΔN keratinocytes in organotypics models (see Chapter 5) and see if there is a reduction in the levels of GLI2 in invading cells.

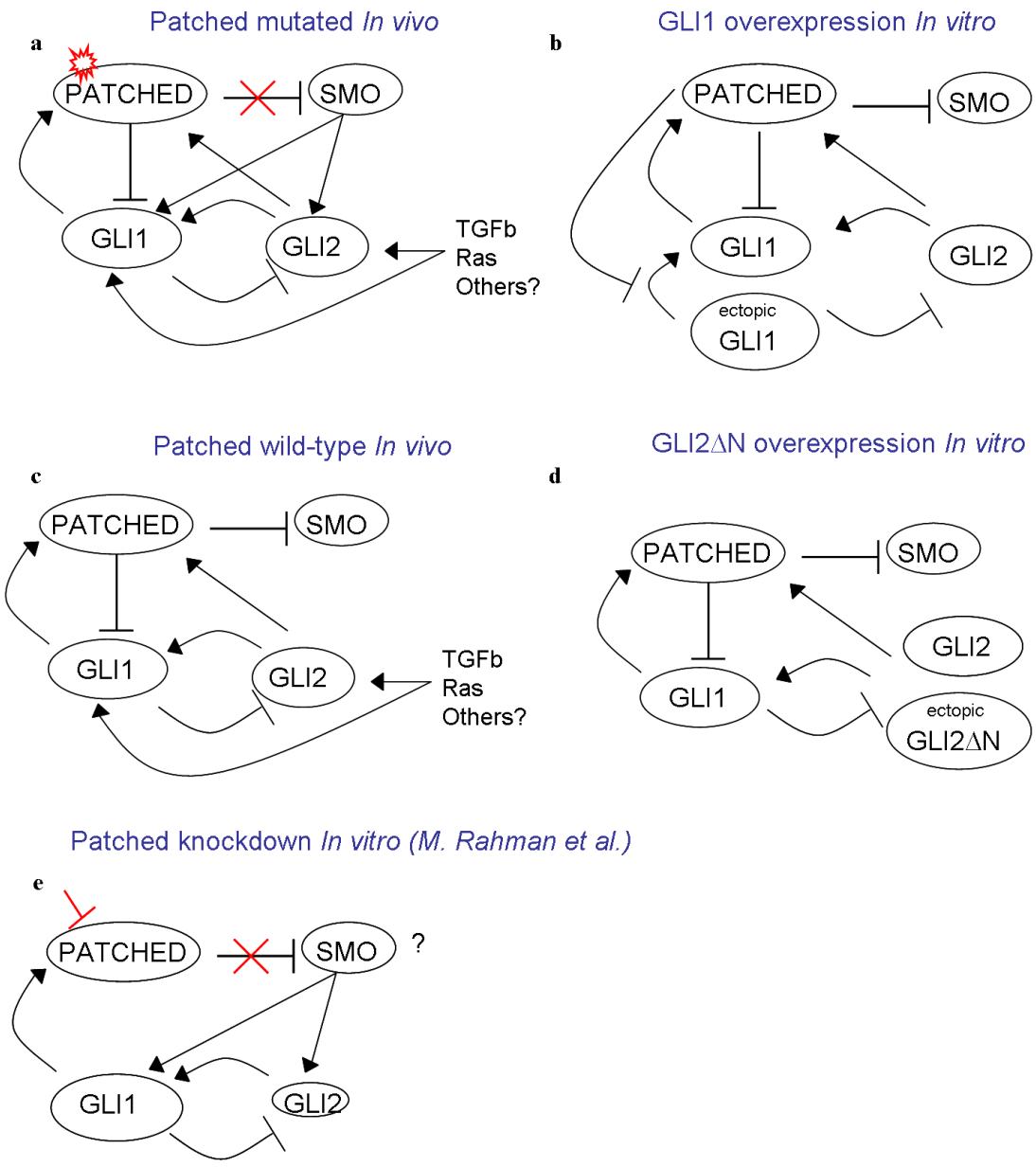

Figure 6.1: Diagram illustrating the potential complex network of interactions that governs GLI expression (both canonical and non-canonical) in vivo and in vitro

- please see text for details

Ectopic overexpression of GLI1 or GLI2ΔN in mouse models result in BCC-like tumour formation, while in the experiment I performed levels of GLI in human BCCs appear heterogeneous seem to bear no correlation with tumour subtype and aggressiveness. This could be due to the differences between human and mice tumorigenesis processes; moreover, overexpression of GLI1 or GLI2ΔN could significantly alter the balance and feedback loops previously described (Fig. 6.1).

The majority of sporadic BCCs display loss of heterozigosity for PTCH1 and this historically suggested its inactivation is an important step in BCC formation (Gailani et al., 1996a). However, an extensive analysis of PTCH1 mutation status in correlation with GLI levels in BCCs has not yet been reported. Different PTCH1 mutations have been described, which may affect one portion of the protein but leave the rest intact. A role for PTCH1 in cell cycle control by means of interaction with cyclin B has been reported (Barnes *et al.*, 2001); moreover, PTCH1 has been recently shown to reduce GLI1 levels, and this function appears not to involve HHG signalling (Rahnama *et al.*, 2006). It is therefore conceivable that PTCH1 could exert some of its activity even if mutated, in addition to the fact that in case of PTCH1 heterozygosity one allele would be fully functional.

Different mouse models of BCCs have been proposed, although it is still debated how closely these mice tumours can mimic their human counterparts. PTCH1 knockout mice (Ptch1 $^{-/-}$) are not viable; PTCH1 (Ptch1 $^{+/-}$) heterozygous mice develop tumours similar to human trichoblastomas, and only if irradiated with U.V. or ionizing radiation develop tumours histologically similar to BCCs (Aszterbaum *et al.*, 1999; Mancuso *et al.*, 2004); the issue of how these radiation can influence tumour development has never been fully addressed. Ectopic expression of GLI1 or GLI2ΔN in mouse skin result in BCC-like tumour formation, though in this case the physiological relevance of the high levels of GLI that are induced should be taken into account, as well as the differences between the human and the mice tumorigenesis processes. As discussed above, overexpression of GLI1 or GLI2ΔN could significantly perturb feedback loops (Fig. 6.1). Moreover, only a small fraction of human BCCs is caused by gain-of-function mutation in GLI factors (Khavari, 2006). Anti-SMO inhibitors appear to be effective in reducing mouse BCC tumour growth but have limited success in humans (Williams *et al.*, 2003; Tang *et al.*, 2011).

This may be due to the fact that in mouse BCC-like tumours the canonical HH signalling may be prevalent and series of complex positive and negative loops present in human tumours may be lost.

In summary, this project has shown that GLI regulation and expression are more complex than previous studies have suggested and that further research is necessary in order to provide better therapies for the treatment of BCCs and possibly other cancers associated with HH pathway deregulation.

7 References

Aberger, F., and Frischauf, A.-M. (2006). GLI genes and their targets in epidermal development and disease. In: Molecular Biology Intelligence Unit, 74-85.

Aberle, H., Bauer, A., Stappert, J., Kispert, A., and Kemler, R. (1997). beta-catenin is a target for the ubiquitin-proteasome pathway. Embo Journal *16*, 3797-3804.

Akgul, B., Garcia-Escudero, R., Ghali, L., Pfister, H.J., Fuchs, P.G., Navsaria, H., and Storey, A. (2005). The E7 protein of cutaneous human papillomavirus type 8 causes invasion of human keratinocytes into the dermis in organotypic cultures of skin. Cancer Research *65*, 2216-2223.

Alcedo, J., Ayzenzon, M., VonOhlen, T., Noll, M., and Hooper, J.E. (1996). The Drosophila smoothened gene encodes a seven-pass membrane protein, a putative receptor for the hedgehog signal. Cell *86*, 221-232.

Alonso, L., and Fuchs, E. (2003). Stem cells of the skin epithelium. Proceedings of the National Academy of Sciences of the United States of America *100*, 11830-11835.

Altaba, A.R.I. (1999). Gli proteins encode context-dependent positive and negative functions: implications for development and disease. Development *126*, 3205-3216.

Annes, J.P., Munger, J.S., and Rifkin, D.B. (2003). Making sense of latent TGF beta activation. Journal of Cell Science *116*, 217-224.

Asada, M., Schaart, F.M., Detmar, M., Mischke, D., Dealmeida, H.L., Gollnick, H., and Orfanos, C.E. (1992). GROWTH-CHARACTERISTICS AND DIFFERENTIATION OF BASAL-CELL CARCINOMA INVITRO IMMUNOHISTOCHEMICAL, GEL-ELECTROPHORETIC, AND ULTRASTRUCTURAL ANALYSIS. Journal of Investigative Dermatology *99*, 474-481.

Aszterbaum, M., Epstein, J., Oro, A., Douglas, V., LeBoit, P.E., Scott, M.P., and Epstein, E.H. (1999). Ultraviolet and ionizing radiation enhance the growth of BCCs and trichoblastomas in patched heterozygous knockout mice. Nature Medicine *5*, 1285-1291.

Aszterbaum, M., Rothman, A., Johnson, R.L., Fisher, M., Xie, J.W., Bonifas, J.M., Zhang, X.L., Scott, M.P., and Epstein, E.H. (1998). Identification of mutations in the human PATCHED gene in sporadic basal cell carcinomas and in patients with the basal cell nevus syndrome. Journal of Investigative Dermatology *110*, 885-888.

Auger, F.A., Rouabhia, M., Goulet, F., Berthod, F., Moulin, V., and Germain, L. (1998). Tissue-engineered human skin substitutes developed from collagen-populated hydrated gels: clinical and fundamental applications. Medical & Biological Engineering & Computing *36*, 801-812.

Aza-Blanc, P., Lin, H.Y., Altaba, A.R.I., and Kornberg, T.B. (2000). Expression of the vertebrate Gli proteins in Drosophila reveals a distribution of activator and repressor activities. Development *127*, 4293-4301.

Bai, C.Y.B., and Joyner, A.L. (2001). Gli1 can rescue the in vivo function of Gli2. Development *128*, 5161-5172.

Bailey, J.M., Mohr, A.M., and Hollingsworth, M.A. (2009). Sonic hedgehog paracrine signaling regulates metastasis and lymphangiogenesis in pancreatic cancer. Oncogene *28*, 3513-3525.

Barnes, E.A., Kong, M., Ollendorff, V., and Donoghue, D.J. (2001). Patched1 interacts with cyclin B1 to regulate cell cycle progression. Embo Journal *20*, 2214-2223.

Behrens, J., vonKries, J.P., Kuhl, M., Bruhn, L., Wedlich, D., Grosschedl, R., and Birchmeier, W. (1996). Functional interaction of beta-catenin with the transcription factor LEF-1. Nature *382*, 638-642.

Belloni, E., Muenke, M., Roessler, E., Traverso, G., SiegelBartelt, J., Frumkin, A., Mitchell, H.F., DonisKeller, H., Helms, C., Hing, A.V., Heng, H.H.Q., Koop, B., Martindale, D., Rommens, J.M., Tsui, L.C., and Scherer, S.W. (1996). Identification of Sonic hedgehog as a candidate gene responsible for holoprosencephaly. Nature Genetics *14*, 353-356.

Berman, D.M., Karhadkar, S.S., Maitra, A., de Oca, R.M., Gerstenblith, M.R., Briggs, K., Parker, A.R., Shimada, Y., Eshleman, J.R., Watkins, D.N., and Beachy, P.A. (2003). Widespread requirement for Hedgehog ligand stimulation in growth of digestive tract tumours. Nature *425*, 846-851.

Bhatia, N., Thiyagarajan, S., Elcheva, I., Saleem, M., Dlugosz, A., Mukhtar, H., and Spiegelman, V.S. (2006). Gli2 is targeted for ubiquitination and degradation by beta-TrCP ubiquitin ligase. Journal of Biological Chemistry *281*, 19320-19326.

Bhowmick, N.A., Neilson, E.G., and Moses, H.L. (2004). Stromal fibroblasts in cancer initiation and progression. Nature *432*, 332-337.

Bishop, C.L., Bergin, A.-M.H., Fessart, D., Borgdorff, V., Hatzimasoura, E., Garbe, J.C., Stampfer, M.R., Koh, J., and Beach, D.H. (2010). Primary Cilium-Dependent and -Independent Hedgehog Signaling Inhibits p16(INK4A). Molecular Cell *40*, 533-547.

Bitgood, M.J., Shen, L.Y., and McMahon, A.P. (1996). Sertoli cell signaling by Desert hedgehog regulates the male germline. Current Biology *6*, 298-304.

Blanpain, C., and Fuchs, E. (2006). Epidermal stem cells of the skin. In: Annual Review of Cell and Developmental Biology, vol. 22, 339-373.

Bonifas, J.M., Pennypacker, S., Chuang, P.T., McMahon, A.P., Williams, M., Rosenthal, A., de Sauvage, F.J., and Epstein, E.H. (2001). Activation of expression of hedgehog target genes in basal cell carcinomas. Journal of Investigative Dermatology *116*, 739-742.

Botchkarev, V.A., and Paus, R. (2003). Molecular biology of hair morphogenesis: Development and cycling. Journal of Experimental Zoology Part B-Molecular and Developmental Evolution *298B*, 164-180.

Boukamp, P., Petrussevska, R.T., Breitkreutz, D., Hornung, J., Markham, A., and Fusenig, N.E. (1988). NORMAL KERATINIZATION IN A SPONTANEOUSLY IMMORTALIZED ANEUPLOID HUMAN KERATINOCYTE CELL-LINE. Journal of Cell Biology *106*, 761-771.

Brewster, R., Mullor, J.L., and Altaba, A.R. (2000). Gli2 functions in FGF signaling during antero-posterior patterning. Development *127*, 4395-4405.

Brownell, I., Guevara, E., Bai, C.B., Loomis, C.A., and Joyner, A.L. (2011). Nerve-Derived Sonic Hedgehog Defines a Niche for Hair Follicle Stem Cells Capable of Becoming Epidermal Stem Cells. Cell Stem Cell *8*, 552-565.

Bumcrot, D., Manoharan, M., Koteliansky, V., and Sah, D.W.Y. (2006). RNAi therapeutics: a potential new class of pharmaceutical drugs. Nature Chemical Biology *2*, 711-719.

Ceilley, R.I., and Del Rosso, J.Q. (2006). Current modalities and new advances in the treatment of basal cell carcinoma. Int. J. Dermatol. *45*, 489-498.

Cerutti, H., and Casas-Mollano, J.A. (2006). On the origin and functions of RNA-mediated silencing: from protists to man. Current Genetics *50*, 81-99.

Chen, J.K., Taipale, J., Young, K.E., Maiti, T., and Beachy, P.A. (2002). Small molecule modulation of Smoothened activity. Proceedings of the National Academy of Sciences of the United States of America *99*, 14071-14076.

Chiang, C., Swan, R.Z., Grachtchouk, M., Bolinger, M., Ying, L.T.T., Robertson, E.K., Cooper, M.K., Gaffield, W., Westphal, H., Beachy, P.A., and Dlugosz, A.A. (1999). Essential role for Sonic hedgehog during hair follicle morphogenesis. Developmental Biology *205*, 1-9.

Chiang, C., Ying, L.T.T., Lee, E., Young, K.E., Corden, J.L., Westphal, H., and Beachy, P.A. (1996). Cyclopia and defective axial patterning in mice lacking Sonic hedgehog gene function. Nature *383*, 407-413.

Chien, A.J., Conrad, W.H., and Moon, R.T. (2009). A Wnt Survival Guide: From Flies to Human Disease. Journal of Investigative Dermatology *129*, 1614-1627.

Clevers, H. (2006). Wnt/beta-catenin signaling in development and disease. Cell *127*, 469-480.

Cooper, M.K., Porter, J.A., Young, K.E., and Beachy, P.A. (1998). Teratogen-mediated inhibition of target tissue response to Shh signaling. Science *280*, 1603-1607.

Crowson, A.N. (2006). Basal cell carcinoma: biology, morphology and clinical implications. Modern Pathology *19*, S127-S147.

Cui, W., Fowlis, D.J., Bryson, S., Duffie, E., Ireland, H., Balmain, A., and Akhurst, R.J. (1996). TGF beta 1 inhibits the formation of benign skin tumors, but enhances progression to invasive spindle carcinomas in transgenic mice. Cell *86*, 531-542.

Dahmane, N., Lee, J., Robins, P., Heller, P., and Altaba, A.R.I. (1997). Activation of the transcription factor Gli1 and the Sonic hedgehog signalling pathway in skin tumours. Nature *389*, 876-881.

Dahmane, N., Sanchez, P., Gitton, Y., Palma, V., Sun, T., Beyna, M., Weiner, H., and Altaba, A.R.I. (2001). The Sonic Hedgehog-Gli pathway regulates dorsal brain growth and tumorigenesis. Development *128*, 5201-5212.

Datto, M.B., Li, Y., Panus, J.F., Howe, D.J., Xiong, Y., and Wang, X.F. (1995). TRANSFORMING GROWTH-FACTOR-BETA INDUCES THE CYCLIN-DEPENDENT KINASE INHIBITOR P21 THROUGH A P53-INDEPENDENT MECHANISM. Proceedings of the National Academy of Sciences of the United States of America *92*, 5545-5549.

Daya-Grosjean, L., and Couve-Privat, S. (2005). Sonic hedgehog signaling in basal cell carcinomas. Cancer Letters *225*, 181-192.

Denef, N., Neubuser, D., Perez, L., and Cohen, S.M. (2000). Hedgehog induces opposite changes in turnover and subcellular localization of patched and smoothened. Cell *102*, 521-531.

Dennler, S., Andre, J., Alexaki, I., Li, A., Magnaldo, T., ten Dijke, P., Wang, X.J., Verrecchia, F., and Mauviel, A. (2007). Induction of sonic hedgehog mediators by transforming growth factor-beta: Smad3-dependent activation of Gli2 and Gli1 expression in vitro and in vivo. Cancer Research *67*, 6981-6986.

Dennler, S., Andre, J., Verrecchia, F., and Mauviel, A. (2009). Cloning of the Human GLI2 Promoter TRANSCRIPTIONAL ACTIVATION BY TRANSFORMING GROWTH FACTOR-beta VIA SMAD3/beta-CATENIN COOPERATION. Journal of Biological Chemistry *284*, 31523-31531.

Derynck, R., Jarrett, J.A., Chen, E.Y., Eaton, D.H., Bell, J.R., Assoian, R.K., Roberts, A.B., Sporn, M.B., and Goeddel, D.V. (1985). HUMAN TRANSFORMING GROWTH FACTOR-BETA COMPLEMENTARY-DNA SEQUENCE AND EXPRESSION IN NORMAL AND TRANSFORMED-CELLS. Nature *316*, 701-705.

di Magliano, M.P., and Hebrok, M. (2003). Hedgehog signalling in cancer formation and maintenance. Nature Reviews Cancer *3*, 903-911.

Dickson, M.A., Hahn, W.C., Ino, Y., Ronfard, V., Wu, J.Y., Weinberg, R.A., Louis, D.N., Li, F.P., and Rheinwald, J.G. (2000). Human keratinocytes that express hTERT and also bypass a p16(INK4a)-enforced mechanism that limits life span become immortal yet retain normal growth and differentiation characteristics. Molecular and Cellular Biology *20*, 1436-1447.

Ding, Q., Motoyama, J., Gasca, S., Mo, R., Sasaki, H., Rossant, J., and Hui, C.C. (1998). Diminished Sonic hedgehog signaling and lack of floor plate differentiation in Gli2 mutant mice. Development *125*, 2533-2543.

Duman-Scheel, M., Weng, L., Xin, S.J., and Du, W. (2002). Hedgehog regulates cell growth and proliferation by inducing cyclin D and cyclin E. Nature *417*, 299-304.

Echelard, Y., Epstein, D.J., Stjacques, B., Shen, L., Mohler, J., McMahon, J.A., and McMahon, A.P. (1993). SONIC-HEDGEHOG, A MEMBER OF A FAMILY OF PUTATIVE SIGNALING MOLECULES, IS IMPLICATED IN THE REGULATION OF CNS POLARITY. Cell *75*, 1417-1430.

Freinkel, R.K., and Woodley, D. (2001). The biology of the skin. Parthenon Publishing Group: New York ; London.

Furue, M., Kato, M., Nakamura, K., Nashiro, K., Kikuchi, K., Okochi, H., Miyazono, K., and Tamaki, K. (1997). Dysregulated expression of transforming growth factor beta and its type-I and type-II receptors in basal-cell carcinoma. International Journal of Cancer *71*, 505-509.

Gailani, M.R., and Bale, A.E. (1997). Developmental genes and cancer: Role of patched in basal cell carcinoma of the skin. Journal of the National Cancer Institute *89*, 1103-1109.

Gailani, M.R., Leffell, D.J., Ziegler, A., Gross, E.G., Brash, D.E., and Bale, A.E. (1996a). Relationship between sunlight exposure and a key genetic alteration in basal cell carcinoma. Journal of the National Cancer Institute *88*, 349-354.

Gailani, M.R., StahleBackdahl, M., Leffell, D.J., Glynn, M., Zaphiropoulos, P.G., Pressman, C., Unden, A.B., Dean, M., Brash, D.E., Bale, A.E., and Toftgard, R. (1996b). The role of the human homologue of Drosophila patched in sporadic basal cell carcinomas. Nature Genetics *14*, 78-81.

Gambichler, T., Skrygan, M., Kaczmarczyk, J.M., Hyun, J., Tomi, N.S., Sommer, A., Bechara, F.G., Boms, S., Brockmeyer, N.B., Altmeyer, P., and Kreuter, A. (2007). Increased expression of TGF-beta/smad proteins in basal cell carcinoma. European Journal of Medical Research *12*, 509-514.

Gao, Z.H., Seeling, J.M., Hill, V., Yochum, A., and Virshup, D.M. (2002). Casein kinase I phosphorylates and destabilizes the beta-catenin degradation complex.

Proceedings of the National Academy of Sciences of the United States of America *99*, 1182-1187.

Gat, U., DasGupta, R., Degenstein, L., and Fuchs, E. (1998). De novo hair follicle morphogenesis and hair tumors in mice expressing a truncated beta-catenin in skin. Cell *95*, 605-614.

Ghali, L., Wong, S.T., Green, J., Tidman, N., and Quinn, A.G. (1999). Gli1 protein is expressed in basal cell carcinomas, outer root sheath keratinocytes and a subpopulation of mesenchymal cells in normal human skin. Journal of Investigative Dermatology *113*, 595-599.

Giles, R.H., van Es, J.H., and Clevers, H. (2003). Caught up in a Wnt storm: Wnt signaling in cancer. Biochimica Et Biophysica Acta-Reviews on Cancer *1653*, 1-24.

Goodrich, L.V., Johnson, R.L., Milenkovic, L., McMahon, J.A., and Scott, M.P. (1996). Conservation of the hedgehog/patched signaling pathway from flies to mice: Induction of a mouse patched gene by Hedgehog. Genes & Development *10*, 301-312.

Goodrich, L.V., Milenkovic, L., Higgins, K.M., and Scott, M.P. (1997). Altered neural cell fates and medulloblastoma in mouse patched mutants. Science *277*, 1109-1113.

Gorlin, R.J. (1995). NEVOID BASAL-CELL CARCINOMA SYNDROME. Dermatologic Clinics *13*, 113-125.

Grachtchouk, M., Pero, J., Yang, S.H., Ermilov, A.N., Michael, L.E., Wang, A., Wilbert, D., Patel, R.M., Ferris, J., Diener, J., Allen, M., Lim, S., Syu, L.-J., Verhaegen, M., and Dlugosz, A.A. (2011). Basal cell carcinomas in mice arise from hair follicle stem cells and multiple epithelial progenitor populations. Journal of Clinical Investigation *121*, 1768-1781.

Grachtchouk, M., Rong, M., Yu, S., Zhang, X.Y., Sasaki, H., Hui, C.C., and Dlugosz, A.A. (2000). Basal cell carcinomas in mice overexpressing Gli2 in skin. Nature Genetics *24*, 216-217.

Grachtchouk, V., Grachtchouk, M., Lowe, L., Johnson, T., Wei, L.B., Wang, A.Q., de Sauvage, F., and Dlugosz, A.A. (2003). The magnitude of hedgehog signaling activity defines skin tumor phenotype. Embo Journal *22*, 2741-2751.

Grando, S.A., Schofield, O.M.V., Skubitz, A.P.N., Kist, D.A., Zelickson, B.D., and Zachary, C.B. (1996). Nodular basal cell carcinoma in vivo vs in vitro - Establishment of pure cell cultures, cytomorphologic characteristics, ultrastructure, immunophenotype, biosynthetic activities, and generation of antisera. Archives of Dermatology *132*, 1185-1193.

Green, J., Leigh, I.M., Poulsom, R., and Quinn, A.G. (1998). Basal cell carcinoma development is associated with induction of the expression of the transcription factor Gli-1. British Journal of Dermatology *139*, 911-915.

Hagedorn, H.G., Tubel, J., Wiest, I., Schleicher, E.D., and Nerlich, A.G. (1998). Prognostic aspects of the loss of epithelial basement membrane components in preinvasive and invasive laryngeal carcinomas. Anticancer Research *18*, 201-207.

Hahn, H., Christiansen, J., Wicking, C., Zaphiropoulos, P.G., Chidambaram, A., Gerrard, B., Vorechovsky, I., Bale, A.E., Toftgard, R., Dean, M., and Wainwright, B. (1996a). A mammalian patched homolog is expressed in target tissues of sonic hedgehog and maps to a region associated with developmental abnormalities. Journal of Biological Chemistry *271*, 12125-12128.

Hahn, H., Wicking, C., Zaphiropoulos, P.G., Gailani, M.R., Shanley, S., Chidambaram, A., Vorechovsky, I., Holmberg, E., Unden, A.B., Gillies, S., Negus, K., Smyth, I., Pressman, C., Leffell, D.J., Gerrard, B., Goldstein, A.M., Dean, M., Toftgard, R., ChenevixTrench, G., Wainwright, B., and Bale, A.E. (1996b). Mutations of the human homolog of Drosophila patched in the nevoid basal cell carcinoma syndrome. Cell *85*, 841-851.

Halpern, A.C., and Hanson, L.J. (2004). Awareness of, knowledge of and attitudes to nonmelanoma skin cancer (NMSC) and actinic keratosis (AK) among physicians. Int. J. Dermatol. *43*, 638-642.

Hannon, G.J., and Beach, D. (1994). P15(INK4B) IS A POTENTIAL EFFECTOR OF TGF-BETA-INDUCED CELL-CYCLE ARREST. Nature *371*, 257-261.

Hardcastle, Z., Mo, R., Hui, C.C., and Sharpe, P.T. (1998). The Shh signalling pathway in tooth development: Defects in Gli2 and Gli3 mutants. Development *125*, 2803-2811.

Hardy, M.H. (1992). THE SECRET LIFE OF THE HAIR FOLLICLE. Trends in Genetics *8*, 55-61.

Hatta, N., Hirano, T., Kimura, T., Hashimoto, K., Mehregan, D.R., Ansai, S., Takehara, K., and Takata, M. (2005). Molecular diagnosis of basal cell carcinoma and other basaloid cell neoplasms of the skin by the quantification of Gli1 transcript levels. Journal of Cutaneous Pathology *32*, 131-136.

He, T.C., Sparks, A.B., Rago, C., Hermeking, H., Zawel, L., da Costa, L.T., Morin, P.J., Vogelstein, B., and Kinzler, K.W. (1998). Identification of c-MYC as a target of the APC pathway. Science *281*, 1509-1512.

Hooper, J.E., and Scott, M.P. (1989). THE DROSOPHILA PATCHED GENE ENCODES A PUTATIVE MEMBRANE-PROTEIN REQUIRED FOR SEGMENTAL PATTERNING. Cell *59*, 751-765.

Hsu, S.M., Raine, L., and Fanger, H. (1981). USE OF AVIDIN-BIOTIN-PEROXIDASE COMPLEX (ABC) IN IMMUNOPEROXIDASE TECHNIQUES - A COMPARISON BETWEEN ABC AND UNLABELED ANTIBODY (PAP) PROCEDURES. Journal of Histochemistry & Cytochemistry *29*, 577-580.

Hu, M., Yao, J., Carroll, D.K., Weremowicz, S., Chen, H., Carrasco, D., Richardson, A., Violette, S., Nikolskaya, T., Nikolsky, Y., Bauerlein, E.L., Hahn, W.C., Gelman, R.S., Allred, C., Bissell, M.J., Schnitt, S., and Polyak, K. (2008). Regulation of in situ to invasive breast carcinoma transition. Cancer Cell *13*, 394-406.

Huelsken, J., Vogel, R., Erdmann, B., Cotsarelis, G., and Birchmeier, W. (2001). beta-catenin controls hair follicle morphogenesis and stem cell differentiation in the skin. Cell *105*, 533-545.

Huntzicker, E.G., Estay, I.S., Zhen, H., Lokteva, L.A., Jackson, P.K., and Oro, A.E. (2006). Dual degradation signals control Gli protein stability and tumor formation. Genes & Development *20*, 276-281.

Hutchin, M.E., Kariapper, M.S.T., Grachtchouk, M., Wang, A.Q., Wei, L.B., Cummings, D., Liu, J.H., Michael, L.E., Glick, A., and Dlugosz, A.A. (2005). Sustained Hedgehog signaling is required for basal cell carcinoma proliferation and survival: conditional skin tumorigenesis recapitulates the hair growth cycle. Genes & Development *19*, 214-223.

Ikram, M.S., Neill, G.W., Regl, G., Eichberger, T., Frischauf, A.M., Aberger, F., Quinn, A., and Philpott, M. (2004). GLI2 is expressed in normal human epidermis and BCC and induces GLI1 expression by binding to its promoter. Journal of Investigative Dermatology *122*, 1503-1509.

Ingham, P.W., and McMahon, A.P. (2001). Hedgehog signaling in animal development: paradigms and principles. Genes & Development *15*, 3059-3087.

Jensen, P.K.A., Norgard, J.O.R., and Bolund, L. (1985). CHANGES IN BASAL-CELL SUBPOPULATIONS AND TISSUE DIFFERENTIATION IN HUMAN EPIDERMAL CULTURES TREATED WITH EPIDERMAL GROWTH-FACTOR AND CHOLERA-TOXIN. Virchows Archiv B-Cell Pathology Including Molecular Pathology *49*, 325-340.

Johnson, R.L., Rothman, A.L., Xie, J.W., Goodrich, L.V., Bare, J.W., Bonifas, J.M., Quinn, A.G., Myers, R.M., Cox, D.R., Epstein, E.H., and Scott, M.P. (1996). Human homolog of patched, a candidate gene for the basal cell nevus syndrome. Science *272*, 1668-1671.

Karhadkar, S.S., Bova, G.S., Abdallah, N., Dhara, S., Gardner, D., Maitra, A., Isaacs, J.T., Berman, D.M., and Beachy, P.A. (2004). Hedgehog signalling in prostate regeneration, neoplasia and metastasis. Nature *431*, 707-712.

Kasper, M., Jaks, V., Are, A., Bergstrom, A., Schwager, A., Barker, N., and Toftgard, R. (2011). Wounding enhances epidermal tumorigenesis by recruiting hair

follicle keratinocytes. Proceedings of the National Academy of Sciences of the United States of America *108*, 4099-4104.

Kasper, M., Regi, G., Frischauf, A.M., and Aberger, F. (2006). GLI transcription factors: Mediators of oncogenic Hedgehog signalling. European Journal of Cancer *42*, 437-445.

Kawano, Y., and Kypta, R. (2003). Secreted antagonists of the Wnt signalling pathway. Journal of Cell Science *116*, 2627-2634.

Khavari, P.A. (2006). Modelling cancer in human skin tissue. Nature Reviews Cancer *6*, 270-280.

King, P., Paul, A., and Laufer, E. (2009). Shh signaling regulates adrenocortical development and identifies progenitors of steroidogenic lineages. Proceedings of the National Academy of Sciences of the United States of America *106*, 21185-21190.

Kinzler, K.W., Bigner, S.H., Bigner, D.D., Trent, J.M., Law, M.L., Obrien, S.J., Wong, A.J., and Vogelstein, B. (1987). IDENTIFICATION OF AN AMPLIFIED, HIGHLY EXPRESSED GENE IN A HUMAN GLIOMA. Science *236*, 70-73.

Kinzler, K.W., Ruppert, J.M., Bigner, S.H., and Vogelstein, B. (1988). THE GLI GENE IS A MEMBER OF THE KRUPPEL FAMILY OF ZINC FINGER PROTEINS. Nature *332*, 371-374.

Kinzler, K.W., and Vogelstein, B. (1990). THE GLI GENE ENCODES A NUCLEAR-PROTEIN WHICH BINDS SPECIFIC SEQUENCES IN THE HUMAN GENOME. Molecular and Cellular Biology *10*, 634-642.

Kogerman, P., Grimm, T., Kogerman, L., Krause, D., Unden, A.B., Sandstedt, B., Toftgard, R., and Zaphiropoulos, P.G. (1999). Mammalian Suppressor-of-Fused modulates nuclear-cytoplasmic shuttling of GLI-1. Nature Cell Biology *1*, 312-319.

Kump, E., Ji, J., Wernli, M., Hausermann, P., and Erb, P. (2008). Gli2 upregulates cFlip and renders basal cell carcinoma cells resistant to death ligand-mediated apoptosis. Oncogene *27*, 3856-3864.

Kurayoshi, M., Oue, N., Yamamoto, H., Kishida, M., Inoue, A., Asahara, T., Yasui, W., and Kikuchi, A. (2006). Expression of Wnt-5a is correlated with aggressiveness of gastric cancer by stimulating cell migration and invasion. Cancer Research *66*, 10439-10448.

Lanske, B., Karaplis, A.C., Lee, K., Luz, A., Vortkamp, A., Pirro, A., Karperien, M., Defize, L.H.K., Ho, C., Mulligan, R.C., AbouSamra, A.B., Juppner, H., Segre, G.V., and Kronenberg, H.M. (1996). PTH/PTHrP receptor in early development and Indian hedgehog-regulated bone growth. Science *273*, 663-666.

Lauth, M., and Toftgard, R. (2007). Non-canonical activation of GLI transcription factors - Implications for targeted anti-cancer therapy. Cell Cycle *6*, 2458-2463.

Lee, M.K., Pardoux, C., Hall, M.C., Lee, P.S., Warburton, D., Qing, J., Smith, S.M., and Derynck, R. (2007). TGF-beta activates Erk MAP kinase signalling through direct phosphorylation of ShcA. Embo Journal *26*, 3957-3967.

Li, X., Deng, W., Lobo-Ruppert, S.M., and Ruppert, J.M. (2007). Gli1 acts through Snail and E-cadherin to promote nuclear signaling by beta-catenin. Oncogene *26*, 4489-4498.

Liotta, L.A., and Kohn, E.C. (2001). The microenvironment of the tumour-host interface. Nature *411*, 375-379.

Liu, F., Hata, A., Baker, J.C., Doody, J., Carcamo, J., Harland, R.M., and Massague, J. (1996). A human Mad protein acting as a BMP-regulated transcriptional activator. Nature *381*, 620-623.

Lo Celso, C., Prowse, D.M., and Watt, F.M. (2004). Transient activation of beta-catenin signalling in adult mouse epidermis is sufficient to induce new hair follicles but continuous activation is required to maintain hair follicle tumours. Development *131*, 1787-1799.

Lo, H.-W., Zhu, H., Cao, X., Aldrich, A., and Ali-Osman, F. (2009). A Novel Splice Variant of GLI1 That Promotes Glioblastoma Cell Migration and Invasion. Cancer Research *69*, 6790-6798.

Lyu, J., and Joo, C.K. (2005). Wnt-7a up-regulates matrix metalloproteinase-12 expression and promotes cell proliferation in corneal epithelial cells during wound healing. Journal of Biological Chemistry *280*, 21653-21660.

Mancuso, M., Pazzaglia, S., Tanori, M., Hahn, H., Merola, P., Rebessi, S., Atkinson, M.J., Di Majo, V., Covelli, V., and Saran, A. (2004). Basal cell carcinoma and its development: Insights from radiation-induced tumors in Ptch1-deficient mice. Cancer Research *64*, 934-941.

Marigo, V., Davey, R.A., Zuo, Y., Cunningham, J.M., and Tabin, C.J. (1996). Biochemical evidence that Patched is the Hedgehog receptor. Nature *384*, 176-179.

Marigo, V., Volpin, D., Vitale, G., and Bressan, G.M. (1994). IDENTIFICATION OF A TGF-BETA RESPONSIVE ELEMENT IN THE HUMAN ELASTIN PROMOTER. Biochemical and Biophysical Research Communications *199*, 1049-1056.

Marsh, D., Dickinson, S., Neill, G.W., Marshall, J.F., Hart, I.R., and Thomas, G.J. (2008). alpha v beta 6 integrin promotes the invasion of morphoeic basal cell carcinoma through stromal modulation. Cancer Research *68*, 3295-3303.

Martins, V.L., Vyas, J.J., Chen, M., Purdie, K., Mein, C.A., South, A.P., Storey, A., McGrath, J.A., and O'Toole, E.A. (2009). Increased invasive behaviour in cutaneous

squamous cell carcinoma with loss of basement-membrane type VII collagen. Journal of Cell Science *122*, 1788-1799.

Massague, J. (1998). TGF-beta signal transduction. Annu. Rev. Biochem. *67*, 753-791.

Massague, J., Blain, S.W., and Lo, R.S. (2000). TGF beta signaling in growth control, cancer, and heritable disorders. Cell *103*, 295-309.

Massague, J., Seoane, J., and Wotton, D. (2005). Smad transcription factors. Genes & Development *19*, 2783-2810.

Matise, M.P., Epstein, D.J., Park, H.L., Platt, K.A., and Joyner, A.L. (1998). Gli2 is required for induction of floor plate and adjacent cells, but not most ventral neurons in the mouse central nervous system. Development *125*, 2759-2770.

Mill, P., Mo, R., Fu, H., Grachtchouk, M., Kim, P.C.W., Dlugosz, A.A., and Hui, C.C. (2003). Sonic hedgehog-dependent activation of Gli2 is essential for embryonic hair follicle development. Genes & Development *17*, 282-294.

Miller, J.R. (2002). The Wnts. Genome Biol *3*, REVIEWS3001.

Miller, S.J. (1995). Etiology and pathogenesis of basal cell carcinoma. Clinics in Dermatology *13*, 527-536.

Mirsky, R., Parmantier, E., McMahon, A.P., and Jessen, K.R. (1999). Schwann cell-derived desert hedgehog signals nerve sheath formation. Charcot-Marie-Tooth Disorders *883*, 196-202.

Miyazono, K., Ichijo, H., and Heldin, C.H. (1993). TRANSFORMING GROWTH-FACTOR-BETA - LATENT FORMS, BINDING-PROTEINS AND RECEPTORS. Growth Factors *8*, 11-22.

Mo, R., Freer, A.M., Zinyk, D.L., Crackower, M.A., Michaud, J., Heng, H.H.Q., Chik, K.W., Shi, X.M., Tsui, L.C., Cheng, S.H., Joyner, A.L., and Hui, C.C. (1997). Specific and redundant functions of Gli2 and Gli3 zinc finger genes in skeletal patterning and development. Development *124*, 113-123.

Montesano, R., and Orci, L. (1988). TRANSFORMING GROWTH FACTOR-BETA STIMULATES COLLAGEN-MATRIX CONTRACTION BY FIBROBLASTS - IMPLICATIONS FOR WOUND-HEALING. Proceedings of the National Academy of Sciences of the United States of America *85*, 4894-4897.

Morin, P.J., Sparks, A.B., Korinek, V., Barker, N., Clevers, H., Vogelstein, B., and Kinzler, K.W. (1997). Activation of beta-catenin-Tcf signaling in colon cancer by mutations in beta-catenin or APC. Science *275*, 1787-1790.

Morley, S.N., Dundas, S.R., James, J.L., Gupta, T., Brown, R.A., Sexton, C.J., Navsaria, H.A., Leigh, I.M., and Lane, E.B. (1995). TEMPERATURE

SENSITIVITY OF THE KERATIN CYTOSKELETON AND DELAYED SPREADING OF KERATINOCYTE LINES DERIVED FROM EBS PATIENTS. Journal of Cell Science *108*, 3463-3471.

Moses, H.L., Branum, E.L., Proper, J.A., and Robinson, R.A. (1981). TRANSFORMING GROWTH-FACTOR PRODUCTION BY CHEMICALLY TRANSFORMED-CELLS. Cancer Research *41*, 2842-2848.

Motoyama, J., Liu, J., Mo, R., Ding, Q., Post, M., and Hui, C.C. (1998). Essential function of Gli2 and Gli3 in the formation of lung, trachea and oesophagus. Nature Genetics *20*, 54-57.

Mullor, J.L., Dahmane, N., Sun, T., and Altaba, A.R.I. (2001). Wnt signals are targets and mediators of Gli function. Current Biology *11*, 769-773.

Murone, M., Luoh, S.M., Stone, D., Li, W.L., Gurney, A., Armanini, M., Grey, C., Rosenthal, A., and de Sauvage, F.J. (2000). Gli regulation by the opposing activities of Fused and Suppressor of Fused. Nature Cell Biology *2*, 310-312.

Nadendla, S.K., Hazan, A., Ward, M., Harper, L.J., Moutasim, K., Bianchi, L.S., Naase, M., Ghali, L., Thomas, G.J., Prowse, D.M., Philpott, M.P., and Neill, G.W. (2011). GLI1 Confers Profound Phenotypic Changes upon LNCaP Prostate Cancer Cells That Include the Acquisition of a Hormone Independent State. Plos One *6*.

Nakano, Y., Guerrero, I., Hidalgo, A., Taylor, A., Whittle, J.R.S., and Ingham, P.W. (1989). A PROTEIN WITH SEVERAL POSSIBLE MEMBRANE-SPANNING DOMAINS ENCODED BY THE DROSOPHILA SEGMENT POLARITY GENE PATCHED. Nature *341*, 508-513.

Neill, G.W., Harrison, W.J., Ikram, M.S., Williams, T.D.L., Bianchi, L.S., Nadendla, S.K., Green, J.L., Ghali, L., Frischauf, A.M., O'Toole, E.A., Aberger, F., and Philpott, M.P. (2008). GLI1 repression of ERK activity correlates with colony formation and impaired migration in human epidermal keratinocytes. Carcinogenesis *29*, 738-746.

Nicolas, M., Wolfer, A., Raj, K., Kummer, J.A., Mill, P., van Noort, M., Hui, C.C., Clevers, H., Dotto, G.P., and Radtke, F. (2003). Notch1 functions as a tumor suppressor in mouse skin. Nature Genetics *33*, 416-421.

Nilsson, M., Unden, A.B., Krause, D., Malmqwist, U., Raza, K., Zaphiropoulos, P.G., and Toftgard, R. (2000). Induction of basal cell carcinomas and trichoepitheliomas in mice overexpressing GLI-1. Proceedings of the National Academy of Sciences of the United States of America *97*, 3438-3443.

Nolan-Stevaux, O., Lau, J., Truitt, M.L., Chu, G.C., Hebrok, M., Fernandez-Zapico, M.E., and Hanahan, D. (2009). GLI1 is regulated through Smoothened-independent mechanisms in neoplastic pancreatic ducts and mediates PDAC cell survival and transformation. Genes & Development *23*, 24-36.

Nusse, R. (2005). Wnt signaling in disease and in development. Cell Research *15*, 28-32.

Nusse, R., Brown, A., Papkoff, J., Scambler, P., Shackleford, G., McMahon, A., Moon, R., and Varmus, H. (1991). A NEW NOMENCLATURE FOR INT-1 AND RELATED GENES - THE WNT GENE FAMILY. Cell *64*, 231-231.

Nussleinvolhard, C., and Wieschaus, E. (1980). MUTATIONS AFFECTING SEGMENT NUMBER AND POLARITY IN DROSOPHILA. Nature *287*, 795-801.

Nystrom, M.L., Thomas, G.L., Stone, M., Mackenzie, I.C., Hart, I.R., and Marshall, J.F. (2005). Development of a quantitative method to analyse tumour cell invasion in organotypic culture. Journal of Pathology *205*, 468-475.

Oft, M., Heider, K.H., and Beug, H. (1998). TGF beta signaling is necessary for carcinoma cell invasiveness and metastasis. Current Biology *8*, 1243-1252.

Okane, S., and Ferguson, M.W.J. (1997). Transforming growth factor beta s and wound healing. International Journal of Biochemistry & Cell Biology *29*, 63-78.

Oro, A.E., and Higgins, K. (2003). Hair cycle regulation of Hedgehog signal reception. Developmental Biology *255*, 238-248.

Ouko, L., Ziegler, T.R., Gu, L.H., Eisenberg, L.M., and Yang, V.W. (2004). Wnt11 signaling promotes proliferation, transformation, and migration of IEC6 intestinal epithelial cells. Journal of Biological Chemistry *279*, 26707-26715.

Pan, Y., Bai, C.B., Joyner, A.L., and Wang, B. (2006a). Sonic hedgehog signaling regulates Gli2 transcriptional activity by suppressing its processing and degradation. Molecular and cellular biology *26*, 3365-3377.

Pan, Y., Bai, C.Y.B., Joyner, A.L., and Wang, B.L. (2006b). Sonic hedgehog signaling regulates Gli2 transcriptional activity by suppressing its processing and degradation. Molecular and Cellular Biology *26*, 3365-3377.

Pan, Y., Wang, C., and Wang, B. (2009). Phosphorylation of Gli2 by protein kinase A is required for Gli2 processing and degradation and the Sonic Hedgehog-regulated mouse development. Developmental Biology *326*, 177-189.

Park, H.L., Bai, C., Platt, K.A., Matise, M.P., Beeghly, A., Hui, C.C., Nakashima, M., and Joyner, A.L. (2000). Mouse Gli1 mutants are viable but have defects in SHH signaling in combination with a Gli2 mutation. Development *127*, 1593-1605.

Peifer, M., McCrea, P.D., Green, K.J., Wieschaus, E., and Gumbiner, B.M. (1992). THE VERTEBRATE ADHESIVE JUNCTION PROTEINS BETA-CATENIN AND PLAKOGLOBIN AND THE DROSOPHILA SEGMENT POLARITY GENE ARMADILLO FORM A MULTIGENE FAMILY WITH SIMILAR PROPERTIES. Journal of Cell Biology *118*, 681-691.

Polakis, P. (2007). The many ways of Wnt in cancer. Current Opinion in Genetics & Development *17*, 45-51.

Porter, J.A., Young, K.E., and Beachy, P.A. (1996). Cholesterol modification of hedgehog signaling proteins in animal development. Science *274*, 255-259.

Prunieras, M., Regnier, M., and Woodley, D. (1983). METHODS FOR CULTIVATION OF KERATINOCYTES WITH AN AIR-LIQUID INTERFACE. Journal of Investigative Dermatology *81*, S28-S33.

Pukrop, T., Klemm, F., Hagemann, T., Gradl, D., Schulz, M., Siemes, S., Trumper, L., and Binder, C. (2006). Wnt 5a signaling is critical for macrophage-induced invasion of breast cancer cell lines. Proceedings of the National Academy of Sciences of the United States of America *103*, 5454-5459.

Quinn, A.G. (1997). Ultraviolet radiation and skin carcinogenesis. British Journal of Hospital Medicine *58*, 261-264.

Rahnama, F., Shimokawa, T., Lauth, M., Finta, C., Kogerman, P., Teglund, S., Toftgard, R., and Zaphiropoulos, P.G. (2006). Inhibition of GLI1 gene activation by patched1. Biochem. J. *394*, 19-26.

Regl, G., Kasper, M., Schnidar, H., Eichberger, T., Neill, G.W., Ikram, M.S., Quinn, A.G., Philpott, M.P., Frischauf, A.M., and Aberger, F. (2004a). The zinc-finger transcription factor GLI2 antagonizes contact inhibition and differentiation of human epidermal cells. Oncogene *23*, 1263-1274.

Regl, G., Kasper, M., Schnidar, H., Eichberger, T., Neill, G.W., Philpott, M.P., Esterbauer, H., Hauser-Kronberger, C., Frischauf, A.M., and Aberger, F. (2004b). Activation of the BCL2 promoter in response to hedgehog/GLI signal transduction is predominantly mediated by GLI2. Cancer Research *64*, 7724-7731.

Regl, G., Neill, G.W., Eichberger, T., Kasper, M., Ikram, M.S., Koller, J., Hintner, H., Quinn, A.G., Frischauf, A.M., and Aberger, F. (2002). Human GLI2 and GLI1 are part of a positive feedback mechanism in Basal Cell Carcinoma. Oncogene *21*, 5529-5539.

Rheinwald, J.G., and Green, H. (1975). SERIAL CULTIVATION OF STRAINS OF HUMAN EPIDERMAL KERATINOCYTES - FORMATION OF KERATINIZING COLONIES FROM SINGLE CELLS. Cell *6*, 331-344.

Rijsewijk, F., Schuermann, M., Wagenaar, E., Parren, P., Weigel, D., and Nusse, R. (1987). THE DROSOPHILA HOMOLOG OF THE MOUSE MAMMARY ONCOGENE INT-1 IS IDENTICAL TO THE SEGMENT POLARITY GENE WINGLESS. Cell *50*, 649-657.

Riobo, N.A., Ke, L., and Emerson, C.P., Jr. (2006a). Hedgehog signal transduction - Signal integration and cross talk in development and cancer. Cell Cycle *5*, 1612-1615.

Riobo, N.A., Lu, K., Ai, X., Haines, G.M., and Emerson, C.P., Jr. (2006b). Phosphoinositide 3-kinase and Akt are essential for Sonic Hedgehog signaling. Proceedings of the National Academy of Sciences of the United States of America *103*, 4505-4510.

Ritzenthaler, J.D., Goldstein, R.H., Fine, A., and Smith, B.D. (1993). REGULATION OF THE ALPHA-1(I) COLLAGEN PROMOTER VIA A TRANSFORMING GROWTH-FACTOR-BETA ACTIVATION ELEMENT. Journal of Biological Chemistry *268*, 13625-13631.

Roessler, E., Ermilov, A.N., Grange, D.K., Wang, A.Q., Grachtchouk, M., Dlugosz, A.A., and Muenke, M. (2005). A previously unidentified amino-terminal domain regulates transcriptional activity of wild-type and disease-associated human GLI2. Human Molecular Genetics *14*, 2181-2188.

Rohatgi, R., Milenkovic, L., and Scott, M.P. (2007). Patched1 regulates Hedgehog signaling at the primary cilium. Science *317*, 372-376.

Rubin, L.L., de Sauvage F.J. (2006). Targeting the Hedgehog pathway in cancer. Nat Rev Drug Discov *5*, 1026-1033.

Rubinfeld, B., Robbins, P., ElGamil, M., Albert, I., Porfiri, E., and Polakis, P. (1997). Stabilization of beta-catenin by genetic defects in melanoma cell lines. Science *275*, 1790-1792.

Ruiz i Altaba, A., Sanchez, P., and Dahmane, N. (2002). Gli and Hedgehog in cancer: Tumours, embryos and stem cells. Nature Reviews Cancer *2*, 361-372.

Ruppert, J.M., Kinzler, K.W., Wong, A.J., Bigner, S.H., Kao, F.T., Law, M.L., Seuanez, H.N., Obrien, S.J., and Vogelstein, B. (1988). THE GLI-KRUPPEL FAMILY OF HUMAN GENES. Molecular and Cellular Biology *8*, 3104-3113.

Ruppert, J.M., Vogelstein, B., Arheden, K., and Kinzler, K.W. (1990). GL13 ENCODES A 190-KILODALTON PROTEIN WITH MULTIPLE REGIONS OF GLI SIMILARITY. Molecular and Cellular Biology *10*, 5408-5415.

Ruppert, J.M., Vogelstein, B., and Kinzler, K.W. (1991). THE ZINC FINGER PROTEIN GL1 TRANSFORMS PRIMARY CELLS IN COOPERATION WITH ADENOVIRUS E1A. Molecular and Cellular Biology *11*, 1724-1728.

Sarangi, A., Valadez, J.G., Rush, S., Abel, T.W., Thompson, R.C., and Cooper, M.K. (2009). Targeted inhibition of the Hedgehog pathway in established malignant glioma xenografts enhances survival. Oncogene *28*, 3468-3476.

Sasaki, H., Nishizaki, Y., Hui, C.C., Nakafuku, M., and Kondoh, H. (1999). Regulation of Gli2 and Gli3 activities by an amino-terminal repression domain: implication of Gli2 and Gli3 as primary mediators of Shh signaling. Development *126*, 3915-3924.

Sato, N., Leopold, P.L., and Crystal, R.G. (1999). Induction of the hair growth phase in postnatal mice by localized transient expression of Sonic hedgehog. Journal of Clinical Investigation *104*, 855-864.

Scales, S.J., and de Sauvage, F.J. (2009). Mechanisms of Hedgehog pathway activation in cancer and implications for therapy. Trends in Pharmacological Sciences *30*, 303-312.

Schmid, P., Itin, P., and Rufli, T. (1996). In situ analysis of transforming growth factors-beta (TGF-beta 1, TGF-beta 2, TGF-beta 3) and TGF-beta type II receptor expression in basal cell carcinomas. British Journal of Dermatology *134*, 1044-1051.

Schnidar, H., Eberl, M., Klingler, S., Mangelberger, D., Kasper, M., Hauser-Kronberger, C., Regl, G., Kroismayr, R., Moriggl, R., Sibilia, M., and Aberger, F. (2009). Epidermal Growth Factor Receptor Signaling Synergizes with Hedgehog/GLI in Oncogenic Transformation via Activation of the MEK/ERK/JUN Pathway. Cancer Research *69*, 1284-1292.

Seifert, J.R.K., and Mlodzik, M. (2007). Frizzled/PCP signalling: a conserved mechanism regulating cell polarity and directed motility. Nature Reviews Genetics *8*, 126-138.

Sellheyer, K., and Krahl, D. (2011). Does the peritumoral stroma of basal cell carcinoma recapitulate the follicular connective tissue sheath? A comparative analysis of nestin expression in basal cell carcinoma, trichoepithelioma, trichoblastoma and the hair follicle. Journal of Cutaneous Pathology *38*, 551-559.

Sheng, H., Goich, S., Wang, A.Q., Grachtchouk, M., Lowe, L., Mo, R., Lin, K., de Sauvage, F.J., Sasaki, H., Hui, C.C., and Dlugosz, A.A. (2002). Dissecting the oncogenic potential of Gli2: Deletion of an NH2-terminal fragment alters skin tumor phenotype. Cancer Research *62*, 5308-5316.

Sheng, T., Chi, S.M., Zhang, X.L., and Xie, J.W. (2006). Regulation of Gli1 localization by the cAMP/protein kinase A signaling axis through a site near the nuclear localization signal. Journal of Biological Chemistry *281*, 9-12.

Shimizu, H., Julius, M.A., Giarre, M., Zheng, Z.L., Brown, A.M.C., and Kitajewski, J. (1997). Transformation by Wnt family proteins correlates with regulation of beta-catenin. Cell Growth & Differentiation *8*, 1349-1358.

Shimokawa, T., Tostar, U., Lauth, M., Palaniswamy, R., Kasper, M., Toftgard, R., and Zaphiropoulos, P.G. (2008). Novel human glioma-associated oncogene 1 (GLI1) splice variants reveal distinct mechanisms in the terminal transduction of the hedgehog signal. Journal of Biological Chemistry *283*, 14345-14354.

Shimomura, Y., and Christiano, A.M. (2010). Biology and Genetics of Hair. In: Annual Review of Genomics and Human Genetics, Vol 11, vol. 11, 109-132.

Smyth, I., Narang, M.A., Evans, T., Heimann, C., Nakamura, Y., Chenevix-Trench, G., Pietsch, T., Wicking, C., and Wainwright, B.J. (1999). Isolation and characterization of human Patched 2 (PTCH2), a putative tumour suppressor gene in basal cell carcinoma and medulloblastoma on chromosome 1p32. Human Molecular Genetics *8*, 291-297.

Snijders, A.M., Huey, B., Connelly, S.T., Roy, R., Jordan, R.C.K., Schmidt, B.L., and Albertson, D.G. (2009). Stromal control of oncogenic traits expressed in response to the overexpression of GLI2, a pleiotropic oncogene. Oncogene *28*, 625-637.

Speek, M., Njunkova, O., Pata, I., Valdre, E., and Kogerman, P. (2006). A potential role of alternative splicing in the regulation of the transcriptional activity of human GLI2 in gonadal tissues. Bmc Molecular Biology *7*.

St-Jacques, B., Dassule, H.R., Karavanova, I., Botchkarev, V.A., Li, J., Danielian, P.S., McMahon, J.A., Lewis, P.M., Paus, R., and McMahon, A.P. (1998). Sonic hedgehog signaling is essential for hair development. Current Biology *8*, 1058-1068.

St-Jacques, B., Hammerschmidt, M., and McMahon, A.P. (1999). Indian hedgehog signaling regulates proliferation and differentiation of chondrocytes and is essential for bone formation. Genes & Development *13*, 2072-2086.

Stecca, B., and Ruiz i Altaba, A. (2009). A GLI1-p53 inhibitory loop controls neural stem cell and tumour cell numbers. Embo Journal *28*, 663-676.

Stecca, B., and Ruiz i Altaba, A. (2010). Context-dependent Regulation of the GLI Code in Cancer by HEDGEHOG and Non-HEDGEHOG Signals. Journal of Molecular Cell Biology *2*, 84-95.

Stenn, K.S., Link, R., Moellmann, G., Madri, J., and Kuklinska, E. (1989). DISPASE, A NEUTRAL PROTEASE FROM BACILLUS-POLYMYXA, IS A POWERFUL FIBRONECTINASE AND TYPE-IV COLLAGENASE. Journal of Investigative Dermatology *93*, 287-290.

Stenn, K.S., and Paus, R. (2001). Controls of hair follicle cycling. Physiological Reviews *81*, 449-494.

Stone, D.M., Hynes, M., Armanini, M., Swanson, T.A., Gu, Q.M., Johnson, R.L., Scott, M.P., Pennica, D., Goddard, A., Phillips, H., Noll, M., Hooper, J.E., deSauvage, F., and Rosenthal, A. (1996). The tumour-suppressor gene patched encodes a candidate receptor for Sonic hedgehog. Nature *384*, 129-134.

Svensson, S., Nilsson, K., Ringberg, A., and Landberg, G. (2003). Invade or proliferate? Two contrasting events in malignant behavior governed by p16(INK4a) and an intact Rb pathway illustrated by a model system of basal cell carcinoma. Cancer Research *63*, 1737-1742.

Taipale, J., Chen, J.K., Cooper, M.K., Wang, B.L., Mann, R.K., Milenkovic, L., Scott, M.P., and Beachy, P.A. (2000). Effects of oncogenic mutations in Smoothened and Patched can be reversed by cyclopamine. Nature *406*, 1005-1009.

Tang, T., Tang, J.Y., Li, D., Reich, M., Callahan, C.A., Fu, L., Yauch, R.L., Wang, F., Kotkow, K., Chang, K.S., Shpall, E., Wu, A., Rubin, L.L., Marsters, J.C., Epstein, E.H., Jr., Caro, I., Jr., and de Sauvage, F.J. (2011). Targeting Superficial or Nodular Basal Cell Carcinoma with Topically Formulated Small Molecule Inhibitor of Smoothened. Clinical Cancer Research *17*, 3378-3387.

Tanimura, A., Dan, S., and Yoshida, M. (1998). Cloning of novel isoforms of the human Gli2 oncogene and their activities to enhance tax-dependent transcription of the human T-cell leukemia virus type 1 genome. Journal of Virology *72*, 3958-3964.

Tetsu, O., and McCormick, F. (1999). beta-catenin regulates expression of cyclin D1 in colon carcinoma cells. Nature *398*, 422-426.

Thayer, S.P., di Magliano, M.P., Heiser, P.W., Nielsen, C.M., Roberts, D.J., Lauwers, G.Y., Qi, Y.P., Gysin, S., Fernandez-del Castillo, C.F., Yajnik, V., Antoniu, B., McMahon, M., Warshaw, A.L., and Hebrok, M. (2003). Hedgehog is an early and late mediator of pancreatic cancer tumorigenesis. Nature *425*, 851-856.

Tian, H., Callahan, C.A., DuPree, K.J., Darbonne, W.C., Ahn, C.P., Scales, S.J., and de Sauvage, F.J. (2009). Hedgehog signaling is restricted to the stromal compartment during pancreatic carcinogenesis. Proceedings of the National Academy of Sciences of the United States of America *106*, 4254-4259.

Tlsty, T.D., and Coussens, L.M. (2006). Tumor stroma and regulation of cancer development. Annual Review of Pathology-Mechanisms of Disease *1*, 119-150.

Todaro, G.J., and Green, H. (1963). Quantitative studies of the growth of mouse embryo cells in culture and their development into established lines. The Journal of cell biology *17*, 299-313.

Tojo, M., Kiyosawa, H., Iwatsuki, K., Nakamura, K., and Kaneko, F. (2003). Expression of the GLI2 oncogene and its isoforms in human basal cell carcinoma. British Journal of Dermatology *148*, 892-897.

Topol, L., Jiang, X.Y., Choi, H., Garrett-Beal, L., Carolan, P.J., and Yang, Y.Z. (2003). Wnt-5a inhibits the canonical Wnt pathway by promoting GSK-3-independent beta-catenin degradation. Journal of Cell Biology *162*, 899-908.

vandenHeuvel, M., and Ingham, P.W. (1996). smoothened encodes a serpentine protein required for hedgehog signalling. Nature *382*, 547-551.

Vanderschroeff, J.G., Evers, L.M., Boot, A.J.M., and Bos, J.L. (1990). RAS ONCOGENE MUTATIONS IN BASAL-CELL CARCINOMAS AND SQUAMOUS-CELL CARCINOMAS OF HUMAN SKIN. Journal of Investigative Dermatology *94*, 423-425.

vandeWetering, M., Cavallo, R., Dooijes, D., vanBeest, M., vanEs, J., Loureiro, J., Ypma, A., Hursh, D., Jones, T., Bejsovec, A., Peifer, M., Mortin, M., and Clevers, H. (1997). Armadillo coactivates transcription driven by the product of the Drosophila segment polarity gene dTCF. Cell *88*, 789-799.

Veeman, M.T., Axelrod, J.D., and Moon, R.T. (2003). A second canon: Functions and mechanisms of beta-catenin-independent wnt signaling. Developmental Cell *5*, 367-377.

Verhaegh, M., Arends, J.W., Majoie, I.M.L., Hoekzema, R., and Neumann, H.A.M. (1997). Transforming growth factor-beta and bcl-2 distribution patterns distinguish trichoepithelioma from basal cell carcinoma. Dermatologic Surgery *23*, 695-700.

Von Hoff, D.D., LoRusso, P.M., Rudin, C.M., Reddy, J.C., Yauch, R.L., Tibes, R., Weiss, G.J., Borad, M.J., Hann, C.L., Brahmer, J.R., Mackey, H.M., Lum, B.L., Darbonne, W.C., Marsters, J.C., de Sauvage, F.J., and Low, J.A. (2009). Inhibition of the Hedgehog Pathway in Advanced Basal-Cell Carcinoma. New England Journal of Medicine *361*, 1164-1172.

Vortkamp, A., Gessler, M., and Grzeschik, K.H. (1995). IDENTIFICATION OF OPTIMIZED TARGET SEQUENCES FOR THE GLI3 ZINC-FINGER PROTEIN. DNA and Cell Biology *14*, 629-634.

Wakefield, L.M., and Roberts, A.B. (2002). TGF-beta signaling: positive and negative effects on tumorigenesis. Current Opinion in Genetics & Development *12*, 22-29.

Wang, B.L., Fallon, J.F., and Beachy, P.A. (2000a). Hedgehog-regulated processing of Gli3 produces an anterior/posterior repressor gradient in the developing vertebrate limb. Cell *100*, 423-434.

Wang, G.Y., Wang, J., Mancianti, M.-L., and Epstein, E.H., Jr. (2011). Basal Cell Carcinomas Arise from Hair Follicle Stem Cells in Ptch1(+/-) Mice. Cancer Cell *19*, 114-124.

Wang, H., Owens, J.D., Shih, J.H., Li, M.-C., Bonner, R.F., and Mushinski, J.F. (2006). Histological staining methods preparatory to laser capture microdissection significantly affect the integrity of the cellular RNA. Bmc Genomics *7*.

Wang, L.C., Liu, Z.Y., Gambardella, L., Delacour, A., Shapiro, R., Yang, J.L., Sizing, I., Rayhorn, P., Garber, E.A., Benjamin, C.D., Williams, K.P., Taylor, F.R., Barrandon, Y., Ling, L., and Burkly, L.C. (2000b). Conditional disruption of hedgehog signaling pathway defines its critical role in hair development and regeneration. Journal of Investigative Dermatology *114*, 901-908.

Watkins, D.N., Berman, D.M., Burkholder, S.G., Wang, B.L., Beachy, P.A., and Baylin, S.B. (2003). Hedgehog signalling within airway epithelial progenitors and in small-cell lung cancer. Nature *422*, 313-317.

Watt, F.M., Lo Celso, C., and Silva-Vargas, V. (2006). Epidermal stem cells: an update. Current Opinion in Genetics & Development *16*, 518-524.

Weeraratna, A.T., Jiang, Y.A., Hostetter, G., Rosenblatt, K., Duray, P., Bittner, M., and Trent, J.M. (2002). Wnt5a signaling directly affects cell motility and invasion of metastatic melanoma. Cancer Cell *1*, 279-288.

Weinberg, R.A. (1995). THE MOLECULAR-BASIS OF ONCOGENES AND TUMOR-SUPPRESSOR GENES. DNA: The Double Helix *758*, 331-338.

Wetmore, C. (2003). Sonic hedgehog in normal and neoplastic proliferation: insight gained from human tumors and animal models. Current Opinion in Genetics & Development *13*, 34-42.

Williams, J.A., Guicherit, O.M., Zaharian, B.I., Xu, Y., Chai, L., Wichterle, H., Kon, C., Gatchalian, C., Porter, J.A., Rubin, L.L., and Wang, F.Y. (2003). Identification of a small molecule inhibitor of the hedgehog signaling pathway: Effects on basal cell carcinoma-like lesions. Proceedings of the National Academy of Sciences of the United States of America *100*, 4616-4621.

Wodarz, A., and Nusse, R. (1998). Mechanisms of Wnt signaling in development. Annual Review of Cell and Developmental Biology *14*, 59-88.

Wong, S.Y., and Reiter, J.F. (2011). Wounding mobilizes hair follicle stem cells to form tumors. Proceedings of the National Academy of Sciences of the United States of America *108*, 4093-4098.

Wrana, J.L., Attisano, L., Carcamo, J., Zentella, A., Doody, J., Laiho, M., Wang, X.F., and Massague, J. (1992). TGF-BETA SIGNALS THROUGH A HETEROMERIC PROTEIN-KINASE RECEPTOR COMPLEX. Cell *71*, 1003-1014.

Wrana, J.L., Attisano, L., Wieser, R., Ventura, F., and Massague, J. (1994). MECHANISM OF ACTIVATION OF THE TGF-BETA RECEPTOR. Nature *370*, 341-347.

Xie, J.W., Murone, M., Luoh, S.M., Ryan, A., Gu, Q.M., Zhang, C.H., Bonifas, J.M., Lam, C.W., Hynes, M., Goddard, A., Rosenthal, A., Epstein, E.H., and de Sauvage, F.J. (1998). Activating Smoothened mutations in sporadic basal-cell carcinoma. Nature *391*, 90-92.

Yamashita, M., Fatyol, K., Jin, C.Y., Wang, X.C., Liu, Z.G., and Zhang, Y.E. (2008). TRAF6 mediates Smad-independent activation of JNK and p38 by TGF-beta. Molecular Cell *31*, 918-924.

Yang, S.H., Andl, T., Grachtchouk, V., Wang, A.Q., Liu, J.H., Syu, L.J., Ferris, J., Wang, T.S., Glick, A.B., Millar, S.E., and Dlugosz, A.A. (2008). Pathological

responses to oncogenic Hedgehog signaling in skin are dependent on canonical Wnt/beta-catenin signaling. Nature Genetics *40*, 1130-1135.

Yauch, R.L., Dijkgraaf, G.J.P., Alicke, B., Januario, T., Ahn, C.P., Holcomb, T., Pujara, K., Stinson, J., Callahan, C.A., Tang, T., Bazan, J.F., Kan, Z., Seshagiri, S., Hann, C.L., Gould, S.E., Low, J.A., Rudin, C.M., and de Sauvage, F.J. (2009). Smoothened Mutation Confers Resistance to a Hedgehog Pathway Inhibitor in Medulloblastoma. Science *326*, 572-574.

Yauch, R.L., Gould, S.E., Scales, S.J., Tang, T., Tian, H., Ahn, C.P., Marshall, D., Fu, L., Januario, T., Kallop, D., Nannini-Pepe, M., Kotkow, K., Marsters, J.C., Rubin, L.L., and de Sauvage, F.J. (2008). A paracrine requirement for hedgehog signalling in cancer. Nature *455*, 406-U461.

Youssef, K.K., Van Keymeulen, A., Lapouge, G., Beck, B., Michaux, C., Achouri, Y., Sotiropoulou, P.A., and Blanpain, C. (2010). Identification of the cell lineage at the origin of basal cell carcinoma. Nature Cell Biology *12*, 299-U111.

Yu, Q., and Stamenkovic, I. (2000). Cell surface-localized matrix metalloproteinase-9 proteolytically activates TGF-beta and promotes tumor invasion and angiogenesis. Genes & Development *14*, 163-176.

Zhao, C., Chen, A., Jamieson, C.H., Fereshteh, M., Abrahamsson, A., Blum, J., Kwon, H.Y., Kim, J., Chute, J.P., Rizzieri, D., Munchhof, M., VanArsdale, T., Beachy, P.A., and Reya, T. (2009). Hedgehog signalling is essential for maintenance of cancer stem cells in myeloid leukaemia. Nature *458*, 776-U117.

Ziegler, A., Leffell, D.J., Kunala, S., Sharma, H.W., Gailani, M., Simon, J.A., Halperin, A.J., Baden, H.P., Shapiro, P.E., Bale, A.E., and Brash, D.E. (1993). MUTATION HOTSPOTS DUE TO SUNLIGHT IN THE P53 GENE OF NONMELANOMA SKIN CANCERS. Proceedings of the National Academy of Sciences of the United States of America *90*, 4216-4220.

8 Appendices

Appendix I

Standard buffers, reagents and cell culture media

Phosphate buffered saline (PBS)

Dulbecco's PBS (1x) without Ca2+ & Mg2+ (PAA Laboratories GmbH, Austria)

Trypsin

Trypsin – EDTA (0.05% - 0.02% in D-PBS), (PAA Laboratories GmbH, Austria)

Versene

Versene 0.2 g/l (0.53 mM) in an isotonically buffered saline (Invitrogen, U.K.)

DMEM Medium

DMEM (PAA Laboratories GmbH, Austria)

10% (v/v) fetal bovine serum (FBS) (Biosera, U.K.)

1% (v/v) L-glutamine (PAA Laboratories GmbH, Austria)

1% (v/v) Penicillin / Streptomycin (PAA Laboratories GmbH, Austria)

RM+ Medium

DMEM: Ham's F12 3:1 (v/v), custom made, (PAA Laboratories GmbH, Austria)

10% (v/v) fetal bovine serum (FBS) (Biosera, U.K.)

1% (v/v) L-glutamine (PAA Laboratories GmbH, Austria)

1% (v/v) Penicillin / Streptomycin (PAA Laboratories GmbH, Austria)

RM+ supplement:

5 μg/ml insulin

0.4 μg/ml hydrocortisone

10 ng/ml epidermal growth factor

5 μg/ml transferrin

20 pM L-lyothyronine.

1 nM cholera toxin (Sigma, U.K.)

Keratinocyte Growth Medium (KGM)

α-MEM (Lonza, U.K.)

10% (v/v) fetal bovine serum (FBS) (Lonza, U.K.)

1% (v/v) L-glutamine (PAA Laboratories GmbH, Austria)

1% (v/v) Penicillin / Streptomycin (PAA Laboratories GmbH, Austria)

1.8×10^{-4} M adenine

1×10^{-10} M cholera toxin

5 μg/ml insulin

0.4 μg/ml hydrocortisone

10 ng/ml epidermal growth factor

(Sigma, U.K.)

RPMI 1640 Medium

RPMI 1640 (PAA Laboratories GmbH, Austria)

10% (v/v) fetal bovine serum (FBS) (Biosera, U.K.)

1% (v/v) L-glutamine (PAA Laboratories GmbH, Austria)

1% (v/v) Penicillin / Streptomycin (PAA Laboratories GmbH, Austria)

Freezing solution

10% (v/v) Dimethyl sulphoxide (DMSO)(BDH Laboratory Supplies, U.K.) in fetal bovine serum (FBS) (Biosera, U.K.)

Antibiotics and Antimycotics

Antibiotic-Antimycotic Solution

(Penicillin 10.000 U/ml, Streptomycin Sulphate 10 mg/ml, Amphotericin B 25 μg/ml in 0.9 % NaCl) (PAA Laboratories GmbH, Austria).

Solution was diluted 1:100 in sterile PBS prior to use

Paraformaldehyde fixative solution (PFA, 1L) pH 7.6

1.3 M Paraformaldehyde (40 g), equal to 4% Paraformaldehyde (w/v)

Paraformaldehyde powder and one pellet of NaOH was dissolved into 1L of distilled water on heating plate at 60°C with a magnetic stirrer; the pH of the solution was then adjusted to 7.6, followed by filtering and storing at +4°C

Scott's tap water (10x, 1L)

811 mM Magnesium sulphate (200g)

238 mM Sodium bicarbonate (20g)

All the reagents were dissolved in 1L of distilled water

Tris buffered saline (TBS, 10x, 1L) pH 7.4

200 mM Tris base (24.2 g)

1.37 M NaCl (80 g)

All the reagents were dissolved in 1L of distilled water, pH adjusted to 7.4 and stored at RT. TBS-T solution was made by adding 0.1% (v/v) Tween 20 (BDH Laboratory Supplies, U.K.) to 1x TBS.

TAE (tris-acetate ethylediaminetetra-acetic acid) buffer (50 x, 1L)

2M Tris base (242 g)

57.1 ml glacial acetic acid

100 mL of 0.5 M EDTA (pH 8.0)

Buffers for Western Blotting

Running buffer (10x, 1L)

0.25 M Tris base (30.29g)

1.92 M Glycine (144.13g)

1 % SDS (10g)

All the reagents were dissolved in 1L of distilled water and stored at RT

Transfer Buffer (10x, 1L)

0.25 M Tris base (30.29g)

1.92 M Glycine (144.13g)

10 % (v/v) Methanol

Tris base and Glycine were dissolved in 1L of distilled water and stored at RT;

Transfer buffer 1x was prepared before use by diluting this solution 1:10 and adding 10 % (v/v) Methanol.

10 % Polyacrylamide Resolving Gel for SDS Gel Electrophoresis (10ml)

4.0 ml dd H2O

3.3 ml Acrylamide/Bis acrylamide mix (30% (w/v) Acrylamide / 0.8% (w/v) Bis acrylamide)

2.5 ml 1.5 mM Tris HCl (pH 8.8)

100 µl 10% SDS

100 µl 10% Ammonium persulfate

4 µl Tetramethylethylenediamine (TEMED)

5 % Polyacrylamide Stacking Gel for SDS Gel Electrophoresis (5ml)

3.4 ml dd H2O

830 µl Acrylamide/Bis acrylamide mix (30% (w/v) Acrylamide / 0.8% (w/v) Bis acrylamide)

630 µl 1.5 mM Tris HCl (pH 6.8)

50 µl 10% SDS

50 µl 10% Ammonium persulfate

5 µl Tetramethylethylenediamine (TEMED)

Lysis buffer boiling buffer A

50 mM Tris HCl pH 8.0

2% (w/v) SDS

1 mM Na_3OV_4

Laemmli buffer (2x)

0.1 M Tris HCl pH 6.8

0.2 M Dithiothreitol (DTT)

4 % (w/v) SDS

0.2% (w/v) Bromophenol blue

20% (w/v) Glycerol

Loading buffer (5x)

125 mM Tris HCl pH 6.8

5% (v/v) β-mercaptoethanol

20 % (v/v) Glycerol

4% (w/v) SDS

0.02% (w/v) Bromophenol blue

Tris buffered saline (TBS, 10x, 1L) pH 7.4

200 mM Tris base (24.2g)

1.37 M NaCl (80g)

All the reagents were dissolved in 1L of distilled water, pH adjusted to 7.4 and stored at RT. TBS-T solution was made by adding 0.1%-0.5% (v/v) Tween 20 (BDH Laboratory Supplies, U.K.) to 1x TBS

Appendix II

List of RNAi sequences

GLI1 si15 (s5815, Silencer Select siRNA, Ambion, U.K.)

Sequence 5'→ 3'

Sense CCAACUUGCCCAAUCACAAtt

Antisense UUGUGAUUGGGCAAGUUGGgt

GLI1 si16 (s5816, Silencer Select siRNA, Ambion, U.K.)

Sequence 5'→ 3'

Sense AGACAGUGCAUGGUCCUGAtt

Antisense UCAGGACCAUGCACUGUCUtg

GLI2 si17 (s5817, Silencer Select siRNA, Ambion, U.K.)

Sequence 5'→ 3'

Sense GGUUCGAGCAGCUCAAGAAtt

Antisense UUCUUGAGCUGCUCGAACCgg

GLI2 si44 (FlexiTube siRNA SI00074844, Qiagen, U.K.)

Sequence 5'→ 3'

Target Sequence TAGGGAGCATTTGGGTTTGAA

Sense GGGAGCAUUUGGGUUUGAATT

Antisense UUCAAACCCAAAUGCUCCCTA

Appendix III

Summary of antigen positions and known isoforms location

GLI1

GLI1 H-300 antibody (GLI1 (H-300) sc-20687, Santa Cruz) was raised against a recombinant protein corresponding to amino acids 781-1080 of GLI1 of human origin (acc# P08151).

The epitope of GLI1 C-18 (GLI1 (C-18) sc-6152, Santa Cruz) maps within the range of amino acids1056-1106 of GLI1 of human origin (acc# P08151).

The GLI1 RD (MAB3324, R&D Systems) antibody was produced using a hybridoma elicited from a rat immunized with purified, E. coli-derived recombinant human GLI1 (aa 1 - 234; Accession # P08151).

The epitope of GLI1 N-16 (GLI1 (N-16) sc-6153, Santa Cruz) maps within the range of amino acid 1-50 of GLI1 of human origin (acc# P08151); this antibody was not used in this thesis but in a publication by Ghali L et al. (Ghali et al., 1999) that investigated GLI1 expression in BCCs by immunohistochemistry; GLI1 N-16 antigen is underlined.

GLSGPPF CHQANLMSGP HSYGPARETN

Amino acids positions 34 to 74 deleted in the tGLI1 isoform described by Lo (Lo *et al.*, 2009).

GLSGPPF CHQANLMSGP HSYGPARETN SCTEGPLFSS PRSAVKLTKK RALSISPLSD ASLDLQTVIR TSPSSLVAFI NSRCTSPGGS YGHLSIGTMS

Amino acids positions 34 to 130 deleted in the GLI1ΔN isoform described by Shimokawa (Shimokawa *et al.*, 2008); first and last three amino acids are highlighted in red and bold font.

MFNSMTPPPI SSYGEPCCLR PLPSQGAPSV GTEGLSGPPF CHQANLMSGP HSYGPARETN SCTEGPLFSS PRSAVKLTKK RALSISPLSD ASLDLQTVIR TSPSSLVAFI NSRCTSPGGS YGHLSIGTMS PSLGFPAQMN HQKGPSPSFG VQPCGPHDSA RGGMIPHPQS RGPFPTCQLK SELDMLVGKC REEPLEGDMS SPNSTGIQDP LLGMLDGRED LEREEKREPE S

Amino acids positions 1 to 231 deleted in the GLI1ΔN isoform described by Altaba (Altaba, 1999) first and last three amino acids are highlighted in blue and bold font.

RGLKLP SLSHTGTTVS RRVGPPVSLE RRSSSSSSIS SAYTVSRRSS LASPFPPGSP
PENGASSLPG LMPAQHYLLR ARYASARGGG TSPTAASSLD RIGGLPMPPW RSRAEYPGYN
PNAGVTRRAS DPAQAADRPA PARVQRFKSL GCVHTPPTVA GGGQNFDPYL PTSVYSPQPP
SITENAAMDA RGLQEEPEVG TSMVGSGLNP YMDFPPTDTL GYGGPEGAAA EPYGARGPGS
LPLGPGPPTN YGPNPCPQQA SYPDPTQETW GEFPSHSGLY PGPKALGGTY SQCPRLEHYG
QVQVKPEQGC PVGSDSTGLA PCLNAHPSEG PPHPQPLFSH YPQPSPPQYL QSGPYTQPPP
DYLPSEPRPC LDFDSPTHST GQLKAQLVCN YVQSQQELLW EGGGREDAPA QEPSYQSPKF
LGGSQVSPSR AKAPVNTYGP GFGPNLPNHK SGSYPTPSPC HENFVVGANR ASHRAAAPPR
LLPPLPTCYG PLKVGGTNPS CGHPEVGRLG GGPALYPPPE GQVCNPLDSL DLDNTQLDFV
AILDEPQGLS PPPSHDQRGS SGHTPPPSGP PNMAVGNMSV LLRSLPGETE FLNSSA

Amino acids positions 515 to 1106 deleted in the GLI1ΔC isoform described by Altaba (Altaba, 1999) first and last three amino acids are highlighted in purple and bold font.

GLI 1

P08151 (GLI1_HUMAN), UniProtKB/Swiss-Prot

```
        10         20         30         40         50         60
MFNSMTPPPI SSYGEPCCLR PLPSQGAPSV GTEGLSGPPF CHQANLMSGP HSYGPARETN

        70         80         90        100        110        120
SCTEGPLFSS PRSAVKLTKK RALSISPLSD ASLDLQTVIR TSPSSLVAFI NSRCTSPGGS

       130        140        150        160        170        180
YGHLSIGTMS PSLGFPAQMN HQKGPSPSFG VQPCGPHDSA RGGMIPHPQS RGPFPTCQLK

       190        200        210        220        230        240
SELDMLVGKC REEPLEGDMS SPNSTGIQDP LLGMLDGRED LEREEKREPE SVYETDCRWD

       250        260        270        280        290        300
GCSQEFDSQE QLVHHINSEH IHGERKEFVC HWGGCSRELR PFKAQYMLVV HMRRHTGEKP

       310        320        330        340        350        360
HKCTFEGCRK SYSRLENLKT HLRSHTGEKP YMCEHEGCSK AFSNASDRAK HQNRTHSNEK

       370        380        390        400        410        420
PYVCKLPGCT KRYTDPSSLR KHVKTVHGPD AHVTKRHRGD GPLPRAPSIS TVEPKREREG

       430        440        450        460        470        480
GPIREESRLT VPEGAMKPQP SPGAQSSCSS DHSPAGSAAN TDSGVEMTGN AGGSTEDLSS

       490        500        510        520        530        540
LDEGPCIAGT GLSTLRRLEN LRLDQLHQLR PIGTRGLKLP SLSHTGTTVS RRVGPPVSLE

       550        560        570        580        590        600
RRSSSSSSIS SAYTVSRRSS LASPFPPGSP PENGASSLPG LMPAQHYLLR ARYASARGGG
```

```
       610        620        630        640        650        660
TSPTAASSLD RIGGLPMPPW RSRAEYPGYN PNAGVTRRAS DPAQAADRPA PARVQRFKSL

       670        680        690        700        710        720
GCVHTPPTVA GGGQNFDPYL PTSVYSPQPP SITENAAMDA RGLQEEPEVG TSMVGSGLNP

       730        740        750        760        770        780
YMDFPPTDTL GYGGPEGAAA EPYGARGPGS LPLGPGPPTN YGPNPCPQQA SYPDPTQETW

       790        800        810        820        830        840
GEFPSHSGLY PGPKALGGTY SQCPRLEHYG QVQVKPEQGC PVGSDSTGLA PCLNAHPSEG

       850        860        870        880        890        900
PPHPQPLFSH YPQPSPPQYL QSGPYTQPPP DYLPSEPRPC LDFDSPTHST GQLKAQLVCN

       910        920        930        940        950        960
YVQSQQELLW EGGGREDAPA QEPSYQSPKF LGGSQVSPSR AKAPVNTYGP GFGPNLPNHK

       970        980        990       1000       1010       1020
SGSYPTPSPC HENFVVGANR ASHRAAAPPR LLPPLPTCYG PLKVGGTNPS CGHPEVGRLG

      1030       1040       1050       1060       1070       1080
GGPALYPPPE GQVCNPLDSL DLDNTQLDFV AILDEPQGLS PPPSHDQRGS SGHTPPPSGP

      1090       1100
PNMAVGNMSV LLRSLPGETE FLNSSA
```

GLI 2

The four known different isoforms of human GLI2 alpha (α), beta (β), gamma (γ) and delta (δ) originate from the combinations of two independent alternative splicing sites (Tanimura et al., 1998). The region between amminoacids positions 394 and 410 is missing in the beta (β) and delta (δ) isoforms (highlighted in purple) while the region between amminoacids positions 1158 and 1586 is missing in the gamma (γ) and delta (δ) isoforms (highlighted in green) (according to UniProtKB/Swiss-Prot database, GLI2_HUMAN, accession number P10070).

GLI2 H-300 (GLI2 (H-300): sc-28674, Santa Cruz) recognises an epitope corresponding to amino acids 841-1140 of GLI2 of human origin. Reactivity is expected with all isoforms of this protein.

GLI2 Abcam (GLI2, ab26056, Abcam) was produced using a synthetic peptide derived from a region between residues 272 - 321 of human GLI2 (600 to 649 according to GLI2 sequence after the discovery of the N-terminal domain (Roessler et al., 2005)). Reactivity is expected with all isoforms of this protein.

GLI 2

P10070 (GLI2_HUMAN), UniProtKB/Swiss-Prot

```
        10         20         30         40         50         60
METSASATAS EKQEAKSGIL EAAGFPDPGK KASPLVVAAA AAAAVAAQGV PQHLLPPFHA

        70         80         90        100        110        120
PLPIDMRHQE GRYHYEPHSV HGVHGPPALS GSPVISDISL IRLSPHPAGP GESPFNAPHP

       130        140        150        160        170        180
YVNPHMEHYL RSVHSSPTLS MISAARGLSP ADVAQEHLKE RGLFGLPAPG TTPSDYYHQM

       190        200        210        220        230        240
TLVAGHPAPY GDLLMQSGGA ASAPHLHDYL NPVDVSRFSS PRVTPRLSRK RALSISPLSD

       250        260        270        280        290        300
ASLDLQRMIR TSPNSLVAYI NNSRSSSAAS GSYGHLSAGA LSPAFTFPHP INPVAYQQIL

       310        320        330        340        350        360
SQQRGLGSAF GHTPPLIQPS PTFLAQQPMA LTSINATPTQ LSSSSNCLSD TNQNKQSSES

       370        380        390        400        410        420
AVSSTVNPVA IHKRSKVKTE PEGLRPASPL ALTQGQVSGH GSCGCALPLS QEQLADLKED

       430        440        450        460        470        480
LDRDDCKQEA EVVIYETNCH WEDCTKEYDT QEQLVHHINN EHIHGEKKEF VCRWQACTRE

       490        500        510        520        530        540
QKPFKAQYML VVHMRRHTGE KPHKCTFEGC SKAYSRLENL KTHLRSHTGE KPYVCEHEGC

       550        560        570        580        590        600
NKAFSNASDR AKHQNRTHSN EKPYICKIPG CTKRYTDPSS LRKHVKTVHG PDAHVTKKQR

       610        620        630        640        650        660
NDVHLRTPLL KENGDSEAGT EPGGPESTEA SSTSQAVEDC LHVRAIKTES SGLCQSSPGA

       670        680        690        700        710        720
QSSCSSEPSP LGSAPNNDSG VEMPGTGPGS LGDLTALDDT PPGADTSALA APSAGGLQLR

       730        740        750        760        770        780
KHMTTMHRFE QLKKEKLKSL KDSCSWAGPT PHTRNTKLPP LPGSGSILEN FSGSGGGGPA

       790        800        810        820        830        840
GLLPNPRLSE LSASEVTMLS QLQERRDSST STVSSAYTVS RRSSGISPYF SSRRSSEASP

       850        860        870        880        890        900
LGAGRPHNAS SADSYDPIST DASRRSSEAS QCSGGSGLLN LTPAQQYSLR AKYAAATGGP

       910        920        930        940        950        960
PPTPLPGLER MSLRTRLALL DAPERTLPAG CPRPLGPRRG SDGPTYGHGH AGAAPAFPHE

       970        980        990       1000       1010       1020
APGGGARRAS DPVRRPDALS LPRVQRFHST HNVNPGPLPP CADRRGLRLQ SHPSTDGGLA

      1030       1040       1050       1060       1070       1080
RGAYSPRPPS ISENVAMEAV AAGVDGAGPE ADLGLPEDDL VLPDDVVQYI KAHASGALDE
```

```
      1090        1100        1110        1120        1130        1140
GTGQVYPTES TGFSDNPRLP SPGLHGQRRM VAADSNVGPS APMLGGCQLG FGAPSSLNKN

      1150        1160        1170        1180        1190        1200
NMPVQWNEVS SGTVDALASQ VKPPPFPQGN LAVVQQKPAF GQYPGYSPQG LQASPGGLDS

      1210        1220        1230        1240        1250        1260
TQPHLQPRSG APSQGIPRVN YMQQLRQPVA GSQCPGMTTT MSPHACYGQV HPQLSPSTIS

      1270        1280        1290        1300        1310        1320
GALNQFPQSC SNMPAKPGHL GHPQQTEVAP DPTTMGNRHR ELGVPDSALA GVPPPHPVQS

      1330        1340        1350        1360        1370        1380
YPQQSHHLAA SMSQEGYHQV PSLLPARQPG FMEPQTGPMG VATAGFGLVQ PRPPLEPSPT

      1390        1400        1410        1420        1430        1440
GRHRGVRAVQ QQLAYARATG HAMAAMPSSQ ETAEAVPKGA MGNMGSVPPQ PPPQDAGGAP

      1450        1460        1470        1480        1490        1500
DHSMLYYYGQ IHMYEQDGGL ENLGSCQVMR SQPPQPQACQ DSIQPQPLPS PGVNQVSSTV

      1510        1520        1530        1540        1550        1560
DSQLLEAPQI DFDAIMDDGD HSSLFSGALS PSLLHSLSQN SSRLTTPRNS LTLPSIPAGI

      1570        1580
SNMAVGDMSS MLTSLAEESK FLNMMT
```

Appendix VI

List of publications where GLI antibodies have been used for immunohistochemistry

GLI1 (H-300), sc-20687, Santa Cruz

Fukaya, M., Isohata, N., Ohta, H., Aoyagi, K., Ochiya, T., Saeki, N., Yanagihara, K., Nakanishi, Y., Taniguchi, H., Sakamoto, H., Shimoda, T., Nimura, Y., Yoshida, T., and Sasaki, H. (2006). Hedgehog signal activation in gastric pit cell and in diffuse-type gastric cancer. Gastroenterology *131*, 14-29.

Chen, B.-Y., Liu, J.-Y., Chang, H.-H., Chang, C.-P., Lo, W.-Y., Kuo, W.-H., Yang, C.-R., and Lin, D.P.C. (2007). Hedgehog is involved in prostate basal cell hyperplasia formation and its progressing towards tumorigenesis. Biochemical and Biophysical Research Communications *357*, 1084-1089.

Kim, K.H., Kim, J.M., Choi, Y.-L., Shin, Y.K., Lee, H.-c., Seong, I.O., Kim, B.K., Chae, S.W., Chung, Y.-S., and Kim, S.-H. (2009b). Expression of Sonic hedgehog signaling molecules in normal, hyperplastic and carcinomatous endometrium. Pathology International *59*, 279-287.

Brunner, M., Thurnher, D., Pammer, J., Heiduschka, G., Petzelbauer, P., Schmid, C., Schneider, S., and Erovic, B.M. EXPRESSION OF HEDGEHOG SIGNALING MOLECULES IN MERKEL CELL CARCINOMA. Head and Neck-Journal for the Sciences and Specialties of the Head and Neck *32*, 333-340.

Wang, G., Zhang, Z., Xu, Z., Yin, H., Bai, L., Ma, Z., DeCoster, M.A., Qian, G., and Wu, G. (2010a). Activation of the sonic hedgehog signaling controls human pulmonary arterial smooth muscle cell proliferation in response to hypoxia. Biochimica Et Biophysica Acta-Molecular Cell Research *1803*, 1359-1367.

Cui, D., Xu, Q., Wang, K., and Che, X. (2010). Gli1 is a potential target for alleviating multidrug resistance of gliomas. Journal of the Neurological Sciences *288*, 156-166.

Mimeault, M., Johansson, S.L., Henichart, J.-P., Depreux, P., and Batra, S.K. (2010). Cytotoxic Effects Induced by Docetaxel, Gefitinib, and Cyclopamine on Side Population and Nonside Population Cell Fractions from Human Invasive Prostate Cancer Cells. Molecular Cancer Therapeutics *9*, 617-630.

Wang, K., Pan, L., Che, X., Cui, D., and Li, C. (2010b). Gli1 inhibition induces cell-cycle arrest and enhanced apoptosis in brain glioma cell lines. Journal of Neuro-Oncology *98*, 319-327.

Singh, R.R., Cho-Vega, J.H., Davuluri, Y., Ma, S., Kasbidi, F., Milito, C., Lennon, P.A., Drakos, E., Medeiros, L.J., Luthra, R., and Vega, F. (2009). Sonic Hedgehog Signaling Pathway Is Activated in ALK-Positive Anaplastic Large Cell Lymphoma. Cancer Research *69*, 2550-2558.

Lo, H.-W., Zhu, H., Cao, X., Aldrich, A., and Ali-Osman, F. (2009). A Novel Splice Variant of GLI1 That Promotes Glioblastoma Cell Migration and Invasion. Cancer Research *69*, 6790-6798.

Xuan, Y., and Lin, Z. (2009). Expression of Indian Hedgehog signaling molecules in breast cancer. Journal of Cancer Research and Clinical Oncology *135*, 235-240.

Liao, X., Siu, M.K.Y., Au, C.W.H., Wong, E.S.Y., Chan, H.Y., Ip, P.P.C., Ngan, H.Y.S., and Cheung, A.N.Y. (2009). Aberrant activation of hedgehog signaling pathway in ovarian cancers: effect on prognosis, cell invasion and differentiation. Carcinogenesis *30*, 131-140.

GLI1 RD, MAB3324, R&D Systems

Li, Y.-C., Deng, Y.-H., Guo, Z.-H., Zhang, M.-M., Zhu, J., Pu, C.-L., Xiang, C.-P., and Guo, C.-B. (2010). PROGNOSTIC VALUE OF HEDGEHOG SIGNAL COMPONENT EXPRESSIONS IN HEPATOBLASTOMA PATIENTS. European Journal of Medical Research *15*, 468-474.

GLI2 (H-300), sc-28674, Santa Cruz

Bishop, C.L., Bergin, A.-M.H., Fessart, D., Borgdorff, V., Hatzimasoura, E., Garbe, J.C., Stampfer, M.R., Koh, J., and Beach, D.H. (2010). Primary Cilium-Dependent and -Independent Hedgehog Signaling Inhibits p16(INK4A). Molecular Cell *40*, 533-547.

Clement, C.A., Kristensen, S.G., Mollgard, K., Pazour, G.J., Yoder, B.K., Larsen, L.A., and Christensen, S.T. (2009). The primary cilium coordinates early cardiogenesis and hedgehog signaling in cardiomyocyte differentiation. Journal of Cell Science *122*, 3070-3082.

Nielsen, S.K., Mollgard, K., Clement, C.A., Veland, I.R., Awan, A., Yoder, B.K., Novak, I., and Christensen, S.T. (2008). Characterization of primary cilia and hedgehog signaling during development of the human pancreas and in human pancreatic duct cancer cell lines. Developmental Dynamics *237*, 2039-2052.

GLI2, ab26056, Abcam

Nakamura, K., Sasajima, J., Mizukami, Y., Sugiyama, Y., Yamazaki, M., Fujii, R., Kawamoto, T., Koizumi, K., Sato, K., Fujiya, M., Sasaki, K., Tanno, S., Okumura, T., Shimizu, N., Kawabe, J.-i., Karasaki, H., Kono, T., Ii, M., Bardeesy, N., Chung,

D.C., and Kohgo, Y. (2010). Hedgehog Promotes Neovascularization in Pancreatic Cancers by Regulating Ang-1 and IGF-1 Expression in Bone-Marrow Derived Pro-Angiogenic Cells. Plos One *5*.

Youssef, K.K., Van Keymeulen, A., Lapouge, G., Beck, B., Michaux, C., Achouri, Y., Sotiropoulou, P.A., and Blanpain, C. (2010). Identification of the cell lineage at the origin of basal cell carcinoma. Nature Cell Biology *12*, 299-U111.

Peacock, Z.S., Cox, D., and Schmidt, B.L. (2010). Involvement of PTCH1 mutations in the calcifying epithelial odontogenic tumor. Oral Oncology *46*, 387-392.

Coon, V., Laukert, T., Pedone, C.A., Laterra, J., Kim, K.J., and Fults, D.W. (2010). Molecular Therapy Targeting Sonic Hedgehog and Hepatocyte Growth Factor Signaling in a Mouse Model of Medulloblastoma. Molecular Cancer Therapeutics *9*, 2627-2636.

Takanaga, H., Tsuchida-Straeten, N., Nishide, K., Watanabe, A., Aburatani, H., and Kondo, T. (2009). Gli2 Is a Novel Regulator of Sox2 Expression in Telencephalic Neuroepithelial Cells. Stem Cells *27*, 165-174.

Kim, J.E., Singh, R.R., Cho-Vega, J.H., Drakos, E., Davuluri, Y., Khokhar, F.A., Fayad, L., Medeiros, L.J., and Vega, F. (2009a). Sonic hedgehog signaling proteins and ATP-binding cassette G2 are aberrantly expressed in diffuse large B-Cell lymphoma. Modern Pathology *22*, 1312-1320.

Syn, W.-K., Witek, R.P., Curbishley, S.M., Jung, Y., Choi, S.S., Enrich, B., Omenetti, A., Agboola, K.M., Fearing, C.M., Tilg, H., Adams, D.H., and Diehl, A.M. (2009). Role for hedgehog pathway in regulating growth and function of invariant NKT cells. European Journal of Immunology *39*, 1879-1892.

Omenetti, A., Popov, Y., Jung, Y., Choi, S.S., Witek, R.P., Yang, L., Brown, K.D., Schuppan, D., and Diehl, A.M. (2008a). The hedgehog pathway regulates remodelling responses to biliary obstruction in rats. Gut *57*, 1275-1282.

Omenetti, A., Porrello, A., Jung, Y., Yang, L., Popov, Y., Choi, S.S., Witek, R.P., Alpini, G., Venter, J., Vandongen, H.M., Syn, W.-K., Baroni, G.S., Benedetti, A., Schuppan, D., and Diehl, A.M. (2008b). Hedgehog signaling regulates epithelial-mesenchymal transition during biliary fibrosis in rodents and humans. Journal of Clinical Investigation *118*, 3331-3342.

Kim, Y., Yoon, J.W., Xiao, X., Dean, N.M., Monia, B.P., and Marcusson, E.G. (2007). Selective down-regulation of glioma-associated oncogene 2 inhibits the proliferation of hepatocellular carcinoma cells. Cancer Research *67*, 3583-3593.